ADAMTS13: Molecular Recognition of von Willebrand Factor

A Thesis Submitted to the University of London for the Degree of Doctor of Philosophy in the Faculty of Medicine

Submitted by Sara Zanardelli,

Medical Biotechnologies Undergraduate Degree, University of Milan

Department of Haematology

Imperial College London

Hammersmith Campus

Commonwealth Building

Du Cane Road W12 ONN

November 2006

ABSTRACT

Von Willebrand factor (VWF) is a multimeric plasma glycoprotein that mediates platelet adhesion and aggregation at sites of vascular injury. VWF platelet tethering function is dependent on its multimeric size. This is regulated by proteolytic cleavage within its A2 domain (Y1605-M1606) by the plasma metalloprotease ADAMTS13. How ADAMTS13 specifically recognises and cleaves VWF is still unclear. To elucidate VWF determinants important for its recognition and cleavage by ADAMTS13, I expressed in *E. coli* four recombinant VWF fragments, spanning different regions of VWF A2 and A3 domains: VWF76 (1593-1668), VWF115 (1554-1668), VWFA2 (1473-1668) and VWF115-A3 (1554-1874). In the absence of denaturants, VWFA2 was quite resistant to proteolysis by ADAMTS13, whereas the other fragments were readily cleaved. Using high pressure liquid chromatography (HPLC) to monitor cleavage, specificity constants (k_{cat}/K_m) for VWF76, VWF115 and VWF115-A3 were derived as 7.83, 6.70 and 6.39 x 10^4 M^{-1} s^{-1}, respectively. The initial rates of VWF115 cleavage at different substrate concentrations were then determined and from this the individual kinetic constants K_m (1.61 μM) and k_{cat} (0.14 s^{-1}) were derived. VWF115 binding interaction with ADAMTS13 was investigated by surface plasmon resonance (SPR) and microtiter plate-based equilibrium assay, both methods revealing high affinity binding (K_D ~20 nM and ~16 nM, respectively). To identify specific residues important for recognition and proteolysis by ADAMTS13, I mutated charged residues of VWF115 predicted to be on the surface of the A2 domain. The study of their proteolysis by ADAMTS13 revealed a reduction (4-12 fold) in k_{cat}/K_m for D1587A, D1614A, E1615A and K1617A VWF115 mutants. SPR analysis showed a significant reduction in ADAMTS13 binding affinity for D1587A, D1614A, E1615A and K1617A VWF115 mutants, suggesting they may be part of a docking site for ADAMTS13 on the surface of A2 domain. This hypothesis was supported by additional binding and competition experiments using VWFA2 and VWF115 fragments, studied in native and denaturing conditions. My work has clarified the way in which ADAMTS13 interacts with VWF and provides a basis for its further investigation.

PUBLICATIONS ARISING FROM THIS THESIS

Zanardelli, S., Crawley, J.T.B., Chan Kwo Chion C.K.N., Lam, J.K., Preston. J.S., Lane D.A., *ADAMTS13 substrate recognition of von Willebrand factor A2 domain.* J Biol Chem, 2006. 281: 1555-63

Zanardelli, S., Chan Kwo Chion C.K.N, Crawley, J.T.B., Moss R., Lenting PJ. Lane D.A., *Regions in von Willebrand factor modulating the interaction with ADAMTS13 and the accessibility of the scissile bond* (paper in preparation).

PERSONAL STATEMENT

I, Sara Zanardelli, confirm that the work presented in this thesis is my own.
Where information has been derived from other sources, I confirm that this has been indicated in the thesis.



ACKNOWLEDGMENTS

I am very grateful to my supervisor Prof. David Lane for giving me the opportunity to study in his laboratory and for his support and guidance throughout the development of my project.

I express my gratitude to Dr. James Rance for his help and supervision at the early stage of this work and to Dr. James Crawley for his advice and for the critical review of this thesis.

I also want to express all my gratitude to Dr. Chan Kwo Chion C.K.N., Alain to his friends, to be my eternal *guru*, at work and in life.

A special thank to fellow PhD students Tom Mc Kinnon and Jonathan Lam for their friendship and for making my stay in this laboratory really enjoyable (definitely!).

I will not forget (of course!) to thank Cristina Razzari, my Italian *pregiata* "connection", because it would have been impossible to work in London without hearing her lovely loud voice!

I also wish to express my gratitude to all the people I had the opportunity to work with during my PhD for making this three-year stays a rewarding experience.

I would like to thank my friend Raffaella Rospo, my little frog, for being always close to me… especially every time I need to print a thesis! …and because *mi squarto!*

I would like to thank Tassos Shalis, my flatmate, neighbour and therapist (…) for getting mad with me during the *boring* formatting of the thesis.

I finally thank Monica Magnani, Roberta Palla, Tiziana Asietti and Claudio Dozza to continuously prove that our friendship goes beyond any distance and my family (animals included) for their unconditioned love and for bearing quite well such a crazy daughter.

I would like to dedicate this thesis to my grandmother Nonna Luigia for "giving me birth" in a magic place as Moneglia.

TABLE OF CONTENTS

ABSTRACT 2

PUBLICATIONS ARISING FROM THIS THESIS 3

ACKNOWLEDGMENTS 4

LIST OF FIGURES 12

LIST OF TABLES 14

ABBREVIATIONS 15

1. INTRODUCTION 18

1.1 HAEMOSTASIS OVERVIEW 18

1.1.1 Platelet plug formation 18

1.1.1.1 Platelet tethering and stable adhesion 18

1.1.1.2 Platelet activation 19

1.1.1.3 Platelet aggregation 20

1.1.2 Coagulation cascade and final clot formation 21

1.2 VWF 23

1.2.1 VWF function 23

1.2.2 Structure and expression of VWF gene 23

1.2.3 Structure of VWF 25

1.2.4 VWF synthesis, storage and secretion 29

1.2.5 VWF plasma clearance 32

1.2.6 Plasma VWF multimers 32

1.2.7 Influence of fluid shear stress upon VWF function 33

1.2.8 VWF structure-function relationship 34

1.2.8.1 Stabilisation of blood coagulation FVIII 34

1.2.8.2 Platelet adhesion to connective tissue 35

1.2.8.2.1 VWF binding to collagen and other extracellular matrix components 35

1.2.8.2.2 VWF binding to platelet GpIbα and GpIIb-IIIa receptors 36

1.2.9 Pathogenesis and classification of von Willebrand's disease (VWD) 36

1.3 ADAMTS13 39

1.3.1 ADAM and ADAMTS families 40

1.3.2 ADAMTS13 gene, synthesis and secretion 43

1.3.3 ADAMTS13 structure 43

1.3.4 ADAMTS13 interaction with VWF 49
1.3.5 ADAMTS13 function 51
1.3.5.1 Role of denaturants/shear stress and chloride ions in VWF cleavage 51
1.3.5.2 Possible location of ADAMTS13 activity *in vivo* 53
1.3.5.3 Regulation of ADAMTS13 activity 54
1.3.6 Thrombotic thrombocytopenic purpura (TTP) 57
1.3.6.1 History of TTP 57
1.3.6.2 Incidence, clinical manifestations, pathophysiology and therapy of TTP 57
1.3.6.3 Congenital TTP 58
1.3.6.4 Acquired TTP 59
1.3.6.5 TTP and other thrombotic microangiopathies 59
1.3.6.6 ADAMTS13 activity assays 60
1.3.6.6.1 CBA 60
1.3.6.6.2 Immunoblotting of VWF multimers 61
1.3.6.6.3 VWF ristocetin cofactor activity 61
1.3.6.6.4 ADAMTS13 cleavage of FRET-VWF73 61
1.3.6.7 Knock out ADAMTS13 mice and TTP 61
1.4 AIMS AND LAYOUT OF MY THESIS 63
2. MATERIALS AND METHODS **65**
2.1 CONSTRUCTION OF EXPRESSION VECTORS 65
2.1.1 ADAMTS13 expression vector 65
2.1.2 VWF76, VWF115, VWF115-A3, VWFA2 expression vectors 66
2.1.2.1 Cloning of VWF fragments 66
2.1.2.2 Transformation of TOP10 competent *E.coli* cells 68
2.1.2.3 Analysis of the transformants by Nhe I and Sac I digestion 68
2.1.2.4 PCR 68
2.1.2.5 Agarose gel electrophoresis 69
2.1.2.6 Gel extraction of DNA 70
2.1.3 Generation of VWF115 and VWF115-A3 mutant constructs 70
2.1.3.1 Site-directed mutagenesis 71
2.1.3.2 Transformation of XL10-Gold ultra competent *E.coli* cells 71
2.1.4 Generation of mutant VWFA2 constructs 71
2.1.4.1 Sub-cloning of D1587A, D1614A and E1615A into VWFA2 pTrcHisA vector 71

2.1.4.2 Transformation of DH5α competent *E.coli* cells 74
2.1.5 Plasmid extraction: miniprep 74
2.1.6 Plasmid extraction: maxiprep 75
2.1.7 Sequencing 76
2.1.8 Glycerol stock 76
2.2 EXPRESSION AND PURIFICATION OF RECOMBINANT PROTEINS 76
2.2.1 ADAMTS13 expression 76
2.2.1.1 Cell culture: general routine 76
2.2.1.2 Reviving HEK293 cells from liquid nitrogen 77
2.2.1.3 Cell passages 77
2.2.1.4 Stable transfection 77
2.2.1.5 Cryopreservation of cell lines 78
2.2.2 ADAMTS13 purification 79
2.2.2.1 Desalting of conditioned medium 79
2.2.2.2 Nickel affinity chromatography and gel filtration chromatography 79
2.2.3 Expression of recombinant VWF fragments in *E. coli* cells 80
2.2.3.1 Overview of expression in Rosetta and Rosetta Gami DE3 *E.coli* cells 80
2.2.3.2 Transformation of competent Rosetta/Rosetta Gami cells 80
2.2.3.3 Expression of VWF fragments in Rosetta/Rosetta Gami cells 81
2.2.4 Purification of VWF fragments 81
2.2.4.1 Isolation of inclusion bodies and soluble citoplasmatic fraction 81
2.2.4.2 Nickel affinity chromatography 82
2.2.5 Total protein quantification (BCA assay) 82
2.2.6 ADAMTS13 Enzyme-Linked ImmunoSorbent Assay (ELISA) 83
2.2.7 SDS polyacrylamide gel electrophoresis (SDS-PAGE) 84
2.2.8 Coomassie staining 84
2.2.9 Western blotting 84
2.3 CHARACTERISATION OF VWF PROTEOLYSIS BY ADAMTS13 85
2.3.1 Cleavage of VWF fragments 85
2.3.2 Overview of HPLC and reverse phase chromatography 86
2.3.3 HPLC analysis and determination of specificity constant k_{cat}/K_m 86

2.3.4 Determination of K_m and k_{cat} 87
2.4 CHARACTERISATION OF ADAMTS13 BINDING TO VWF FRAGMENTS 88
2.4.1 Overview of Surface Plasmon Resonance (SPR) and the BIAcore system 88
2.4.1.1 Principles and components of BIAcore system 88
2.4.1.2 Ligand immobilisation 91
2.4.1.3 Amount of ligand to immobilise 92
2.4.1.4 Mass transport 92
2.4.1.5 Regeneration conditions 92
2.4.2 Kinetic analysis using BIAcore 93
2.4.2.1 Langmuir model 93
2.4.2.2 Heterogeneous ligand model 94
2.4.3 Determination of ADAMTS13 binding affinity for wild type and mutant VWF115 fragments using SPR 94
2.4.3.1 Immobilisation of ADAMTS13 on a CM5 sensor chip using monoclonal antibodies 95
2.4.3.2 Immobilisation of VWF115 on a CM5 sensor chip using monoclonal antibodies 95
2.4.3.3 Direct immobilisation of VWF115 on a CM5 sensor chip 96
2.4.3.4 Direct immobilisation of ADAMTS13 on a CM5 sensor chip 96
2.4.4 Determination of ADAMTS13 binding affinity for VWF fragments using a microtiter plate-based binding assay 96
2.4.5 Competition binding studies 98
2.4.5.1 Soluble and plate-bound VWFA2 competition 98
2.4.5.2 Competition between soluble and immobilised VWF115 and VWFA2 fragments 98
2.4.5.3 Calculation of IC50 and the dissociation constant K_i 99
3. RESULTS **100**
3.1 PREPARATION OF ADAMTS13 100
3.1.1 Introduction 100
3.1.2 Expression and purification of recombinant ADAMTS13 100
3.1.3 Further purification of ADAMTS13: gel filtration 102
3.1.4 Determination of the concentration of ADAMTS13 104
3.1.4.1 BCA assay 104

3.1.4.2 ELISA for ADAMTS13 104
3.1.5 Discussion 105
3.2 GENERATION AND CHARACTERISATION OF VWF A DOMAIN FRAGMENTS AS ADAMTS13 SUBSTRATES 107
3.2.1 Introduction 107
3.2.2 VWF fragment cloning 109
3.2.3 VWF76, VWF115 and VWF115-A3 expression and purification 111
3.2.3.1 Expression and purification of VWF76 112
3.2.3.2 Expression and purification of VWF115 113
3.2.3.3 Expression and purification of VWF115-A3 114
3.2.4 Proteolysis of VWF76, VWF115, VWF115-A3 by ADAMTS13 115
3.2.4.1 Qualitative analysis of cleavage 115
3.2.4.2 Quantitative analysis of cleavage 119
3.2.4.3 Determination of K_m and k_{cat} for VWF115 cleavage 121
3.2.5 Discussion 122
3.3 CHARACTERISATION OF ADAMTS13 RECOGNITION OF VWF115 124
3.3.1 Introduction 124
3.3.2 Characterisation of ADAMTS13 binding to VWF115 by SPR 124
3.3.2.1 Immobilisation of ADAMTS13 or VWF115 on a CM5 chip using monoclonal antibodies 124
3.3.2.2 Direct immobilisation of VWF115 on a CM5 chip 128
3.3.2.3 Direct immobilisation of ADAMTS13 on a CM5 chip 130
3.3.3 Characterisation of ADAMTS13 binding to VWF115 using a microtiter plate-based immunoassay 131
3.3.4 Discussion 133
3.4 TYPE 2A VWD MUTATIONS AND VWF115 PROTEOLYSIS 136
3.4.1 Introduction 136
3.4.2 Site-directed mutagenesis of type 2A VWD mutations 136
3.4.3 Expression and purification of type 2A VWD mutants 138
3.4.4 Influence of type 2A VWD mutations on ADAMTS13 proteolysis 139
3.4.5 Discussion 140
3.5 IDENTIFICATION OF CHARGED RESIDUES IN VWF115 INVOLVED IN ADAMTS13 BINDING 142

3.5.1 Introduction 142
3.5.2 Site-directed mutagenesis of surface charged residues inVWF115 142
3.5.3 Expression and purification of VWF115 charged mutants 144
3.5.4 Analysis of the cleavage of VWF115 charged mutants 144
3.5.5 VWF115 residues involved in ADAMTS13 binding 147
3.5.6 Discussion 149
3.6 BINDING AND PROTEOLYSIS OF VWF A2 DOMAIN BY ADAMTS13 151
3.6.1 Introduction 151
3.6.2 Bacterial expression of VWFA2 151
3.6.3 Denaturants enhance VWFA2 proteolysis 153
3.6.4 Sub-cloning of D1587A, D1614A and E1615A in VWF A2 domain 155
3.6.5 Expression and purification of VWFA2 mutants 156
3.6.6 ADAMTS13 cleavage of VWFA2 variants 156
3.6.7 Wild type VWFA2 binding to ADAMTS13 158
3.6.8 Soluble and plate-bound VWFA2: competition experiments 159
3.6.9 Competition between soluble and immobilised VWF115 and VWFA2 fragments 161
3.6.10 Discussion 165
4. ON-GOING AND FUTURE WORK **168**
4.1 INVESTIGATION OF OTHER VWF REGIONS IMPORTANT FOR ITS CLEAVAGE/BINDING BY ADAMTS13 168
4.1.1 Site-directed mutagenesis of charged residues in VWFA2 N-terminal region 168
4.1.2 Site-directed mutagenesis of VWF cleavage site and surrounding residues 170
4.1.3 Characterisation of ADAMTS13 binding to VWFD'D3, VWFA1A2A3, VWFD'A3 AND VWFA1CK 172
4.2 ROLE OF CALCIUM IONS IN VWF-ADAMTS13 BINDING 173
4.3 INHIBITION OF VWFA2 PROTEOLYSIS BY ITS CLEAVAGE PRODUCTS 174
5. DISCUSSION **176**
REFERENCES **184**
APPENDICES **204**

COPY OF THE PUBLICATION ARISING FROM THE WORK IN THIS THESIS

208

LIST OF FIGURES

Figure1.1 Clot formation 22

Figure 1.2 Domain structure of VWF 25

Figure 1.3 VWF A domains 28

Figure 1.4 Maturation process of pro-VWF 31

Figure 1.5 Plasma VWF multimers 33

Figure 1.6 Distribution of VWF multimers in VWD 39

Figure 1.7 Schematic diagrams of ADAM, ADAMTS metalloproteases and ADAMTS13 42

Figure 1.8 Mechanism of peptide hydrolysis 46

Figure 1.9 Structural model of ADAMTS13 catalytic domain 46

Figure 1.10 VWF Y1605-M1606 cleavage site 52

Figure 1.11 VWF cleavage by ADAMTS13 52

Figure 1.12 Sites of ADAMTS13 action 56

Figure 2.1 Schematic representation of pcDNA 3.1/myc-His vector 65

Figure 2.2 Schematic representation of pTrcHisA vector 67

Figure 2.3 Schematic representation of pET100/D-TOPO vector 67

Figure 2.4 Schematic representation of sub-cloning of D1587A, D1614A and E1615A into VWFA2 pTrcHisA vector 73

Figure 2.5 Illustration of sensor chip, detector and IFC 90

Figure 2.6 SPR sensogram 90

Figure 2.7 Amine coupling of the ligand to the surface of a CM5 sensor chip 91

Figure 2.8 Representation of VWF115/VWFA2-ADAMTS13 plate-based binding assay 98

Figure 3.1 Purification of recombinant ADAMTS13 101

Figure 3.2 Gel filtration of affinity purified ADAMTS13 103

Figure 3.3 ADAMTS13 purified after adding protease inhibitor cocktail to the Optimem medium 103

Figure 3.4 Standard curve for BCA 104

Figure 3.5 Standard curve for ADAMTS13 ELISA 105

Figure 3.6 Recombinant VWF A domain fragments 108

Figure 3.7 Gel electrophoresis of PCR products encoding VWF76, VWF115 and VWF115-A3 109

Figure 3.8 Screening of VWF115-A3 pET100 positive clones 110
Figure 3.9 Site-directed mutagenesis of C1669 and C1670 residues in VWF115-A3 111
Figure 3.10 VWF115 soluble fraction and inclusion bodies 112
Figure 3.11 Purification of recombinant VWF76 113
Figure 3.12 Purification and refolding of VWF115 from inclusion bodies 114
Figure 3.13 Purification and refolding of VWF115-A3 from inclusion bodies 115
Figure 3.14 VWF76, VWF115, VWF115-A3 cleavage by ADAMTS13 118
Figure 3.15 Proteolysis of VWF115 is independent of its concentration 120
Figure 3.16 Proteolysis of VWF76, VWF115 and VWF115-A3 by ADAMTS13 under low substrate concentrations 120
Figure 3.17 *Michaelis-Menten* plot of VWF115 cleavage by ADAMTS13 121
Figure 3.18 Immobilisation of ADAMTS13 via an anti-CUB antibody and VWF115-ADAMTS13 binding 126
Figure 3.19 Immobilisation of VWF115 via Anti-His G antibody and VWF115-ADAMTS13 binding 127
Figure 3.20 Immobilisation of VWF115 and hEPCR 129
Figure 3.21 ADAMTS13 binding to VWF115 directly coupled to a CM5 chip 130
Figure 3.22 VWF115 binding to ADAMTS13 directly coupled to a CM5 chip 131
Figure 3.23 VWF115-ADAMTS13 binding (plate-based binding assay) 132
Figure 3.24 VWF115 type 2A (II) mutants 137
Figure 3.25 Purification of VWF115 type 2A mutants 138
Figure 3.26 HPLC analysis of proteolysis of VWF115 type 2A mutants 139
Figure 3.27 VWF115 charged mutants 143
Figure 3.28 Gel electrophoresis following PCR reaction 143
Figure 3.29 Purification of VWF115 charged mutants 144
Figure 3.30 Proteolysis of VWF115 charged mutants by ADAMTS13 146
Figure 3.31 Binding between ADAMTS13 and immobilised wild type VWF115 and D1587A, D1614A, E1615A and DEK1614/5/7AAA variants 148
Figure 3.32 Binding between ADAMTS13 and immobilised D1614A mutant 148
Figure 3.33 Binding between wild type and mutant VWF115 fragments and immobilised ADAMTS13 149
Figure 3.34 Recombinant VWFA2 fragment 152
Figure 3.35 Purification of wild type VWFA2 152
Figure 3.36 Wild type VWFA2 proteolysis followed by SDS-PAGE and

Coomassie staining 154
Figure 3.37 Wild type VWFA2 proteolysis followed by HPLC 154
Figure 3.38 Gel electrophoresis following Kpn I and Pvu I digestion 155
Figure 3.39 VWFA2 mutants examined with SDS-PAGE and Coomassie staining 156
Figure 3.40 Proteolysis of wild type and mutant VWFA2 fragments 157
Figure 3.41 VWFA2-ADAMTS13 binding 158
Figure 3.42 Soluble and plate-bound VWFA2 competition 160
Figure 3.43 Competition for ADAMTS13 binding between immobilised and soluble VWFA2 160
Figure 3.44 Competition for ADAMTS13 binding between immobilised VWFA2 and soluble VWF115 or VWFA2 162
Figure 3.45 Competition for ADAMTS13 binding between immobilised VWF115 and soluble VWF115 or VWFA2 163
Figure 3.46 IC50 and K_i values for the inhibition of ADAMTS13 binding to immobilised VWFA2 or VWF115, using soluble VWF115 or VWFA2 as competitors 164
Figure 4.1 Location of 23 charged residues on the surface of A2 domain 169
Figure 4.2 Residues surrounding the cleavage site 171
Figure 4.3 SPR analysis of binding between ADAMTS13 and immobilised wild type VWF115 and YM1605/6AA variant 171
Figure 4.4 Recombinant VWF fragments 172
Figure 4.5 VWF A2 domain cleavage products 175
Figure 4.6 Binding of VWF NCleav to ADAMTS13 175
Figure 5.1 A proposed mechanism for VWF binding to and proteolysis by ADAMTS13 183

LIST OF TABLES

Table 2.1 PCR cycling conditions used to amplify the VWF fragments 69

ABBREVIATIONS

A	absorbance
ADAMTS	A Disintegrin and Metalloprotease with ThromboSpondin motif
ADP	adenosine diphosphate
APC	activated protein C
AU	absorbance unit
B	binding
BCA	bicinchoninic acid
BGH	bovine growth hormone
B_{max}	maximal binding
bp	base pair(s)
BSA	bovine serum albumin
CBA	collagen binding assay
cDNA	complementary deoxyribonucleic acid
CM	carboxymethylated
CMV	cytomegalovirus
CO_2	carbon dioxide
C-terminal	carboxy terminal
CUB	Complement components C1r/C1s, Uegf and Bone morphogenic protein 1
DDAVP	1-deamino-8-D-arginine vasopressin
DIC	disseminated intravascular coagulation
DMSO	dymethyl sulfoxide
DNA	deoxyribonucleic acid
dNTP	deoxynucleoside triphosphate
E. coli	*Escherichia coli*
EDC	1-ethyl-3-93-dimethylaminopropyl carbodiimide
EDTA	ethylenediaminetetraacetic acid
EGF	epidermal growth factor
EK	enterokinase
ELISA	enzyme-linked immunosorbent assay
EMEM	Eagle minimal essential medium
EPCR	endothelial protein C receptor
eq.	equation
F	clotting factor
Fa	activated clotting factor
FBS	fetal bovine serum
FGF-2	fibroblast growth factor-2
FPLC	fast protein liquid chromatography
FRET	fluorescence resonance energy transfer
GAG	glycosaminoglycan
Gp	glycoprotein
HEK	human embryonic kidney fibroblast
HIV	human immunodeficiency virus
HPLC	high pressure liquid chromatography
HRP	horseradish peroxidase
HUS	haemolytic uremic syndrome
IC50	half maximal inhibitory concentration
IFC	integrated microfluidic cartridge
Ig	immunoglobulin

IL-6	interleukin-6
IPTG	isopropyl-β-D-thiogalactoside
k_a	association rate constant
kb	kilobase
k_{cat}	catalytic constant or turnover number
k_{cat}/K_m	catalytic efficiency or specificity constant
k_d	dissociation rate constant
K_D	equilibrium dissociation constant
kDa	kilodaltons
K_i	inhibition constant
K_m	*Michaelis-Menten* constant
lacO	lac operator
Lad	ladder
LB	Luria-Bertani
Log	logarithm
LPR	lipoprotein receptor-related protein
mins	minutes
MMP	matrix metalloproteinase
mRNA	messenger ribonucleic acid
MW	molecular weight
NEAA	non-essential amino acids
NHS	N-hydroxysuccinimide
NR	non-reducing
N-terminal	amino terminal
OD	optical density
OPD	o-phenylenediamine dihydrochloride
ORF	open reading frame
pAb	polyclonal antibody
PAGE	polyacrilamide gel electrophoresis
PAR	protease-activated receptors
PBS	phosphate bufferred saline
PC	protein C
PCR	polymerase chain reaction
PLC	phospholipase C
PVDF	polyvinylidene difluoride
R	reducing
RBS	ribosome binding site
RI	refractive index
R_{max}	analyte binding capacity
RNA	ribonucleic acid
rpm	revolutions per minute
RT-PCR	reverse transcription-polymerase chain reaction
RU	resonance unit
S.E.	standard error
SDS	sodium dodecyl sulphate
SPR	surface plasmon resonance
SVMP	snake venom metalloproteinase
Ta	annealing temperature
TACE	TNF-α converting enzyme
TBE	tris-borate-EDTA
TF	tissue factor
TFA	trifluoroacetic acid

TFPI	tissue factor pathway inhibitor
TM	thrombomodulin
TNF-α	tumor necrosis factor-α
TSP-1	thrombospondin-1
TSR	thrombospondin repeat
TTP	thrombotic thrombocitopenic purpura
U	unit
UL-VWF	ultra large von Willebrand Factor
UV	ultaviolet
V	volt
v/v	volume per unit volume
V_0	initial velocity
VEGF	vascular endothelial growth factor
V_{max}	maximal velocity
VWD	von Willebrand's disease
VWF	von Willebrand factor
w/v	weight per unit volume

1. INTRODUCTION

1.1 HAEMOSTASIS OVERVIEW

Haemostasis is a precisely regulated response to vessel injury, in which the vessel wall, platelets, the coagulation proteins, the anticoagulant system and the fibrinolytic proteins interact with each other to prevent blood loss, while maintaining blood fluidity. The haemostatic response can be schematically divided in four phases: vasoconstriction, primary platelet plug formation, the coagulation cascade and fibrinolysis. Vasoconstriction of the vessel wall is the first anti-haemorrhagic mechanism to occur. It is a reflex which limits the blood flow to the site of vessel damage. Subsequently, the formation of a primary platelet plug limits bleeding and provides a surface for clotting factors to assemble and become activated. The initial platelet plug is unstable, since platelets can detach from the exposed sub-endothelial surface. Fibrin, generated from the coagulation cascade, forms an insoluble scaffold which stabilises the primary platelet plug. The final step in the haemostatic response involves removal of fibrin by the fibrinolytic enzyme system. This thesis is primarily related to the plasma glycoprotein VWF, which is involved in the tethering of platelets to the damaged endothelium, one of the initial events in platelet plug formation.

1.1.1 Platelet plug formation

Platelets are disc-shaped cell fragments derived from megakaryocytes largely confined within the bone marrow. Platelets circulate in blood in a resting state. When damage to the endothelial cell layer occurs, they undergo a series of reactions (initial tethering and stable adhesion, activation and aggregation) which ultimately lead to the formation of the primary platelet plug (Fig. 1.1).

1.1.1.1 Platelet tethering and stable adhesion

The initial platelet interaction with the exposed extracellular matrix is mainly mediated by their binding to collagen. Under conditions of high shear stress such as are present in arterioles and capillaries (see Section 1.2.7), platelets do not to interact directly with collagen because the strength of this binding is not enough to resist the haemodynamic forces of the flowing blood. In these conditions, VWF is essential to initiate platelet adhesion (see Section 1.2.7). Following its interaction with the exposed collagen (see Section 1.2.8.2.1), VWF becomes able to bind to the platelet surface receptor

glycoprotein GpIbα [1] (see Section 1.2.8.2.2), part of the GpIb-IX-V complex and a member of the leucine-rich repeat protein family [2] (Fig. 1.1 A). The association rate between VWF and GpIbα is very fast and they can interact with each other even when the velocity of flowing platelets near the vessel wall is elevated [3]. However, the VWF-GpIbα interaction is also characterised by a fast dissociation rate and consequently it does not provide irreversible platelet adhesion [3]. Studies using a parallel-plate flow chamber have reported that platelets tethered to the vessel wall move constantly in the direction of flow ("rolling"), continuously establishing new interactions with the adjacent thrombogenic surface [3]. During this slow translocation, the continuous contact between platelets and VWF induces an activation process (see Section 1.1.1.2) and another platelet surface receptor (GpIIb-IIIa) then becomes available [1]. This receptor is also able to interact with VWF (see Section 1.2.8.2.2). However, in contrast to the VWF-GpIbα interaction, this consists of tight binding, which arrests the rolling of platelets and stabilises their adhesion to the damage sub-endothelium [1,3].

Another platelet surface receptor taking part in the tethering process has been recently identified, GpVI. It is a glycoprotein of the immunoglobulin superfamily which binds directly to collagen on the exposed sub-endothelium [4,5]. A critical role for this glycoprotein has been suggested, since its interaction with collagen stimulates both platelet adhesion and activation [6]. It is also responsible for the activation of surface integrins, such as GpIa-IIa (also known as Integrin $\alpha_2\beta_1$), which also binds to collagen favouring platelet adhesion [7,8]. The direct binding of platelets to collagen (both via GpVI and GpIaIIa) represents the preferential anchoring mechanism in conditions of low shear stress (such as in the venous circulation), but it also supports tethering in high shear stress conditions complementing that caused by GpIbα-VWF binding.

1.1.1.2 Platelet activation

Once platelets are immobilised to sites of vascular injury, they are activated by a range of agonists released or generated locally (such as collagen and thrombin), which bind different G protein coupled receptors on the platelet surface [9] (Fig. 1.1 B). Both VWF binding to GpIbα and collagen interaction with GpVI and GpIa-IIa generate intracellular signals, which activate specific intracellular protein kinases, leading to platelet activation [10-13]. Furthermore, thrombin generated by the coagulation cascade (see Section 1.1.2) is also a potent activator, cleaving protein G-coupled protease-activated receptors (PAR) on the platelet surface and generating intracellular signals

which activate phospholipase C (PLC) β [9,14-16]. Epinephrine binding to α-adrenergic receptor potentiates platelet activation caused by other agonists [17,18].

Platelet activation results in cytoskeleton changes associated with changes in platelet shape. Platelets are transformed from a discoid into a spherical shape and extrude extensive pseudopodia that help anchoring. The platelet membrane is also subjected to a general rearrangement, leading to the exposure of negatively charged phospholipids (phospatidylserine and phosphatidylinositol), which create a surface for optimal binding of coagulation factors [19-22] (see Section 1.1.2).

Platelet activation also causes the secretion of VWF, fibrinogen, fibronectin, thrombospondin-1 (TSP-1), vitronectin and some coagulation factors from platelet α-granules and of ADP and thromboxane A_2 from platelet dense granules [23] (Fig.1.1 B). Fibronectin, TSP-1 and vitronectin are adhesive proteins which also take part in platelet adhesion and aggregation [24-34].

ADP and thromboxane A_2 are also potent activators of platelets. ADP binds to the G-coupled P2Y1 and P2Y12 receptors and signalling through both these pathways amplifies platelet responses induced by other agonists [18,23,35-37]. Thromboxane A_2 binds to the TPα and TPβ receptors, both activating G_q and G_{12-13} signaling, inducing platelet shape change, secretion from dense granules and platelet aggregation [38-41].

During platelet activation, two new receptors become presented on the platelet surface: GpIIb-IIIa [23,42] and P-selectin [43]. GpIIb-IIIa binds to VWF and fibrinogen [44,45], both stabilising the initial VWF-GpIbα contact (see Section 1.1.1.1) and mediating platelet aggregation (see Section 1.1.1.3). P-Selectin binding to GpIbα also induces platelet aggregation (see Section 1.1.1.3).

1.1.1.3 Platelet aggregation

Aggregation consists in the recruitment of platelets to sites of vascular injury to which platelets have already adhered. Aggregation is mediated by VWF and fibrinogen, interacting with GpIbα and GpIIb-IIIa (the former) and with GpIIb-IIIa (the latter) (Fig. 1.1 C). At high fluid shear rates, fibrinogen alone cannot support the formation of stable platelet aggregates. Therefore, the role of VWF becomes critical, with its multimeric conformation conferring resistance to rheological forces of the circulating blood [46,47]. P-selectin exposed on the surface of activated platelets seems also to play a role in the aggregation process, establishing interactions with GpIbα [48] (Fig. 1.1 C).

1.1.2 Coagulation cascade and final clot formation

As stated above, the primary platelet plug is temporary and unstable. Its formation is spatially and temporally coordinated with the activation of the blood coagulation system (Fig.1.1 D). This consists in a series of proteolytic reactions, finally leading to the generation of fibrin which stabilise the platelet plug. In each proteolytic reaction, a clotting factor precursor (denoted as F) is transformed in its active form (Fa), which in turn acts as a serine protease in the subsequent step. Activation of the coagulation cascade takes place on the negatively charged surface provided by the reorganisation of the platelet membrane during the activation process. Upon vessel injury, sub-endothelial tissue factor (TF) is exposed [49,50] and it binds circulating FVII/VIIa, initiating the so called extrinsic pathway. The TF/FVIIa complex activates FX to FXa, which by itself can catalyse the conversion of small amounts of prothrombin to thrombin. The trace amounts of thrombin generated via the extrinsic pathway can activate platelets and cause the exposure of negatively charged phospholipids [51]. Amplification of thrombin generation is achieved by a positive feedback mechanism, in which the initial amount of generated thrombin activates FVIII to FVIIIa and FV to FVa [52]. FXa activity is markedly enhanced in the presence FVa, calcium and phospholipid membrane (prothrombinase complex) [53]. The TF/FVIIa complex can also activate FIX, a component of the intrinsic pathway. FIXa forms a complex with FVIIIa and FX, in the presence of calcium, on the surface of activated platelets (tenase complex) and it leads to the generation of FXa, which proteolytically converts prothrombin to thrombin. Once thrombin is generated, it converts fibrinogen into fibrin. The fibrin fibrils are cross-linked by FXIIIa and they form a scaffold to stabilise the platelet plug [54] (Fig. 1.1 D).

In order to localise coagulation to the site of injury, several anticoagulant mechanisms exist that regulate the coagulation cascade. First, tissue factor pathway inhibitor (TFPI), a member of the Kunitz family of inhibitors, can bind to TF-FVIIa and FXa to form a quaternary complex that inhibits both FVIIa and FXa [55]. Second, antithrombin, a member of the serpin family, inhibits thrombin, FXa, FXIa and FIXa [56]. Third, the protein C (PC) pathway down-regulates the clotting cascade by inactivating FVIIIa and FVa, cofactors required for the tenase and prothrombinase complexes respectively [57-59].

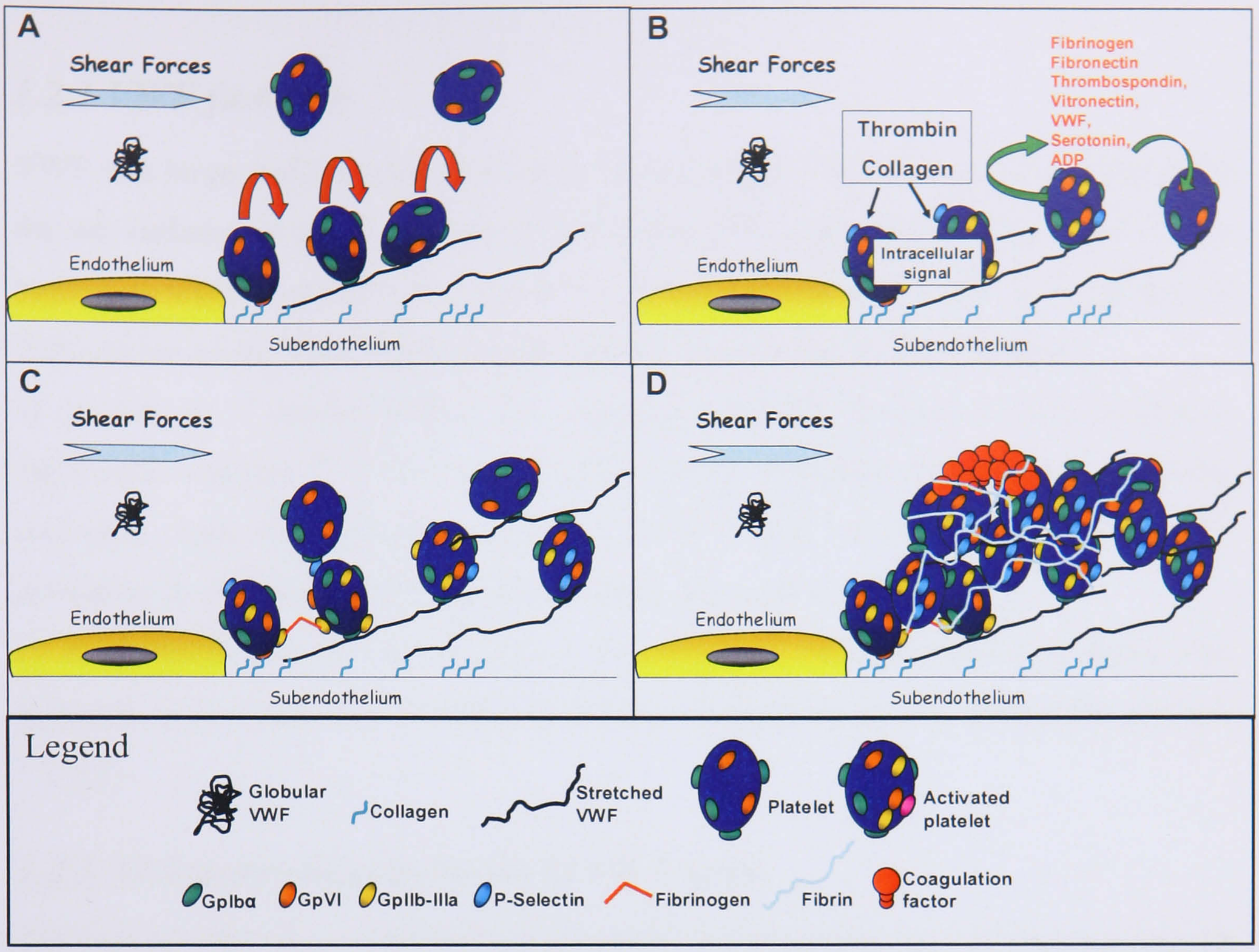


Fig. 1.1 Clot formation. (A) Platelet tethering. At sites of vascular injury, sub-endothelial proteins (such as collagen) are exposed. VWF anchors to collagen and unfolds by shear stress. Consequently, the binding site for platelet receptor GpIbα on VWF becomes exposed. However, VWF-GpIbα interaction is not stable (due to a fast dissociation rate) and platelets tethered to the vessel wall keep moving constantly ("rolling") in the direction of flow (see red arrows). Another platelet receptor (GpVI) takes part in the initial platelet tethering to the surface of the vessel damage, interacting directly with the exposed collagen. **(B) Platelet activation and stable adhesion.** During the "rolling" process, platelets are activated by binding of collagen and thrombin (generated from the coagulation cascade) to specific platelet surface receptors. Upon activation, platelets change their shape and rearrange their membrane (not shown). They secrete the content of their granules (green arrow): some of the secreted substances are agonists, which in turn activate other platelets. They also express the surface receptors GpIIb-IIIa which promote a stable platelet adhesion to the immobilised VWF. They also exposed on their surface P-selectin. **C) Platelet aggregation.** During aggregation, new platelets are recruited from the circulation and cluster at the site of vascular injury. The binding between platelets is mainly mediated by VWF and fibrinogen, which bind to GpIbα and GpIIIaIIb (the former) and to GpIIbIIIa (the latter). P-Selectin also plays a role in this step, binding to GpIbα. **D) Stabilisation of the platelet plug.** The coagulation cascade is activated on the surface of platelet phospholipids, leading to thrombin generation and fibrin deposition, which stabilises the platelets plug.

1.2 VWF

1.2.1 VWF function

VWF is a large and complex multimeric glycoprotein, which is present in plasma, in the sub-endothelial matrix, in platelet α-granules and in endothelial cell Weibel-Palade bodies. A VWF monomer has a molecular weight of 250 kDa and it is comprised of 2050 amino acids. VWF has two important functions in normal haemostasis:

1) It acts as a carrier protein for coagulation FVIII, forming a non-covalently associated complex [60]. FVIII complexed to VWF is protected from degradation by proteases, such as activated protein C (APC) [61], and its clearance is reduced [62], extending its otherwise short half-life in blood (see Section 1.2.8.1).

2) It supports platelet attachment to thrombogenic sub-endothelial surfaces and augments platelet-platelet interactions at sites of vessel injury (see above and Section 1.2.8.2).

1.2.2 Structure and expression of VWF gene

The human VWF gene (*VWF*) is located at the tip of the short arm of chromosome 12 (region 12p13.2) and spans approximately 180 kb [63]. It contains 52 exons: exon 1 represents 5'-untranslated sequence [64]; exons 2-18 encode the signal peptide and the propeptide; the remaining exons encode the domains of the mature VWF subunit [63] (see Section 1.2.3). A *VWF* pseudogene is located on human chromosome 22 (region 22q11.2). It spans approximately 29 kb and it represents a duplication of the region spanning exons 23 through 34 of the *VWF*, which encodes domains A1-A2-A3. The *VWF* pseudogene and gene sequences are 97% identical, suggesting a relatively recent creation of the pseudogene [65,66]. The pseudogene does not encode a protein that exerts VWF function. Expression of *VWF* is restricted to endothelial cells and megakaryocytes. The *VWF* promoter includes a core region of 90 nucleotides upstream of the transcription initiation site, two positive regulatory regions (one located 200 nucleotides upstream of the transcription initiation site, and the second within exon 1), and two negative regulatory regions upstream of the positively acting sequences. The positive regulatory regions contain potential GATA and Sp1 binding sites. GATA and Sp1 are transcription factors, which have been implicated in the regulation of expression of various genes in haematopoietic cells [67-69] and in endothelial cells [70-72]. The negative regulatory sites contain NF1-like protein binding sites that are involved in suppressing transcription in non-endothelial/megakaryocytic

cells [73-77]. To date, little is known about the mechanisms that regulate VWF expression *in vivo*. Immunohistochemical studies, quantitative RT-PCR and transgenic mice showed that VWF gene expression is heterogeneous in the porcine [78-80], canine [81] and murine [74,82,83] vascular systems. High levels of VWF expression are present in lung, spleen, aorta and brain. Low levels are reported in liver, skeletal muscle and kidney. Furthermore, VWF is expressed at higher levels in venous than in arterial endothelial cells. Taken together, all these studies suggest the presence of a specific transcriptional control of *VWF* gene in endothelial cells of different organs. The significance of this endothelial cell heterogeneity and the specific transcriptional network involved are still to be fully elucidated. It has been shown [83] that administration of lipopolysaccharide or tumor necrosis factor-α (TNF- α) in mice increased plasma VWF levels but they had variable effect on VWF mRNA levels. The expression of the murine VWF gene was down-regulated in some tissue and up-regulated in others. Increased VWF mRNA levels have been detected in human colon carcinoma samples by quantitative RT-PCR [84]. In the same study, it was shown that vascular endothelial growth factor (VEGF) and fibroblast growth factor-2 (FGF-2) (potent angiogenesis inducers over-expressed in a variety of tumors) up-regulated both VWF mRNA and protein levels in cultured endothelial cells.

1.2.3 Structure of VWF

Mature VWF multimers are composed of a variable number of VWF subunits, each containing discrete functional sites that mediate interactions with other molecules. A diagram of the domain structure of each VWF monomer is shown below (Fig. 1.2).

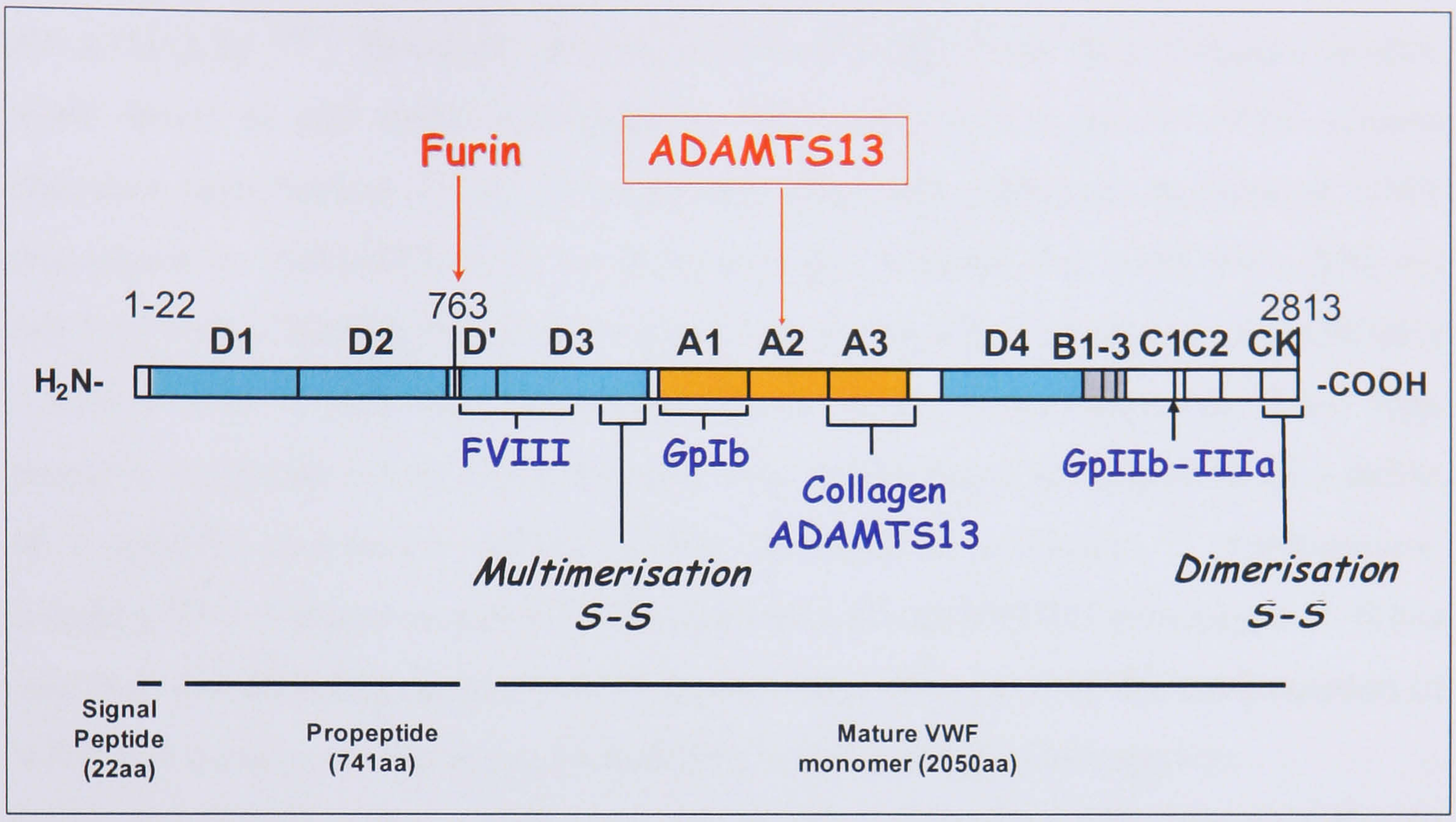


Fig. 1.2 Domain structure of VWF. The diagram shows VWF domain structure, highlighting the position of the repeated domains (five D domains, three A domains, three B domains, two C domains). Major ligand binding sites and regions involved in dimerisation and multimerisation are highlighted below the diagram. Furin and ADAMTS13 cleavage sites are indicated by red arrows. The three black lines beneath the diagram indicate the extension of the signal peptide, the propeptide and the mature VWF, respectively. Amino acid numbering is given above, starting from the first amino acid of the signal peptide.

The mature protein is remarkably rich in cysteines (169 cysteine residues out of 2050 residues). Cysteine is abundant in all the domains except the three A domains, which together contain only six cysteines. Two regions of the mature subunit are involved in intermolecular disulphide bonds formation: one in the N-terminal portion of the molecule (residues 1046-1242) and the other in the C-terminal portion (residues 2671-2813) (amino acid numbering from the start of the signal peptide). In the secreted protein, there are no detectable free sulphydryl groups, suggesting that all cysteine residues not forming intermolecular disulphide bridges are paired in intramolecular disulphide bonds [85-87].

The mature subunit is extensively glycosylated (see Section 1.2.4): it contains 22 carbohydrate side chains, 10 of which are *O*-linked to serine or threonine residues and 12 *N*-linked to asparagine residues. The estimated carbohydrate content of VWF varies between 10% and 19% of the total mass of the mature subunit. The *N*-linked oligosaccharides contain ABO blood group oligosaccharides [88,89]. It has been shown that ABO blood group antigens are a determinant of plasma VWF levels (O<A<B<AB) [90,91]. However, the mechanism through which they influence plasma VWF levels is still under investigation. They may play a role in VWF plasma clearance (see Section 1.2.5). Alternatively, they may influence the rate of VWF proteolysis by ADAMTS13. It has been recently reported that VWF with different ABO groups exhibited different susceptibility to specific cleavage by ADAMTS13 (O>B>A>AB) [92]. Another study found plasma VWF levels similar or lower than group O in a group of individual with the very rare Bombay phenotype (with a defect of a specific enzymes involved in the carbohydrate synthesis) [93]. Furthermore, Bombay VWF showed an increased susceptibility to ADAMTS13 proteolysis [93]. It has been hypothesised that the presence of glycan structures may alter the conformation of VWF and thereby modulate the accessibility to ADAMTS13 cleavage site.

Each VWF monomer has a multi-domain structure, consisting of four types of distinct repeated domains [86] (Fig. 1.2). There are five D domains, three A domains, three B domains, two C domains. Each of the four D domains (D1-D2-D'-D3) located in the N-terminal part of pro-VWF is approximately 360 residues in length and contains between 32 and 36 cysteine residues. The D domains have significant sequence homology and the position of most cysteine residues is conserved, suggesting that their tertiary structure may be similar. They are involved in the multimerisation process (see Section 1.2.6): D1 and D2 represent the propeptide, and D3 contains cysteine residues involved in the formation of intermolecular disulphide bonds between VWF monomers [86,87,94,95]. Moreover the D' and D3 domains bind to FVIII [96] (see Section 1.2.8.1) and to heparin [97] (see Section 1.2.8.2.1).

The three homologous A domains span residues 1260 to 1874 (Fig. 1.3). The A1 domain contains an intramolecular disulphide bond between C1272 and C1458 that forms a loop of 187 residues. The A3 domain also contains an intramolecular disulphide bond, C1686-C1872, which generates a loop of identical length. The A2 domain primary sequence is similar to A1 and A3, but it lacks the conserved cysteine residues. A domains are present in a wide variety of proteins, including components of extracellular matrix (non fibrillar collagen and cartilage matrix protein), proteins

involved in cellular adhesion (integrins, leukocyte adhesion receptors. collagen receptors) and defence mechanisms (complement components). In all these molecules, it has been shown that A domains play an important role in establishing specific interactions with macromolecular ligands [98]. In VWF, the A1 domain contains the interaction site for platelet GpIbα, promoting tethering of circulating platelets [99-102] (see Sections 1.1.1.1 and 1.2.8.2.2). A heparin binding site [97,101], a minor binding site for collagen type I [101,103] and a binding site for collagen type VI [104,105] are also located in the A1 domain.

The A2 domain contains the site of cleavage by ADAMTS13 occurring between Y1605 and M1606 of VWF [106] (see Section 1.3.5).

The A3 domain mediates the binding between VWF and collagen types I and III. present in the perivascular connective tissue, and collagen type VI of the sub-endothelial matrix [105]. It has been shown recently that the A3 domain also may contain a high affinity binding site for ADAMTS13 [107].

The C domains of VWF have sequence similarity to corresponding domains in TSP-1 and alpha-procollagen types I and III. The C1 domain contains an Arg-Gly-Asp (RGD) sequence, which is a typical recognition site for adhesion receptor of the integrin superfamily. It has been shown that the C domains bind to the platelet GpIIb/IIIa receptor, present on the surface of activated platelets [108] (see Sections 1.1.1.1 and 1.2.8.2.2). The CK domain contains the cysteines involved in the dimerisation process (see Section 1.2.4).

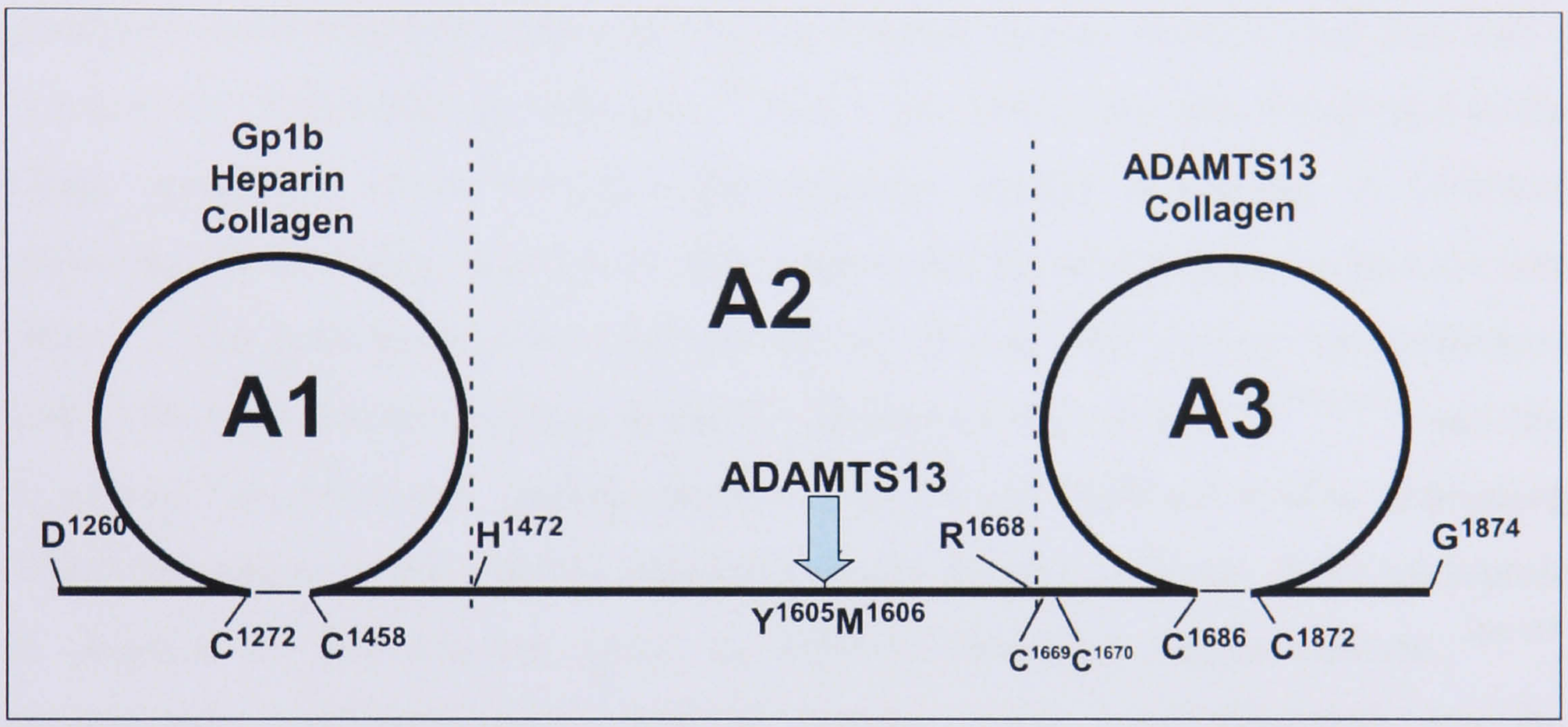


Fig. 1.3 VWF A domains. Diagram of the VWF A1A2A3 domains is shown. Both A1 and A3 domains contain an intramolecular disulphide bond between cysteine residues, leading to the formation of a loop of 187 amino acids. Major ligands for each domain are highlighted above. The ADAMTS13 cleavage site (Y1605-M1606) is located in the middle of A2 domain, see blue arrow.

1.2.4 VWF synthesis, storage and secretion

VWF is synthesised by endothelial cells and megakaryocytes as a prepropolypeptide of 2813 amino acids. This includes a 22 amino acid signal peptide, a 741 amino acid propeptide and the mature protein consisting of 2050 amino acids. The prepro-VWF undergoes a maturation process in the rough endoplasmic reticulum and in the Golgi complex (Fig.1.4). In the rough endoplasmic reticulum, following the removal of the signal peptide, initial *N*-linked glycosylation and dimerisation take place (Fig. 1.4 a and b) [86,108-110]. It has been shown that inhibition of *N*-linked glycosylation blocks the dimerisation process [111]. The dimerisation of the pro-VWF subunits is achieved by disulphide bond formation between cysteine residues located in the C domains, and it is known as "tail-to-tail" dimerisation [85]. The VWF dimers are then transported to the Golgi apparatus, where *O*-linked glycosylation, further processing of N-linked glycosylation (including addition of ABO sugars) and the multimerisation process take place [85]. The propeptide drives the association of pro-VWF dimers into multimers linked through cysteine residues in the D3 domain of each subunit [87,94,112,113] and this is termed "head-to-head" multimerisation (Fig. 1.4 c). Different studies expressing VWF truncations in mammalian cells have shown that the presence of the propeptide is required in this process, since its deletion abolished multimerisation [114-117]. Interestingly, multimerisation could be restored when free propeptide was co-expressed in the same cells [118]. It has been suggested that the propeptide acts as a thiol-disulphide oxidoreductase and that the vicinal cysteines in the D1 (C159 and C162) and D2 (C521 and C524) domains promote VWF interdimer disulphide bond formation [115]. After multimerisation, the propeptide is cleaved by furin, a calcium-dependent serine protease (Fig. 1.4 d). Propeptide cleavage is not necessary for multimerisation, since the mutation R763G, which inhibits the cleavage, results in multimers composed of pro-VWF subunits [119]. After cleavage, the propeptide still remains non-covalently bound to VWF multimers, since this association is promoted by the acidic pH and high calcium concentration of the Golgi [120].

After maturation, VWF can follow a constitutive pathway of secretion, the rate of secretion being directly linked to that of VWF synthesis. The majority of VWF (95%) follows this pathway and polymers of varying size are released as soon as their synthesis is completed. They are secreted both into circulating blood and into the sub-endothelial matrix. The remaining 5% of newly synthesised VWF (predominantly the longest multimers) is stored in subcellular organelles called Weibel-Palade bodies in

endothelial cells [121] or in α-granules within platelets [122]. It has been shown that VWF targeting to storage granules requires the propeptide region. Its deletion causes constitutive secretion of VWF [123-126]. The stored VWF can be released after specific stimulation, for example by thrombin or histamine or vasopressin and its analogue 1-deamino-8-D-arginine vasopressin (DDAVP). Each agonist interacts with a particular extracellular receptor on the surface of platelets or endothelial cells, generating a specific intracellular signal which ultimately leads to the secretion of the contents of α-granules and/or Weibel-Palade bodies [9,14-18,127-130]. After secretion, the propeptide dissociates from VWF multimers and circulates in plasma as a non-covalent homodimer (vWAgII) [131,132]. VWF multimers (see Section 1.2.6) are present in plasma at a concentration of ~5-10 μg/ml and with a half life of ~12 hours [132,133].

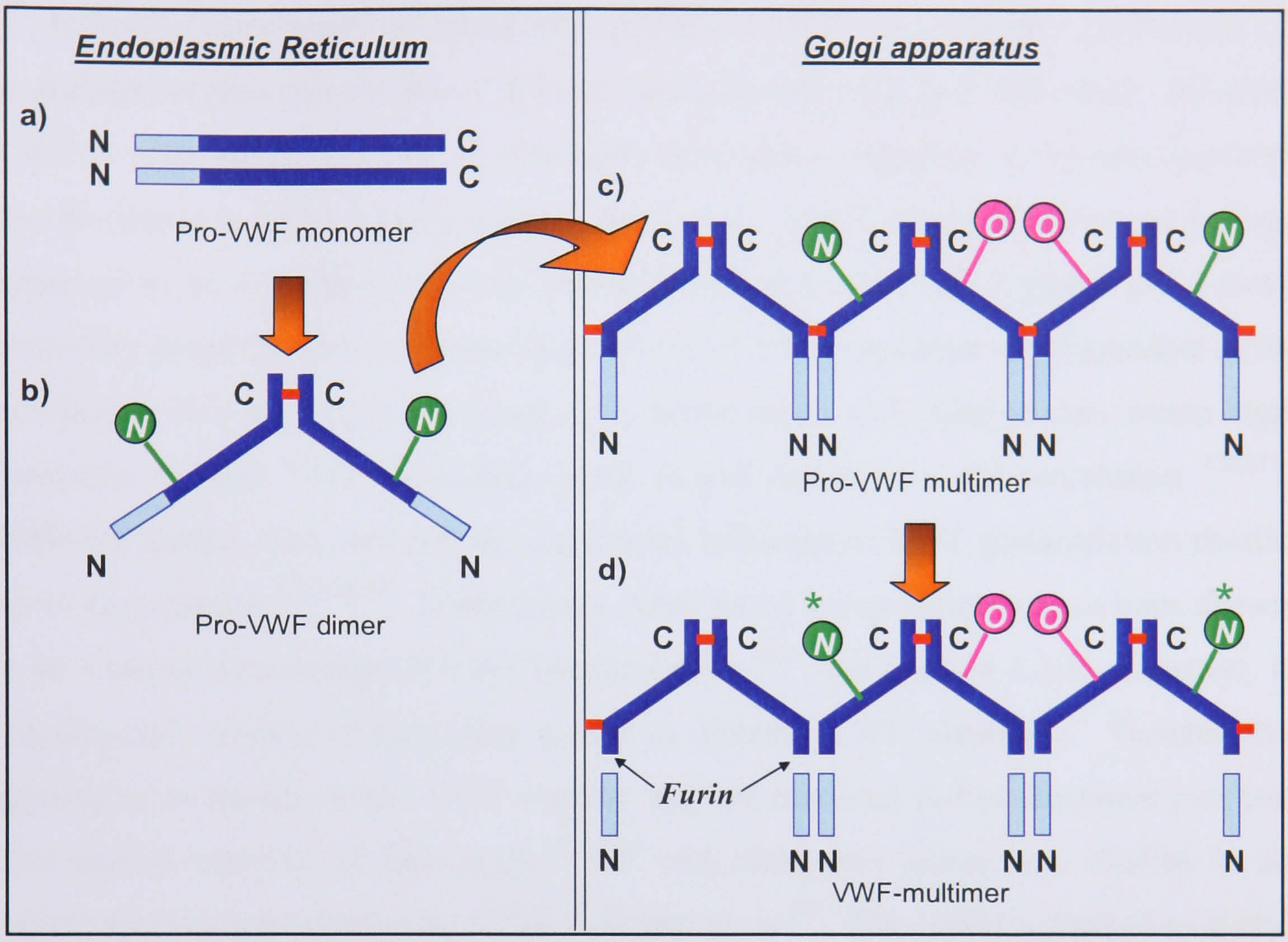


Fig. 1.4 Maturation process of pro-VWF. In the endoplasmic reticulum the dimerisation between two pro-VWF monomers (a) takes place, by the formation of a disulphide bond in the C-terminal region (highlighted with a red line) (b). *N*-linked glycosylation (shown as green spheres) also starts in the endoplasmic reticulum. Pro-VWF dimers then traslocate to the Golgi apparatus, where the propeptide contributes to the initiation of the multimerisation process. After dimers have been linked through disulphide bonds in the N-terminal region (c), the propeptide is removed by furin cleavage (d). In the Golgi, *N*-linked glycosylation is completed and ABO groups are added (*). *O*-linked glycosylation (shown as pink spheres) also takes place at this stage (Adapted from [134]).

1.2.5 VWF plasma clearance

VWF biosynthesis, post-translational modifications and secretion have been widely studied in the last two decades (see Section 1.2.4).Little is known. however. regarding its plasma clearance. VWF biodistribution was studied in a VWF-deficient mice model [135], following intravenous injection of radiolabeled VWF. The analysis of radioactivity in different organs showed that VWF was predominantly targeted to the liver. Whether VWF is taken-up in the liver in a receptor-mediated mechanism or by extravasation into the tissue is still not known. In the same study, VWF disappearance from plasma appeared to be a biphasic process, characterised by a rapid initial phase and a slow secondary phase. It was also found that the rate of VWF clearance is independent of its multimeric size. However, this result is in contradiction with other studies where high molecular weight VWF multimers were cleared faster from the circulation [136,137]. Different studies have reported the significant influence of VWF glycosylation profile upon its clearance [136,138,139]. Furthermore, ABO blood group antigens have been shown to be a major determinant of VWF plasma levels [90,91] (see Section 1.2.3). However, it remains still unclear if they play a role in altering VWF clearance. Besides the glycosylation profile, some VWF regions may be involved in the clearance process. The plasma survival of full-length VWF and some truncations was studied in an experimental model employing VWF-deficient mice [135]. The results indicated a central role for A1-A2-A3 region in promoting VWF clearance, making it the major candidate to contain a receptor-recognition site. The region D4-CK showed a regulatory function, by enhancing A1-A2-A3-mediated clearance. Conversely, D'-D3 region seemed to play a negative regulatory role, by reducing the rate of clearance. Furthermore, the effect of some mutations (C1130F, C1149R, C2671Y, R1205H, S2179F) leading to VWF deficiency (see Section 1.2.9) have been studied both in patients and VWF-deficient animal models and they have been associated with increased rate of VWF clearance [135,140,141]. Residues C1130, C1149 and R1205 are located in the D3 domain, C2671 in the region between C2 and CK domains and S2179 in the D4 domain.

1.2.6 Plasma VWF multimers

A wide range of VWF multimers (ranging from 500 kDa to 20 000 kDa), which differ only in the number of constituent VWF monomers, is found in normal plasma [142-144]. The multimeric pattern can be visualised by agarose gel electrophoresis in non-

denaturing conditions, followed by Western blotting [142-144] (Fig 1.5). Purified VWF visualised by electron microscopy appears either as filamentous structure (diameter 2-3 nm, length of up to 1300 nm) or as coiled compact molecules [145,146]. The properties of circulating VWF are, in part, dependent upon its molecular size and its conformation. The largest VWF multimers termed ultra large VWF (UL-VWF) contain multiple sites of interaction with platelets and vessel wall components, thus having enhanced thrombogenic potential [147]. Moreover, they can more readily undergo more marked conformational changes in response to the rheological forces exerted by the circulating blood [148] (see Section 1.2.7). Under normal flowing conditions, VWF multimers circulate in a "globular" form. However, when VWF is exposed to increased shear forces these molecules respond by unravelling into a "string-like" conformation [149]. This increases the number of exposed platelet/matrix binding sites and thus enhances the platelet aggregating potential of the VWF molecule. Smaller multimeric forms do not respond to shear forces to the same extent as UL-VWF.

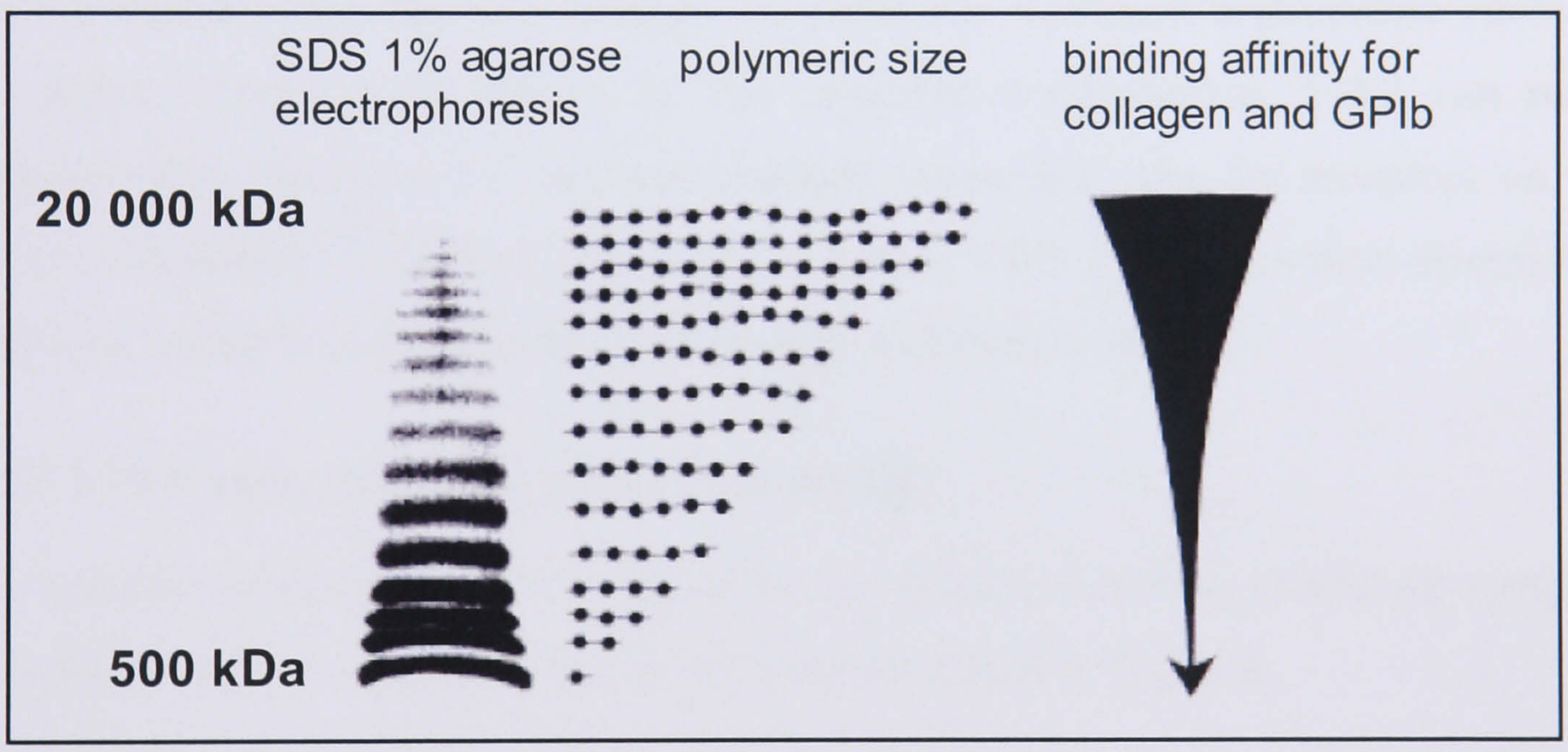


Fig. 1.5 Plasma VWF multimers. Sodium dodecyl sulphate (SDS)-1% agarose gel electrophoresis in non reducing condition of normal plasma VWF, followed by Western blotting using a peroxidase-labeled reabbit IgG against human VWF (*left panel*). The polymeric size of each band is shown in the *middle panel*. The bottom band correspond to the size of a dimer (MW~500 kDa). Each multimer differs from the adjacent one by one dimeric unit. The arrow in the *right panel* indicates the decrease in the binding affinity for collagen and GpIbα in the smaller VWF multimers. (Picture taken from [150])

1.2.7 Influence of fluid shear stress upon VWF function

To perform their haemostatic function, platelets have to bind irreversibly at site of vascular injury, opposing the blood flow adjacent to the luminal surface. As blood flows through a vessel, velocity is maximal in the centre and falls to zero near the

wall. The blood can thus be imagined as being divided in a series of adjacent layers (laminae) moving at a different velocity one to another. The shear rate (expressed in s^{-1}) is the rate of change of velocity with respect to distance measured perpendicularly to the direction of flow. Inversely from the velocity, shear rate is greater near the vessel wall and zero at the center. Shear stress (expressed in Pa or N/m^2) is the tangential force per unit area of contact between the laminae. The relationship between shear stress and shear rate is linear and the proportionality constant is the viscosity of the fluid. This means that shear stress is directly proportional to shear rate and fluid viscosity [95]. In small arterioles and arterial capillaries shear rate vary between 470 and 4700 s^{-1} [151]. In arteries partially occluded by atherosclerotic plaques, shear rate can exceed 5000 s^{-1}[152,153]. In veins and normal arteries shear rate is much lower (~100 s^{-1}) and thus circulating platelets can directly interact with the exposed collagen at sites of vascular injury (see Section 1.1.1.1) and VWF function become less relevant. VWF function is crucial to establish platelet-surface contact at shear rate above 500-1000 s^{-1}, when platelets alone cannot directly attach to the sub-endothelial components. Once VWF is bound to the exposed collagen, its particular molecular architecture allows it to "unravel" under shear forces. In this stretched conformation, VWF can resist haemodynamic forces and it exposes multiple interaction sites for receptors on the platelet membrane [149]. In arterioles and capillaries, VWF function is thus essential in creating a bridge between platelets and the sub-endothelial surface.

1.2.8 VWF structure-function relationship

The multiple functions of VWF depend on its distinct domains, mediating complex interactions with other proteins involved in the haemostatic response.

1.2.8.1 Stabilisation of blood coagulation FVIII

An important VWF function is to protect FVIII from plasma clearance and degradation by APC, increasing its stability and half-life and contributing, indirectly, to its function in the generation of fibrin. FVIII circulates in plasma bound to VWF, in a high affinity non-covalently associated complex (99% VWF and 1% FVIII). Factor VIII binds to VWF with a K_D of 200 to 400 pM [60]. All sizes of VWF multimers bind FVIII with similar affinity [154]. The region of VWF which interacts with FVIII is located within the N-terminal part of the mature subunit, in the D' and D3 domains (residues 763-1035, amino acid numbering from the start of the signal peptide), with a possible crucial role for residues 841 to 859 [96,155,156]. The N-terminal region of VWF

contains an intra-chain disulphide bond, which seems to be essential for FVIII binding [157]. The complementary VWF binding sites on FVIII is located near the amino-terminus of the 80 kDa light chain [158-160] and in the carboxy-terminal region of the C2 domain [158,161]. Inhibition studies [61,162] showed that binding sites for APC and VWF on FVIII are overlapping. VWF therefore protects FVIII from APC catalysis by direct inhibition of APC binding. It has also been shown that VWF binding to FVIII reduced the rate of its clearance by decreasing the efficiency of FVIII internalisation and degradation by the liver lipoprotein receptor-related protein (LPR) [62]. During blood coagulation, FVIII is activated by thrombin cleavage after R372, R740 and R1689, causing the release of FVIII B domains [163]. This cleavage disrupts VWF binding site, releasing FVIIIa, which can take part in the coagulation cascade [164-166]. The importance of VWF function in contributing in FVIII stability is highlighted by the fact that severe deficiencies in VWF or a specific defect in the interaction of VWF with FVIII (see Section 1.2.9) both cause a secondary deficiency of FVIII. Thus, these patients may have symptoms characteristic of haemophilia, such as bleeding into joints or soft tissue.

1.2.8.2 Platelet adhesion to connective tissue

Under normal physiological conditions, platelets and VWF circulate in plasma without interacting with each other and with the endothelial surface. In the presence of a vascular lesion, the sub-endothelial components are exposed and platelets attach to them directly or via VWF, in order to form the platelet plug to prevent blood loss (see Section 1.1.1.1). The multimeric molecular architecture of VWF is well suited to resist large haemodynamic forces, such that present in the arterioles and capillaries, which might oppose platelet adhesion (see Section 1.2.7). Once it tethers to exposed collagen, VWF "unravel" under blood flowing and offers an array of interactions sites for platelet membrane glycoprotein GpIbα.

1.2.8.2.1 VWF binding to collagen and other extracellular matrix components

Collagen is the main component of extracellular matrix capable of binding VWF (see also Sections 1.1.1.1 and 1.2.3). Different types of collagen may interact with VWF and their respective roles may vary, depending on the degree of the vascular endothelium damage. The main collagen types involved in VWF anchoring to perivascular connective tissue are types I and types III [167-170]. Collagen type VI, present in the sub-endothelial matrix, also seems to play a role in mediating VWF localisation on the site of lesion [171]. The crystal structures of the VWF A1 [102] and A3

[172] domains, alanine-scanning mutagenesis studies [173,174] and the use of proteolytic [103] or recombinant [105,175] VWF fragments have been carried out to exactly localise the collagen-binding sites in VWF. These studies suggest the major collagen-binding site is within A3 domain, which can interact both with collagen type I, type III and type VI. Residues located at the bottom of one of the side faces of A3 domain (residues 1725-1729, 1744-1760, 1022-1026) [103,173,175] have been identified to be necessary for the binding to both type I and type III collagen. A minor collagen type I binding site (residues 1212-1491, particularly the 1275-1436 region) [101,103] and a collagen type VI binding site (residues 1260-1479) [104,105] have both been identified in the A1 domain. However, other structural matrix components, such as glycosaminoglycans (GAGs), may be involved in the immobilisation of VWF to the sub-endothelial surface. The A1 domain contains a heparin binding site which may interact with matrix heparin-like GAGs [101,102]. A second (lower affinity) heparin-binding site is located in the D' and D3 domains, in the same region that interacts with FVIII [97].

1.2.8.2.2 VWF binding to platelet GpIbα and GpIIb-IIIa receptors

Plasma VWF does not bind tightly to circulating platelets, because of its folded complex tertiary structure conformation. Only when VWF is anchored to sub-endothelium and thus exposed to elevated shear stress condition (see Section 1.2.7), it can assume a "stretched" conformation and thus reveal the multiple binding sites for GpIbα [99-102,149] (see also Sections 1.1.1.1 and 1.2.3). This particular VWF conformation suitable for platelet interaction can also be induced by certain soluble modulators (the antibiotic ristocetin and the snake borocetin) [176,177] or by specific mutations (see Section 1.2.9). The GpIbα binding site on VWF has been mapped to domain A1 [102]. Alanine scanning mutagenesis studies [101] and A1 domain crystal structure [102] have lead to the identification of a large number of charged residues in discontinuous sequence location, which contribute to this binding. As previously described (see Section 1.1.1.1), GpIbα mediate the initial contact between VWF and platelets, causing platelet "rolling". Upon platelet activation, another receptor (GpIIb-IIIa) becomes available and it can interact with the Arg-Gly-Asp motif in the C1 domain of VWF, stabilising platelet adhesion (see Section 1.1.1.1).

1.2.9 Pathogenesis and classification of von Willebrand's disease (VWD)

The importance of the role of VWF is highlighted by its deficiency states. Von Willebrand's disease (VWD) is the most common human congenital bleeding disorder.

with a prevalence of 100 per million population in Scandinavia [178], where the first case of VWD was identified. It appears to be less common elsewhere [179]. VWD results from either a qualitative or quantitative deficiency in VWF, caused by mutations at the *VWF* locus. The symptoms can vary widely between patients with VWD, but usually they are those of platelet dysfunction and include nose bleeding, oral cavity bleeding, prolonged bleeding from trivial wounds, skin bruises and haematomas. Severe deficiency of VWF or abnormalities in its interaction with FVIII (see type 2N VWD), causes a secondary moderate deficiency of FVIII, with typical haemophilia symptoms.

VWD is a heterogeneous disorder. It is classified into three major categories: partial quantitative deficiency (type 1), qualitative deficiency (type 2) and total deficiency (type 3) (reviewed in [180]):

Type 1 VWD is the most common VWD deficiency (70% of all VWD patients). It is characterised by decreased VWF levels in blood. However, all the multimeric forms of VWF are decreased proportionally, resulting in a normal multimers distribution (Fig 1.6). It is caused by mutations that impair VWF synthesis and/or secretion or increase VWF plasma clearance. Type I VWD can be inherited as a dominant or recessive trait, depending on the specific mutation and on the variable penetrance.

Type 3 VWD is characterised by no or minimal detectable VWF protein in plasma (Fig 1.6). It is a recessive disorder and its pathophysiology is not different from that of VWD type 1. The distinction between the two forms is made from a clinical point of view, since type 3 VWD have more severe symptoms and a distinct therapy.

Type 2 VWD is characterised by normal plasma VWF antigen, but loss of certain functions. It includes a series of subtypes (2A, 2B, 2M, 2N). Inheritance is dominant, with the exception of type 2N and a rare variant of type 2A.

Type 2A VWD is the most common qualitative deficiency. It is associated with the absence of large and intermediate molecular weight VWF multimers (Fig 1.6), which are the most effective in haemostatic activity. Type 2A VWD is usually transmitted as a dominant disorder caused by single amino acid substitution usually within the A1 and A2 domains. Two distinct molecular mechanisms are involved in causing the type 2A VWD phenotype and the corresponding causative mutations are designated group I and group II [181]. Group I mutations are associated with impaired assembly and secretion of normal VWF multimers [182]. It is assumed that only the larger multimers carrying these mutations are retained in the endoplasmic reticulum, since they have incorporated a large number of mutant subunits interfering with processing and

secretion process. Group II mutations are associated with normal processing and secretion of VWF multimers. Loss of large and intermediate molecular weight multimers then occurs in plasma, due to increased susceptibility to proteolysis by ADAMTS13 [106,183-186] (see Section 1.3). Molecular modelling of the A2 domain suggests that these mutations may change the conformation of the molecule, leading to an unfolded domain more susceptible to proteolytic cleavage. A distinct set of mutations within the propeptide causes a recessive form of type 2A VWD, also by impairing multimer assembly in the Golgi. The basis for the recessive clinical phenotype is not completely understood.

Type 2B VWD is characterised by increased affinity of VWF for platelet GpIbα. Different point mutations have been identified all clustered in the region of the A1 domain, which contains the GpIbα binding site [187,188]. Paradoxically, this abnormality does not lead to thrombosis but to a bleeding phenotype. This can be explained by the presence of increased clearance of both VWF and platelets, leading to absence of haemostatically effective high molecular weight multimers in plasma (Fig 1.6) and intermittent thrombocytopenia.

Type 2M VWD is characterised by normal VWF multimers distribution but decreased platelet adhesion. Mutations associated with this particular phenotype have been identified in GpIbα binding site in A1 domain and they cause a disruption of this interaction [189].

Type 2N VWD shows preserved platelet-dependent functions and normal VWF multimeric pattern, but decreased FVIII binding and subsequently low FVIII levels due to enhanced clearance. All the mutations described are located in the region of VWF containing FVIII binding site (i.e D'D3). The phenotype is autosomal recessive, since FVIII binding to VWF is not dependent on VWF multimeric size. Furthermore, VWF is physiologically in excess compared to FVIII and thus the amount of VWF synthesized by a single allele is sufficient to bind all the circulating FVIII [190,191].

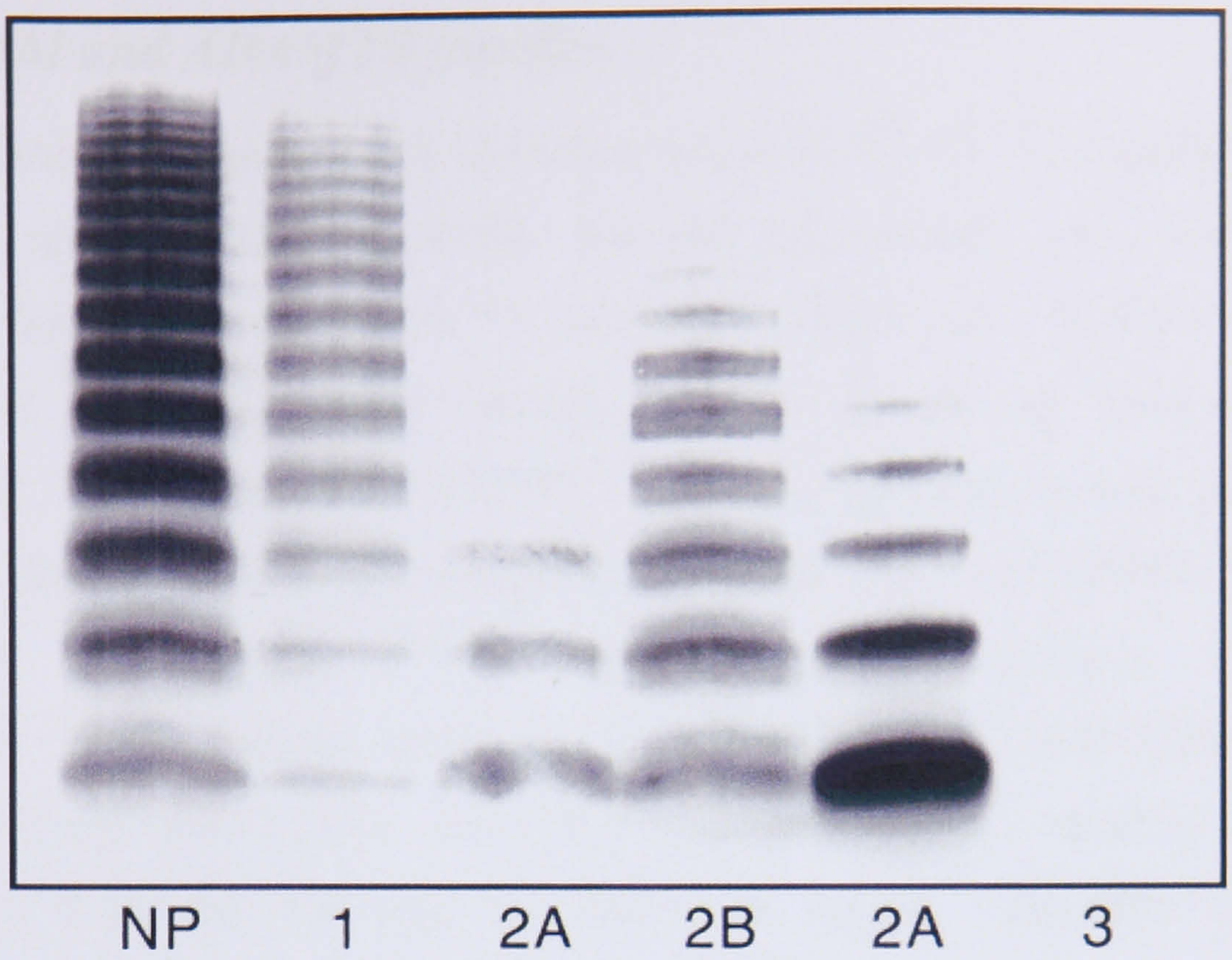


Fig. 1.6 Distribution of VWF multimers in VWD. 1.3% agarose/SDS gel followed by Western blotting using anti VWF antibody of plasma samples from normal individual (NP) and from patients with VWD types 1, 2A, 2B and 3. VWF multimer distribution is normal in type 1 VWD, whereas type 2A and type 2B lack the large and medium multimers. No VWF is detected in type 3 VWD. (Picture taken from [192])

1.3 ADAMTS13

As already stated, VWF platelet-tethering function depends on its multimeric size. The largest VWF multimers show an enhanced haemostatic potential (see Section 1.2.6). Consequently, the size of plasma VWF multimers needs to be physiologically regulated to prevent abnormal thrombus formation. This is finely modulated by the plasma metalloprotease ADAMTS13, which cleaves VWF between Y1605 and M1606 within the A2 domain (see Section 1.3.5). Mature ADAMTS13 is a 1353 residue glycoprotein with a molecular weight of approximately 200 kDa, which circulates in plasma as an active enzyme with a concentration of 1 μg/ml (~ 5 nM) and an estimated half life of two or three days [193-195]. It was first identified in 1996 [147,196] and initially called VWF-cleaving protease, due to its function of regulating VWF multimeric size. A few years later, following its cloning, purification and domain structure characterisation, it was classified as the 13th member of the ADAMTS (A Disintegrin and Metalloprotease with ThromboSpondin motif) metalloproteinase family [194,195,197,198].

1.3.1 ADAM and ADAMTS families

The first ADAMTS member to be identified was ADAMTS1 [199] and after that, a large number of proteases sharing similar domain organisation were described. The ADAMTS family now includes 19 proteases, which are involved in different physiological functions. These include collagen processing from procollagen (ADAMTS2, ADAMTS3, ADAMTS14) [200,201], cleavage of the matrix proteoglycans aggrecan, rich in the cartilage (ADAMTS1, ADAMTS4, ADAMTS5, ADAMTS8, ADAMTS9, ADAMTS15) [202-207], inhibition of angiogenesis (ADAMTS1, ADAMTS8) [208,209], gonadal development (ADAMTS9, ADAMTS20) [206], VWF cleavage (ADAMTS13). Some ADAMTS members have no function or substrate identified to date and therefore are known as orphan ADAMTS (ADAMTS6, ADAMTS7, ADAMTS10, ADAMTS12, ADAMTS16, ADAMTS19).

Some ADAMTS members appear to be important in organogenesis: it has been shown that ADAMTS1 knock out mice present growth retardation and several developmental defects in different organs (adipose tissue, kidneys, uterus, ovaries) [210]. Recently, it has been shown that some ADAMTS proteases show an altered expression in pathological conditions, such as arthritis [207] and cancers. ADAMTS1 expression appears to be down-regulated in pancreatic cancer and hepatocellular carcinoma, probably favouring local invasion and tumour metastasis [211]. The expression of eleven of the ADAMTS members appeared to be dysregulated in invasive breast carcinoma: some of them are down-regulated (ADAMTS1, ADAMTS3, ADAMTS5, ADAMTS8, ADAMTS9, ADAMTS10, ADAMTS18), others are up-regulated (ADAMTS4, ADAMTS6, ADAMTS14, ADAMTS20) [212].

The ADAMTS family represents a branch of the M12B ADAM (a disintegrin and metalloprotease-like, or adamalysin) subfamily of metalloendopeptidases, based on the similarity of their metalloprotease domain to that of snake venom metalloproteinases (SVMPs). The adamalysins (both ADAMTS and ADAM) belong to the family of metzincins (zinc-dependent proteases), which also included the matrix metalloproteinases (MMP), astacins and serralysins [213,214]. The name metzincins derives from the fact that they have a zinc ion in the active site (see Section 1.3.3) and also a conserved methionine downstream from the catalytic site, which generates a "Met-turn".

ADAMTS and ADAM members show a high similarity in their domain structure (Fig. 1.7 panels 1 and 2): they both contain a signal peptide, a propeptide, a metalloprotease domain, a disintegrin-like domain and a cysteine-rich domain (Cys-rich). But ADAM

metalloproteases are usually transmembrane proteins (growth factors and adhesion receptors), whereas ADAMTS members are secreted enzymes. They also differ by the presence of epidermal growth factor (EGF)-like repeats in the ADAM sequence; whereas a spacer domain and at least one Thrombospondin Type 1 Repeat (TSR) are present in the ADAMTS sequence, together with additional C-terminal domains.

The non-catalytic domains in ADAMTS family member perform various functions, participating in tissue localisation and substrate recognition: in ADAMTS1 the Cys-rich/spacer domain and three TSRs are involved in binding to heparin and extracellular matrix [215,216], whereas the C-terminal TSR binds to endothelial cells and VEGF [209,216]; in ADAMTS4 TSRs are required for aggrecan cleavage [203], whereas the Cys-rich/spacer domain binds to glycosaminoglycans [217]; in ADAMTS12, TSRs bind to extracellular matrix [218].

ADAMTS13 shows the highest divergence from any other member of the ADAMTS family, due to the presence of a smaller propeptide and two C-terminal CUB domains (Fig. 1.7 panel 3). The function of its different domains is not completely understood and is still under investigations (see Section 1.3.3).

To date, the crystal structures have been solved only for two ADAM catalytic domains [ADAM17 [219] (also known as TNF-α converting enzyme, TACE) and ADAM33 [220]], while none is available for the ADAMTS family. Nevertheless, structural models of the catalytic domains have been generated for all the ADAM and ADAMTS members, using modeling programs [221], where ADAM17 [219] or the snake venom metalloproteinase adamalysin II [222] were chosen as templates (see Fig. 1.9 Section 1.3.3).

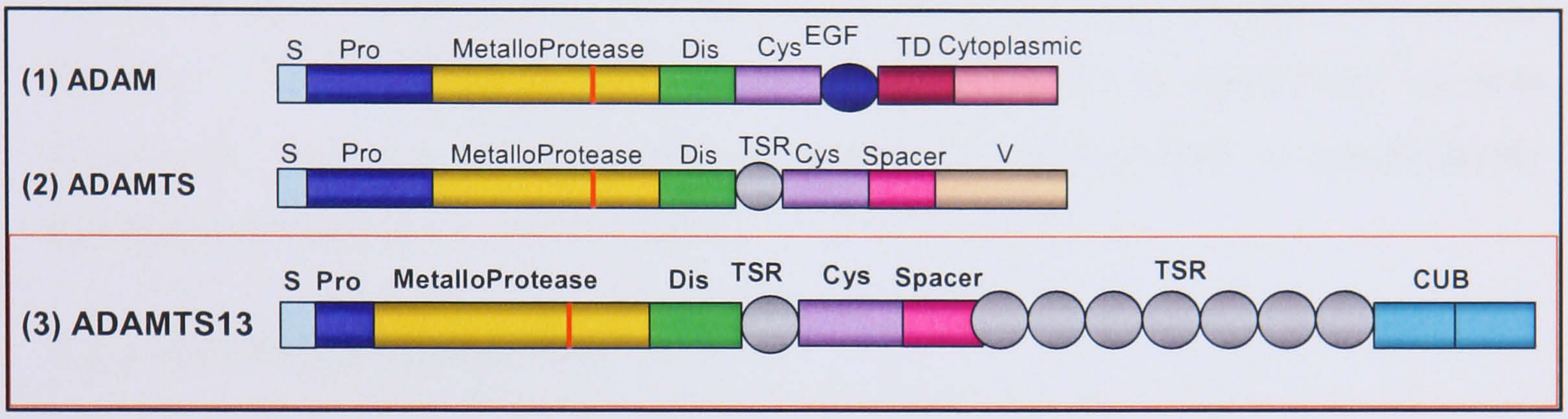


Fig. 1.7. Schematic diagrams of ADAM, ADAMTS metalloproteases and ADAMTS13. The ADAM **(1)** and the ADAMTS **(2)** proteases show a high similarity in the organization of the domains: they both have a signal peptide (S), a propeptide (Pro), a metalloprotease domain (the location of the zinc-binding site is highlighted with a red line), a disintegrin-like domain (Dis) and a Cys-rich domain (Cys). In the ADAM metalloproteases there are also an EGF-like domain, a transmembrane domain (TD) and a cytoplasmic region. The ADAMTS family are characterised by the presence of at least one Thrombospondin Type 1 Repeat (TSR), a spacer domain and a C-terminal variable region. ADAMTS13 **(3)** is the only ADAMTS family member to possess two CUB domains (Adapted from [223]).

1.3.2 ADAMTS13 gene, synthesis and secretion

The human *ADAMTS13* gene is located on chromosome 9 at position 9q34. It spans approximately 37 kb and contains 29 exons [197]. *ADAMTS13* mRNA is approximately 5 kb and encodes a 1427 amino acid protein, with a predicted molecular weight of 145 kDa, differing from the observed molecular mass of purified plasma ADAMTS13 (180-200 kDa) [194,224]. This discrepancy is due to glycosylation, since there are 10 potential *N*-glycosylation sites [196,225]. Northern blot analysis using human tissue or cDNA libraries derived from human tissues reported that ADAMTS13 is synthesised primarily in the stellate cells of the liver [226,227], but it has also been found in a wide number of adult tissues (brain, prostate, ovary, placenta, heart, skeletal muscle and platelets) [195,197,228]. A recent study found that ADAMTS13 is synthesised by both venous and arterial endothelial cells in culture [229]. ADAMTS13 is constitutively secreted into blood as an active enzyme.

1.3.3 ADAMTS13 structure

The 1427 amino acids of the precursor of ADAMTS13 consists of a signal peptide (residues 1-33), a propeptide, a metalloprotease domain, a Thrombospondin Type-1 motif (TSR), a Cys-rich domain, a spacer domain, seven additional TSRs and two CUB domains [195] (Fig.1.7, panel 3).

Propeptide domain (residues 34-74). The ADAMTS13 propeptide is shorter (41 residues) by comparison to other ADAMTS/ADAM family propeptides (160-230 residues) (see Fig. 1.7 Section 1.3.1). Like other metalloproteases, ADAMTS13 propeptide presents a typical proprotein processing site (RQRR), which has been shown to be a furin cleavage site [195]. In other metalloproteases, the propeptide is essential to assist protein folding and to maintain enzymatic latency, due to the presence of a cysteine residue, which coordinates the catalytic Zn^{2+} ion, maintaining it in an inactive state [230]. ADAMTS13 propeptide seems to be dispensable for normal folding, since deletion of the propeptide does not affect secretion of active enzyme [231]. Moreover, it has been shown that mutation in furin consensus recognition site leads to secretion of an active pro-ADAMTS13 [231]. This suggests that ADAMTS13 propeptide does not confer enzymatic latency (probably because it lacks the "cysteine-switch" motif). Detection of anti-propeptide antibodies in some patients with TTP suggests that not all plasma ADAMTS13 has this sequence removed [194].

Metalloprotease domain (residues 75-289). It contains the protease active site, which is highly conserved amongst the metzincin family (see Section 1.3.1). It includes a conserved zinc binding motif, "**H**EXX**H**XXGXX**H**Z", where X represents any amino acid residue and Z indicates a subfamily specific conserved residue, which is D for both ADAM and ADAMTS members. The Zn^{2+} ion is essential for the hydrolysis of the target peptide bond and it is coordinated by the three histidines (H). The glutamate (E) following the first zinc-binding histidine has a catalytic role [232], polarizing through hydrogen bonding a water molecule, which is stabilised by coordination with the Zn^{2+} ion and it is responsible for the nucleophilic attack on the carbonyl of the substrate scissile peptide bond (reviewed in [233]) (Fig 1.8). The conserved methionine is located 10-20 amino acids after the third histidine [214].

A predicted model of ADAMTS13 protease domain structure has been generated in our laboratory using adamalysin II as a template [221] and it is shown in Fig. 1.9. The catalytic Zn^{2+} ion is coordinated by three histidine residues (H224, H228 and H234). The conserved catalytic glutamate residue (E225) is also highlighted in the figure.

Another divalent cation which plays an essential role in ADAMTS13 activity is calcium. The precise role of calcium has not been completely clarified. However, it has been shown that in its absence the proteolysis of VWF is markedly slowed [147,196]. A potential calcium binding site (conserved in most of the ADAM and ADAMTS member) is predicted to lie on the opposite side of the zinc catalytic domain and it may involve residues E83, D173, C281 and D284 (Fig. 1.9). This could suggest that the interactions between calcium and zinc ions may be mediated through a conformational change in the protein structure. The importance of zinc and calcium ions explains why ADAMTS13 function is completed inhibited by metal ions chelators, such as ethylenediaminetetraacetic acid (EDTA) [196]. In a recent study it has been demonstrated that ADAMTS13 activity in citrated-anticoagulated plasma was enhanced two fold by zinc ions, three fold by calcium ions and six fold by both [234], suggesting a cooperative activation by the two ions. In the same study, the contribution of calcium and zinc has been investigated using recombinant ADAMTS13 (free from citrate or other metal chelators) and its apparent binding affinity for calcium and zinc was calculated (K_D of 4.8 and 0.5 μM, respectively). Since the normal plasma concentration of calcium and zinc are 1.2-2.6 mM and 12-18 μM respectively, it is likely that ADAMTS13 circulating in normal plasma is fully saturated by both ions. Zinc concentrations higher than 50 μM showed an inhibitory effect, perhaps due to the formation of $Zn(OH)^{+}$ that bind to the catalytic glutamic acid in the active site [235].

Different studies using C-terminal truncations of recombinant ADAMTS13 have shown that the metalloprotease domain alone was not able to cleave plasma VWF [236,237] or a short A2 domain peptide, VWF73 (residues 1596-1668) [238]. However, in the last mentioned study it was found that the metalloprotease alone could cleave the substrate after long incubation times (16-24 hours) but at a different site than the predicted Y1605-M1606. These experiments demonstrated that the protease domain alone, even if functional, is not sufficient to recognise and cleave specifically the VWF cleavage site, suggesting that the other downstream domains are responsible for determining substrate specificity of cleavage.

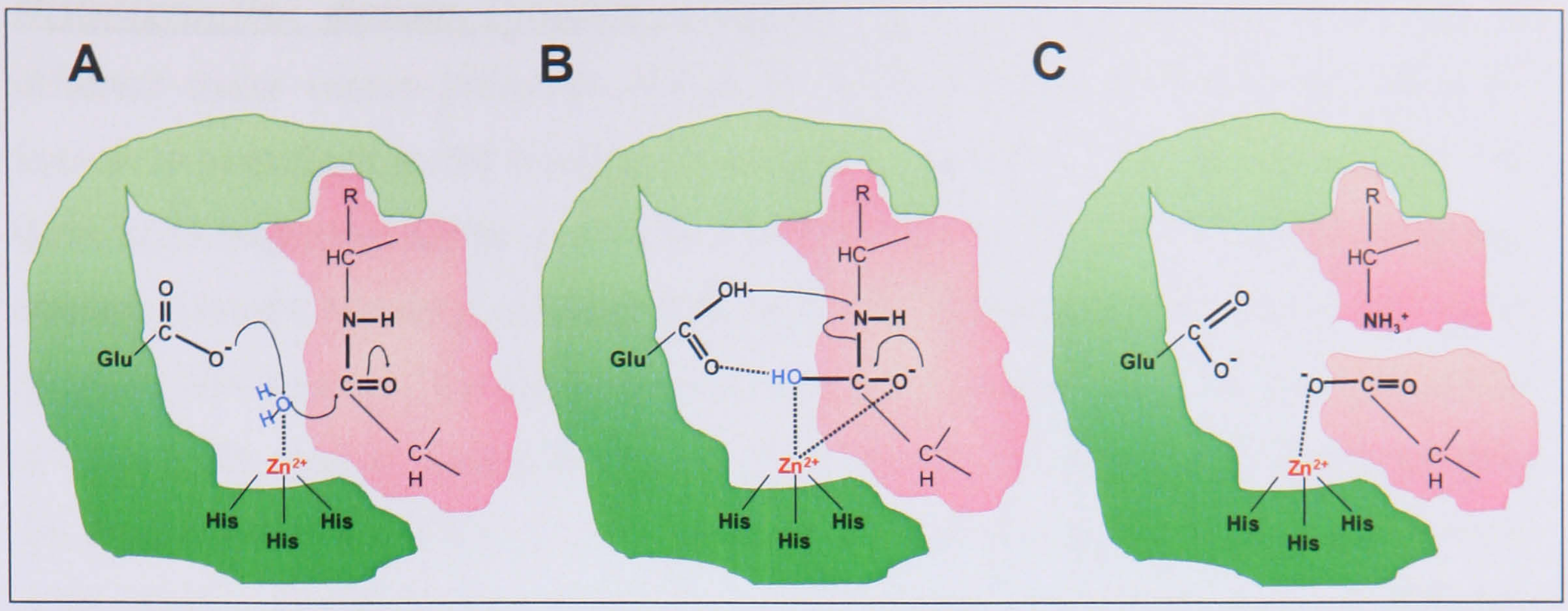


Fig. 1.8 Mechanism of peptide hydrolysis. The metalloprotease is shown in green, the substrate in pink (R= side lateral chain), the catalytic zinc ion in red and a molecule of water in blue. A) The catalytic glutamate (Glu) in the enzyme active site attacks the molecule of water (coordinated to the Zn^{2+}), polarizing it through hydrogen bonding. The water molecule promotes the nucleophilic attack on the carbonyl of the substrate scissile peptide bond. B) Reaction intermediate resulting from the previous step is illustrated. This intermediate can collapse with proton donation from the hydroxyl group of the glutamate to the peptide amino group, leading to a substantial electron rearrangement. C) Hydrolysis products are shown, just after the final step resulting in the rupture of the peptidyl bond. (Based upon [233,239])

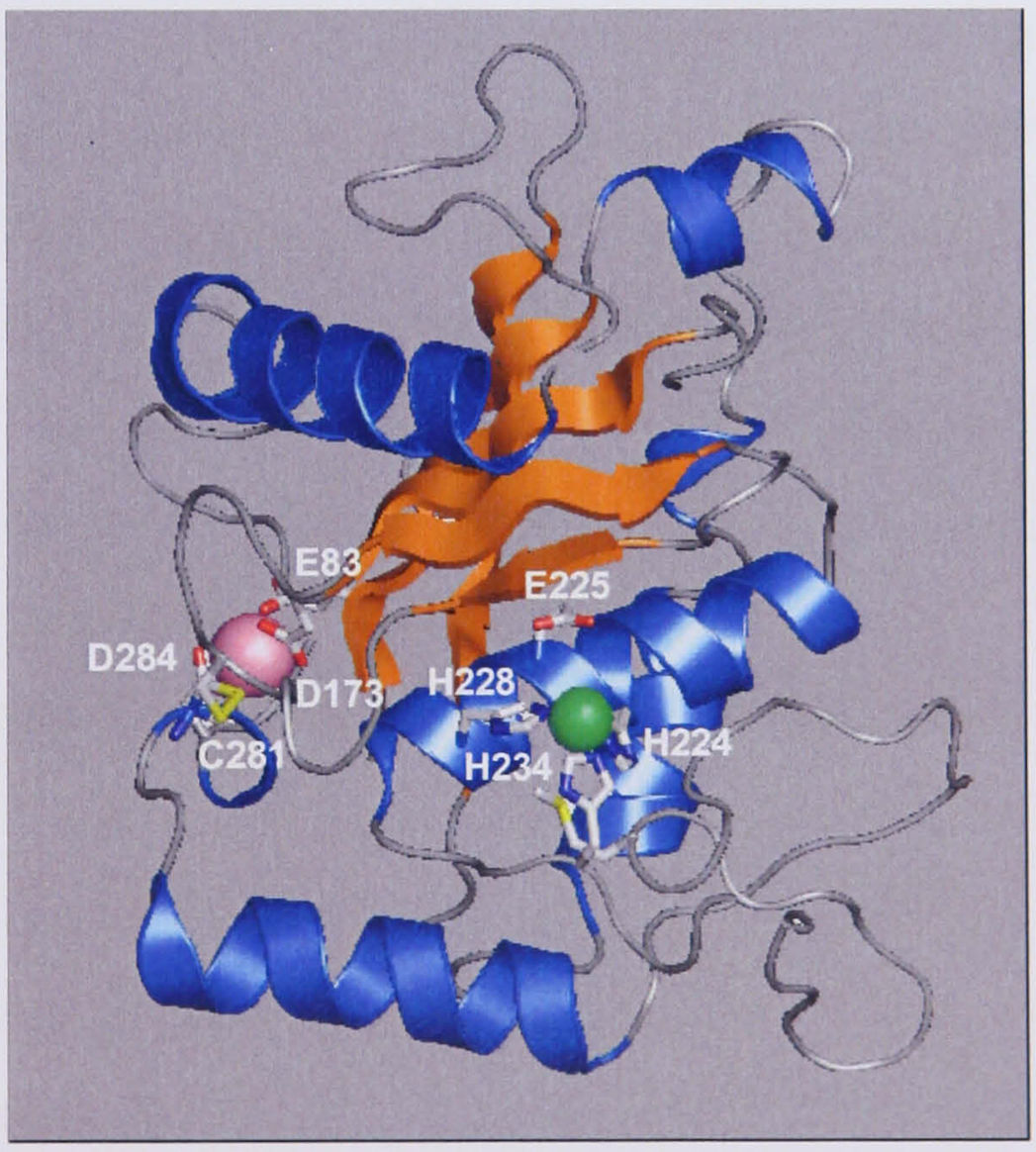


Fig. 1.9 Structural model of ADAMTS13 catalytic domain. The model was generated with the program Modeller6v2, using the venom metalloprotease adamalysin II as a template [221]. It consists in a core of five stranded β-sheet (brown), wrapped by five α-helixes (blue). The zinc and calcium ions are shown as green and pink spheres, respectively. The three catalytic histidines (H224, H228, H234), coordinating the zinc ion, are represented in stick form. E225 is also shown. The predicted calcium-binding site (left) involves four predicted residues (E83, D173, C281, D284).

Disintegrin-like domain (residues 290-385). Disintegrin domains are present in different snake venom proteases and in the ADAM family proteases and they are known to contribute to the binding of integrins on platelet or other cell surface, via their RGD sequence. All the members of ADAMTS family possess a disintegrin-like domain. Despite its name and high sequence identity with the mentioned disintegrin domains, this domain does not actually have an RGD integrin binding sequence and it is not known to bind integrins. To date, it is not clear if this domain has a specific function or just a structural role [195]. However, some mutations have been found in the ADAMTS13 disintegrin-like domain in some patients with inherited ADAMTS13 deficiency (see Section 1.3.6), but whether they actually affect ADAMTS13 activity or they just impair secretion is not clear [197,240].

Cys-rich domain (residues 440-555). As name suggests, this domain is rich in cysteines (10 residues), the role of which is uncertain. It also contains a potential integrin-binding sequence (RGD), but mutations of the RGD sequence do not impair ADAMTS13 secretion and function *in vitro* [237]. However, the importance of this domain is highlighted by the identification of a polymorphism, P475S, in the Japanese population. This altered ADAMTS13 activity but not its secretion [225] (see Section 1.3.6.3). Furthermore, a mutation found in a patient with inherited ADAMTS13 deficiency (Q449stop) causing a premature stop after the first TSR resulted in a truncated protein which was secreted normally but possessed very low enzymatic activity [225] (see Section 1.3.6.3). It is possible that the Cys-rich domain is involved in VWF binding (see Section 1.3.4), since it was found that the snake venom metalloproteinase Atrolysin A binds to VWF via its Cys-rich domain, blocking its binding to collagen and inhibiting platelet aggregation [241].

Spacer domain (residues 556-685). This domain has been shown to be essential for efficient ADAMTS13 VWF-cleaving activity [236,237]. ADAMTS13 fragments truncated after the metalloprotease domain, the disintegrin domain, the first TSR or the Cys-rich domain were not able to cleave full-length VWF, whereas addition of the spacer region restored protease activity [236,237]. Furthermore, some missense mutations have been mapped to the spacer domain and associated with congenital ADAMTS13 deficiency, but most of them have not been fully characterised [225,242]. Moreover, it has been shown that patients with acquired ADAMTS13 deficiency develop antibodies against this region. Whether such antibodies cause loss of enzyme activity or accelerate its clearance has not been clarified yet [237,243]. *In vitro* experiments have shown that a monoclonal antibody against the Cys-rich/spacer domain completely

abolished ADAMTS13 binding and cleavage of both VWF73 and full-length VWF [244]. It is likely that this domain plays a crucial role in ADAMTS13-VWF interaction (see Section 1.3.4)

TSRs. TSRs are protein modules, initially identified in TSP-1, a multifunctional protein present in platelet α-granules and released upon activation (see Sections 1.1.1.2 and 1.3.5.3). Subsequently, other proteins sharing TSRs, have been identified, most of them playing a role in the nervous system development, probably directing cell migration [245]. TSRs frequently have positively charged patches and they have high affinity for the negatively charged GAGs and CD36 receptor present on endothelial cell surface [246-248].

ADAMTS13 has eight TSRs: the first one (residues 386-439) is located between the disintegrin-like domain and the Cys-rich domain; the other seven (residues 686-1131) are located between the spacer domain and the two C-terminal CUB domains. TSRs may play a role in binding GAGs and/or CD36, localising ADAMTS13 to the surface of endothelial cells (see Section 1.3.5.2). Supporting this hypothesis, anti-CD36 antibodies have been frequently found in patients with thrombotic thrombocytopenic purpura (see Section 1.3.6): Tandon *et al* [249] found that 75% (21/28) of total analysed patients were positive to anti-CD36 antibodies. Schultz *et al* [250] obtained a similar result, with 71% (10/14) of total patients positive. However, it has been shown that soluble anti-CD36 antibodies do not completely block UL-VWF cleavage on the endothelial cell surface [251], suggesting that, if ADAMTS13 interacts with endothelial cells, it might use a different cell receptor. Alternatively, ADAMTS13 TSRs may be involved in VWF interaction, similarly to plasma TSP-1 which bind to VWF A3 domain [252,253] (see Section 1.3.4).

CUB domains (residues 1192-1408). These domains are uniquely found in ADAMTS13 among the ADAMTS family, but they are present in other proteins involved in developmental processes (embryogenesis, organogenesis, innervation), suggesting they can have a role in protein-protein interactions [254]. The name "CUB" is an acronym for the three proteins in which this domain was firstly identified: Complement components C1r/C1s, Uegf (sea urchin fibropellins) and Bone morphogenic protein 1 (Bmp1). To date, the function of ADAMTS13 CUB domains is controversial. Three different recent studies using C-terminal truncations of ADAMTS13 have shown that these domains are not required for VWF-cleaving activity under static [236,237] and flow [255] conditions. Moreover, several natural strains of phenotypically normal mice express a C-terminal truncation of ADAMTS13 after

TSR7, suggesting that the CUB domains, at least in mice, are not necessary for ADAMTS13 function *in vivo* [256]. Furthermore, autoantibodies against the CUB domains have been found in patients with acquired TTP, but it is unknown whether they compromise ADAMTS13 function or lead to ADAMTS13 depletion by the formation of antibody-antigen complexes [243]. Mutations located in the CUB domains have been reported in patients with congenital TTP [240,257]. It has been suggested a possible role for CUB domains in modulating ADAMTS13-VWF interaction under flowing conditions (see Section 1.3.4)

1.3.4 ADAMTS13 interaction with VWF

In order to precisely map the VWF binding site on ADAMTS13, a plate-based binding assay was optimised [238,258]. Either the full-length VWF [258] or the short substrate VWF73 [238] were coated on a 96-well plate and their binding to full-length ADAMTS13 and to a series of ADAMTS13 truncations was tested. These studies highlighted the complexity of the interaction between ADAMTS13 and VWF, as different domains seem to be involved. Certain regions appear as main candidates for a crucial role in VWF interaction, i.e Cys-rich and spacer domains (see below). Other domains may have a role in modulating the binding, i.e. TSRs and CUB domains (see below).

In accordance with the activity experiments [236-238] (see Section 1.3.3), no binding was detected between the metalloprotease domain alone and both the full-length VWF and VWF73 [238,258]. No binding was observed also when ADAMTS13 truncated after the disintegrin-like domain was incubated with full-length VWF coated onto the wells [258]. However, Ai *et al* [238] have shown that the isolated disintegrin-like domain alone can bind to the VWF73 substrate with a K_D of 489 nM. Another recent study [244] has demonstrated that a monoclonal antibody against the disintegrin-like domain abolished binding and activity against both VWF73 and full-length VWF. Thus, it may be possible that the disintegrin-like domain is partially involved in VWF recognition. A major role for the Cys-rich/spacer domain region in VWF recognition has been suggested. ADAMTS13 truncated after the first TSR bound full-length VWF with a K_D of 206 nM whereas ADAMTS13 truncated after the spacer domain bound to it with a K_D of 23 nM. This is comparable to the K_D of 14 nM found for full-length ADAMTS13 interaction with full-length VWF [258]. Similar results were obtained testing the binding to VWF73: ADAMTS13 truncated after the spacer domain bound to VWF73 with a K_D of 7 nM, comparable to that obtained using full-length

ADAMTS13 (K_D 4.6 nM), whereas further truncation drastically reduced the binding. Moreover, it was found that antibodies against the Cys-rich domain completely abolished binding and activity against VWF73, indicating a crucial role for this region [244]. Ai *et al* [238] have expressed recombinant ADAMTS13 domains individually (disintegrin, first TSR, Cys-rich, spacer) and they found they bound to VWF73 with a K_D of 489 nM, 136 nM, 121 nM and 108 nM, respectively. This data suggested that all the proximal C-terminal domains may act in cooperation to confer an efficient recognition of the substrate. Even if the absence of the last seven TSRs and the two CUB domains did not affect ADAMTS13 activity against full-length VWF [236,237] and VWF73 [238], they both seem to take part in the modulation of VWF binding. Truncations after the seventh TSR and the eight TSR bound to full-length VWF with K_D of 6.9 and 45 nM, respectively [258]. Comparing the K_D of 23 nM found for the truncation after the spacer domain with the K_D of 14 nM for the full-length ADAMTS13 suggests that the first six C-terminal TSRs and the two CUB domains may modulate ADAMTS13-VWF binding positively, whereas the last TSR negatively. Furthermore, competitive binding studies using a parallel flow chamber system, have found that recombinant CUB-1 domain (not CUB-2) inhibited UL-VWF-cleaving activity and UL-VWF-ADAMTS13 interaction under flowing conditions, but not under static conditions, suggesting a potentially important physiological functional role for this region under flow [259]. In the same study, it was also shown that both the two CUB peptides could bind UL-VWF in flowing conditions, but the binding of CUB-2 was unstable at elevated shear stress. This is also suggested by a second study [260]. On the basis of these findings, Tao *et al* [259] proposed the following 2-site model of ADAMTS13 binding to UL-VWF strings. ADAMTS13 circulates in plasma in equilibrium between a closed state (where the CUB-1 binding site is exposed but a second cryptic binding site is hidden) and an open state (where both the two binding sites are exposed). The close conformation is favoured when ADAMTS13 is in solution. It has been suggested that when ADAMTS13 binds to UL-VWF via its CUB-1 domain, it assumes the open conformation, revealing the cryptic binding site which then stabilises the interaction. This model is supported by the fact that truncation of ADAMTS13 up to the TSR8 reduced VWF binding (see above) by three fold, confirming CUB-domains role in modulating the binding. The fact that truncations before the spacer domain drastically reduced VWF binding (see above) suggests that this region can represent the cryptic binding site. This model also explains why CUB anchoring function is less important under static conditions. The model is also

supported by another study under flow conditions, in which it was reported that truncation after the spacer cleaved UL-VWF more efficiently than wild type ADAMTS13, possibly because truncation could expose the cryptic binding site [261].

1.3.5 ADAMTS13 function

1.3.5.1 Role of denaturants/shear stress and chloride ions in VWF cleavage

ADAMTS13 cleaves the peptidyl bond Y1605-M1606 in the A2 domain of VWF [106] (Fig. 1.10 A and B), and in this way regulates its plasma multimeric size (Fig. 1.11). *In vitro*, ADAMTS13 can only cleave VWF in the presence of denaturants (Guanidine-HCl or urea) and by use of extended incubation times [196]. *In vivo,* its activity seems to be shear-dependent [149]. The conformation of VWF is therefore a critical determinant of its susceptibility to proteolysis, since it needs to be unfolded to be effectively cleaved. Shear stress and denaturants probably induce conformational changes that expose the cleavage site, which appear to be buried in the centre of the molecule, in a predicted model of A2 domain generated in our laboratory (Fig. 1.10 B) (see Section 3.4.2 for details of the model).

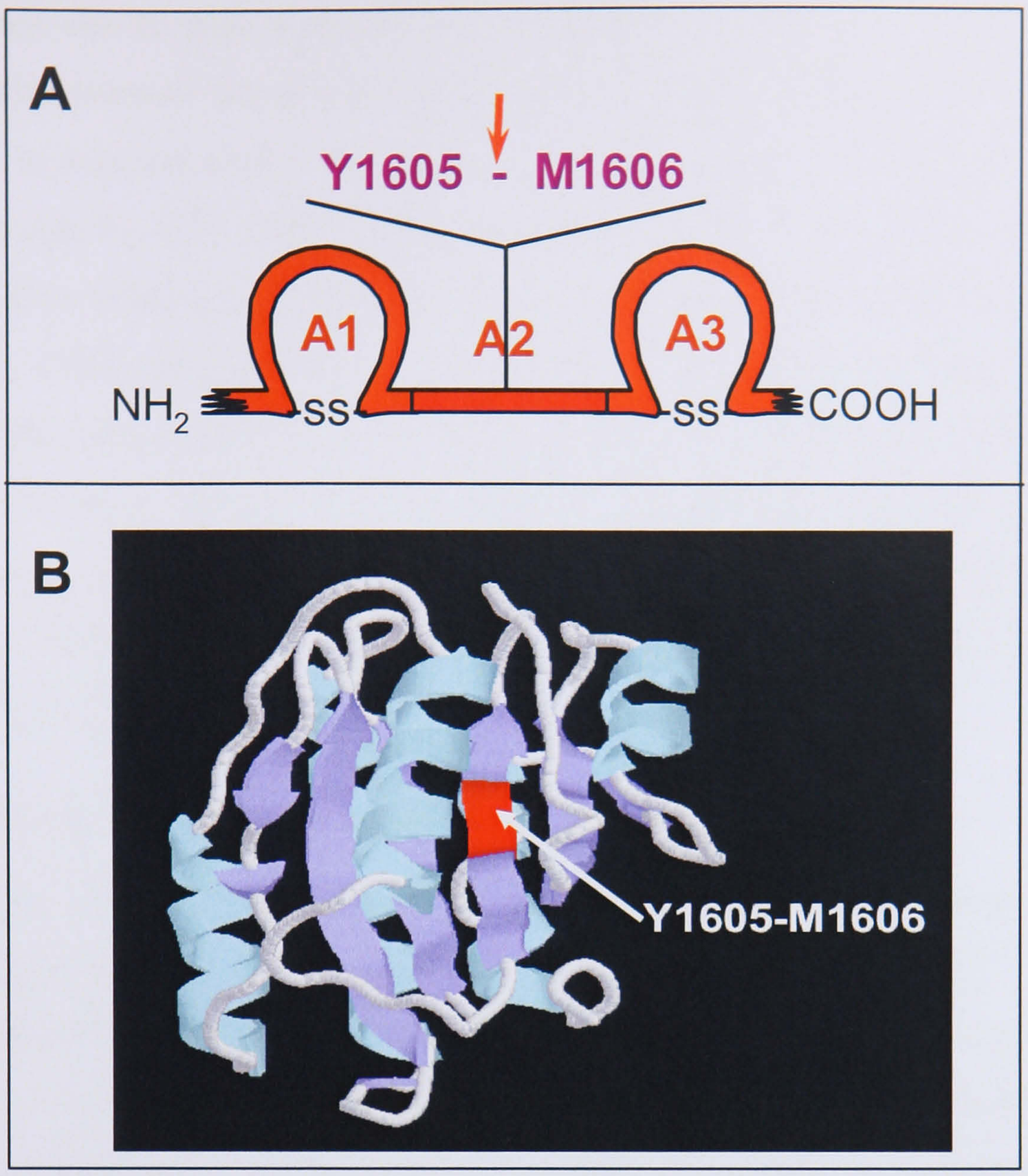


Fig. 1.10 VWF Y1605-M1606 cleavage site. A) Schemating representation of VWF A1, A2 and A3 domains. The ADAMTS13 cleavage site (Y1605-M1606) is located in the A2 domain and it is highlighted by a red arrow. B) Predicted model of VWF A2 domain. The cleavage site (Y1605-M1606) is highlighted in red within the centre of the A2 domain.

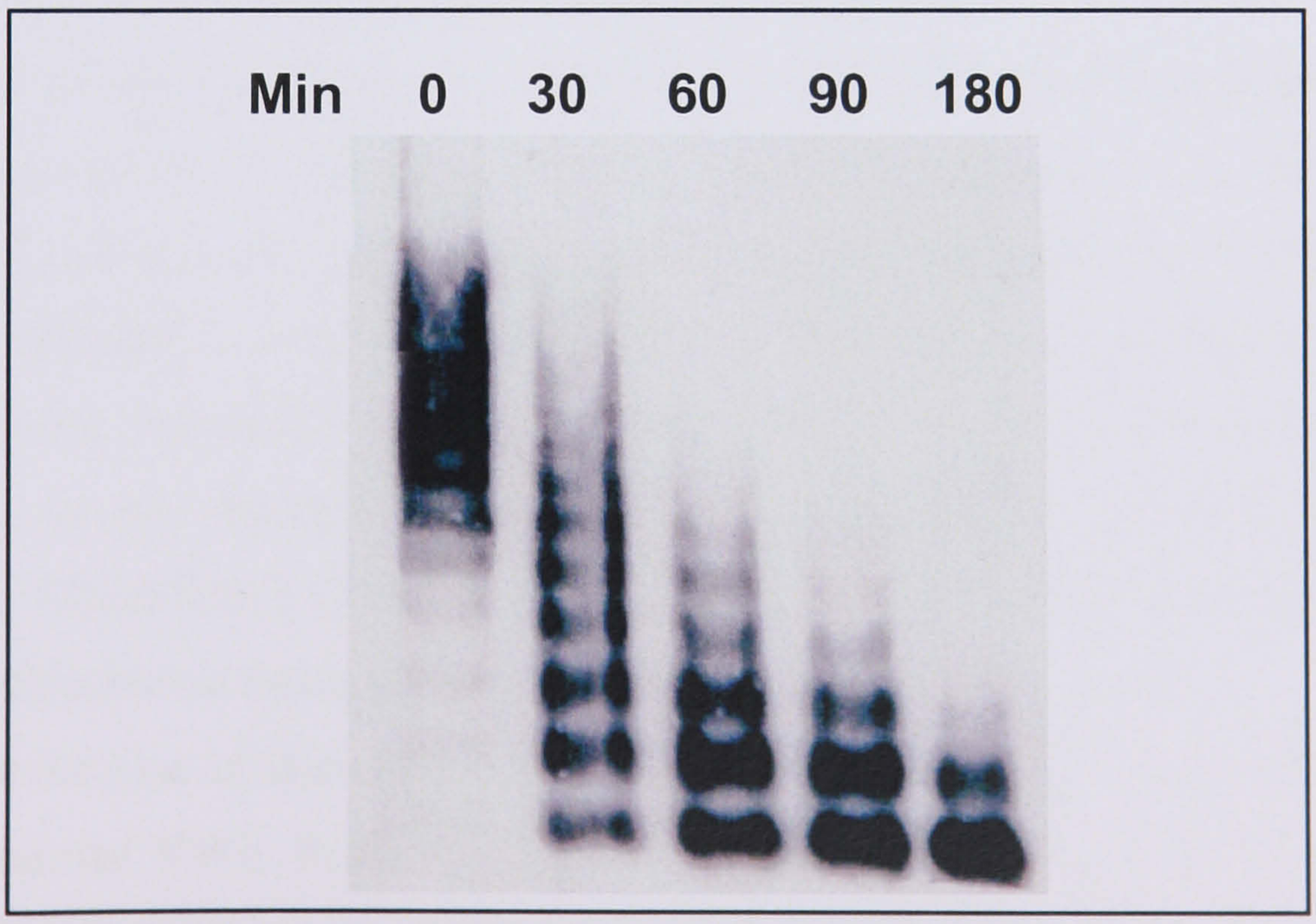


Fig. 1.11 VWF cleavage by ADAMTS13. 1.1% agarose gel electrophoresis of purified plasma VWF multimers cleavage by recombinant ADAMTS13 (in denaturing conditions) at different time points. The disappearance of the VWF high molecular weight forms can be detected over time (kindly supplied by Tom McKinnon).

NaCl seems also to play a crucial role in regulating VWF-ADAMTS13 interaction. Early studies showed that physiological concentrations of NaCl inhibit hydrolysis of VWF [147]. In a recent study, the catalytic efficiency k_{cat}/K_m of full-length multimeric VWF cleavage by ADAMTS13 was calculated to be 3.4 x 10^4 $M^{-1}s^{-1}$ in the absence of NaCl [262]. This value was ~10-fold decreased in the presence of 1.5 M NaCl. Ristocetin binding to VWF could reverse this inhibitory effect. Spectroscopic studies suggested that chloride ions present in the extracellular environment bind to VWF, stabilising it in a conformation which is quite resistant to ADAMTS13 proteolysis. Only when VWF changes its conformation by GpIbα binding or shear stress conditions, chloride affinity for VWF markedly decreases and VWF is stabilised in a conformation suitable for ADAMTS13 interaction.

1.3.5.2 Possible location of ADAMTS13 activity in vivo

The precise location of ADAMTS13 action *in vivo* is still under debate. Circulating VWF appears as a folded globular molecule by electron microscopy [145,146]. However, newly released VWF expressed by endothelial cells after histamine-stimulation forms extremely long string-like structures (UL-VWF) on the surface of endothelial cells, under flow conditions. These strings are rapidly cleaved in the presence of normal plasma or partially purified ADAMTS13, suggesting that a primary site of ADAMTS13 action is on endothelial bound VWF [263,264]. Another study has demonstrated that these UL-VWF multimers anchor to endothelial surface, binding P-selectin [265].

Based on all these findings, the following model has been proposed (Fig 1.12). A possible location of ADAMTS13 activity may be in plasma. Since ADAMTS13 is present in plasma in an active form, regulation of the cleavage is mainly dependent on VWF conformation. VWF is normally present in plasma in a globular and condensed conformation, which cannot interact with platelets or ADAMTS13 (Fig. 1.12 A). However, in the presence of high shear stress, VWF can spontaneously unravel, exposing ADAMTS13 cleavage site. In this way, ADAMTS13 proteolysis prevents unwanted thrombus formation in the normal circulation (Fig. 1.12 B).

A second location of ADAMTS13 activity is on the surface of endothelial cells, upon newly secreted VWF. Following endothelial cell stimulation, VWF is secreted from Weibel-Palade bodies as a very large polymer (UL-VWF), with a high haemostatic potential. UL-VWF appears to tether to P-selectin (also present in Weibel-Palade bodies) on the surface of endothelial cell surface, and get unravelled upon release.

These elongated strings can thus expose ADAMTS13 binding and cleavage sites, leading to immediate proteolysis. This represents a mechanism to down regulate UL-VWF hyper reactive activity and prevent spontaneous platelet adhesion (Fig. 1.12 C). The cleavage of UL-VWF on the endothelial surface raises the hypothesis that ADAMTS13 may need to anchor to the endothelial surface to perform its activity. ADAMTS13 might bind to GAGs and/or endothelial receptors via TSRs and/or CUB domains. However, there is yet no direct evidence to confirm this hypothesis.

It is not known if a similar regulation upon secretion is present for VWF multimers following the direct secretion pathway. It may be that these VWF species do not required immediate proteolysis, since they do not include high molecular weight multimers. Alternatively, the regulation of their size may be controlled by ADAMTS13 activity in plasma (as described above). According to this model, plasma multimers may be the result of a complex dynamic process involving VWF release and proteolysis.

1.3.5.3 Regulation of ADAMTS13 activity

As already stated, proteolysis by ADAMTS13 seems to be mainly controlled by VWF conformation, since shear forces or denaturants are required to "unravel" VWF and permit the enzyme to access the cleavage site. At sites of endothelial disruption, VWF binds to collagen and unfolds in response to shear forces, facilitating platelet tethering and therefore platelet plug formation. However, this unfolding is also predicted to allow ADAMTS13 to access and cleave the VWF scissile bond, preventing efficient platelet adhesion and thrombus formation. The presence of a specific inhibitor which regulates ADAMTS13 activity seems to be required (Fig. 1.12 D, scenario 1). In a recent study, it was found that thrombin cleaved ADAMTS13 at different sites, inactivating it [266]. This suggests that thrombin generated locally at sites of vascular perturbation may regulate ADAMTS13 activity by proteolytic inactivation. The same study investigated a possible role for thrombomodulin (TM) in modulating ADAMTS13 proteolysis by thrombin. TM is a trans-membrane protein expressed on endothelial cells. When TM binds thrombin, it inhibits thrombin pro-coagulant properties and enables it to interact with the anti-coagulant PC [267]. This mechanism limits thrombin pro-coagulant activities to the site of vascular injury. It was found that ADAMTS13 inhibition by thrombin was remarkably reduced if thrombin was pre-incubated with TM [266], suggesting that ADAMTS13 activity is not compromised at the edge of the disrupted endothelium, limiting platelet aggregation from spreading

beyond the site of injury (Fig. 1.12 D, scenario 2). In the same study, it was shown that also FXa and plasmin can cleave and inactivate ADAMTS13. Another recent study, suggested that TSP-1 has an inhibitory role upon ADAMTS13 activity [30]. It showed that platelet recruitment onto stimulated endothelium was impaired in *Tsp1*$^{-/-}$ mice, compared with wild type mice. Soluble TSP-1 injection or neutralising anti-ADAMTS13 antibodies corrected the defective platelet tethering and adhesion, suggesting ADAMTS13 is inhibited by TSP-1 during platelet plug formation. This result was confirmed by *in vitro* perfusion studies, where VWF cleavage by ADAMTS13 was indeed inhibited by TSP-1. The mechanism for inhibition is probably due to TSP-1 binding to VWF A3 domain, masking in this way ADAMTS13 binding site [252,253]. Another candidate in inhibiting ADAMTS13 activity at sites of vascular injury is collagen. VWF anchoring to collagen via its A3 domain may mask ADAMTS13 docking site. This possibility is currently under investigation in our laboratory. It has been reported that also interleukin-6 (IL-6) inhibits ADAMTS13 activity, but the specific mechanism of this remains uncertain [268]. Moreover, a study using haemolytic serum from a paediatric patient with ADAMTS13 deficiency suggested that plasma haemoglobin at concentration of 2 mg/ml or higher may inhibit ADAMTS13 activity [269]. The physiological significance of both IL-6 and haemoglobin is uncertain. They both might be involved in ADAMTS13 regulation only under pathological conditions.

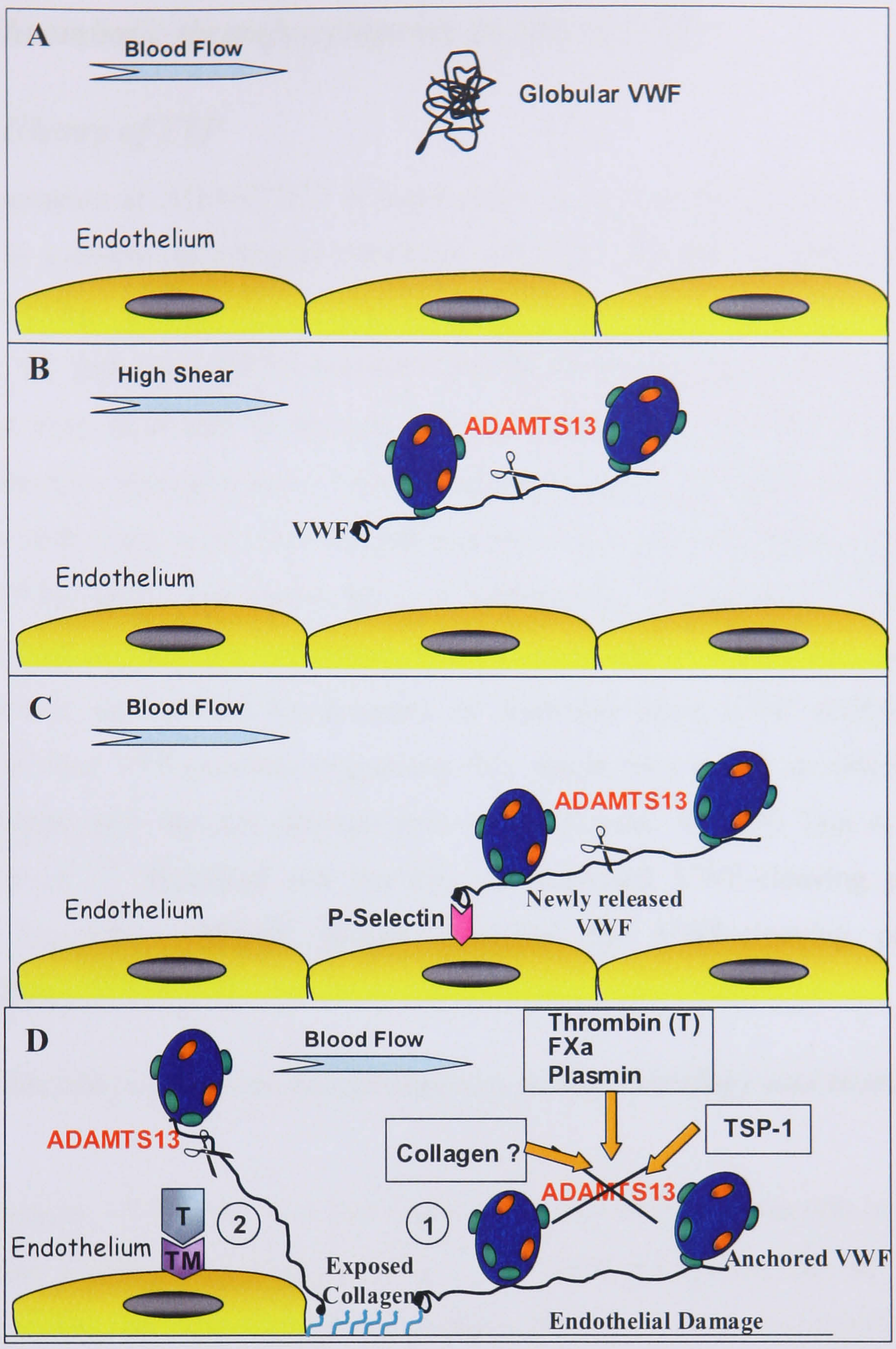


Fig. 1.12 Sites of ADAMTS13 action. (A) In normal flow, VWF maintains a globular structure that protects it from ADAMTS13 proteolysis. **(B)** In conditions of high shear stress, VWF can be unravelled and platelets can bind to it via GpIbα receptor. ADAMTS13 is present in blood as an active enzyme and it cleaves VWF in order to prevent unwanted platelet aggregation. **(C)** Newly released UL-VWF multimers secreted from Weibel-Palade bodies are anchored to P-selectin on the surface of endothelial cells, and become stretched under fluid shear stress. These strings are rapidly cleaved by ADAMTS13. Probably, platelets bind to VWF strings via GpIbα and contribute in maintaining VWF in the stretched conformation. **(D)** At site of vascular injury (1), VWF binds to collagen and unfolds in response to shear forces, facilitating platelet tethering. Thrombin, FXa, plasmin, TSP-1 and collagen may have a crucial role in inhibiting ADAMTS13 activity. On the other hand, ADAMTS13 activity should not be compromised at the edge of the disrupted endothelium (2), limiting platelet aggregation from spreading beyond the site of injury. It has been suggested that thrombin (T) binding to thrombomodulin (TM) probably masks ADAMTS13 binding site on thrombin, inhibiting its proteolytic cleavage.

1.3.6 Thrombotic thrombocytopenic purpura (TTP)

1.3.6.1 History of TTP

The importance of ADAMTS13 is highlighted by its genetic or acquired deficiency leading to a severe pathological condition, known as Thrombotic Thrombocytopenic Purpura (TTP).

In 1924, the first case of TTP was described by Eli Moschcowitz [270]. It was a young girl presenting fever and haemolytic anemia, rapidly leading to coma and death. A similar disorder was reported in 1960 by Schulman *et al* [271] and later on by Upshaw *et al* [272]. In both these latter cases the patients responded well to plasma infusion. Since then, TTP has been of interest in terms of pathogenesis. Moake *et al* [273] suggested for the first time in 1982 the correlation between decreased VWF proteolysis and TTP pathogenesis: he reported the presence of unusually large VWF multimers in the plasma of four TTP patients, suggesting they might play a role in determining the VWF-platelet rich thrombi characteristic of the disease. In 1996 Tsai *et al* [196] and Furlan *et al* [147] identified and partially characterised VWF-cleaving protease in plasma. In 2001, different groups identified the VWF-cleaving protease as ADAMTS13 [194,195,197,198].

1.3.6.2 Incidence, clinical manifestations, pathophysiology and therapy of TTP

The incidence of TTP has been estimated to be 4 cases per 1 000 000 in the United States, but it appears to be increasing [274,275]. Although the severity of the disease among affected individuals varies significantly, the common clinical manifestations of this syndrome are thrombocytopenia and microangiopathic haemolytic anemia, sometimes accompanied by fever, neurological deficits, renal abnormalities, abdominal pain, elevated pancreatic enzymes and/or cardiac arrhythmias [273]. TTP is caused by lack of VWF-cleaving activity, generally less than 5%. The consequence is elevated levels of circulating UL-VWF, which remain unprocessed after secretion. UL-VWF can spontaneously unravel under the high shear forces characteristic of capillaries, enabling platelet tethering. This results in the formation of platelet-rich, fibrin-poor thrombi in the microcirculation, leading to tissue ischemia or injury [276]. Untreated TTP is almost always fatal, but plasma exchange/infusion therapy has reduced mortality from 90% to less than 20% [277].

1.3.6.3 Congenital TTP

Congenital TTP usually occurs immediately after birth or during childhood, although some exceptions have been reported where the disease became manifested in adulthood or not still appeared in the third decade of life (incomplete penetrance) [278-284]. Congenital TTP is caused by mutations in ADAMTS13 gene, affecting protein secretion or function and it is autosomal recessive inherited. To date, more than 50 mutations have been documented in patients with familial TTP [197,225,240,242,257,285-289]. Analysis of the location of the mutations on the ADAMTS13 gene reveals no evident mutation hot spots. However, 75% of the missense mutations are found in the N-terminal part of the molecule, up to the spacer domain. Most (60%) of the identified mutations are missense; the remaining 40% (nonsense, frameshift, splicing mutations) generates truncated forms of the protein. The majority of the mutations cause reduced ADAMTS13 secretion [225,286,287]. Interestingly, three mutations have been fully characterised and found to cause significantly reduced ADAMTS13 activity. P475S is a common polymorphism in the Japanese population (10% of the population is heterozygous), located in the Cys-rich domain. Recombinant P475S ADAMTS13 mutant was expressed *in vitro*. It was secreted normally, but it showed a markedly lower activity in cleaving VWF multimers, compared with the wild type enzyme[225]. However, a slight loss of high molecular weight VWF was observed, suggesting this mutant still retain a quite significant activity. In the same study, another mutation was found to have normal secretion levels but lower enzymatic activity, Q449stop, which generated a protein truncated after the first TSR. Q449stop possessed lower enzymatic activity than P475S, since no cleavage was detected upon VWF multimers. Another mutation (T196I), found in the metalloprotease domain, has been reported to have less than 25% VWF-cleaving activity, compared to the wild type [197]. No patient had obvious null mutations on both alleles, suggesting that a complete deficiency of ADAMTS13 may be lethal. This is consistent with the fact that low levels of residual VWF-cleaving activity were detectable in all patients with TTP studied. Patients with congenital TTP usually do not required plasma exchange, since they respond well to plasma infusion. A periodic plasma infusion every 2-3 weeks is sufficient to supply enough ADAMTS13 to alleviate the thrombotic tendency, a consequence of the long plasma half-life of the enzyme.

1.3.6.4 Acquired TTP

Acquired TTP usually occurs in individual between 20 and 60 years old, in the absence of any obvious inciting event [290]. However, it can also arise secondary to other conditions, such as use of antiplatelet drugs (ticlopidine [291] and clopidogrel [292]). Acquired TTP is caused by autoantibodies (IgG) against ADAMTS13, which compromise its function and/or elevate its clearance. In 1998, anti-ADAMTS13 antibodies were identified for the first time in a patient with acute acquired TTP [293]. Since then, autoantibodies inhibiting ADAMTS13 activity have been detected in most patients with acquired TTP [237,243,294-298]. Epitope specificity of anti-ADAMTS13 antibodies have been recently investigated [237,243]. From the data collected from these studies, it can be inferred that in most of the cases the autoantibody response is polyclonal, directed against various epitopes of the molecule. However, all analysed plasma contained antibodies directed against the Cys-rich/spacer domain region and these were the only anti-ADAMTS13 antibodies found in three patients, suggesting that antibodies against this region are sufficient to induce acquired ADAMTS13 deficiency. Interestingly, a recent study [299] reported the case of two identical twins both developing anti-ADAMTS13 antibodies, suggesting that a genetic predisposition can be present even in the acquired form of the disease.

In contrast to congenital form, the therapy for acquired TTP consists of plasma exchange, required to remove the inhibiting autoantibodies.

1.3.6.5 TTP and other thrombotic microangiopathies

Different conditions can occasionally lead to a clinical phenotype (microangiopatic haemolysis and thrombocytopenia) similar to TTP: HIV [300], bone marrow transplantation [301,302], pregnancy [303], autoimmunodisorders (systemic lupus erythematosus) [304], neoplastic disorders [305,306], liver cirrhosis, various acute inflammatory disorders and postoperative period [307]. Mildly decreased levels of ADAMTS13 activity have been found in some of the above conditions.

Decreased ADAMTS13 activity has been often reported in other two thrombotic microangiopathic diseases: disseminated intravascular coagulation (DIC) [308,309] and haemolytic uremic syndrome (HUS) [310-312]. However, it should be noticed that ADAMTS13 activity levels in these conditions were 20-50%, rather then less then 5-10% found in TTP.

HUS has been subject of much debate, since it presents similar symptoms to TTP. HUS is usually diagnosed in young children (less then 5 years old) who present the

characteristics of haemorragic diarrhea and acute renal failure, associated with thrombocytopenia and microangiopathic haemolytic anemia. Most of the cases are caused by infections from *E. coli*, *Shigella dysenteriae* and related bacteria which produce shigatoxin. The clinical symptoms in TTP and HUS are often overlapping. Although attempts have been made to differentiate TTP from HUS on the basis of ADAMTS13 deficiency (less than 5% in TTP) [295,297,313,314], the current method of discrimination is still mainly based on the clinical diagnosis. Acute renal failure is the principle abnormality in HUS, whereas it is usually mild (if present) in TTP. HUS differs from TTP also for the nature of the microvascular thrombi: they are mainly composed of VWF and platelet in TTP, whereas of both fibrin and platelets in HUS.
To date, therefore, the sensitivity and specificity of ADAMTS13 deficiency for the diagnosis of TTP remains controversial.

1.3.6.6 ADAMTS13 activity assays

Laboratory assays should reliably identify severe ADAMTS13 deficiency (typical of TTP) and distinguish it from moderately decreased levels found in HUS or in the other conditions described in the previous Section. A critical point is the variability in the methods currently used to measure ADAMTS13 activity in different laboratories, making direct comparison among assays very difficult. In an effort of standardization, some studies have been carried out to compare several tests used in different laboratories [315,316]. To date collagen binding assay (CBA), immunoblotting of VWF multimers and ristocetin cofactor activity appeared to be the most reliable [317-320].

1.3.6.6.1 CBA

This assay is an ELISA assay, based on the preferential binding of high molecular weight VWF multimers to collagen [319]. Dilutions of the plasma sample to be analysed and of the standard plasma pool are added to normal human plasma in which ADAMTS13 was previously inactivated by EDTA and dialysed. The cleavage reaction is performed in the presence of urea and $BaCl_2$ ions and stopped at different time points. The sub-samples are then added to a microtiter plate previously coated with collagen type III. The binding is measured using a peroxidase-conjugated anti-VWF antibody. The proteolytic degradation of VWF leads to the generation of low molecular weight multimers which show impaired binding to collagen. The course of the cleavage reaction over time can be measured as a progressive decrease in collagen binding.

1.3.6.6.2 Immunoblotting of VWF multimers

Purified VWF, prepared from cryoprecipitate of normal plasma by gel filtration, is incubated with dilutions of the plasma to be tested and of the normal human plasma. The cleavage reaction is performed in the presence of $CaCl_2$ or $BaCl_2$ and stopped at different time points with EDTA. The extent of VWF degradation (visible as loss of high molecular weight multimers) is assessed by SDS-1.4% agarose gel electrophoresis, followed by Western blot using an anti-human VWF antibody [147]. An alternative method consists in the detection of N and C-terminal linked dimers (200 and 350 kDa respectively) generated after VWF cleavage. The fragments can be separated by SDS-PAGE and detected by Western blot [196].

1.3.6.6.3 VWF ristocetin cofactor activity

VWF ristocetin cofactor activity tests the ability of VWF to bind platelet GpIbα in the presence of ristocetin, measuring the agglutination of platelets. Ristocetin dimers bind both to VWF and platelets GpIbα leading to the cross-linking of platelets. High molecular weight multimers show a higher ristocetin cofactor activity. The disappearance of high molecular weight multimers after incubation with the plasma sample (containing ADAMTS13) can thus be followed over time by the diminishing of the ristocetin cofactor activity and can be compared with that obtained using a plasma standard [321].

1.3.6.6.4 ADAMTS13 cleavage of FRET-VWF73

New diagnostic tests using smaller VWF fragments as ADAMTS13 substrate have been developed. Kokame *et al* [322] reported a fluorescence resonance energy transfer (FRET) assay for ADAMTS13 activity, using a fluorescent VWF substrate where two amino acids have been modified (FRET-VWF73). One modified amino acid is able to be excited at 340 nm and the fluorescence resonance energy is transferred to the second modified amino acid which acts as a quencher. When the bond between Y1605 and M1606 is cleaved by ADAMTS13 the quencher is no more able to absorb the fluorescence then thus is emitted at 440 nm. In this way, the cleavage reaction can be monitored over time following the increase in fluorescence emission.

1.3.6.7 Knock out ADAMTS13 mice and TTP

In order to further explore the pathogenesis of TTP *in vivo*, ADAMTS13 knock out mice were generated and studied by two different groups [323,324]. In both studies, ADAMTS13 deficient mice were obtained by gene targeting. Surprisingly, ADAMTS13 homozygous mice were viable, fertile and exhibited normal survival.

Analysis of peripheal blood and tissue analysis showed no sign of thrombocytopenia, haemolytic anemia or microvascular thrombosis. However, UL-VWF multimers were detected in their plasma but not in wild type mice. Moreover, thrombus formation and growth on a collagen surface in flowing conditions was enhanced in homozygous ADAMTS13 deficient mice, compared with wild type mice [324]. Two explanations can be considered for these findings. ADAMTS13 deficiency may cause a milder phenotype in mice than in human, reflecting differences in the haemostatic system functioning in these two species. Generally, VWF multimers in mice are larger than those in humans, possibly related to higher shear rates in mice. This may explain why ADAMTS13 deficient mice are viable, whereas there are no ADAMTS13 homozygous null patients. Alternatively, ADAMTS13 deficiency may be prothrombotic, but insufficient to induce a TTP episode, suggesting additional genetic factors or environmental triggers are required to provoke the disease, both in mice and human. Indeed, Motto *et al* [323] have shown that ADAMTS13 knock out mice crossed with the CASA/Rk strain (elevated plasma VWF levels) and challenged with shigatoxin lead some of them to developed TTP-like symptoms. Similarly, Banno *et al* [324] have found that, following intravenous injection of a mixture of collagen and epinephrine, thrombocytopenia was more severely induced in ADAMTS13 knock out homozygotes than in wild type mice. Such observations may be of relevance to humans, where ADAMTS13 deficiency has been reported to be asymptomatic until adulthood [284] or where patients with identical ADAMTS13 genotypes have different symptoms [311] or where the Japanese population does not have a high frequency of TTP even though 10% of the population is heterozygous for a polymorphism (P475S) shown to be associated with lower ADAMTS13 activity *in vitro* [225]. Another recent study [325] showed the spontaneous thrombus formation in activated microvenules of ADAMTS13 deficient mice by intravital microscopy. Infusion of anti-ADAMTS13 antibodies into wild type mice resulted in a similar phenotype, with platelet aggregation and thrombus formation upon activated microvenules. Furthermore, in ADAMTS13 deficient mice, the thrombus formation upon injured arterioles was more rapid than the one observed in wild type mice. Infusion of recombinant human ADAMTS13 inhibited thrombus growth by destabilisation of platelet aggregates in both deficient and wild type mice. These results suggest that ADAMTS13 prevents thrombi in activated microvenules and modulate the thrombotic response in injured arterioles. On the base of its antithrombotic effects, recombinant ADAMTS13 should be considered as a promising alternative therapy in TTP patients.

1.4 AIMS AND LAYOUT OF MY THESIS

In the previous Sections, I have discussed the crucial role of VWF in the haemostatic response, allowing platelet tethering and adhesion at site of vascular injury. I have also highlighted the importance of the metalloproteinase ADAMTS13 in regulating VWF multimeric size and the consequent prevention of unwanted platelet plug in the circulation. In the presence of calcium ions and denaturing/high shear conditions, ADAMTS13 cleaves the peptidyl bond Y1605-M1606 in VWF A2 domain (see Section 1.3.5.1). However, little is still known about the specific interaction between the two molecules and the precise mechanism of proteolysis. In Section 1.3.4, I have presented evidence from recent studies which have investigated the binding site for VWF on ADAMTS13. These studies suggest a crucial role for the Cys-rich/spacer domain of ADAMTS13.

The aim of the present study was to investigate which domains and residues in VWF are important for its binding to ADAMTS13 and its proteolysis. My starting point was the VWF A2 domain, where the ADAMTS13 scissile bond is located. However, in view of a report implicating a role for the VWF A3 domain in binding ADAMTS13 [107], this domain was also considered. The specific aims of my study can be summarised as follows:

1) Preparation of high purity recombinant ADAMTS13
2) Optimisation of a simple and reproducible method to express and purify a large amount of recombinant VWF A2/A3 domain fragments
3) Optimisation of a reliable and quantitative technique to analyse the cleavage of the VWF fragments by ADAMTS13
4) Mutation of specific residues in VWF A2/A3 domain fragments to analyse their impact on VWF proteolysis by ADAMTS13
5) Analysis of the binding of wild type and mutant VWF fragments to ADAMTS13

In the following Chapters, I will first explain the methods I have utilised for my experiments (Chapter 2) and I will subsequently report the Results of my investigation (Chapter 3). The Results have been divided into sub-sections, each dealing with a specific issue. In each case, I will provide an introduction to explain the rationale for the experiment, then present the results, followed by a brief discussion, including limitations and advantages of the employed methods (when appropriate). In Chapter 4, the on-going and future work will be presented. Finally, in Chapter 5 a general

discussion is given, where my results are considered in broader context and where I present my working model of ADAMTS13-VWF interaction.

2. MATERIALS AND METHODS

2.1 CONSTRUCTION OF EXPRESSION VECTORS

2.1.1 ADAMTS13 expression vector

Full-length human ADAMTS13 cDNA (4.3 kb) was previously cloned by Dr. James Rance in-frame into the mammalian expression vector pcDNA 3.1/myc-His (Invitrogen) (Fig. 2.1). The pcDNA3.1 vector is 5.5 kb in length and it includes a cytomegalovirus (CMV) immediate-early promoter to drive high-level gene expression in mammalian cells, multiple cloning site, a myc epitope to facilitate immunodetection, a C-terminal polyhistidine (6xHis) tag to allow purification, an ampicillin resistance gene to perform the selection of the vector in bacteria cells and a neomycin resistance gene to allow the selection in mammalian cells, a PUC origin which allows high-copy number replication and growth in *E.coli* and a SV40 origin which allows episomal replication in cells expressing the SV40 large T antigen.

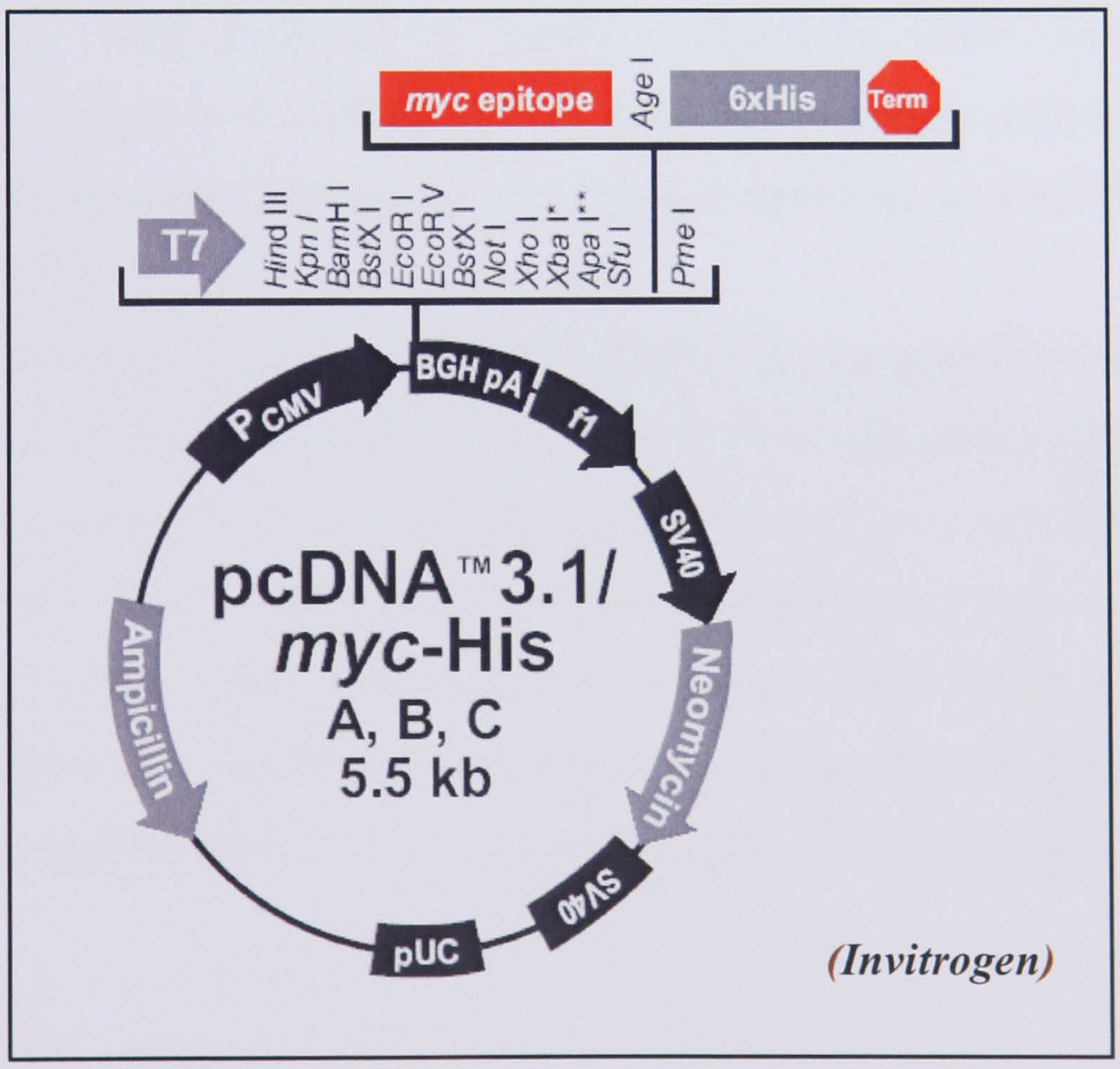


Fig. 2.1 Schematic representation of pcDNA 3.1/myc-His vector. The features of the vector are shown in the picture above: CMV promoter/priming site, multiple cloning site, myc-epitope, C-terminal polyhistidine tag, bovine growth hormone (BGH) polyadenilation signal, SV40 replication origin, SV40 promoter which allows efficient expression of the neomycin resistance gene, SV40 polyadenilation signal, pUC origin, ampicillin resistance gene. (Picture taken from Invitrogen).

2.1.2 VWF76, VWF115, VWF115-A3, VWFA2 expression vectors

2.1.2.1 Cloning of VWF fragments

Recombinant VWF fragments (VWF76, VWF115, VWF115-A3, VWFA2) (see Fig. 3.6 in Section 3.2) were cloned into two different bacterial expression vectors. VWFA2 was previously cloned by Dr Chan K.N.K Chion into pET101/D-TOPO vector (Invitrogen), which contains a 6xHis tag and a V5 epitope at C-terminus. The fragment was then sub-cloned into pTrcHisA (Invitrogen) (Fig. 2.2), a 4.4 kb vector which includes an ampicillin-resistance gene, an inducible trc promoter, one polyhistidine tag and an Xpress epitope at N-terminus. After the sub-cloning, the fragment had two polyhistidine tags, one at each terminus.

VWF76, VWF115, VWF115-A3 were cloned into pET100/D-TOPO vector (Invitrogen) (Fig. 2.3), which is 5764 bp in length and contains an ampicillin-resistance gene for selection in *E. coli*, an inducible T7 promoter for high-level expression, a 6xHis tag at the N-terminus for purification and an Xpress epitope to allow detection with a specific antibody.

All the fragments were prepared by specific polymerase chain reaction (PCR) amplification, as described in Section 2.1.2.4. PCR products were analysed using 1% agarose gel electrophoresis (see Section 2.1.2.5) and thereafter purified from the gel (see Section 2.1.2.6).

After PCR amplification, VWF76, VWF115, VWF115-A3 fragments were cloned into pET100/D-TOPO, which is an open vector with a blunt end and a protruding end (GTGG), which anneals with the sequence CACC present on a 5'-terminus of the insert (see Section 2.1.2.4). Both vector ends are covalently bound to *Vaccinia* virus topoisomerase I, which catalyses the ligation reaction. The cloning reaction was performed as follows. 0.5-4 µl PCR product, 1 µl salt solution (Invitrogen), 1 µl vector and water to a final volume of 6 µl were incubated at room temperature for 10 minutes.

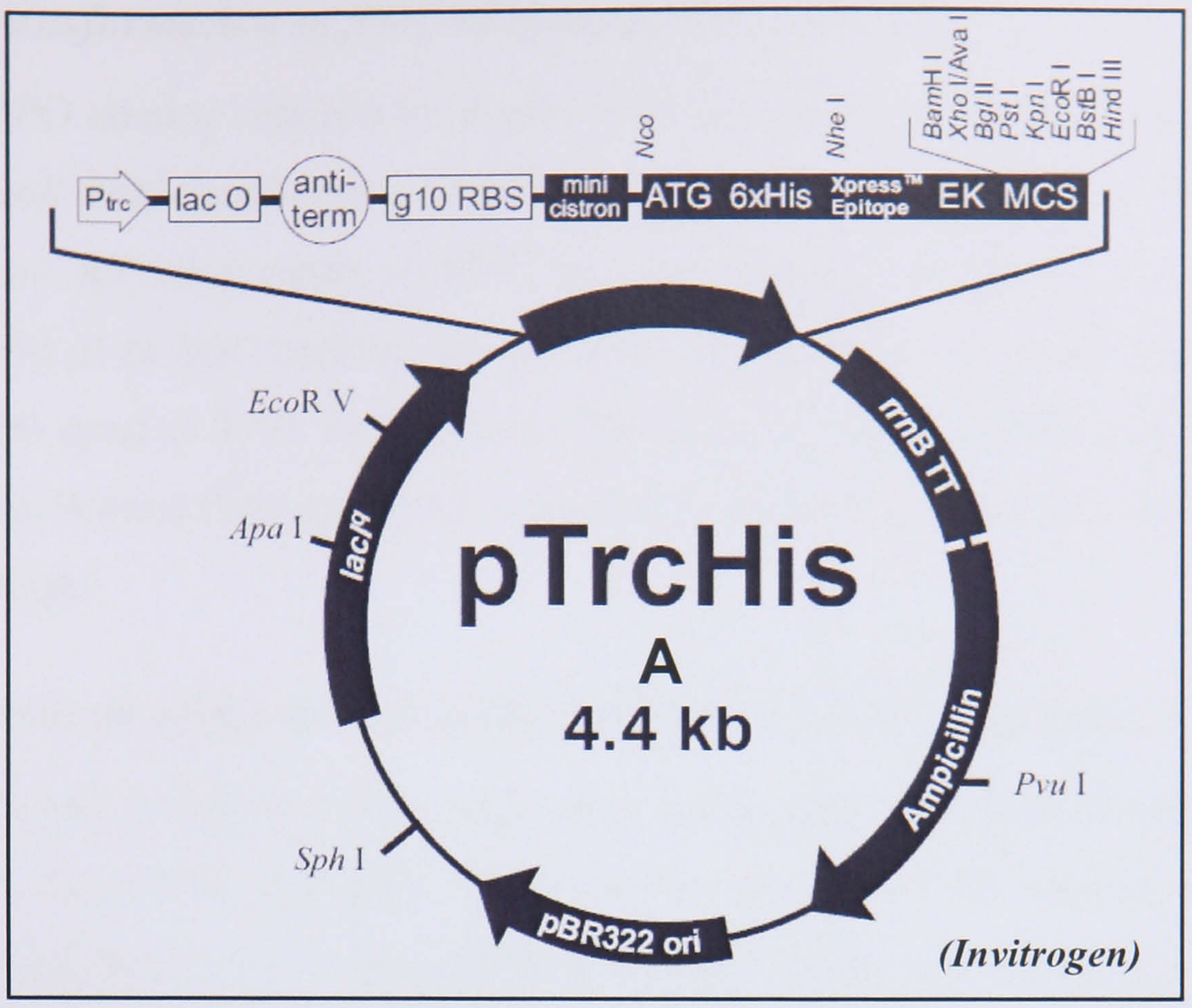


Fig. 2.2 Schematic representation of pTrcHisA vector. The features of the vector are shown in the picture above: trc promoter, lac operator (lacO), ribosome binding site (RBS), initiation codon ATG, 6xHis tag, Xpress epitope, enterokinase (EK) recognition site, multiple cloning site, rrnB transcription termination sequence, ampicillin resistance gene, pBR322 replication origin which allows low-copy number replication in *E.coli*, lacI Open Reading Frame (ORF) encoding for the lac repressor. (Picture taken from Invitrogen).

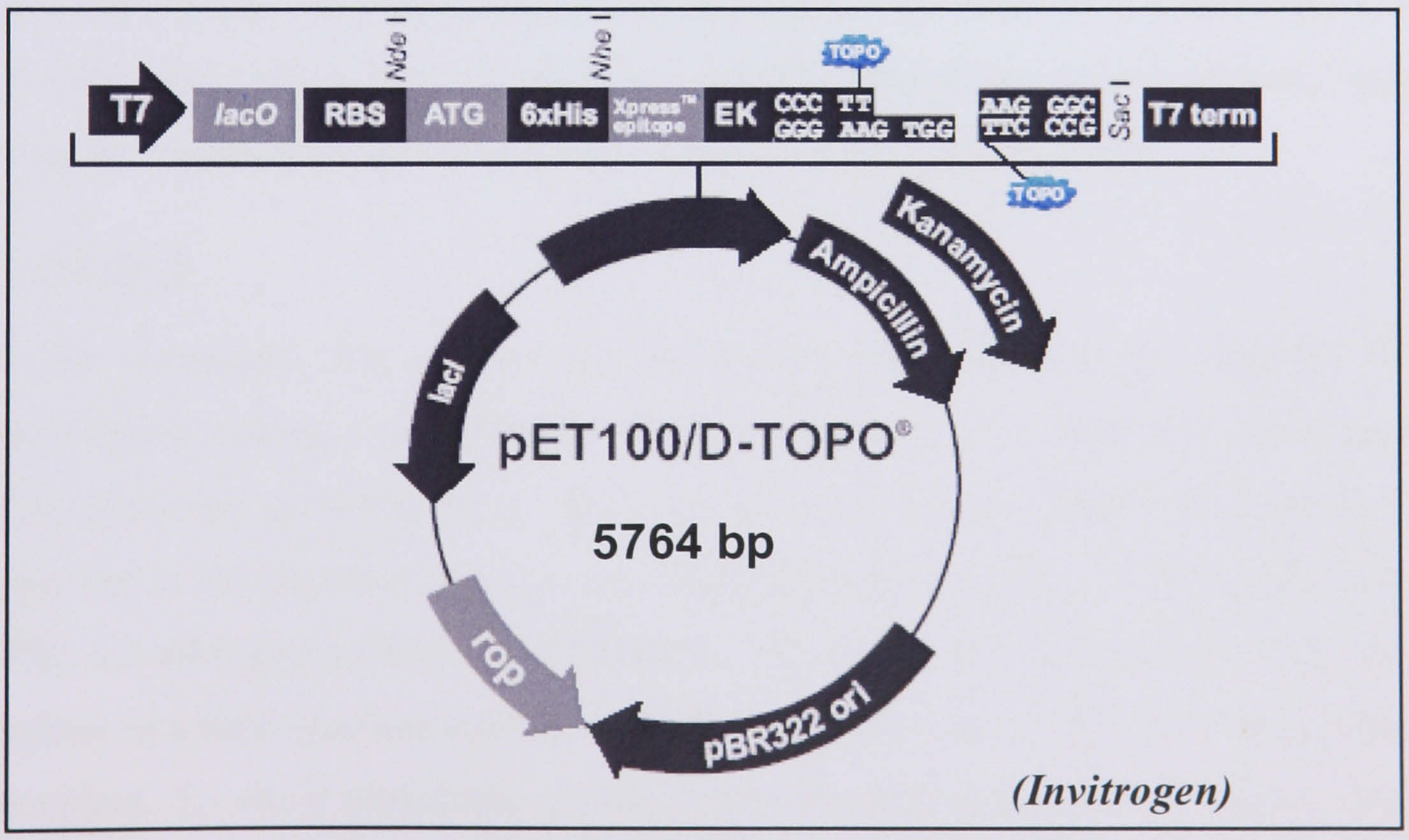


Fig. 2.3 Schematic representation of pET100/D-TOPO vector. The features of the vector are shown in the picture above: T7 promoter/priming site, lacO, RBS, initiation codon ATG, 6xHis tag, Xpress epitope, EK recognition site, TOPO cloning site, T7 reverse priming site and transcription termination region, ampicillin resistance gene, pBR322 replication origin for low-copy number replication in *E.coli*, lacI ORF. (Picture taken from Invitrogen).

2.1.2.2 Transformation of TOP10 competent E.coli cells

3 µl of TOPO cloning reaction were used to transform 50 µl of chemically competent TOP10 *E.coli* cells (Invitrogen). After incubation on ice for 20 minutes, the cells were heat-shocked for 30 seconds at 42ºC and immediately transferred on ice for two minutes. 250 µl of SOC medium (Invitrogen) was added to the transformed cells and shaken (200 rpm) at 37ºC for one hour. 50-250 µl of liquid culture was then plated onto a Luria-Bertani (LB) agar plate, containing 100 µg/ml ampicillin and incubated at 37ºC overnight.

2.1.2.3 Analysis of the transformants by Nhe I and Sac I digestion

After collecting 6 colonies from each plate and performing plasmid extraction (see Section 2.1.5), a first screening to ensure the success of the cloning of VWF76, VWF115 and VWF115-A3 into pET100/D-TOPO vector was obtained by digesting the minipreps with the Nhe I and Sac I restriction endonucleases (New England Biolabs). As shown in Fig. 2.3, the two enzymes cut in close proximity to the cloning site. Approximately 1 µg of each vector were digested with 10 units (U) Nhe I and 10 U Sac I, in the appropriate 1X buffer (NEB), 1X bovine serum albumin (BSA) in a final volume of 20 µl. The reaction mixtures were incubated at 37ºC for 2 hours. The digested reaction was then analysed on a 1% agarose gel (see Section 2.1.2.5). If the insert was correctly cloned, a band corresponding to the insert size was detected on the gel. Otherwise, only a band of 5687 bp corresponding to the cleaved parental vector appeared. The positive clones were then sequenced (see Section 2.1.7).

2.1.2.4 PCR

All the fragments that needed to be cloned were prepared by specific PCR amplification, using a high-fidelity DNA polymerase (Platinum *Pfx*, Invitrogen), which possesses proofreading 3' to 5' exonuclease activity. The PCR reaction was performed in the presence of 1-2 U of platinum *Pfx* polymerase, 1X *Pfx* amplification buffer, 0.3 mM (each) dNTP, 1 mM $MgSO_4$, 15 pmol of each primer and 150 ng DNA template in a final reaction volume of 50 µl. The full-length VWF cDNA was used as a template. To allow directional cloning, each forward primer included the sequence CACC at its 5` end (in frame with the ATG present in the pET100/D-TOPO vector), which pairs with the overhang complementary sequence on the vector (see Section 2.1.2.1). The reverse primer contained a stop codon in its 5` end. Primers were generated and their purity assessed by HPLC (Thermo Electron Corporation,

Germany). Primers sequences and annealing temperatures (Ta) are listed in Table 1 in the Appendix I. The cycling conditions are shown below, in Table 2.1. The PCR cycles were performed using a GeneAmp PCR system 2700 (Applied Biosystems).

	Cycles	***Temperatures***	***Time***
Initial denaturation	1	94°C	5min
Denaturation ***Annealing*** ***Extension***	30	94°C Ta 68°C	30sec 30sec 1min
Final Extension	1	68°C	10min

Table 2.1 PCR cycling conditions used to amplify the VWF fragments. PCR consists of an initial denaturation step (94°C), followed by 30 cycles of denaturation (94°C), re-annealing (Ta for each fragment are listed in Table 1 in the Appendix I) and extension (68°C), and a final extension step (68°C).

2.1.2.5 Agarose gel electrophoresis

Agarose gel electrophoresis allows the separation of double-strand DNA fragments according to their size. When a direct current is applied to the gel, DNA (negatively charged) migrates towards the positive electrode. Agarose gels were prepared at a final agarose concentration of 0.8-1% (w/v) in 1X Tris-borate-EDTA (TBE) buffer. The concentration was established depending on the size of the DNA fragments to be separated. Agarose was dissolved by heating in the microwave oven. The agarose was cooled and ethidium bromide (a fluorescent dye which intercalates between bases of DNA and RNA) was added to a final concentration of 5 µg/ml. After being cast and set, gels were immersed in 1X TBE. An appropriate amount of loading buffer was added to each sample and applied to the wells of the gel. The loading buffer contained glycerol to allow the sample to deposit into wells, and bromophenol blue and xilene cyanol (see Appendix II), two tracking dyes which migrate in the gel and allow visual monitoring of how far the electrophoresis has proceeded. In each run, a DNA ladder (1kb or 100bp) (NEB) was used to identify the precise molecular weight of the samples. Gels were electrophoresed at 60-70 V for 30-60 minutes and DNA fragments

were then visualised using an ultraviolet (UV) transilluminator lightbox (fotoprep II Fotodyne).

2.1.2.6 Gel extraction of DNA

The band containing the desired fragment was excised from the agarose gel using a scalpel. The purification was performed using the QIAquick gel extraction kit (QIAgen). The gel slice was weighed and 3 volumes of the solubilisation and binding Buffer QG were added. The sample was incubated for 10 minutes at 50°C until the gel slice had been dissolved. After the addition of 1 volume of isopropanol, the sample was applied to a resin column (silica-gel membrane) to bind DNA. The addition of isopropanol increases the yield of DNA fragments smaller than 500 bp or bigger than 4 kb. The sample was centrifuged for 1 minute at 13 000 rpm (~17 900 x g) in a microcentrifuge 5417R (Eppendorf) and the flow-through was discarded. During this step, DNA is adsorbed to the silica-membrane, whereas contaminants (primers, nucleotides, enzymes, agarose, dyes and ethidium bromide) pass through the column. 0.5 ml of Buffer QG were applied to the column and centrifuged for 1 minute. This step allows the removal of all the traces of agarose. A washing step was then performed, adding 0.75 ml of Buffer PE and centrifuging for 1 minute twice. The DNA was finally eluted, adding 50 µl of Buffer EB (10 mM Tris-Cl, pH 8.5) and centrifuging for 1 minute.

2.1.3 Generation of VWF115 and VWF115-A3 mutant constructs

Two adjacent cysteines (C1669 and C1670) in VWF115-A3 were converted into alanines, in order to ensure the formation of the right disulphide bond (C1686-C1872) and, consequently, the right folding of the molecule (see Sections 3.2.2 and 3.2.3.3).
Some type 2A mutations (group II) (R1597Q, R1597W, D1614G, I1628T, G1629R, E1638K) were individually introduced into VWF115 (see Section 3.4). Some charged residues on the surface of a predicted model of A2 domain (R1583, D1587, D1614, E1615, K1617, E1638, E1640) were also selected to be individually mutated to alanine into VWF115 (see Section 3.5). Also a triple mutant (DEK1614/5/7AAA) was generated.
All the above mentioned mutations were introduced into VWF115 or VWF115-A3 pET100/D-TOPO vectors using the QuikChange® XL site-directed mutagenesis kit (Stratagene).

2.1.3.1 Site-directed mutagenesis

QuikChange® XL site-directed mutagenesis kit (Stratagene) was used to introduced mutations in the VWF115 and VWF115-A3 pET100 vectors. PCR reaction was performed using 2.5 U of high fidelity *Pfu* Ultra DNA polymerase, 125 ng of complementary primers containing the mutation of interest, 10 ng of ds DNA template (VWF115 or VWF115A3 pET100/D-TOPO), 1X reaction buffer, 10 mM dNTP, 3 µl of QuikSolution in a final volume of 50 µl. The primers used in each amplification reaction are shown in Table 2 in the Appendix I, with the introduced mutation underlined and in bold. The PCR amplification consisted in an initial denaturation (95°C, 1 minute); 18 cycles of denaturation (95°C, 50 seconds), annealing (60°C, 50 seconds) and extension (68°C, 10 minutes); and a final extension at 68°C for 7 minutes. Subsequently, PCR products were digested with 10 U of Dpn I for 2 hours at 37°C, in order to remove the methylated parental DNA template (without desired mutation).

2.1.3.2 Transformation of XL10-Gold ultra competent E.coli cells

1 µl of the digestion reaction was then used to transform 20 µl XL10-Gold ultra competent *E.coli* cells (Stratagene), and then incubated on ice for 30 minutes. The cells were heat-shocked at 42ºC for 30 seconds and placed immediately on ice for two minutes. 200 µl of SOC medium was added to the transformed cells and they were incubated at 37ºC, for 1 hour, with shaking (250 rpm). 150 µl of the transformed liquid culture was then plated onto a LB agar plate containing 100 µg/ml ampicillin and incubated at 37ºC overnight. The next day, colonies were collected from each plate and plasmid extraction was performed as described in Section 2.1.5. The presence of the desired mutation was checked by sequencing (see Section 2.1.7).

2.1.4 Generation of mutant VWFA2 constructs

2.1.4.1 Sub-cloning of D1587A, D1614A and E1615A into VWFA2 pTrcHisA vector

Mutations D1587A, D1614A and E1615A introduced in the VWF115 pET100/D-TOPO vector were then sub-cloned in the VWFA2 pTrcHisA vector, as it is schematically represented in Fig 2.4. Both VWF115 (D1587A, D1614A, E1615A) pET100 and VWFA2 pTrcHisA vectors (approximately 1µg of each) were sequentially digested with 10 U KpnI and 10 U PvuI restriction endonucleases (New

England Biolabs), in the appropriate 1X buffer (NEB), 1X BSA in a final volume of 30 µl. The reaction mixtures were incubated at 37°C for 2 hours. In order to prevent the recircularisation of the vector during the ligation reaction, the linearised vector was first dephosphorylated using 5 U Calf Intestinal Alkaline Phosphatase (Invitrogen), in the appropriate provided buffer and incubated at 37°C for one hour. This enzyme catalyses the removal of 5'-phosphate groups from both ends of the linearised vector, leaving it with 5'-hydroxyltermini. Both digestion products were run on a 0.8% agarose gel (see Section 2.1.2.5). A 1.2 kb band, from the digestion of each mutated VWF115 pET100 vectors, and one of 3.6 kb, from the digestion of VWFA2 pTrcHisA vector, were excised and purified from the gel, as described in Section 2.1.2.6, and respectively used as insert and vector in the following ligation step. The reaction was performed using a molar ratio of 3:1 insert to vector, in the presence of 0.5 U T4 DNA ligase (Invitrogen) and 1X ligation buffer, in a final reaction volume of 20 µl. The enzyme catalyses the formation of phosphodiester bonds between adjacent 3'-hydroxyl and 5'-phosphate termini. Each ligation reaction was incubated at room temperature for 90 minutes. The region of the vector containing the C-terminal His-tag was cut with the sub-cloning procedure and the final vector contained only the N-terminal His-tag.

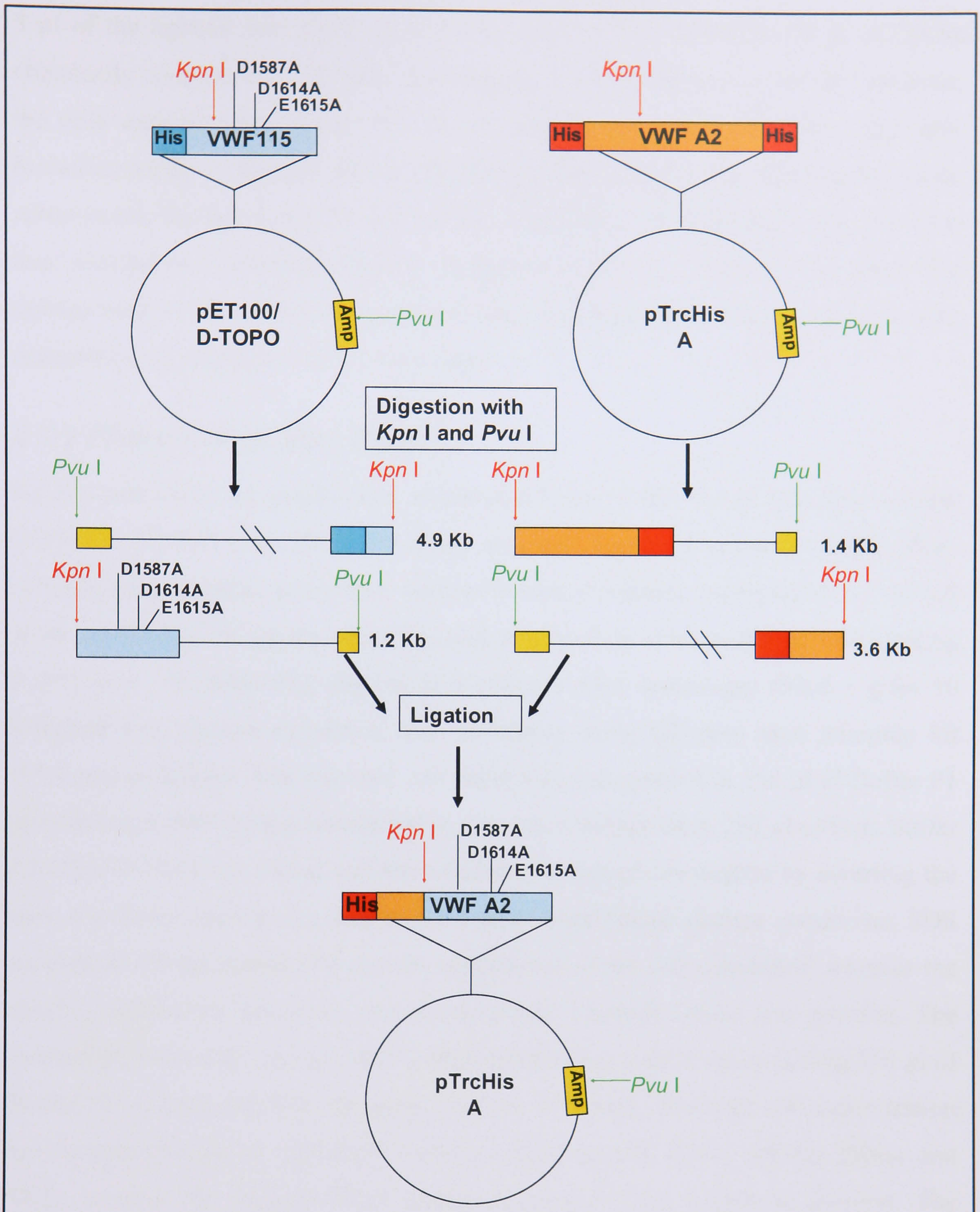


Fig. 2.4 Schematic representation of sub-cloning of D1587A, D1614A and E1615A into VWFA2 pTrcHisA vector. The maps of VWF115 pET100 (with the individual mutation D1587A, D1614A or E1615) and VWFA2 pTrcHisA vectors are shown in the top part of the picture. The two vectors were digested with Kpn I and Pvu I, giving the illustrated cleaved products. Ligation of the 1.2 kb and 3.6 kb products originated the vector shown in the bottom part of the picture, VWFA2 pTrcHisA carrying one of each mutation. The final vector encodes for VWF fragments with only one N-terminal His-tag.

2.1.4.2 Transformation of DH5α competent E.coli cells

5 µl of the ligation mix (1-10 ng of DNA) were used to transform 50 µl of DH5α chemically competent *E.coli* cells (Invitrogen). After incubation on ice for one hour, the cells were heat-shocked at 37°C for 20 seconds and immediately after they were placed on ice for 2 minutes. 950 µl of LB broth were added to the cells and they were subsequently incubated at 37°C for one hour, with shaking (250 rpm). The cells were then pelleted in a microcentrifuge at maximum speed for 2 minutes. The pellet was resuspended in 100 µl of LB and plated onto a LB agar plate containing 100 µg/ml ampicillin and incubated at 37°C overnight.

2.1.5 Plasmid extraction: miniprep

Small-scale analytical preparations of plasmid DNA (VWF76/wild type and mutated VWF115/ VWF115-A3 pET100 vectors and wild type and mutated A2 pTrcHisA vectors) were prepared as follows. Isolated bacterial colonies were placed in 7 ml LB broth containing 100 µg/ml ampicillin and incubated at 37°C overnight with shaking (~250 rpm). The following day bacterial cultures were centrifuged (5000 x g for 10 minutes) and plasmid extraction was performed using QIAprep spin miniprep kit (QIAgen) as follows. The bacterial cell pellet was resuspended in 250 µl of Buffer P1 (containing RNase A) and transferred to a microcentrifuge tube. 250 µl of lysis Buffer P2 (NaOH/SDS) was added and the solution was mixed thoroughly by inverting the tube 4-6 times. During this step bacteria were lysed under alkaline conditions: SDS solubilised phospholipids and protein components of the cell membrane, whereas the alkaline conditions denatured chromosomal and plasmid DNAs and proteins. The lysate was neutralised and adjusted to high-salt binding conditions by adding 350 µl of Buffer N3 and mixing it by inverting the tube 4-6 times. The high salt concentration led to precipitation of denatured proteins, chromosomal DNA, cellular debris and SDS, whereas the plasmid DNA renatured correctly and stayed in solution. The solution was centrifuged for 10 minutes at 13 000 rpm in a microcentrifuge, leading to the formation of a compact insoluble pellet. The supernatant was then applied to a QIAprep spin column and centrifuged for 1 minute. During this step, DNA was absorbed onto the silica membrane of the column. The flow-through was discarded and the column washed by adding 0.5 ml of Buffer PB and subsequently 0.75 ml of Buffer PE. The elution of DNA was performed adding 50µl of Buffer EB to the centre of the column, followed by 1 minute centrifugation. The typical yield from miniprep was 5-10 µg (concentration 100-200 ng/µl).

2.1.6 Plasmid extraction: maxiprep

For large-scale plasmid extraction (ADAMTS13 pcDNA 3.1/myc-His vector). a 100 ml cell culture in LB broth was grown, shaking overnight at 37°C. Bacterial cells were then harvested by centrifugation at 5000 x g for 15 minutes at 4°C and plasmid maxiprep purification was performed using Endofree plasmid maxi kit (QIAgen). The bacterial pellet was resuspended in 10 ml of buffer P1 (containing RNase A) and subsequently 10 ml of lyses Buffer P2 was added to the solution, mixed by inverting the tube 4-6 times and incubated at room temperature for 5 minutes to allow alkaline lysis to take place. The lysate was neutralised by adding 10 ml of chilled Buffer P3 and mixing it by inverting the tube 4-6 times. This step led to precipitation of cell debris, proteins, genomic DNA and detergents, whereas the plasmid DNA stayed in solution. The lysate was poured into the barrel of the QIAfilter Cartridge, incubated at room temperature for 10 minutes and filtered. 2.5 ml of Buffer ER were added to the filtered lysate, mixed by inverting the tube 10 times and incubated on ice for 30 minutes. Buffer ER is a specific endotoxin removal buffer, which prevents lipopolysaccharides molecules from binding to the resin in the following step. The filtered lysate was then applied to the QIAgen-tip 500, which is an anion-exchange resin which binds to plasmid DNA under appropriate low-salt and pH conditions. The column was previously equilibrated by applying 10 ml of the equilibration Buffer QBT, which ensured low salt conditions and pH 7. The lysate was filtered trough the column by gravity flow. Two washing steps were then performed adding 30 ml of Buffer QC. Plasmid DNA was eluted from the column in 15 ml of high-salt buffer (Buffer QN) and then concentrated and desalted by isopropanol precipitation (10.5 ml of 0.7 volumes of isopropanol and centrifugation at 15 000 x g for 30 minutes at 4°C). The pellet was then washed with 10 ml of 70% ethanol and centrifuged at 15 000 x g for 10 min. The pellet was then redissolved in a suitable volume of Buffer TE.

To determine the yield of the purification, the optical density (OD) was measured at 260 nm, using UV-1601 spectrophotometer (Shimadzu). Purity was checked by the OD_{260nm}/OD_{280nm} ratio (DNA/protein). A ratio equal or bigger than 1.8 provided a pure DNA preparation, whereas a lower ratio suggested protein contamination.

A simple equation was employed to calculate DNA concentration:

DNA (μg/ml) = D x A x K, where

D is the dilution factor, A is the absorbance at 260 nm, K is a constant (Boltzmann constant) and its value is 50. A double-strand DNA at a concentration of 50 μg/ml has an OD of 1 at 260 nm.

Yields were in the range of 300-500 μg.

2.1.7 Sequencing

All the vectors generated were verified by sequencing to ensure the absence of any unwanted PCR-introduced errors and to check the presence of the correct insert or the mutation introduced by site-directed mutagenesis. The primers used for sequencing are listed in Table 3 in the Appendix I. DNA sequencing was performed at the Imperial College-MRC Genetics Core Facility using ABI 3700 DNA analyser (Perkin-Elmer).

2.1.8 Glycerol stock

To store bacteria transformed with the vector constructs, 900 μl of the liquid culture was placed into 100 μl glycerol (Sigma), to prevent the formation of ice crystals, vortexed and stored at –70°C.

2.2 EXPRESSION AND PURIFICATION OF RECOMBINANT PROTEINS

2.2.1 ADAMTS13 expression

The ADAMTS13 pcDNA 3.1/myc-His construct was stably expressed in human embryonic kidney fibroblast (HEK) 293 cells. Stable transfection allowed the generation of a large amount of protein that, after purification (see Section 2.2.2), could be used for all the activity and binding assays (see Sections 2.3 and 2.4).

2.2.1.1 Cell culture: general routine

All cell culture experimentation was carried out in a class II flow cabinet (FASTER BHG 2004, JENCONS-PLS), using aseptic techniques, in a designated laboratory. All surfaces of the flow cabinet and incoming materials (flasks, tubes, bottles) were thoroughly cleaned with 70% ethanol before starting, to reduce the possibility of contamination of culture.

Each cell line was grown in humidified incubators (BIOHIT, Biological Instrumentation Service, Lancashire, UK) set to 37°C, in an atmosphere containing 5% CO_2. Each incubator contained a tray with an aqueous, saturated solution of copper sulphate (BDH), which maintained humidity and prevented against contamination.

Frozen cells were kept in a liquid nitrogen container, at a temperature around -180°C.

Cultured cells were visualised under an inverted microscope CK2 (Olympus, Japan).

2.2.1.2 Reviving HEK293 cells from liquid nitrogen

HEK293 cells stored in 10% Dimethyl Sulfoxide (DMSO) (SIGMA) in liquid nitrogen (see Section 2.2.1.5) were thawed at room temperature and centrifuged at 100 x g for 5 minutes, in order to remove residual DMSO and dead cells. The medium was decanted and the cell pellet resuspended in fresh growth medium consisting of Eagle Minimal Essential Medium (EMEM) (Sigma) supplemented with 10% Fetal Bovine Serum (FBS) (Biosera), 5 mM Penicillin/Streptomycin (Invitrogen), 5 mM L-Glutamine (Invitrogen) and 1X non-essential amino acids (NEAA) (Sigma). HEK293 cells were then seeded into a small (T25) tissue culture flask (Nunc) and incubated at 37°C and 5% CO_2 until cells had reached the desired confluence.

2.2.1.3 Cell passages

Once HEK293 cells had reached full confluence on the flasks/plate, adherent cells were passaged and seeded into larger tissue culture flasks. Cells were washed twice with autoclaved Phosphate Buffered Saline (PBS) (Sigma), detached from the surface using 0.25% trypsin/EDTA (Sigma). Trypsin was added in the amount necessary to cover the cells layer and the excess was immediately removed. The cells were then incubated for 5 minutes at 37°C. Trypsin was inactivated adding serum containing growth medium and the cells seeded into a larger tissue culture flask (Nunc).

2.2.1.4 Stable transfection

Stable transfection allows the identification and growth of cells that have stably integrated plasmid DNA into one or more sites in the host's chromosomes. After DNA transfection, cells are subjected to selective pressure. Subsequently, colonies that are resistant to the selective antibody are isolated. The purpose of stable transfection is to generate an individual clone containing the transfected DNA permanently integrated into the chromosome.

Plasmid DNA was stably transfected into HEK293 cells by my colleague Jonathan Lam using the lipofectin reagent (Invitrogen), a liposome preparation formulated from cationic lipids. $2x10^5$ HEK293 cells were seeded into a 3.5 cm^2 (6 well) dish and grown in 2 ml of growth media for 24 hours at 37°C with 5% CO_2 until cells were 30-50% confluent. 4 µg plasmid DNA was mixed with 100 µl Optimem serum-free medium (Invitrogen) and in a separate reaction 1 µg lipofectin was mixed with 100 µl Optimem. Both reactions were incubated at room temperature for 30 minutes. Subsequently, the two solutions were combined and incubated at room temperature for

15 minutes. During the incubation, HEK293 cells were washed twice with 2 ml sterile PBS buffer and resuspended in 1.8 ml Optimem. The lipofectin/DNA mix was then added to the cells and incubated overnight at 37°C with 5% CO_2. The following day, the DNA-containing medium was removed and replaced with fresh complete growth medium. They were then incubated at 37°C with 5% CO_2 until fully confluent. HEK293 cells were then trypsinised and seeded onto a 10 cm^2 dish with growth medium containing 50 µg/ml of the antibiotic geneticin G418 (Sigma), a neomycin analogue that selects for transfected cells. The growth medium supplemented with G418 was replaced every two days to maintain the selective pressure. A non-transfected control was used as a negative control to indicate when clones could be selected. Screening of high expressing clones was done using ADAMTS13 ELISA (see Section 2.2.6) and verified by Western blotting (see Section 2.2.9). The selected clones were then expanded progressively in T25, T75, T175 cm^2 flasks and finally to a T175 cm^2 triple flask (Nunc). When the cells were 80-90 % confluent, the growth medium was then replaced with Optimem medium supplemented with a protease inhibitor cocktail (SIGMA) and incubated for 3-4 days at 37°C 5%CO_2. The protease inhibitor cocktail is a mixture of six protease inhibitors (aprotinin, 4-(2-aminoethyl) benzenesulfonyl fluoride, bestatin hydrochloride, N-(trans-epoxysuccinyl)-L-leucine-4-guanidinobutylamide, leupeptin hemisulfate salt and pestatin A) with a broad specificity for serine, cysteine and acid proteases and aminopeptidases and it is useful to prevent the degradation of the secreted proteins. The conditioned medium was then collected and filtered through a 0.5 mm Nalgene filter to remove cell debris.

2.2.1.5 Cryopreservation of cell lines

For long-term storage of cells in liquid nitrogen, cell lines were trypsinised and resuspended in growth medium containing EMEM, 2 mM L-Glutamine, 1X NEAA, 10% FBS and 10% DMSO (Sigma). DMSO protects cells from rupture by formation of ice crystals at low temperatures. 1 ml aliquots of the cell suspension were stored in cryovials (Nunc) and placed in an appropriate freezing container with 200 ml isopropanol (VWR) and stored at –70°C overnight. This assured slow freezing of cells (about 1°C per minute). These were then stored in liquid nitrogen.

2.2.2 ADAMTS13 purification

2.2.2.1 Desalting of conditioned medium

Filtered serum-free conditioned medium (see Section 2.2.1.4) was concentrated and desalted using a Hi Prep^{TM} 26/10 desalting column (Amerham Pharmacia, UK) coupled to an AKTA FPLC machine (Amerham Pharmacia, UK). This column uses the principle of gel filtration chromatography to separate high molecular weight (> 5 kDa) from low molecular weight (<1 kDa) molecules. It allows rapid exchange of buffers or salts in protein preparation: protein larger than 5 kDa do not enter the beads and remain in the mobile phase, which can have a different salt and buffer composition than that originally present in the protein sample. In contrast, small molecules such as small proteins and salts are retained inside the beads of the resin, and they will be eluted afterwards.

The column was washed with 256 ml ddH_2O at 18ml/min before being equilibrated with the desired buffer (20 mM Tris-HCl (pH 7.8), 500 mM NaCl and 20 mM imidazole). The early fraction containing proteins was collected and kept.

2.2.2.2 Nickel affinity chromatography and gel filtration chromatography

Thereafter, ADAMTS13 was purified by nickel affinity chromatography on a 5 ml Ni^{2+}His trap chelating column (Amersham Pharmacia, UK). This column allowed the His-tagged fusion proteins to bind, whereas most contaminant proteins did not. Briefly, the desalted medium was passed over the nickel-chelating column, washed with 15 ml 20 mM Tris-HCl (pH 7.8), 500 mM NaCl and 35 mM imidazole and eluted with 20 mM Tris-HCl (pH 7.8), 500 mM NaCl and 500 mM imidazole. The eluted fraction was dialysed into 20 mM Tris-HCl (pH 7.8), using 10 kDa molecular weight cut-off dialysis membrane (Pierce). High purity ADAMTS13 preparation was required in some experiments. In these particular cases, ADAMTS13 was further purified by my colleague Jonathan Lam, using a Superdex^{TM} 200 HR 10/30 gel filtration column (Amersham Pharmacia). The column is composed of cross-linked porous agarose beads and dextran, which allow separation of proteins in the range of 10-600 kDa. The sample is injected into the column in 20 mM Tris-HCl (pH 7.8) and 150 mM NaCl at a flow rate of 0.25 ml/min. The slow flow rate is required to have a good resolution of the peaks.

To analyse the amount and the purity of the purification, the sample was subjected to SDS-PAGE (see Section 2.2.7) on a 4-15% Tris-HCl polyacrylamide gel and analysed

by Coomassie staining (see Section 2.2.8) and by Western blot analysis. Western blot analysis was performed as described in Section 2.2.9, using a monoclonal antibody specific for the protease domain or an anti-myc epitope antibody. ADAMTS13 was then quantified using a total protein BCA assay (see Section 2.2.5) or a specific ELISA (see Section 2.2.6).

2.2.3 Expression of recombinant VWF fragments in E. coli cells

2.2.3.1 Overview of expression in Rosetta and Rosetta Gami DE3 E.coli cells

Wild type VWF76, wild type and mutant VWF115 and VWFA2 fragments were expressed in Rosetta DE3 *E.coli* cells (Novagen). These cells have been genetically modified by the addition of sequences encoding eukaryotic tRNA species that are rare in bacteria, which encourage eukaryotic protein synthesis. VWF 115-A3 was expressed in Rosetta Gami DE3 *E.coli* cells (Novagen). These particular cells allow cytoplasmic disulphide bond formation, since they have mutations that inactivate the reducing enzymes present in the cell (glutathione reductase and thioredoxin reductase). Both cell strains carry the DE3 bacteriophage lambda lysogen, which includes the *lacI* gene and the *T7 RNA polymerase* gene under the control of lacUV5 promoter. The expression of T7 RNA polymerase is necessary to drive the expression of the gene of interest in the pET100 vector (see Fig. 2.3 in Section 2.1.2.1), whereas the expression of the gene in the pTrcHisA (see Fig. 2.2 in Section 2.1.2.1) just requires the *E.coli* RNA polymerase. The lac repressor (encoded by *lacI*) binds to the lac Operator region and represses the expression of both the gene of interest and T7 RNA polymerase (in pET100 vector). Induction of expression can be achieved using isopropyl-β-D-thiogalactoside (IPTG), a synthetic inducer, which can bind to the lac repressor protein, causing an allosteric change in it. The lac repressor dissociates from the lac Operator region, allowing the transcription of the gene of interest by RNA polymerase.

2.2.3.2 Transformation of competent Rosetta/Rosetta Gami cells

20 µl of competent Rosetta/Rosetta Gami cells were transformed with ~ 1 ng of the vector containing the fragment of interest. After incubation on ice for 5 minutes, the cells were heat-shocked at 42°C for 30 seconds and immediately after they were placed on ice for 2 minutes. 80 µl of SOC medium was added to the cells and they were subsequently incubated at 37°C for one hour, with shaking (250 rpm). The cells were then plated onto a LB agar plate containing 100 µg/ml ampicillin and incubated at 37°C overnight.

2.2.3.3 Expression of VWF fragments in Rosetta/Rosetta Gami cells

Isolated bacterial colonies were placed in 10 ml of LB broth containing 100 μg/ml ampicillin and incubated at 37°C with shaking (~250 rpm). The culture was grown to an OD_{600nm} ~ 0.6-1, which corresponds to the exponential phase of bacterial growth. The bacterial culture was then used to inoculate 1L 2X YT broth, a rich medium optimal for favouring protein synthesis. The culture was grown to an OD_{600nm} ~ 0.6-1 and the expression of the recombinant protein was induced adding 1 mM IPTG for 16 hours. Bacterial cells were harvested by centrifugation (5000 x g for 30 minutes at 4°C). The supernatant was discarded and the cell pellet stored at -70°C.

2.2.4 Purification of VWF fragments

2.2.4.1 Isolation of inclusion bodies and soluble citoplasmatic fraction

If the recombinant protein assumed the correct folding, it was likely to be found soluble in the cytoplasm, whereas if it was miss-folded (and therefore insoluble) it was sequestered in inclusion bodies. Cell pellets were lysed using BugBuster reagent, Benzonase® Nuclease and rLysozyme™ Solution (Novagen). BugBuster reagent is a mixture of non-ionic detergents capable of cell wall perforation. Addition of rLysozyme™ Solution enhances the efficiency of protein extraction, as this enzyme specifically catalyses the hydrolysis of bacterial cell wall components. Benzonase® Nuclease is an endonuclease which degrades all forms of DNA and RNA and thus reduces the viscosity of the preparation. After centrifugation, the bacterial cell pellet was resuspended in BugBuster reagent (5 ml reagent/g wet cell paste). 1 μl (25 U) of Benzonase® Nuclease per 1 ml of BugBuster reagent was added. rLysozyme™ Solution was also added in order to have a final concentration of 1 KU/ml. The cell suspension was incubated on a shaking platform for 30 minutes at room temperature. Centrifugation at 5000 x g for 30 minutes allowed the separation between soluble and insoluble fraction (inclusion bodies). To purify proteins from the insoluble fraction, the inclusion body pellet was resuspended in 5 ml BugBuster reagent/g wet cell paste and rLysozyme™ Solution (1 KU/ml) added. After 10 minutes incubation, sequential centrifugation and washing steps using 1:10 diluted BugBuster were required to obtain a clean inclusion body pellet. Both the soluble and the inclusion body fractions were analysed by SDS-PAGE followed by Coomassie staining (see Sections 2.2.7 and 2.2.8). VWF 115-A3, wild type and mutant VWF115 and wild type and mutant

VWFA2 were predominantly present in the insoluble fraction, whereas VWF76 was in the soluble cytoplasmic fraction.

2.2.4.2 Nickel affinity chromatography

The soluble VWF76 protein was directly loaded onto a nickel-chelating column (Amersham Pharmacia), previously equilibrated with a buffer containing 20 mM Tris-HCl (pH 7.8), 500 mM NaCl and 20 mM imidazole. This column allowed the binding of the His-tagged VWF76, whereas most of bacterial proteins could not bind. A stringent washing step using a buffer containing 20 mM Tris-HCl (pH 7.8), 500 mM NaCl and 35 mM imidazole was performed to elute eventual bacterial proteins bound to the column. VWF76 was then eluted using a buffer containing 20 mM Tris-HCl (pH 7.8), 500 mM NaCl and 500 mM imidazole.

The insoluble proteins (VWF115, VWF115-A3 and VWFA2) present in the inclusion bodies were solubilised in a buffer containing 20 mM Tris-HCl (pH 7.8), 500 mM NaCl, 20 mM imidazole and 8 M urea, before being passed over a nickel-chelating column. Insoluble proteins needed to gradually regain their native conformation. This was achieved with an on-column refolding technique, using an 8M-0M urea linear gradient (20 minutes for VWF115; 60 minutes for VWF115-A3 and VWFA2). After refolding, the soluble proteins were eluted with a 500 mM imidazole step gradient, while some eventual insoluble proteins still bound to the column were stripped with a buffer containing 20 mM Tris-HCl (pH 7.8), 500 mM NaCl, 6 M guanidine-HCl and 50 mM EDTA. Both eluted and stripped proteins were dialysed in 20 mM Tris-HCl (pH 7.8) overnight at 4°C using the 10 kDa molecular weight cut-off dialysis membrane (Pierce). For the VWFA2 fragment, this gradual dialysis helped proteins still insoluble after purification to refold properly. The purity of the expressed proteins was checked by SDS-PAGE (see Section 2.2.7) followed by Coomassie staining (see Section 2.2.8) and Western blot analysis (see Section 2.2.9). The amount of purified proteins was quantified by BCA total protein assay kit (see Section 2.2.5).

2.2.5 Total protein quantification (BCA assay)

The total protein concentration was determined using a BCA total protein assay kit (Pierce, UK). This method is based on the property of proteins to reduce Cu^{+2} to Cu^{+1} (cuprous ion) in an alkaline medium. The purple-colored reaction product is formed by the chelation of two molecules of bicinchoninic acid (BCA) with one cuprous ion. The colorimetric intensity correlates to the protein concentration. A series of dilutions of

known concentrations of BSA (range 15-2 000 µg/ml) were prepared and used as a standard. Different dilutions (neat, 1:5, and 1:10) of the unknown sample were prepared simultaneously. 25 µl of each standard or unknown sample were pipetted in replicates into a 96 well polyvinyl plate (Nunc). 200 µl of the working reagent was added to each well and incubated at 37°C for 30 minutes on a plate shaker. The absorbance was measured at 540 nm using an automated plate reader (iEMS Reader MF, LabSystems). The protein concentration of the unknown sample was determined by reading from the BSA standard curve.

2.2.6 ADAMTS13 Enzyme-Linked ImmunoSorbent Assay (ELISA)

ADAMTS13 concentration was also determined by a specific ELISA, previously optimised in our laboratory by Dr James Crawley [326]. 500 µg rabbit anti ADAMTS13 polyclonal antibody (pAb) (depleted from antibodies against TSR (2-4)) in 50 mM sodium carbonate buffer (pH 9.6) was immobilised onto the wells of a 96 well plate (Nunc) and incubated overnight at 4°C. The plate was washed three times with 200 µl washing buffer (phosphate buffered saline (PBS) (Sigma)-0.1% Tween (Sigma)), and the wells blocked with 200 µl of PBS-2.5 % BSA (Sigma) for one hour shaking at room temperature. A series of dilutions of a highly pure gel-filtered ADAMTS13 (range 0-100 ng/ml) in PBS-1% BSA, the concentration of which was determined by BCA assay, were used as a standard. The unknown sample was diluted 1:10 000, 1:20 000 and 1:40 000 in PBS-1% BSA. Each sample was added to the correspondent well and incubated at room temperature for two hours. The plate was then washed three times with 200 µl washing buffer and 100 µl of 0.5 µg/ml primary antibody (rabbit biotinylated anti-TSR (2-4) pA) in PBS-1% BSA was applied for two hours shaking at room temperature. The plate was washed three times with 200 µl washing buffer and 100 µl of streptavidin conjugated with horseradish peroxidase (HRP) (Amersham Bioscience) in PBS-1% BSA applied for one hour at room temperature. The wells were washed as before and 200 µl o-phenylenediamine dihydrochloride (OPD) (Sigma) added as a chromogenic substrate, which could be hydrolysed by the peroxidase. The reactions were stopped with 100 µl 1.4 M sulphuric acid (H_2SO_4) and the absorbance read at 492 nm. The concentration of the unknown protein was determined by reading it on the standard curve.

2.2.7 SDS polyacrylamide gel electrophoresis (SDS-PAGE)

The electrophoretic separation of proteins is determined by their size, charge and conformational structure. SDS is an anionic detergent which denatures proteins (reducing them to primary structure) and confers them a negative charge in proportion to their length, so that the charge densities per unit is equal. In SDS-PAGE electrophoresis therefore, separation of protein is determined only by molecular weight. An appropriate amount of loading buffer was added to each sample. Where it was necessary to reduce disulphide bridges, 4% (w/v) 2-mercaptoethanol (BD Biochemicals) were added to the sample. This was then denatured at 95°C for 5 minutes and loaded onto a polyacrilamide gel (BIORAD). Gels with different concentrations of polyacrilamide were used to solve proteins of different molecular weights. The electrophoresis was performed at 90-100 V for 70-90 minutes.

2.2.8 Coomassie staining

The Coomassie staining procedure utilises a dye, Coomassie blue Safe Stain (Invitrogen), which indistinguishly stains all the proteins contained in the electrophoresed sample. After SDS-PAGE, the gel was rinsed three times with 100 ml ddH_2O for five minutes before applying 25 ml Coomassie blue Safe Stain for one hour. The gel was then destained by rinsing it with 100 ml ddH_2O for one hour, before being dried using a gel Dryer 583 (Biorad) for two hours.

2.2.9 Western blotting

The Western blotting technique allows the detection of a specific peptide/protein present in an electrophored sample, using an appropriate antibody. After electrophoresis of samples on a SDS-PAGE gel, the gel was placed in transfer buffer to be equilibrated. Proteins were transferred to either a Hybond ECL nitrocellulose or Hydrophobic polyvinylidene difluoride (PVDF) membrane (Amersham Pharmacia, UK), using a Trans-Blot Electrophoretic Transfer Cell (Bio-Rad), in the presence of ice to prevent overheating. In the transfer tank, the gel was arranged adjacent to the cathode electrode, and the membrane next to the gel closer to the anode electrode. The transfer electrophoresis conditions were 90 V for 65 minutes. After transferring, non-specific binding sites were blocked by immersing the membrane in 5% blocking reagent (Amerham Pharmacia, UK) in PBS (Sigma)-0.1% Tween (Sigma) for one hour to overnight, shaking at room temperature. After washing with PBS-0.1% Tween, the membrane was incubated with the appropriate diluted primary antibody in 1%

blocking reagent for one hour, shaking at room temperature. ADAMTS13 was detected using a mouse anti human ADAMTS13 protease domain monoclonal antibody (1.1 mg/ml) (a kind gift from Dr. Scheiflinger, Baxter), at a 1:6300 dilution. Alternatively, the anti-myc antibody (Invitrogen) was used. Whereas, VWF fragments were detected using a mouse anti X-press epitope or anti V5 epitope antibody (2 mg/ml) (Invitrogen) at a 1:5000 dilution. After three washings with PBS-0.1% Tween, the secondary antibody, a goat anti mouse pAb coniugated with HRP (Dako) at a 1:1500 dilution, was added for an hour, shaking at room temperature. Finally, the membrane was washed with PBS-0.1% Tween four times and detected by exposure with ECL chemiluminescent kit (Amerham Pharmacia, UK). Briefly, the membrane is covered with a mixture of an equal volume of the two detection solutions provided by the kit, incubated for one minute and finally detected by exposing it to an autoradiography film.

2.3 CHARACTERISATION OF VWF PROTEOLYSIS BY ADAMTS13

2.3.1 Cleavage of VWF fragments

To analyse the cleavage of VWF fragments by ADAMTS13, time course experiments were set up as follows. Purified recombinant ADAMTS13 (5.5-16.5 nM) was incubated without the recombinant VWF fragment at 37°C for 30 minutes in reaction buffer (20 mM Tris-HCl (pH 7.8), 150 mM NaCl and 5 mM $CaCl_2$) in a final volume of 65 µl for each time point. The substrate (VWF76, wild type and mutant VWF115, VWF115-A3, wild type and mutant VWFA2) was added to start each reaction. VWFA2 cleavage was analysed both in the absence and presence of 1 M urea. Each reaction was stopped by adding 5 µl of 0.5 M EDTA at different time points (0, 30, 45, 60, 90, 120, 180, 240, 360 minutes) and then analysed by SDS-PAGE (16.5% Tris-Tricine gel)/Coomassie staining (see Sections 2.2.7 and 2.2.8) and HPLC analysis (see Section 2.3.3). Repeated time course experiments were performed using different substrate concentrations, since visualisation by Coomassie staining required high substrate concentrations (6 µM), whereas accurate determination of the specificity constant (also known as catalytic efficiency), k_{cat}/K_m, was performed at low substrate concentrations (0.25-0.5 µM).

2.3.2 Overview of HPLC and reverse phase chromatography

HPLC is based on the separation of molecules through a chromatography column under high pressure conditions. The stationary phase is defined as the immobile packing material in the column, whereas the mobile phase refers to the solvent being continuously applied to the column and in which the sample has been dissolved. The chemical interactions of the mobile phase (and the sample) with the column, determine the degree of migration and separation of components contained in the sample. The mobile phase can be altered in order to manipulate the interactions between the sample and the stationary phase, leading to different grade of resolutions of the molecules contained in a mixture.

In reverse phase chromatography, the stationary phase is hydrophobic, whereas the mobile phase is polar. Biomolecules strongly adsorbed to the surface of a reverse phase matrix under aqueous conditions. Subsequently, the mobile phase composition is modified to favour desorption of the solute from the stationary phase back into the mobile phase. The polarity of the mobile phase is gradually decreased by adding organic modifiers such as acetonitrile (apolar). Proteins are eluted at different points of the acetonitrile gradient based on their hydrophobic properties. Ion-pairing agents such as trifluoroacetic acid (TFA) are also added to the mobile phase in order to maintain a low pH environment (below 7.5).

2.3.3 HPLC analysis and determination of specificity constant k_{cat}/K_m

To quantify the cleavage, 50 µl of the stopped reaction were loaded onto an AKTA Basic10 HPLC machine (Amersham Pharmacia, UK) and passed over a BioBasic C4 HPLC column (Thermo) for reversed phase chromatography, monitored by the control system UNICORN™ (Amersham). Initially, the full-length substrate and the two cleavage products were eluted using a 0-100% gradient of acetonitrile (Sigma,UK), after a specific retention time, on the base of their hydrophobic properties. Once the retention time for each peptide was known, the gradient could be shortened in each case (20-55% for VWF76, 25-45% for VWF115, 20-65% for VWF115-A3, 25-60% for VWFA2). The resolution of each peak was achieved by alteration of the rate of the gradient. Comparing the peaks originated from the cleavage of the different VWF fragments, it was possible to identify which peptide was contained in each eluted peak. To confirm this, mass spectrometry was performed at the Imperial College-MRC Clinical Sciences Centre proteomics facility, Hammersmith Campus. Unicorn analysis software was used to calculate the areas under each peak. The rate of cleavage for each

fragment was determined monitoring the appearance of the peak corresponding to the N-cleavage product. The specificity constant k_{cat}/K_m of the cleavage of each fragment was calculated by plotting the rate of cleavage over time and by fitting the curve using Enzfitter software to the equation:

$$k_{cat}/K_m = \frac{-\ln(1-[AP]/[APf])}{et} \qquad [eq.1]$$

where [AP] is the area under curve at time *t*, [APf] is the area under curve after complete substrate cleavage, *e* is the enzyme concentration, *t* is the time.

2.3.4 Determination of K_m and k_{cat}

Separate estimates of catalytic constants for wild type VWF115 were obtained from the dependence of the initial rates of cleavage upon its concentration. Purified recombinant ADAMTS13 (8.5 nM) was incubated, as before, without the substrate at 37°C for 30 minutes in reaction buffer (20 mM Tris-HCl (pH 7.8), 150 mM NaCl and 5 mM $CaCl_2$). Different concentrations (0.25-25 μM) of the substrate were added to start each reaction and incubated at 37°C. Each reaction was stopped by adding 5 μl of 0.5 M EDTA at early time points (0, 5, 10 minutes), in order to have a cleavage less than 15%. This condition is required to work in first-order kinetics. Samples were analysed by HPLC and initial velocity (in nM/sec) of the cleavage reaction was plotted against substrate concentration, using Graph Pad Prism 4 software. The data were fitted to the *Michaelis-Menten* equation:

$$V = \frac{V_{max} \times [S]}{K_m + [S]} \qquad [eq.2]$$

where V is the initial velocity, V_{max} is the maximal velocity reached at high substrate concentration when the enzyme is saturated, [S] is the substrate concentration and K_m is the *Michaelis-Menten* constant, which represents the substrate concentration at which the reaction velocity is half-maximal.

In this way, K_m and V_{max} were determined and therefore k_{cat} (in sec^{-1}) from the ratio $V_{max}/[E]$, where [E] refers to enzyme concentration. K_{cat} is known as catalytic constant or turnover number, and represents the number of reaction processes that each active site catalyses per unit of time. Finally, the specificity constant could be calculated from the ratio k_{cat}/K_m.

2.4 CHARACTERISATION OF ADAMTS13 BINDING TO VWF FRAGMENTS

2.4.1 Overview of Surface Plasmon Resonance (SPR) and the BIAcore system

2.4.1.1 Principles and components of BIAcore system

The affinity constants of the binding between the wild type and mutant VWF115 fragments and full-length ADAMTS13 were determined using a dual flowcell BIAcore X biosensor system (BIAcore, AB), which monitors biomolecular interactions in real-time on a metal layer through the phenomenon of surface plasmon resonance (SPR). SPR is an electron charge density wave phenomenon that arises when light is reflected under certain conditions from a conducting film at the interface between two media of different refractive index (RI) (Fig. 2.5). The SPR phenomenon results in a reduction in the intensity of the reflected light at a specific angle, which varies according to the refractive index of the solution. In the Biacore system, the interaction between molecules occurs on the surface of a sensor chip, which provides the physical condition necessary to generate the SPR signal. It consists of a glass surface coated with a thin gold layer, which is covered with a matrix surface (usually dextran), where the biomolecule (known as *ligand*) can be attached. The glass and the sample solution represent the two media with different RI, whereas the gold film is required for the SPR detection principle. Another component of the BIAcore system is a microfluidic system which delivers the sample containing the other interactant biomolecule (known as *analyte*) to the sensor surface. The microfluidic system consists of a series of channels and valves in a plastic block, the Integrated Microfluidic Cartridge (IFC). The IFC channels are pressed against the sensore surface to form the flow cells (1 and 2). The ligand should be immobilised on flow cell 2, whereas a molecule of a similar molecular weight (which is thought not to interact with the analyte) should be immobilised on flow cell 1 as a control. The injected solutions follow the IFC channels and are delivered first to flow cell 1 and, subsequently, to flow cell 2. When the analyte in the sample binds to the ligand immobilised on the sensor surface, the concentration and therefore the RI at the surface increase. SPR response is detected as a decrease in the angle of incidence, monitored as a change in the detector position, and it is measured in resonance unit (RU). Plotting the response against time provides a quantitative measure of the

progress of the interaction. This plotted is called sensogram (Fig. 2.6). During the association phase, the reduction of the reflection angle can be monitored. At the end of the injection, the sample is replaced by a flow of buffer and the dissociation phase can be observed. The analyte can thus be stripped from the ligand using different regeneration conditions (see Section 2.4.1.5) and the chip is thus available to study another injection.

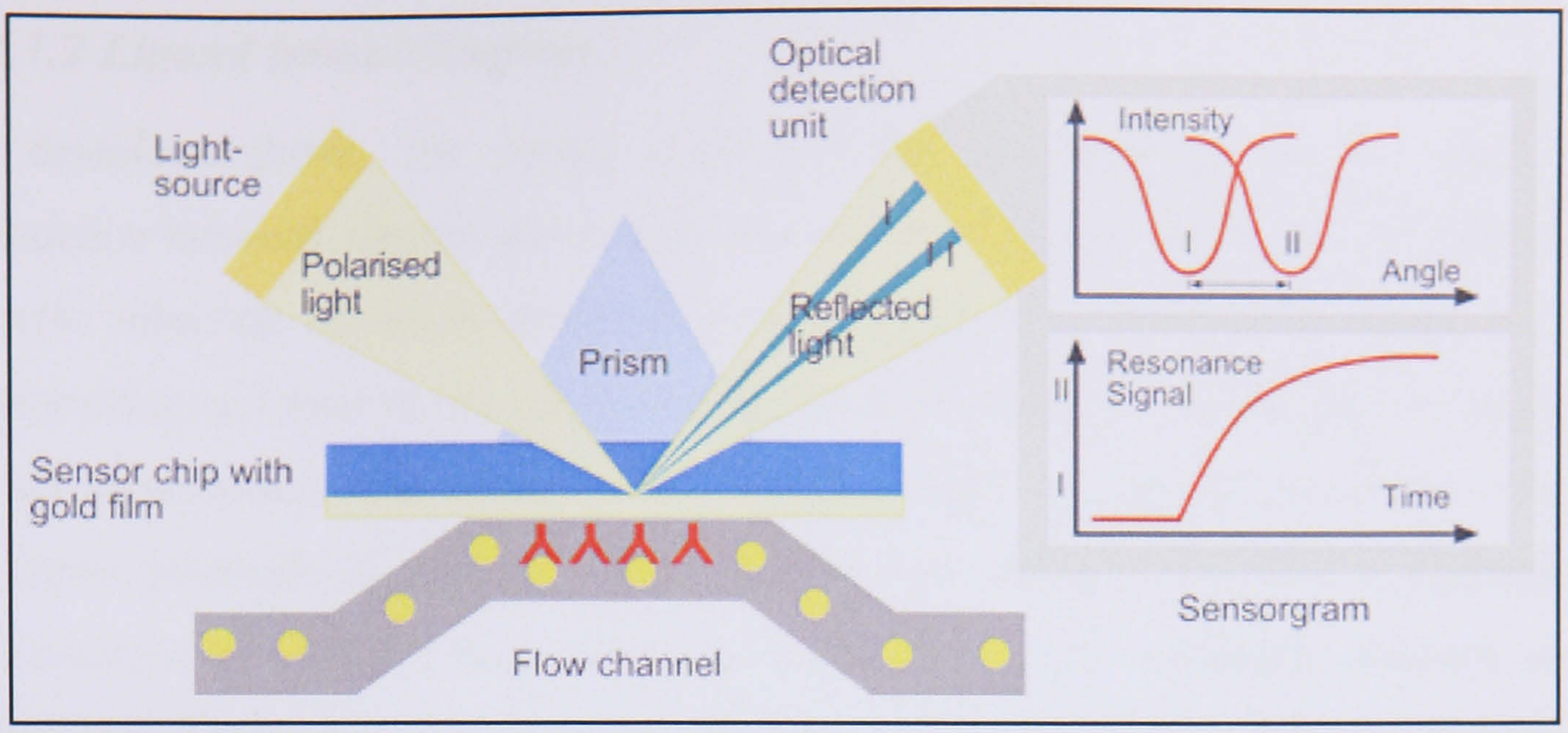


Fig. 2.5 Illustration of sensor chip, detector and IFC. SPR records changes in mass at the surface of a sensore chip by measuring changes in the reflection angle of a polarised light which is reflected at the interface of two media with different RI. The change in the angle is detected by the optical detection unit, as a change in the detector position (from I to II). During the course of analyte-lygand interaction, the response, expressed in RU, is plotted against time. (Picture taken from BIAcore Technology).

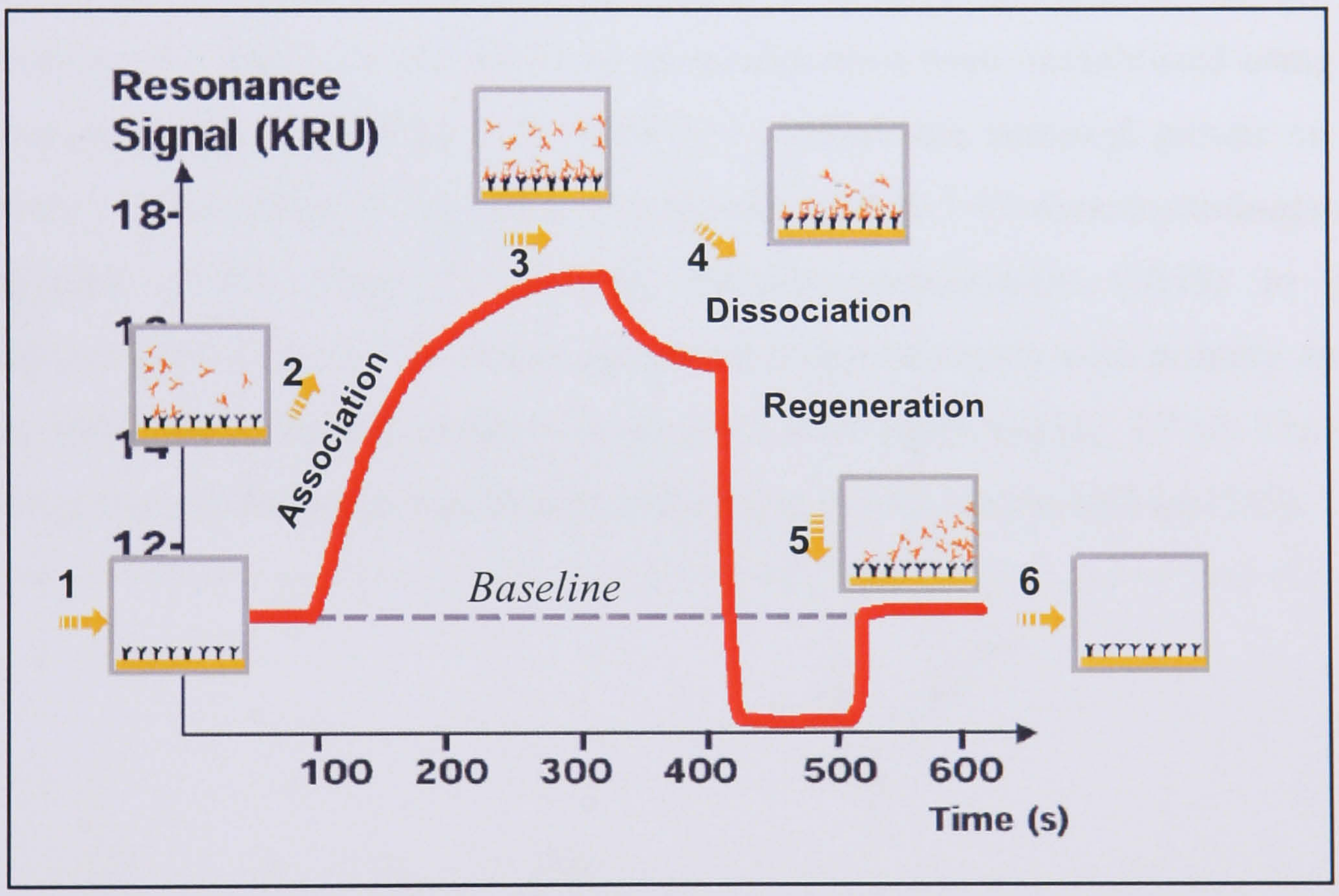


Fig. 2.6 SPR sensogram. The real-time interaction of biomolecules monitored by SPR is plotted in a sensogram. Before the analyte is delivered to the sensorchip surface, where the ligand is immobilised (**1**), a stable flat line is recorded, correspondingt to the ligand level and adjusted to 0 RU (Baseline). As sample is flowing over the chip surface, the analyte comes in contact with the ligand (**2**) and the association takes place over time. The increase in the number of molecules which bind to the ligand is recorded as an increase in the RU, until the steady state is reached (**3**). This point corresponds to a dymamic equilibrium, where the number of molecules associating and dissociating per unit of time is the same. At the end of the sample injection, the dissociation of the analyte from the ligand (**4**) is detected as a decrease in the response. The chip surface can be regenerated (**5**) using specific solutions, which disrupt the analyte-lygand interaction, re-establishing the basal condition where no analyte is bound to the immobilised ligand (**6**). (Picture modified from BIAcore Technology).

2.4.1.2 Ligand immobilisation

As described above, the sensor chip provides the physical surface where the interaction between biomolecules takes place and where the SPR signal is generated. A wide selection of sensor chips (BIAcore) is available. They differ in the surface composition and thus in the series of molecules that can be immobilised on them. In all my experiments, I have used a CM5 chip, in which the surface consists in a matrix of carboxymethylated dextran. This carbohydrate polymer provides a hydrophilic environment to which a wide range of molecules can be covalently attached using different techniques (amine coupling, thiol coupling, aldhehyde coupling). The ligand can be directly immobilised on this surface or, alternatively, using a capturing molecule, i.e a specific monoclonal antibody. The direct coupling of the ligand upon the surface leads to a random immobilisation, whereas the capturing approach offers the advantage of immobilising the ligand in a specific orientation. In all my experiments, the ligands or the capturing molecules have been immobilised using the amine coupling approach (Fig. 2.7). With this method, the carboxyl groups on the sensor chip surface (Fig. 2.7 a) are activated with 1-ethyl-3-93-dimethylaminopropyl carbodiimide (EDC) (Fig. 2.7 b) and N-hydroxysuccinimide (NHS) to give succinimide esters (Fig. 2.7 c). These groups react spontaneously with primary amine groups, which are present in different numbers in most proteins (Fig. 2.7 d). The free reactive groups of the surface are then blocked using ethanolamine-HCl (pH 8.5).

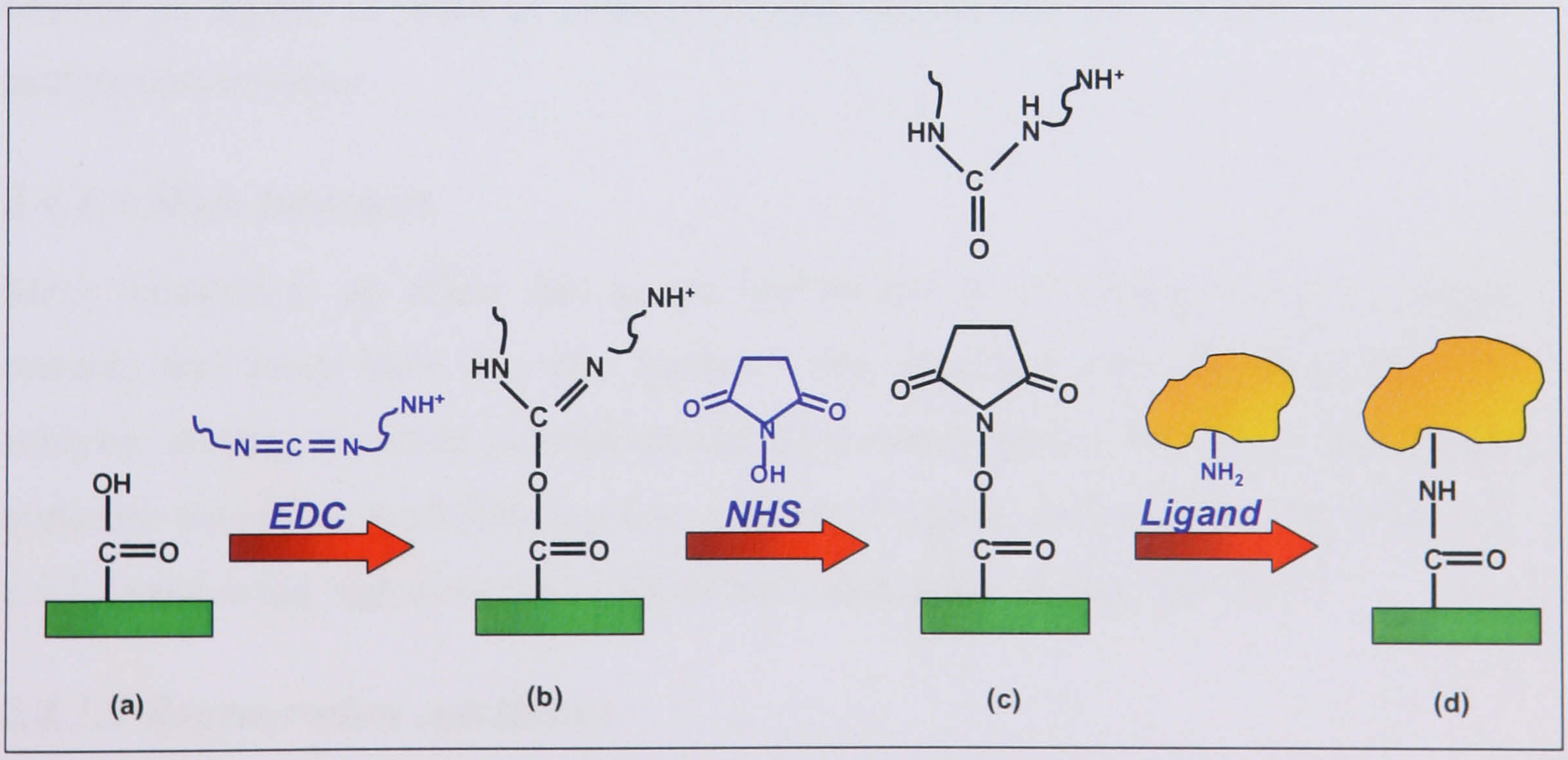


Fig. 2.7 Amine coupling of the ligand to the surface of a CM5 sensor chip. The carboxyl group of a CM5 sensor chip (a) reacts sequentially with EDC (b) and NHS, leading to the formation of a reactive succinimide esters (c). This spontaneously reacts with amine groups of the ligand. The ligand is thus covalently immobilised on the dextran matrix (d).

2.4.1.3 Amount of ligand to immobilise

For kinetic analysis, it is recommended to use the lowest amount of immobilised ligand in order to work in pseudo first order condition. If the concentration of the ligand is much lower than that of the analyte, then the concentration of the analyte can be considered to remain constant during the all course of the experiment. This is also ensured by a continuous supply of new sample during the analyte injection. The amount of the ligand to immobilise in order to satisfy these conditions depends on the relative molecular weights of the ligand and analyte, since the SPR signal is directly proportional to the mass of the material present on the surface, and it can be calculated as follows:

$$\text{Immobilised ligand (RU)} = \text{analyte binding capacity (RU)} \cdot \frac{\text{ligand MW}}{\text{analyte MW}} \qquad \text{[eq.3]}$$

The analyte binding capacity (R_{max}) is the theoretical binding which is reached at infinite analyte concentrations and infinite contact time. This value should be around 100-300 RU in order to have the optimal condition for the fitting. From equation 3 it appears that if the ligand is large and the analyte is small, responses will be generally low. It is thus advised to immobilise a quite large amount of ligand. On the other hand, if the ligand is small and the analyte is large, it is suggested to immobilise a moderate amount of ligand, in order to avoid crowding effects and steric hindrance at high analyte concentration.

2.4.1.4 Mass transport

Mass transport is an effect due to the analyte not being transported fast enough towards and away from the chip surface. Mass transport may confound the SPR analysis, leading to slower association and dissociation phases. It is thus important to minimise this effect immobilising low amount of ligand on the surface (see Section 2.4.1.3) and using high flow rates (>20 µl/min) during the analyte injection.

2.4.1.5 Regeneration conditions

After the binding of the analyte to the immobilised ligand, the dissociation may be very slow. It is thus useful to determine suitable regeneration conditions in order to efficiently remove the bound analyte from the chip surface, without damaging the ligand activity. When the response returns to baseline, the chip is ready for another

analyte injection. Different regeneration solutions are provided from BIAcore and they can be tested. Low pH (10 mM glycine-HCl pH 1.5-3), high pH (1-100 mM NaOH) and high ionic strength (up to 5 M NaCl or 4 M $MgCl_2$) are the most commonly used.

2.4.2 Kinetic analysis using BIAcore

After a series of curves have been generated following the injections of different concentrations of analyte and after the subtraction of the signal from the control flow cell (flow cell 2- flow cell 1), the data are ready to be kinetically analysed. The provided BIAevaluation software 3.0 (BIAcore) allows the determination of the association and dissociation rate constants (k_a and k_d, respectively) and the equilibrium dissociation constant ($K_D=k_d/k_a$). The association and dissociation phases of all sensograms are fitted simultaneously: this means it is possible to calculate a single set of kinetic constants which best fit all the data sets. The BIAevaluation software provides different mathematical models to which the binding curves could be fitted.

2.4.2.1 Langmuir model

The Langmuir model represents the simplest situation in biomolecular interaction, where the soluble analyte (A) and the immobilised ligand (B) bind reversibly in a 1:1 complex (AB):

$$A + B \underset{k_d}{\overset{k_a}{\rightleftharpoons}} AB$$

The net rate complex formation is given by the differential equation:

$$d[AB]/dt = k_a [A] [B] - k_d [AB] \qquad [eq. 4]$$

where [A] is the concentration of the analyte (in M), [B] is the concentration of the immobilised ligand (in RU), [AB] is the concentration of the ligand-analyte complex (in RU), k_a is the association constant (in $M^{-1} s^{-1}$) and k_d is the dissociation constant (in s^{-1}).

I have used this model to analyse the curves obtained when wild type VWF115 or VWF115 mutants were immobilised onto the chip as a ligand and ADAMTS13 was passed over it as an analyte.

2.4.2.2 Heterogeneous ligand model

The heterogeneous ligand model represents the situation where the immobilised molecule is heterogeneous (B and B*) with regard to analyte (A) binding:

$$A + B \underset{k_d1}{\overset{k_a1}{\rightleftharpoons}} AB$$

$$A + B^* \underset{k_d2}{\overset{k_a2}{\rightleftharpoons}} AB^*$$

When the data fit best to this model it may represent the situation in which two binding sites are present in the ligand. The interaction of each binding site with the analyte is thus characterised by specific binding constants (k_a1 and k_d1 for one binding site, k_a2 and k_d2 for the second one), which are all calculated by the fitting software using the sum of two integrated rate equations (as in equation 4). Alternatively, the random amine coupling (see Section 2.4.1.2) may result in a heterogeneous population of immobilised ligands, where the binding site may be or be not completely exposed. Although a true representation of this require a whole range of interactions, from the tightest to the weakest, it can usually be successfully approximated by a simple two-population model, representing the two extremer interactions. The tighter interaction of the two may be considered the one which represents the binding of the analyte to the optimally-immobilised ligand. This model was used to fit the binding of immobilised ADAMTS13 to wild type and mutant VWF115 fragments.

2.4.3 Determination of ADAMTS13 binding affinity for wild type and mutant VWF115 fragments using SPR

In order to study the binding between ADAMTS13 and wild type or mutant VWF115 fragments, different approaches were attempted. All the experiments were performed using a dual flowcell BIAcore® X Biosensor system (BIAcore, AB, Uppsala, Sweden) at a constant temperature of 25°C. BIAcore HBS-P buffer (10 mM HEPES pH 7.4, 150 mM NaCl, 0.005% Surfactant P20, filtered and degassed) was pumped continuously through the machine, during the all course of the analysis. The analyte was previously dialysed in the same buffer, at 4 °C overnight. A CM5 sensor chip (BIAcore) was used in each case, and the coupling technique (see Section 2.4.1.2) employed to immobilise the ligand (ADAMTS13 or VWF115) on the surface, either using a specific

monoclonal antibody (see Sections 2.4.3.1 and 2.4.3.2) or directly (see Sections 2.4.3.3 and 2.4.3.4).

2.4.3.1 Immobilisation of ADAMTS13 on a CM5 sensor chip using monoclonal antibodies

Initially, different attempts were made to use specific monoclonal antibodies to immobilise ADAMTS13 on the surface of a CM5 sensor chip. Both flow cell surfaces were activated with 0.4 M EDC and 0.1 M NHS (flow rate 7 µl/min, contact time 7 minutes). 100 µl of anti-CUB monoclonal antibody (a kind gift from Dr. Scheiflinger, Baxter, Austria) (50 µg/ml) in acetate buffer (pH 5.0) was injected over both flow cells at a flow rate of 7 µl/min. Free reactive groups of the surface were blocked with 35 µl of 1 M ethanolamine-HCl (pH 8.5). 100 µl of ADAMTS13 (2 µM) was passed over flow cell 2 only (flow rate 7 µl/min) and it bound to the immobilised antibody. When the reading became stable, different concentrations of VWF115 (62.5, 125 and 250 nM) were injected over both flow cells (flow rate 30 µl/min, contact time 1-2 minutes). Specific binding response could be detected in flow cell 2, after subtraction of non-specific response in flow cell 1 (reference cell). The chip could be regenerated with a 5-10 seconds pulse of 10 mM glycine-HCl (pH 2). The same protocol was used when other antibodies were employed: anti myc-tag (Invitrogen) and anti disintegrin-like domain monoclonal antibodies (a kind gift from Dr. David Motto, University of Michigan), and anti TSR (2-4) pAb.

2.4.3.2 Immobilisation of VWF115 on a CM5 sensor chip using monoclonal antibodies

Similar attempts were tried to immobilise VWF115 on the surface of a CM5 sensor chip, using alternatively an anti-His G antibody (Invitrogen) or an anti-Xpress antibody (Invitrogen). The CM5 chip was activated with 0.4 M EDC and 0.1 M NHS (flow rate 7 µl/min, contact time 7 minutes). 50 µl of antibody (30 µg/ml) in acetate buffer (pH 5.0) was injected over both flow cells at a flow rate of 7 µl/min. The sensor surface was blocked with 35 µl of 1 M ethanolamine-HCl (pH 8.5). 80 µl of VWF115 (300 µg/ml) was injected over flow cell 2 only and it bound to the antibody. 30 µl of ADAMTS13 (1 µM) was injected over both flow cells (flow rate 30 µl/min). The non-specific response in flow cell 1 was subtracted from the one observed in flow cell 2.

2.4.3.3 Direct immobilisation of VWF115 on a CM5 sensor chip

Wild type or mutant VWF115 was directly immobilised on the surface of a CM5 sensor chip, by amine coupling. After surface activation with 0.4 M EDC and 0.1 M NHS (flow rate 7 µl/min, contact time 7 minutes), 10 µl of wild type or mutant VWF115 (10 µg/ml) in acetate buffer (pH 5.0) was injected over flow cell 2 and directly immobilised on the surface. All free reactive surface groups were then blocked using 1 M ethanolamine-HCl (pH 8.5). 50 µl of 2.5 µM human endothelial protein C receptor (hEPCR) (40 kDa) was injected and immobilised on flow cell 1, which was used as a reference cell to monitor non-specific binding. Different concentrations (10, 20, 27.5 and 55 nM) of ADAMTS13 were injected over both the active and control flow cells (flow rate 30 µl/min, contact time 1-2 minutes). After each ADAMTS13 injection, the surface was regenerated using 5 µl of 10 mM NaOH (flow rate 30 µl/min, contact time 10 seconds). Data analysis was performed using the BIAevaluation software 3.0 (BIAcore), fitting the derived sensograms to 1:1 Langmuir model (see Section 2.4.2.1) and dermining values of k_a, k_d and K_D.

2.4.3.4 Direct immobilisation of ADAMTS13 on a CM5 sensor chip

To directly immobilise ADAMTS13 on the sensor chip the same strategy was used as for VWF115 wild type. After surface activation with NHS/EDC, 25 µl of ADAMTS13 (10 µg/ml) in acetate buffer (pH 5.0) was injected over flow cell 2. 30 µl of anti-hEPCR RCR-2 antibody (a kind gift from Dr. K Fukudome) (10 µg/ml) was immobilised over flow cell 1 as a control. Different concentrations of wild type or mutant VWF115 (62.5, 125 and 250 nM) were injected over both flow cells (flow rate 30 µl/min, contact time 1-2 minutes). After each VWF115 injection, the surface was regenerated using 5 µl of 10 mM NaOH (flow rate 30 µl/min, contact time 10 seconds). The data were fitted using the BIAevaluation software 3.0 (BIAcore) to the heterogeneous ligand model (see Section 2.4.2.2). Two sets of binding constants were calculated.

2.4.4 Determination of ADAMTS13 binding affinity for VWF fragments using a microtiter plate-based binding assay

A plate-based binding assay was performed as an alternative method to assess ADAMTS13 binding to VWF115 and VWFA2. A similar method was previously used [258], but some modifications were introduced. A 96 well microtiter plate (Nunc) was coated with 100 µl of 140 nM VWF115 or VWFA2 diluted in 50 mM sodium

carbonate buffer (pH 9.6) overnight at room temperature. Unbound VWF was removed and the plate was washed three times with 200 µl washing buffer (PBS-0.1% Tween). The wells were then blocked with 200 µl blocking buffer (PBS-2.5% BSA) for 60 minutes shaking at room temperature. 100 µl of different ADAMTS13 concentrations (1.56-100 nM), in dilution buffer (PBS-1% BSA), in the absence or presence of 50 mM EDTA, were applied to the wells and incubated for 3 hours shaking at 37°C. 100 µl of dilution buffer only was added to the well which was supposed to be used as a blank. The plate was washed three times with 200 µl washing buffer and 100 µl of 0.1 µg/ml of biotinylated anti-TSR (2-4) pAb in dilution buffer was applied and incubated for 90 minutes shaking at room temperature. The plate was again washed three times and 100 µl of Streptavidin-HRP (Amersham Bioscience) diluted 1:1000 in dilution buffer was applied and incubated for 1 hour shaking at room temperature. 200 µl of OPD solution was applied to each well and incubated until developing of the colour (~3 minutes).The reactions were stopped with 50 µl 3 M H_2SO_4 and the plate read at 492 nm. A schematic representation of the binding assay is given in Fig. 2.8.

The absorbance values (after subtraction of the blank) were plotted against the ADAMTS13 concentration, using Graph Pad Prism 4 software. The data were fitted to the one binding site model, using the equation:

$$B = \frac{B_{max} \times [X]}{K_D + [X]} \qquad [eq.5]$$

where B is the binding expressed in absorbance unit, B_{max} is the maximal binding when saturation is reached, [X] is the ligand (ADAMTS13) concentration and K_D is the equilibrium dissociation constant.

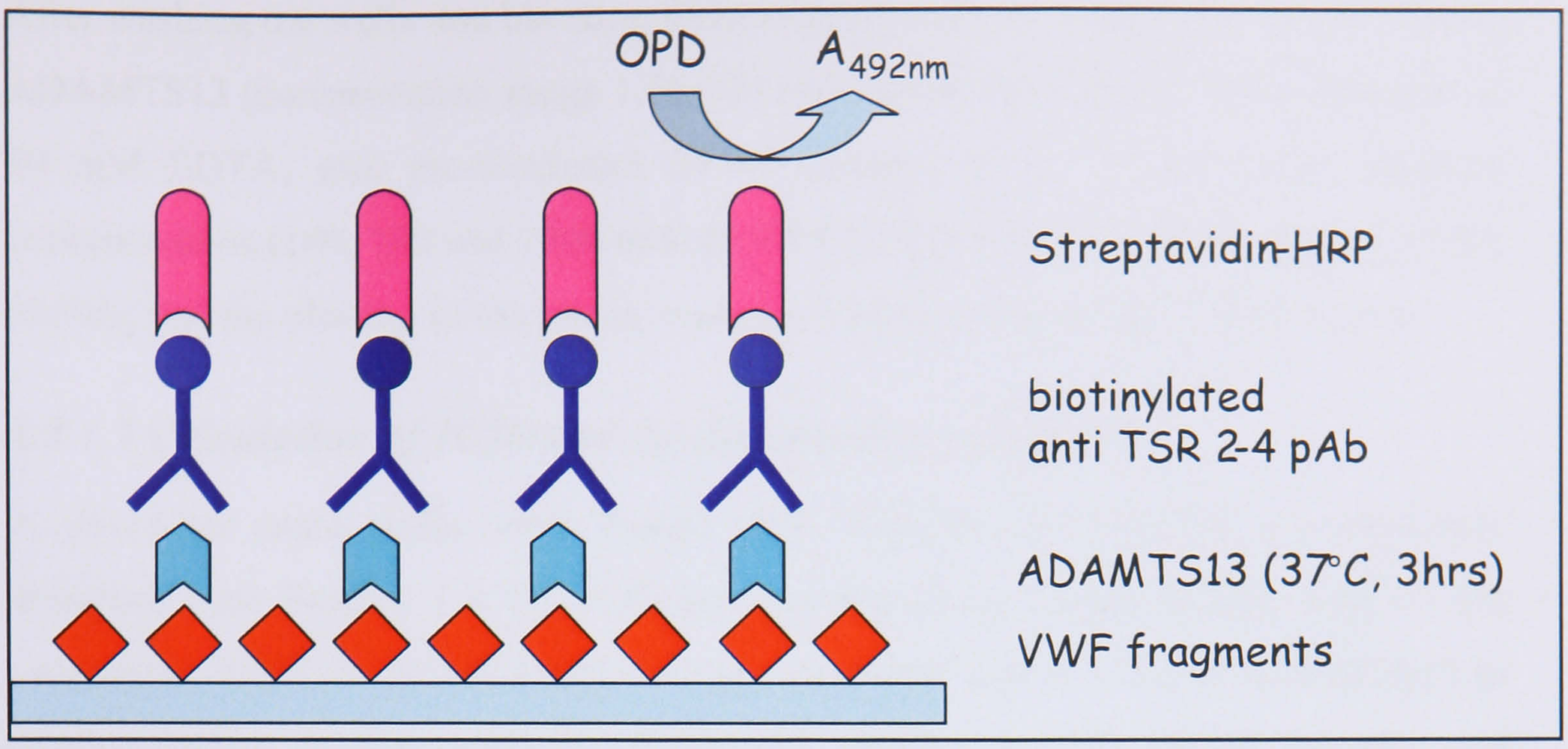


Fig. 2.8 Representation of VWF115/VWFA2-ADAMTS13 plate-based binding assay. After VWF115/VWFA2 immobilisation, ADAMTS13 was added and incubated at 37°C for 3 hours. Biotinylated anti-TSR (2-4) pAb was applied and incubated for 90 minutes at room temperature. Subsequently, Streptavidin-HRP was applied and incubated for 1 hour at room temperature. The chromogenic substrate OPD was finally added and hydrolysed by the peroxidase. The reaction was stopped with H_2SO_4 and the absorbance read at 492 nm.

2.4.5 Competition binding studies

2.4.5.1 Soluble and plate-bound VWFA2 competition

To investigate if the binding site for ADAMTS13 is exposed when VWFA2 is in solution in a folded conformation, a competition experiment was set up as follows. VWFA2 was immobilised into the wells of a microtiter plate as previously described (see Section 2.4.4). Different ADAMTS13 concentrations (1.56-100 nM), in dilution buffer, in the presence of 50 mM EDTA, were pre-incubated at 37 ºC for 40 minutes with 1400 nM of either VWFA2 (in the absence and presence of 1 M urea) or R1597Q VWFA2. 100 µl of each mix was added to the wells, previously blocked and washed as described in Section 2.4.4, and incubated at 37 ºC for 3 hours. The detection of the binding and the plotting of the curves were performed as before (see Section 2.4.4).

2.4.5.2 Competition between soluble and immobilised VWF115 and VWFA2 fragments

Similar competition experiments were set up to investigate if VWFA2 contains important residues for ADAMTS13 binding, which are not present in VWF115. Either

VWFA2 or VWF115 was coated into the plate wells as before (see Section 2.4.4). After washing the wells and blocking them as previously described (see Section 2.4.4). ADAMTS13 (concentration range 1.56-100 nM), in dilution buffer, in the presence of 50 mM EDTA, was pre-incubated for 40 minutes at 37 °C with three different concentrations (140, 700 and 1400 nM) of VWF115 (or VWFA2). The detection of the binding and the plotting of the curves were performed as described in Section 2.4.4.

2.4.5.3 Calculation of IC50 and the dissociation constant K_i

A microtiter plate wells were coated with VWFA2 or VWF115 as previously described (see Section 2.4.4.). Different concentrations (range 0-2240 nM) of the competitor (VWF115 or VWFA2) were pre-incubated with 6.5 nM of ADAMTS13 in dilution buffer, in the presence of 50 mM EDTA, at 37°C for 40 minutes and subsequently added to the wells. The detection of the binding was performed as described in Section 2.4.4. The binding in the absence of soluble inhibitor was taken as 100%. The result was plotted as a percentage of this maximal binding against the logarithm of inhibitor concentration. The curves were fitted using Graph Pad Prism 4 software to the one site competition model:

$$Y = \text{Bottom} + \frac{(\text{Top} - \text{Bottom})}{(1 + 10^{(\text{X-Log IC50})})} \qquad \text{[eq.6]}$$

where IC50 is the half maximal inhibitory concentration and it represents the concentration of the competitor required to compete for half the specific binding. *Top* and *Bottom* represent the maximum and minimum values for the Y, respectively. If the blank value (see Section 2.4.4) has been subtracted from the Y values and they they have been plotted as a percentage of total binding (in the absence of inhibitor), *Top* can be fixed to 100 and *Bottom* to 0.

The IC50 value depends on the concentration of the immobilised substrate. The inhibition constant (K_i) can be calculated from IC50 using the following equation:

$$K_i = \frac{\text{IC50}}{1 + \frac{[\text{immobilised substrate}]}{K_D}} \qquad \text{[eq.7]}$$

3. RESULTS

3.1 PREPARATION OF ADAMTS13

3.1.1 Introduction

My first objective was to prepare highly pure recombinant ADAMTS13. The purity of the recombinant protein was a crucial issue for the kinetic work and the binding experiments I had planned. In this Section I will describe the purification protocol, the evaluation of the purity of the expressed ADAMTS13 and the determination of its concentration using a total protein BCA assay and an ELISA.

3.1.2 Expression and purification of recombinant ADAMTS13

Recombinant ADAMTS13 pcDNA 3.1/myc-His expression vector was stably transfected into HEK293 cells as described in Section 2.2.1 and expressed into Optimem serum-free conditioned medium. Collected medium was filtered, concentrated and desalted (Fig. 3.1 A). ADAMTS13 was then purified by nickel-chelating affinity chromatography (Fig. 3.1 B) (see Section 2.2.2). The sample was subjected to non-reducing SDS-PAGE on a 4-15% Tris-HCl polyacrylamide gel and analysed by Western blotting (Fig. 3.1 C) and Coomassie staining (Fig. 3.1 D). The purified ADAMTS13 migrated predominantly as a single band of approximately 200 kDa (Fig. 3.1 C and 3.1 D, lanes 4 and 5). However, some faint bands of higher molecular weight were visible, previously demonstrated by my colleague Dr. James Rance to be the result of different glycosylated forms of the protein, which do not influence its proteolytic activity. Faster mobility bands present in the Coomassie stained gel and not in the Western blotting represented minor low molecular weight protein contaminants.

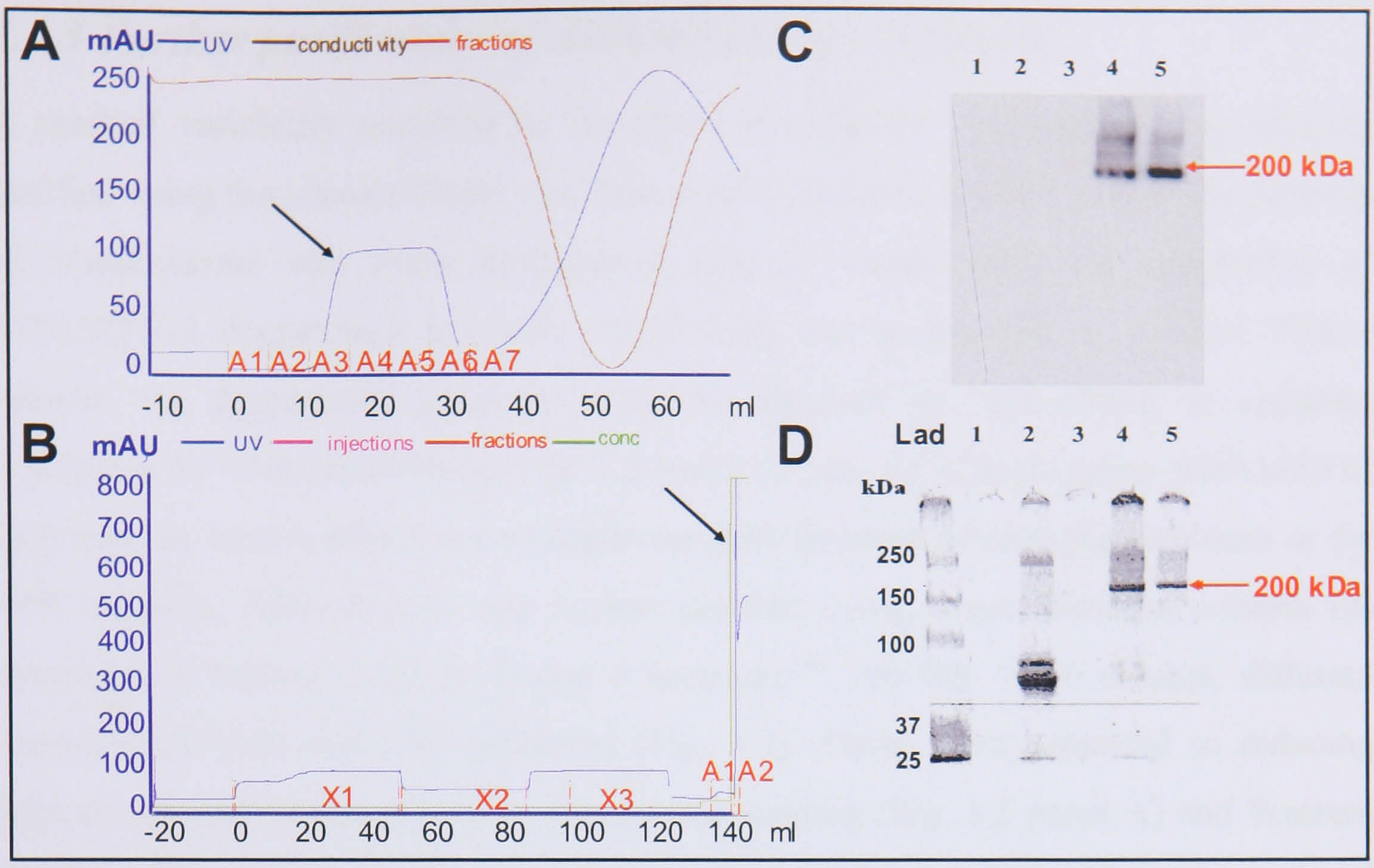


Fig. 3.1 Purification of recombinant ADAMTS13. (A) Serum-free conditioned medium was desalted on a Hi Prep^{TM} 26/10 desalting column. Before the injection of the sample, the column was equilibrated with a buffer containing 20 mM Tris-HCl (pH 7.8), 500 mM NaCl and 20 mM imidazole. Desalted material was eluted first. It was collected in fractions A3-A6 (highlighted by an arrow) and it was used for the following purification step. Salts and small proteins (< 5 kDa) were eluted in fraction A7. **(B)** Affinity purification of ADAMTS13 using a nickel-chelating column. The column was initially equilibrated in a buffer containing 20 mM Tris-HCl (pH 7.8), 500 mM NaCl and 20 mM imidazole. After repetitive injections of the sample (X1, X2 and X3), the column was washed with 15 ml of a buffer containing 20 mM Tris-HCl (pH 7.8), 500 mM NaCl and 35 mM imidazole (fraction A1). ADAMTS13 was then eluted with a buffer containing 20 mM Tris-HCl (pH 7.8), 500 mM NaCl and 500 mM imidazole. The eluted fraction (A2) is highlighted by an arrow. **(C)** Non-reducing SDS-PAGE on a 4-15 % Tris-HCl gel analysed by Western blotting, using anti-protease domain antibody: desalting column fraction A7 (lane 1), affinity column flow through (lane 2), elution with 35 mM imidazole (lane 3), elution with 500 mM imidazole (lanes 4 and 5). No protein was detected by the antibody in lanes 1, 2 and 3. In lanes 4 and 5, the red arrow highlights a major band of 200 kDa, corresponding to the expected molecular weight of ADAMTS13. **(D)** Non-reducing SDS-PAGE on a 4-15 % Tris-HCl gel followed by Coomassie staining: desalting column fraction A7 (lane 1), affinity column flow through (lane 2), elution with 30 mM imidazole (lane 3), elution with 500 mM imidazole (lanes 4 and 5). Most of the contaminant proteins did not bind to the column (lane 2). However, some minor contaminants are present in lanes 4 and 5. Lad: ladder of protein molecular weight markers.

3.1.3 Further purification of ADAMTS13: gel filtration

A marked variability occurred in the purity of different ADAMTS13 preparations purified using the above affinity chromatography method. In some cases, the presence of contaminants was more pronounced than in others. Also the appearance of ADAMTS13 degradation products varied from one preparation to another. Where present, the degradation products could be detected on SDS-PAGE in reducing conditions by Western blotting (Fig. 3.2 panel A, lane S). If high purity ADAMTS13 preparations were required, for example for determination of catalytic constants or for SPR analysis, ADAMTS13 was further purified using a gel filtration column (as described in Section 2.2.2.2). Using a Superdex^{TM} 200 HR 10/30 column, different fractions (A1-A5) could be separated (Fig. 3.2). These were subjected to reducing SDS-PAGE and analysed both by Coomassie staining (Fig. 3.2 panel A) and Western blotting (Fig. 3.2 panel B). On the Coomassie stained gel, fractions A1 and A2 appeared as a single band of approximately 200 kDa, whereas in fraction A3 a slightly faster mobility band was also present, possibly a degradation product originating from cleavage in the N-terminal part of the molecule. Western blot analysis of the same fractions showed that ADAMTS13 degradation products were still present (fig. 3.2 panel B). They were less apparent in fraction A2, but it should be noticed that that particular sample was less concentrated. It might be that degradation products could not be separated from the intact ADAMTS13 by gel filtration because they were formed by internal cleavage and they were held together by disulphide bonds. Although gel filtration seemed not to remove all degradation products, it was useful to remove a 65 kDa contaminant protein, possibly albumin, which was eluted in fraction A5 (visible in the Coomassie stained-gel but not in Western blotting). Since the degradation products probably originated by cleavage of ADAMTS13 occurring after ADAMTS13 secretion into the conditioned medium, I decided to add a protease inhibitor cocktail (see Section 2.2.1.4) during the 3-4 days of incubation with Optimem medium. The collected medium was purified both by affinity chromatography and gel filtration, as described above, and it appeared as a single band of ~ 200 kDa when analysed by Western blotting (Fig. 3.3). After dialysis in 20 mM Tris-HCl at 4°C overnight, smaller aliquots (10-20 µl each, with a concentration of ~1 mg/ml) were prepared from the ADAMTS13 stock and stored at -70°C.

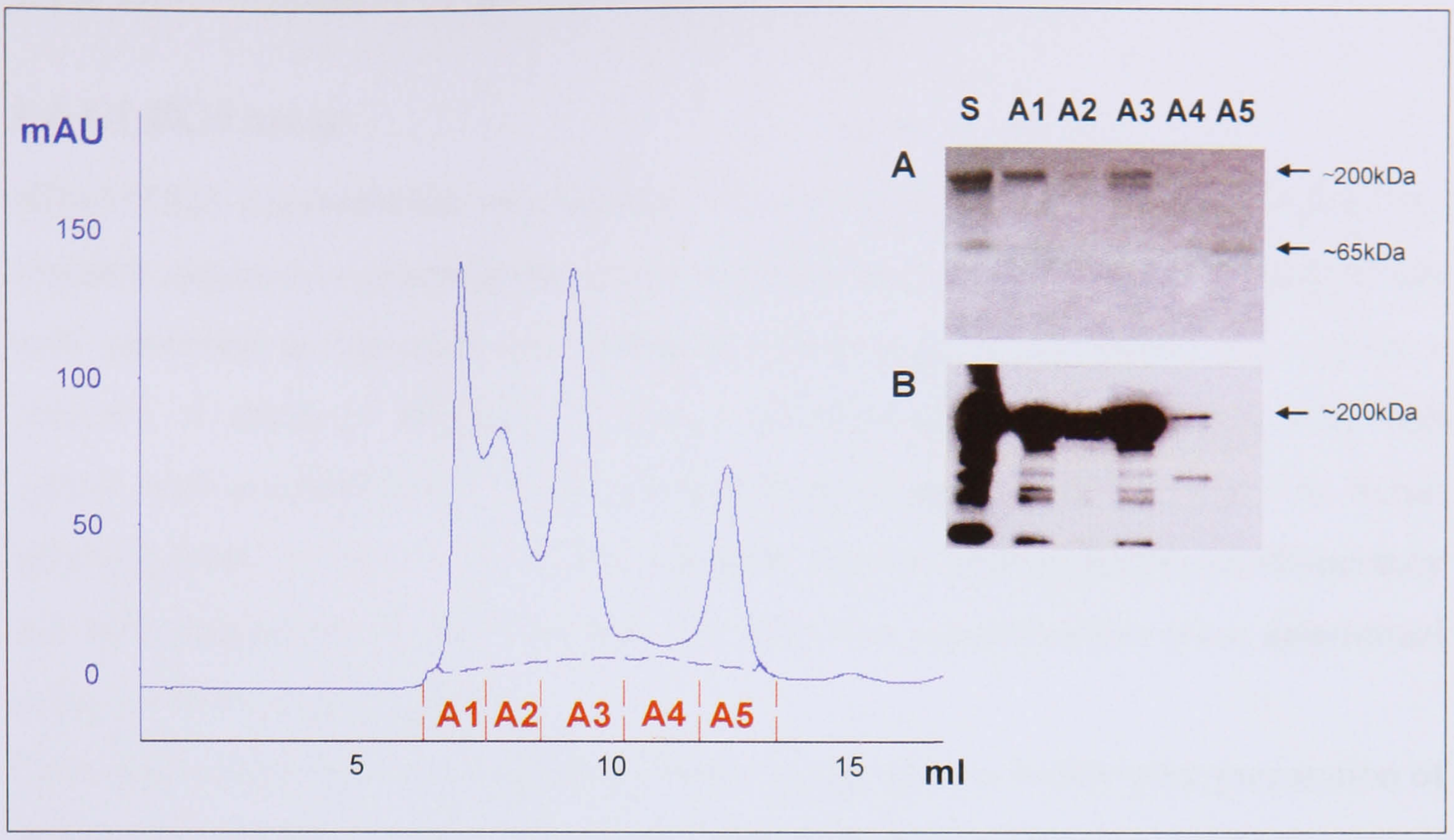


Fig. 3.2 Gel filtration of affinity purified ADAMTS13. In order to remove protein contaminants and ADAMTS13 degradation products, affinity purified ADAMTS13 was passed over a Superdex^{TM} 200 HR 10/30 gel filtration column and different fractions (A1-A5) were collected. The starting material (S) and the gel-filtered fractions (A1-A5) were subjected to reducing SDS-PAGE on a 4-15% Tris-HCl polyacrylamide gel and analysed both by Coomassie staining (panel A) and Western blotting using anti-myc antibody (panel B). The Western blot analysis showed that ADAMTS13 degradation products were still present in fractions A1, A2 and A3. However, gel filtration was useful to eliminate a 65 kDa contaminant protein, possibly albumin, which was eluted in fraction A5.

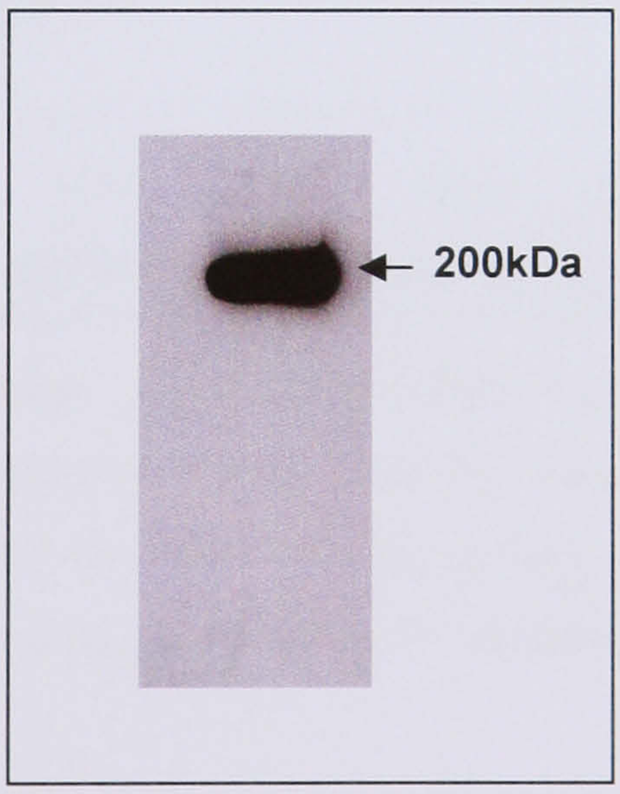


Fig. 3.3 ADAMTS13 purified after adding protease inhibitor cocktail to the Optimem medium. In order to avoid ADAMTS13 cleavage after secretion from HEK293 cells, a protease inhibitor cocktail was added to the Optimem medium. After purification on a nickel-chelating column and gel filtration, ADAMTS13 degradation was assessed by reducing SDS-PAGE on a 4-15% Tris-HCl gel followed by Western blotting. The anti-myc antibody was employed for detection. ADAMTS13 appeared as a pure single band of ~ 200 kDa, with no evidence of degradation products.

3.1.4 Determination of the concentration of ADAMTS13

3.1.4.1 BCA assay

ADAMTS13 concentration was initially determined by BCA total protein assay. The reagents required to generate the colour response and the principle of the method are both described in Materials and Methods (see Section 2.2.5). BSA was used as a standard. A series of dilutions of known concentrations of BSA (range 15-2 000 µg/ml) were prepared and plotted against their absorbance at 540 nm (Fig. 3.4). Serial dilutions (neat, 1:5 and 1:10) of the unknown sample were prepared simultaneously and their absorbance read at 540 nm. The unknown concentrations were determined using the BSA standard curve.

Since this method detects all proteins present in the sample, highly pure preparation of ADAMTS13 were required to have an accurate estimation of its concentration.

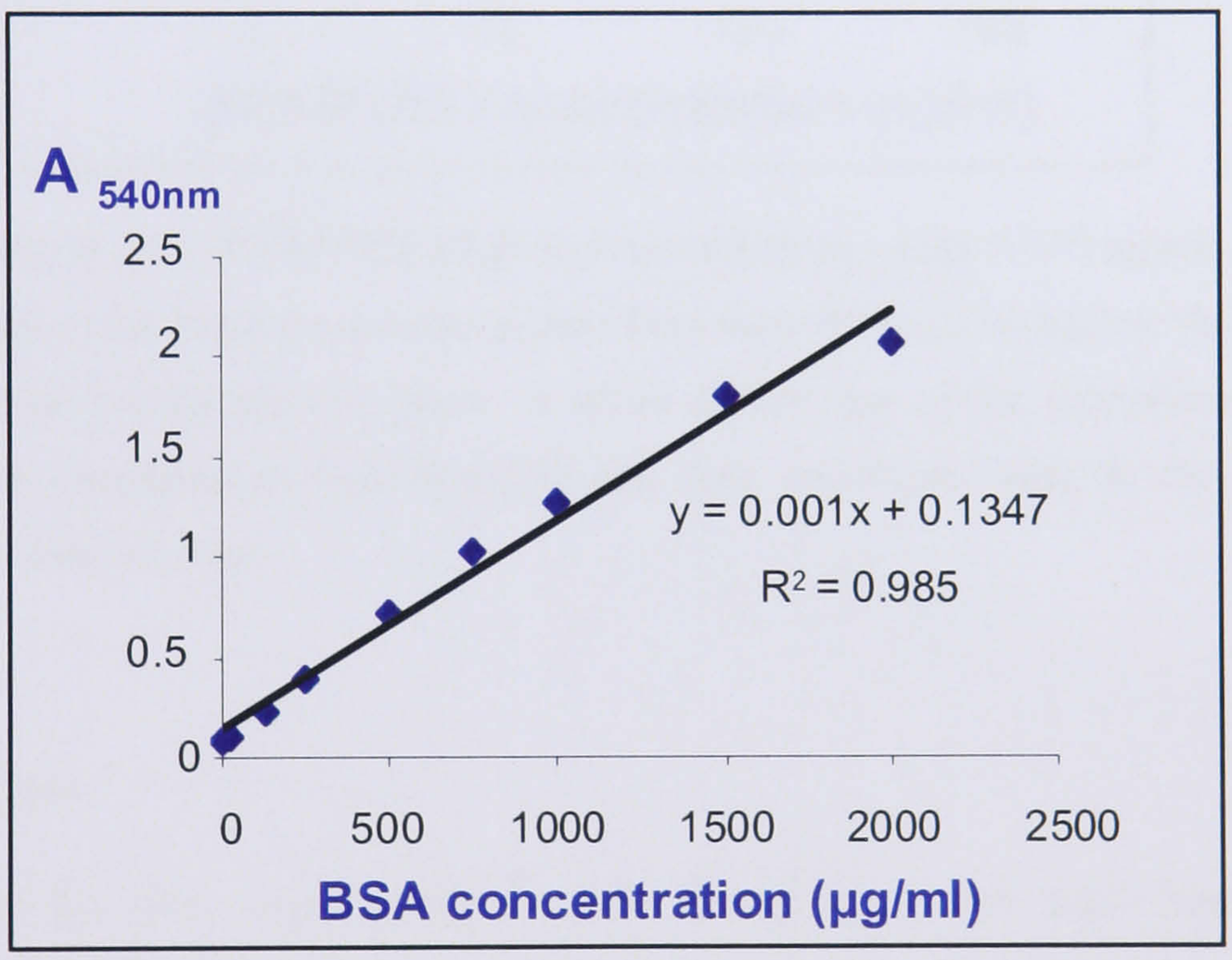


Fig. 3.4 Standard curve for BCA assay. A series of dilutions of known concentrations of BSA (range 15-2 000 µg/ml) were prepared and plotted against their absorbance at 540 nm. The equation for the curve is given. The absorbance at 540 nm of serial dilutions (neat, 1:5, 1:10) of the unknown sample were determined using the standard curve, giving values for its concentration.

3.1.4.2 ELISA for ADAMTS13

Subsequently, a specific ELISA for ADAMTS13 was optimised in our laboratory, as described in Materials and Methods (see Section 2.2.6). This allowed a precise determination of ADAMTS13 concentration even when protein contaminants were present, provided a reliable standard was available. Serial dilutions (range 0-100

ng/ml) of a highly pure gel-filtered preparation of ADAMTS13 quantified by BCA were prepared. The absorbance of these was read at 492 nm and used to generate the standard curve for the ELISA (Fig. 3.5). The unknown sample was diluted 1:10 000, 1:20 000 and 1:40 000 and the absorbance was read at 492 nm. The concentration of the unknown sample was derived using the standard curve.

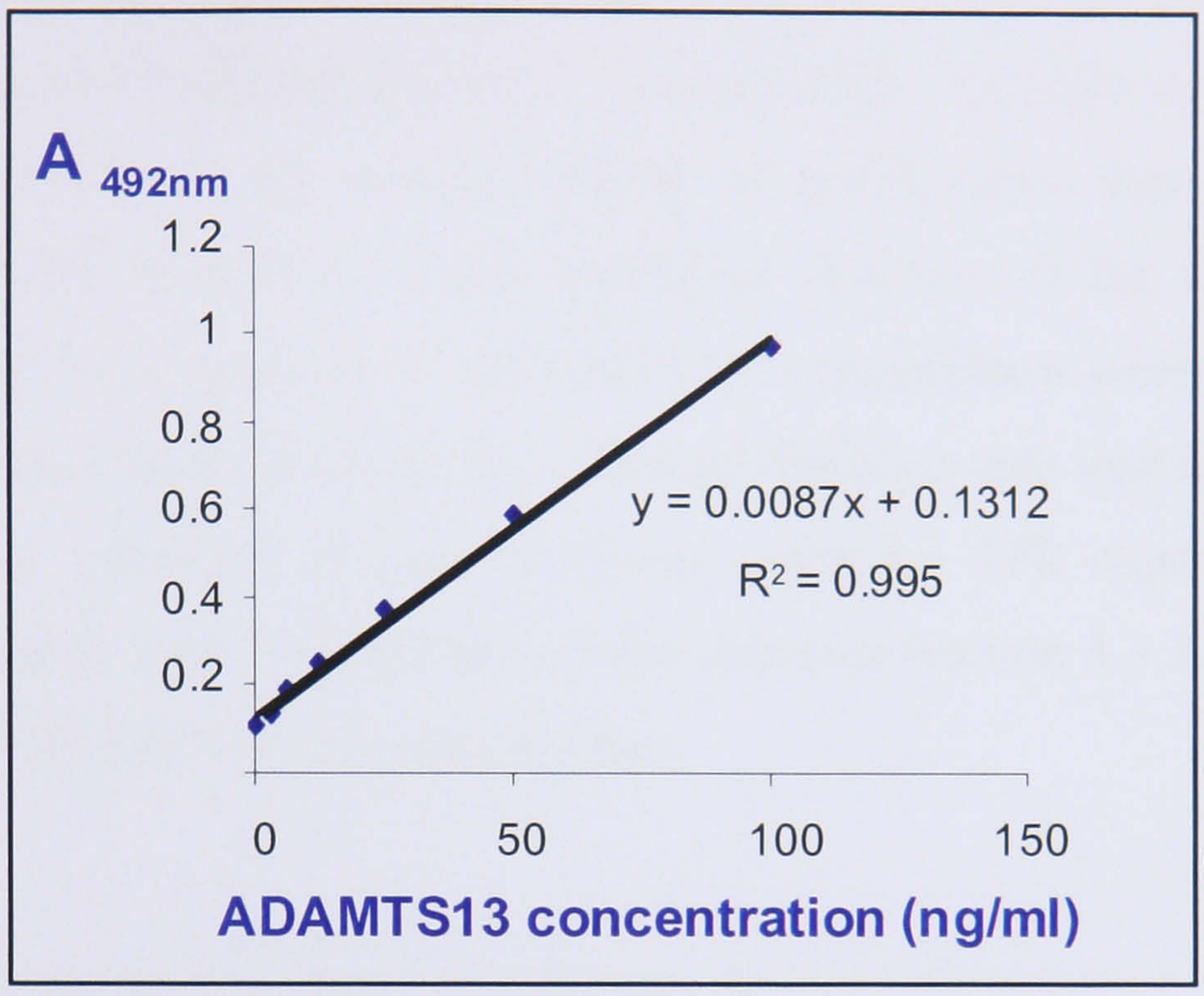


Fig. 3.5 Standard curve for ADAMTS13 ELISA. Serial dilutions (range 0-100 ng/ml) of a gel-filtered ADAMTS13 of known concentration were prepared. They were then plotted against their absorbance at 492 nm. The equation for the curve is given. A series of dilutions of the recombinant ADAMTS13 sample of unknown concentration were prepared and their absorbance read on the standard curve, giving values for its concentration.

3.1.5 Discussion

The prerequisite for the experiments I will describe in the next Sections was to optimise an efficient system to express and purify recombinant ADAMTS13. Recombinant myc/6xHis-tagged ADAMTS13 was expressed by stably-transfected HEK293 cells. ADAMTS13 was concentrated and purified by affinity chromatography on a nickel-chelating column (Fig. 3.1). The average yield after purification was ~3 mg of ADAMTS13 per litre of culture. Because protein contaminants and/or degradation products were present in this material, other approaches were adopted, including a further purification using a gel filtration column and addition of protease inhibitor cocktail to the collected medium. The gel filtration step helped to remove a 65 kDa contaminant protein (possibly albumin) (Fig. 3.2). The protease inhibitor cocktail was effective in reducing ADAMTS13 degradation by proteases active in the Optimem medium (Fig. 3.3). Some quantitative experiments,

such as determination of kinetic and binding constants, required a precise measurement of ADAMTS13 concentration. This was initially calculated using the BCA assay. Since this method detects indistinctively the presence of any protein, it was important that the sample to be analysed was highly pure. Therefore, both ADAMTS13 purification steps were required. For qualitative analysis or preliminary results, the precise ADAMTS13 concentration was not so crucial. In such cases, only purification on a nickel-chelating column was necessary. This also avoided significant loss of sample which usually occurred during the gel-filtration step. Subsequently, a specific ELISA for ADAMTS13 was optimised. Because of the specificity of the method, reliable determinations of ADAMTS13 concentration were possible even if contaminants were present in the sample. The gel-filtration step was thus not necessary most of the time. However, in some particular cases, i.e. SPR experiments in which ADAMTS13 was directly immobilised on the chip (see Section 3.3.2.3), a highly pure preparation of ADAMTS13 was still required.

3.2 GENERATION AND CHARACTERISATION OF VWF A DOMAIN FRAGMENTS AS ADAMTS13 SUBSTRATES

3.2.1 Introduction

ADAMTS13 regulates VWF multimeric size by cleaving the peptide bond Y1605-M1606 in VWF A2 domain [106,147,196] (see Section 1.3). However, the circulating VWF adopts a non-permissive conformation which cannot be cleaved by ADAMTS13 (see Section 1.3.5.2 and Fig. 1.12 A), probably because the cleavage site is located in the centre of VWF A2 domain (see Fig. 1.10 in Section 1.3.5.1). In the presence of high shear-stress, VWF can spontaneously unravel and expose the cleavage site (see Fig. 1.12 B). This provides context for *in vitro* investigations of ADAMTS13 activity, using full-length VWF as a substrate. Use of denaturants in static assays or of high-shear rates in flow chamber systems are necessary to unfold VWF to a conformation which can be cleaved by ADAMTS13 [149,196,327]. An alternative method consists in expressing shorter VWF fragments, which may be easily cleaved by ADAMTS13 in the absence of denaturants.

Since the ADAMTS13 cleavage site is located in the A2 domain and a binding site for ADAMTS13 was reported in the A3 domain [107], I decided to express three VWF fragments spanning different regions of these domains (Fig. 3.6): VWF76 (1593-1668), VWF115 (1554-1668) and VWF115-A3 (1554-1874). The short length of the fragments and their relatively simple structure (only one disulphide bond in the A3 domain), suggested that they could be expressed in bacteria. Their expression in *E. coli* and the subsequent purification using a nickel-chelating column (in association with the refolding on the column technique, if necessary) was thought to be a rapid method to produce large amount of protein. Once the VWF fragments had been generated, their proteolysis by ADAMTS13 could be studied, in the presence of calcium ions and under physiological ionic conditions. The cleavage reactions were firstly analysed by SDS-PAGE followed by Coomassie staining in order to have an initial qualitative estimation of the rate of cleavage. HPLC analysis was then performed to obtain a precise measurement of the catalytic efficiency (k_{cat}/K_m) of each cleavage reaction.

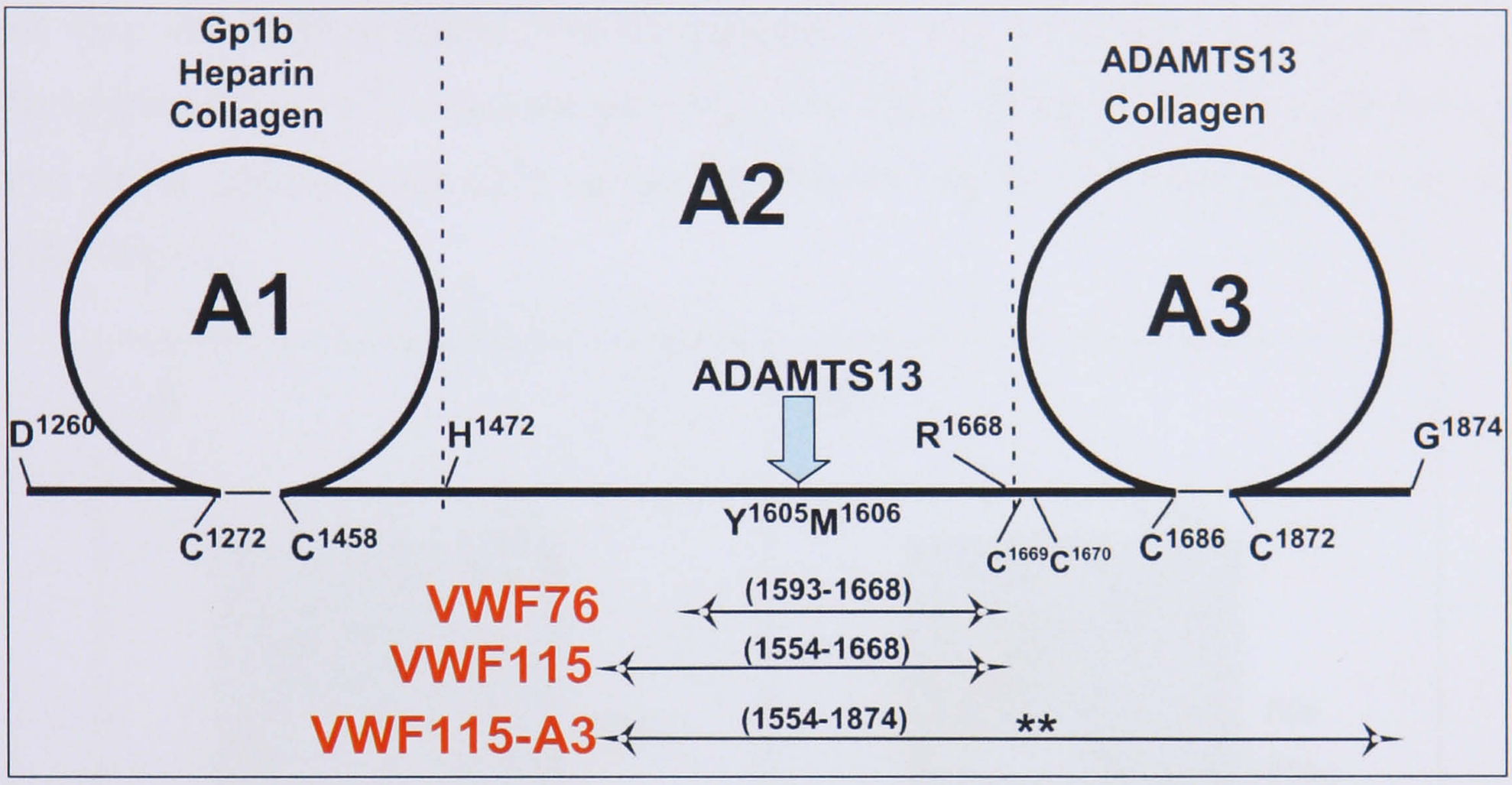


Fig. 3.6 Recombinant VWF A domain fragments. Recombinant VWF fragments (VWF76, VWF115, and VWF115-A3) are shown as arrows beneath the diagram of the VWF A1A2A3 domains (residues 1260-1874). The ADAMTS13 cleavage site (Y1605-M1606) and major ligands for each domain are highlighted above the diagram. All the VWF fragments were made with a His-tag and an Xpress epitope at the N-terminus. The amino acid numbering of each substrate is given in brackets. In VWF115-A3, the two adjacent cysteine residues at 1669 and 1670 mutated into alanines (see text) are indicated by **.

3.2.2 VWF fragment cloning

VWF76, VWF115, VWF115-A3 fragments were cloned into pET100/D-TOPO bacterial expression vector, as described in Section 2.1.2.1. This vector contains an N-terminal His-tag and an Xpress epitope.

All the fragments were prepared by specific PCR amplification, using full-length VWF cDNA as a template. PCR primers were designed as described in Section 2.1.2.4 and they are listed in Table 1 in the Appendix I. PCR products were analysed by electrophoresis on a 1% agarose gel (Fig. 3.7). They all appeared as a predominant band of the expected size (228 bp for VWF76, 345 bp for VWF115 and 963 bp for VWF115-A3).

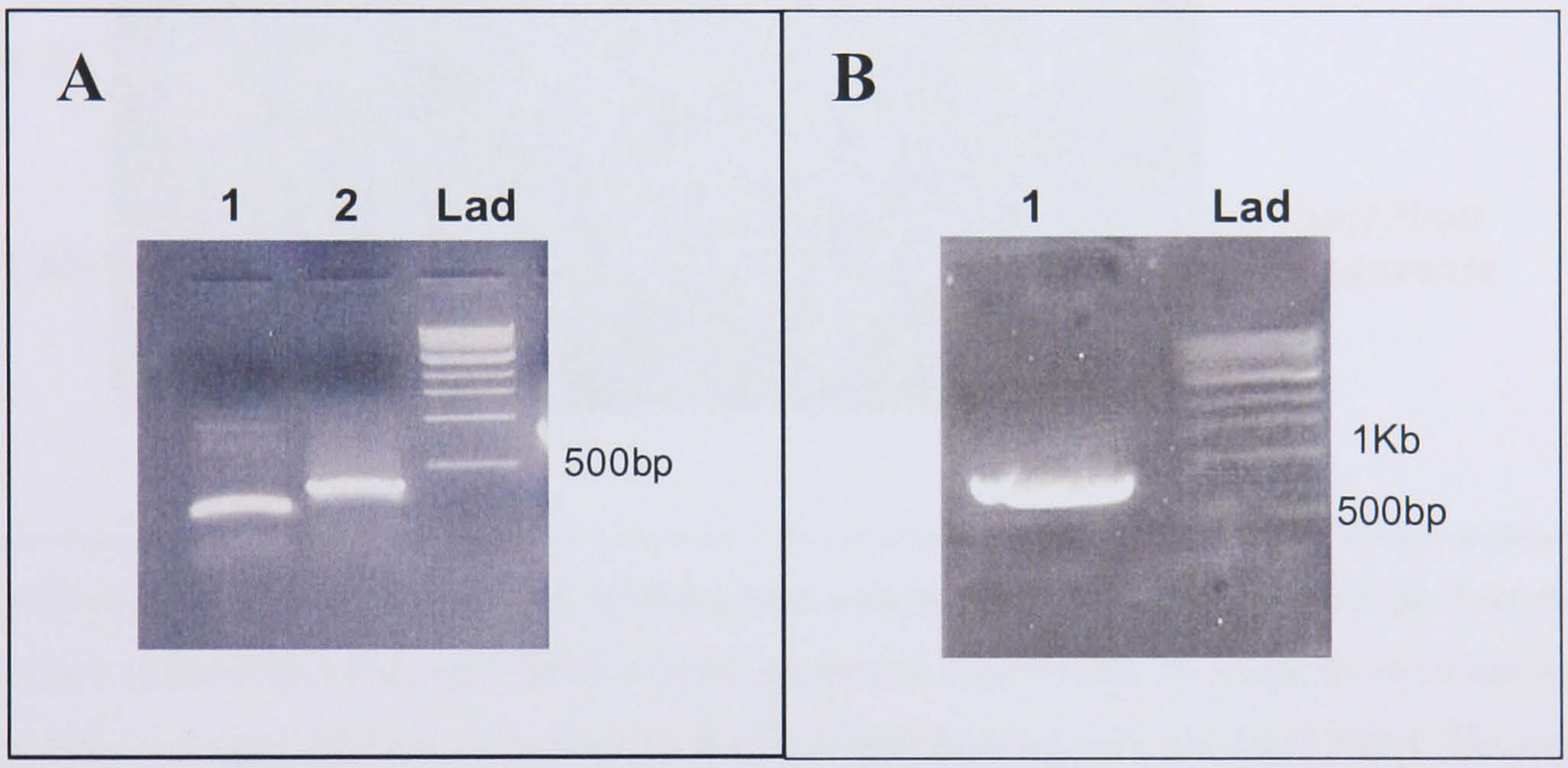


Fig. 3.7 Gel electrophoresis of PCR products encoding VWF76, VWF115 and VWF115-A3. PCR products were analysed on a 1% agarose gel (running conditions: 70 V, 30 minutes). Viewed under UV light, a predominant band corresponding to the expected product size was detected in each case. VWF76 and VWF115 PCR products can be seen in lane 1 and 2, respectively (panel A). VWF115-A3 PCR product is shown in panel B. In both A and B, 1kb ladder (Lad) was used to assess the size of the fragments.

The PCR bands were extracted from their gels and cloned into pET100/D-TOPO vector as described in Sections 2.1.2.1 and 2.1.2.6, respectively. The cloning reactions were then used to transform TOP10 competent *E.coli* cells (see Section 2.1.2.2). Six colonies for each fragment were collected and plasmid extraction performed as described in Section 2.1.5. A first screening to ensure the success of the cloning was obtained by digesting the minipreps with the restriction enzymes Nhe I and Sac I, which cut in close proximity to the cloning site (see Section 2.1.2.3 and Fig. 2.3). In Fig. 3.8, the screening for VWF115-A3 positive clones is depicted as an example.

After digestion with Nhe I and Sac I, the positive clones were identified on a 1% agarose gel by the presence of a band of 1040 bp corresponding to the cloned insert. If the cloning procedure was not successful, only a band of 5687 bp, corresponding to the cleaved parental vector, was visible. A similar strategy was employed for the screening of the other two fragments (not shown). The positive clones were then sequenced to confirm the presence of the correct insert and to ensure the absence of any unwanted PCR-introduced errors.

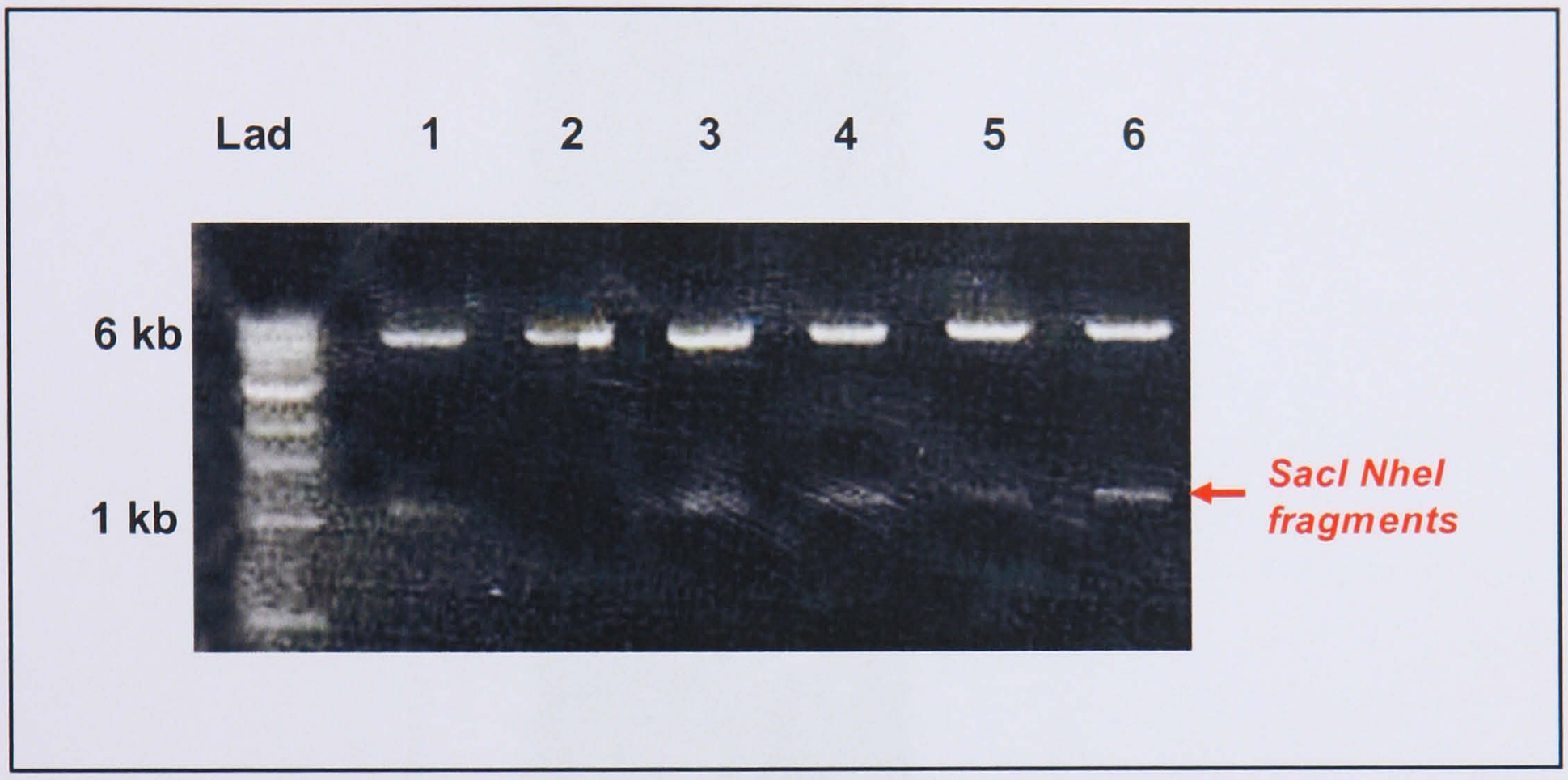


Fig. 3.8 Screening of VWF115-A3 pET100 positive clones. After VWF115-A3 PCR product cloning into pET100 vector and transformation of TOP10 competent *E.coli* cells, six colonies were screened as follows. After miniprep plasmid extraction, each vector was digested with Sac I and Nhe I. The digested reaction was then analysed on a 1% agarose gel (running conditions: 70 V, 30 minutes). If the cloning procedure was successful, a band of 1040 bp corresponding to the insert was detected (lane 1, 3, 4, 5, 6). Otherwise, only a band of 5687 bp corresponding to the cleaved parental vector was visible (lane 2). Lad: 1kb ladder of molecular weight markers.

The VWF115-A3 fragment contains an intra-molecular disulphide bond between cysteines C1686 and C1872 (see Fig. 3.6 in Section 3.2.1). These residues are conserved in the A1 domain and assumed to be important for correct domain structure. At the junction of the A2/A3 domain of VWF there are two other cysteines (C1669 and C1670), which probably pair to each other. I decided to mutate these into alanines, in order to ensure the formation of the C1686-C1872 disulphide bond and the correct folding of the molecule, minimising the generation of VWF115-A3 polymers due to the formation of inter-chain disulphide bonds. It has been found previously that these mutations do not compromise A3 domain function (M.A. Cruz, personal communication). The two mutations were introduced into VWF 115-A3 pET100/D-TOPO by site-directed mutagenesis (see Section 2.1.3.1). The primers used are listed

in Table 2 in the Appendix I. The PCR product was run on a 1% agarose gel and a single band of 6727 bp was detected under UV light (Fig. 3.9). After digestion with Dpn I to remove the parental metylated DNA, the reaction was used to transform XL10-Gold ultra competent *E.coli* cells (as described in Section 2.1.3.2). Following plasmid extraction, sequencing of the vector confirmed the introduced mutations.

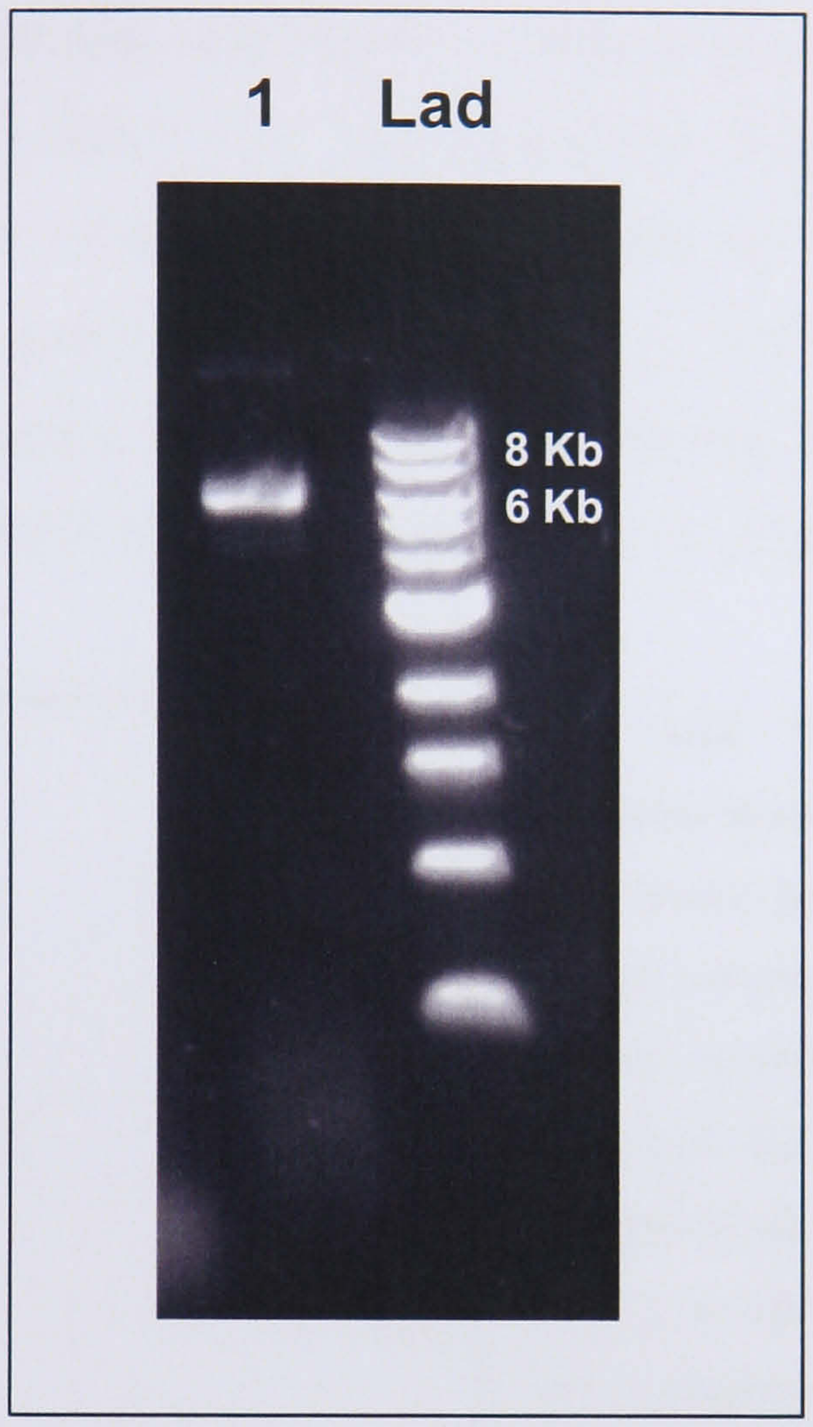


Fig. 3.9 Site-directed mutagenesis of C1669 and C1670 residues in VWF115-A3. C1669 and C1670 were mutated to alanines in pET100 VWF115-A3. After site-directed mutagenesis, the PCR product was run on a 1% agarose gel (running condition: 70 V, 60 minutes). A single band of the expected molecular weight of 6727 bp was detected under UV light (Lane 1). Lad: 1 kb ladder of molecular weight markers.

3.2.3 VWF76, VWF115 and VWF115-A3 expression and purification

VWF fragments were expressed in Rosetta or Rosetta Gami *E.coli* cells (see below), as described in Section 2.2.3. Induction of expression was achieved by adding 1 mM IPTG to the bacteria culture for 16 hours. IPTG induces the expression of both T7 RNA polymerase and the gene of interest. Subsequently, bacterial cells were harvested and lysed using BugBuster reagents (see Section 2.2.4.1). If the recombinant protein assumed the correct folding, it was found soluble in the cytoplasm together with bacteria proteins, whereas if it was miss-folded (and therefore insoluble) it was

sequestered in inclusion bodies. For each fragment, both soluble and insoluble fractions were collected and analysed by SDS-PAGE followed by Coomassie staining and Western blotting. As an example, Coomassie staining analysis of VWF115 soluble fraction and inclusion bodies is shown in Fig. 3.10. Most of this fragment was found in inclusion bodies (highlighted by an arrow in lane 2). After purification (see below for details), each fragment was dialysed in Tris-HCl 20 mM (pH 7.8) at 4°C overnight. The recovered material was centrifuged to remove eventual precipitated proteins and its purity checked by SDS-PAGE and Coomassie staining (see Fig. 3.11, 3.12 and 3.13). The high purity of the preparations allowed me to use the BCA total protein assay to measure the protein concentrations. The yield of the purification was quite high for all the fragments (>10 mg per litre of culture). The largest amount of material was recovered for VWF115 (up to 50 mg per litre of culture).

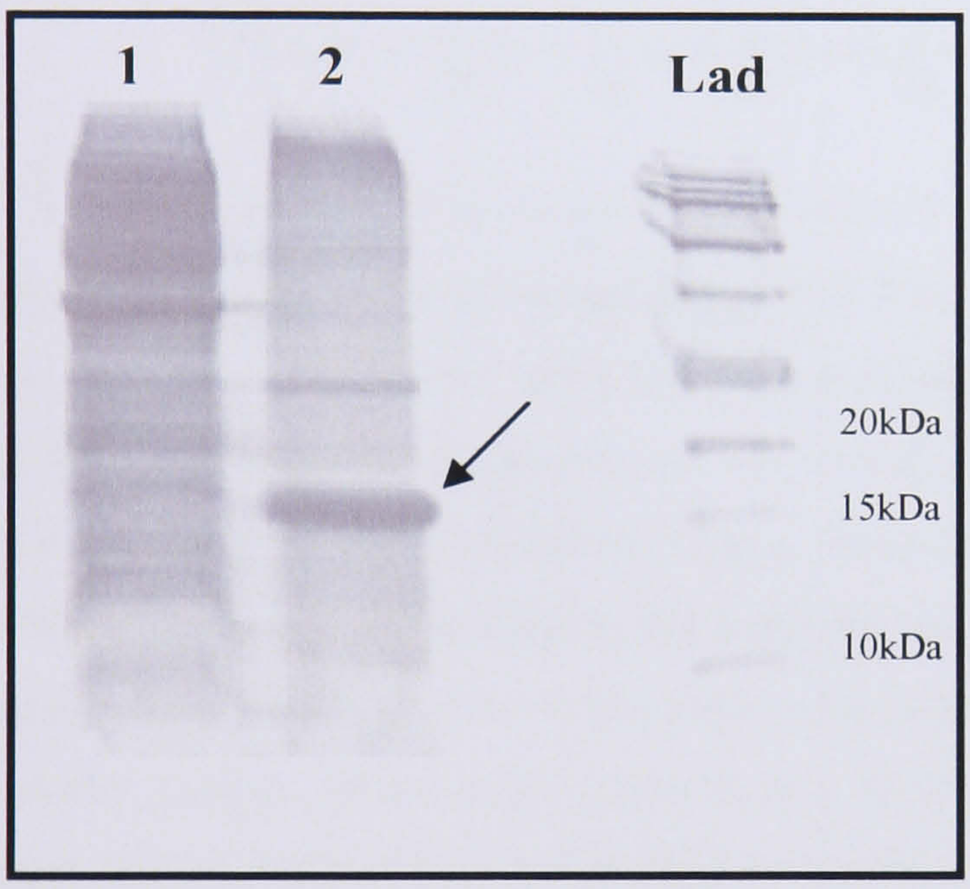


Fig. 3.10 VWF115 soluble fraction and inclusion bodies. Coomassie staining on a 16.5% Tris-Tricine gel of VWF115 soluble fraction (lane 1) and inclusion bodies (lane 2). Lad: ladder of protein molecular weight markers. The arrow highlights the presence of the 16.9 kDa band, corresponding to VWF115 expected molecular weight, in the inclusion bodies fraction. Western blot analysis using anti Xpress antibody confirmed that that band corresponded to the VWF115 fragment (not shown).

3.2.3.1 Expression and purification of VWF76

VWF76 was expressed in Rosetta *E. coli* cells and recovered from the soluble cytoplasmic fraction. Although this may appear as an advantage since the recombinant protein is soluble, most of the bacterial proteins are also present in the cytoplasmic fraction and they need to be removed during the purification step. The soluble material was directly loaded onto a nickel-chelating column, previously equilibrated with a buffer containing 20 mM imidazole. This column allowed the binding of the His-tagged VWF76, whereas most of bacterial proteins could not bind (Fig 3.11, left panel). However, some bacterial proteins may contain hystidine residues which promote binding to the column. To remove these bacterial contaminants, a stringent

washing step using 35 mM imidazole was necessary. VWF76 was finally eluted using 500 mM imidazole (highlighted by an arrow in Fig. 3.11, left panel).

The eluted fraction was then dialysed and analysed by SDS-PAGE followed by Coomassie staining. It migrates as a single band of the expected molecular weight of 12.5 kDa (Fig. 3.11, right panel).

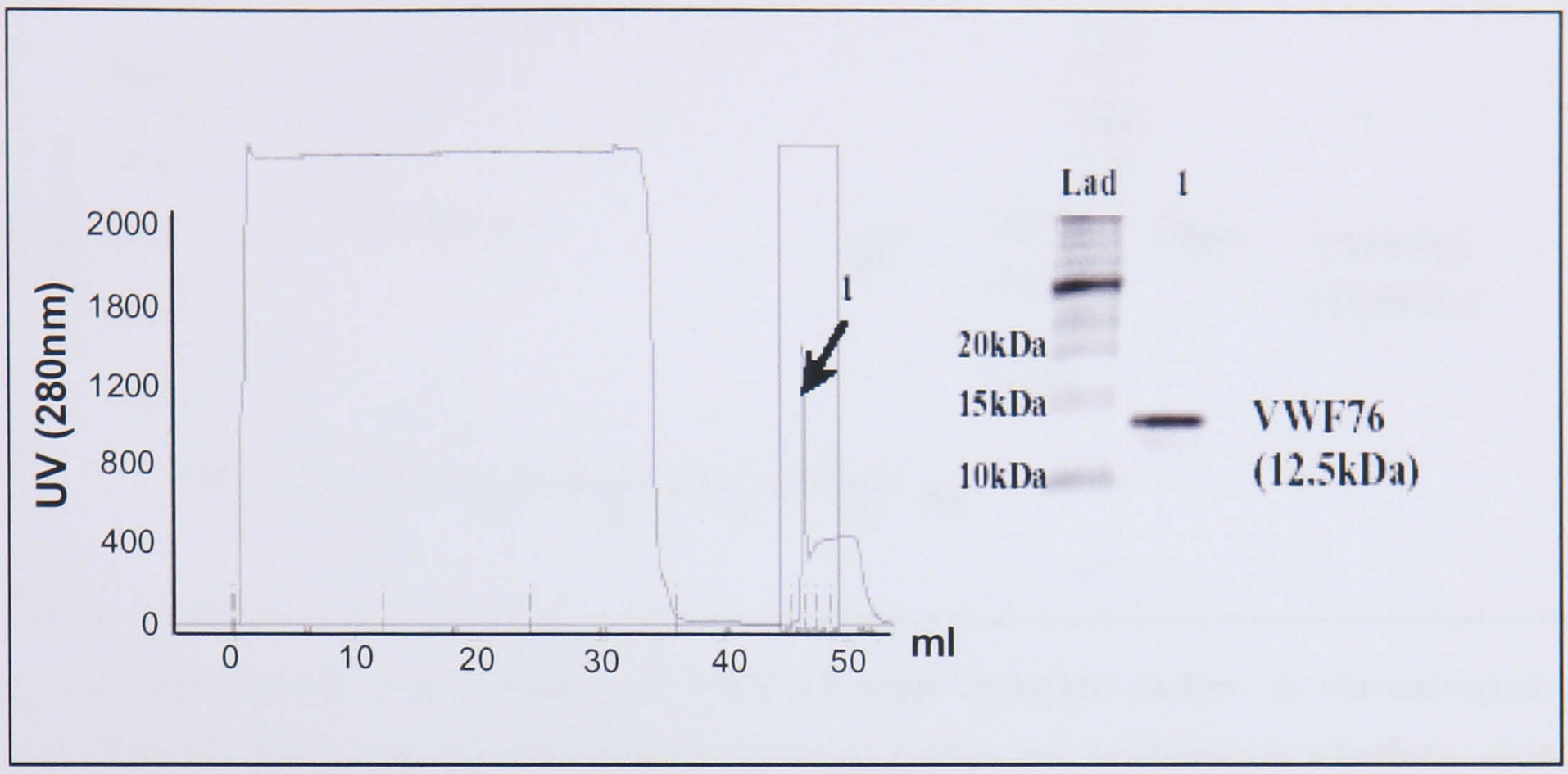


Fig. 3.11 Purification of recombinant VWF76. VWF76 was purified from the soluble cytoplasmic fraction of Rosetta *E. coli*, using a nickel-chelating column. Chromatogram of purification is shown on the left. The material was loaded onto the column in a buffer containing 20 mM Tris-HCl (pH 7.8), 500 mM NaCl and 20 mM imidazole. After a stringent washing step using 20 mM Tris-HCl (pH 7.8), 500 mM NaCl and 35 mM imidazole, the recombinant protein was eluted by increasing the concentration of imidazole to 500 mM. The eluted peak is highlighted by an arrow (1). On the right panel, Coomassie staining analysis of the eluted fraction on a 16.5% Tris-Tricine gel showed a single band of 12.5 kDa (lane 1). Lad: ladder of protein molecular weight markers.

3.2.3.2 Expression and purification of VWF115

VWF115 was expressed in Rosetta *E. coli* cells and mainly recovered in the insoluble inclusion body preparation, suggesting a miss-folding of the protein. An on-column refolding technique was attempted (Fig. 3.12, left panel) in order to allow the protein to gradually regain its native conformation. The inclusion bodies were solubilised in 8 M urea, before being passed over a nickel-chelating column. A linear gradient 8M-0M urea was performed. The gradual removal of urea allowed a slow renaturing of the protein immobilised on the column. After refolding, the protein was eluted with a 500 mM imidazole step gradient. A large amount of highly pure soluble recombinant protein could be recovered using this technique. This is due to the presence of only few bacterial proteins in the inclusion bodies, thus avoiding the stringent washing

steps which would have been required for the purification from the soluble cytoplasmic fraction. SDS-PAGE and Coomassie staining analysis showed the presence of a single band of 16.9 kDa (Fig. 3.12, right panel).

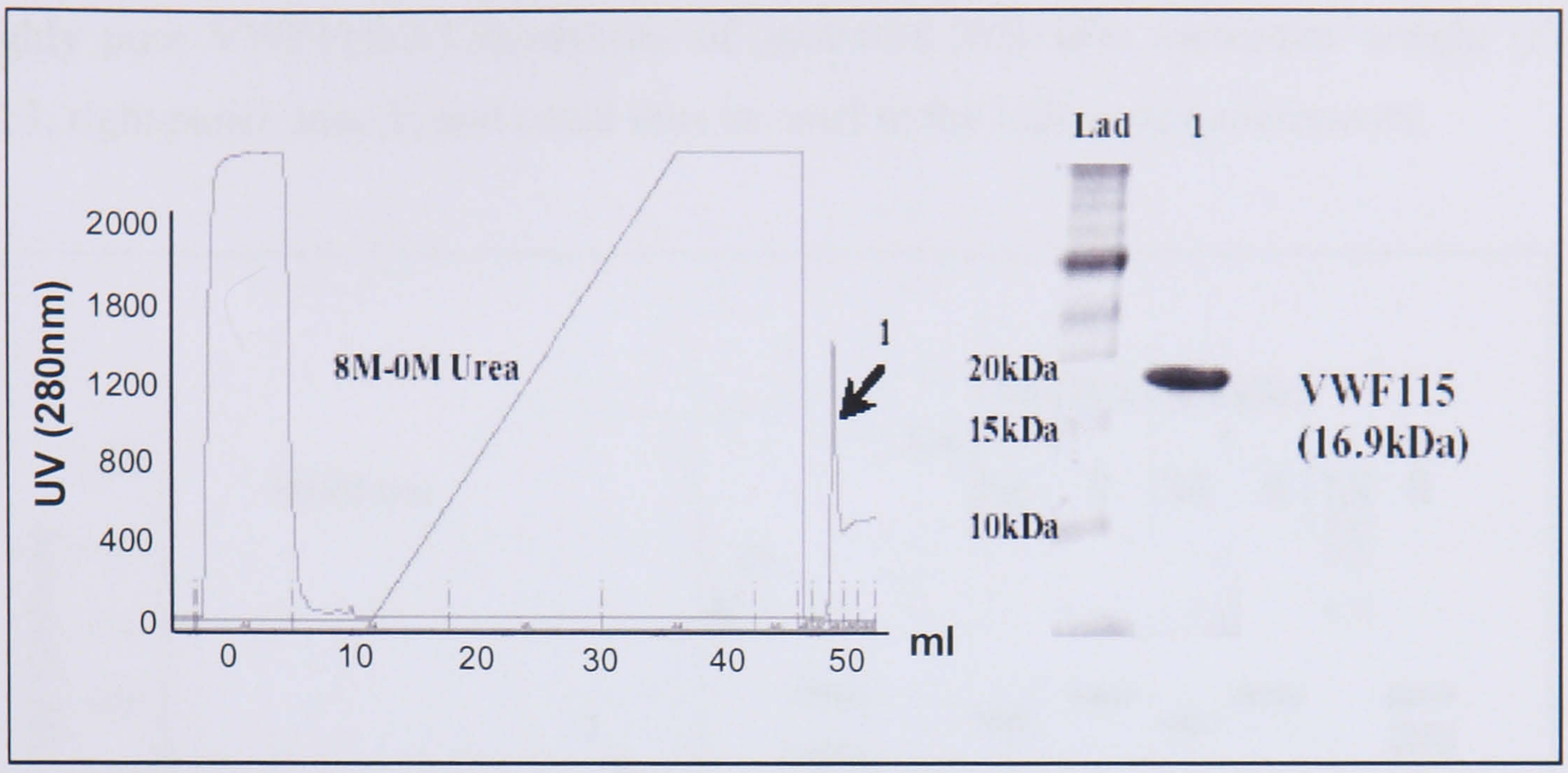


Fig. 3.12 Purification and refolding of VWF115 from inclusion bodies. A chromatogram of VWF115 purification is shown in the left panel. Inclusion bodies were solubilised in a buffer containing 20 mM Tris-HCl (pH 7.8), 500 mM NaCl, 20 mM imidazole and 8 M urea and refolded on the column using an 8M-0M urea linear gradient. The protein was eluted using 20 mM Tris-HCl (pH 7.8), 500 mM NaCl and 500 mM imidazole. The eluted peak is highlighted by an arrow. Coomassie staining analysis on a 16.5% Tris-Tricine gel is depicted in the right panel and it showed a single band of 16.9 kDa (lane 1). Lad: ladder of protein molecular weight markers.

3.2.3.3 Expression and purification of VWF115-A3

VWF115-A3 (with mutations C1669A and C1670A) was expressed in Rosetta-Gami *E. coli.* These particular cells allow cytoplasmic disulphide bond formation, since they have mutations, which inactivate some reducing enzymes (see Section 2.2.3.1). VWF115-A3 was recovered in inclusion bodies and purified using the technique of refolding on the column (Fig. 3.13, left panel). However, after elution, only a small amount of soluble, refolded material was recovered (peak 1, arrowed). After SDS-PAGE and Coomassie staining, it was visualised as a single band of the expected molecular weight of 38.6 kDa. The presence of the disulphide bond between cysteines 1686 and 1872 was confirmed by the mobility shift seen under reducing condition (Fig. 3.13, right panel lane 1, compare NR and R). In order to increase the yield of the purification, the column was subsequently stripped with a buffer containing 6 M guanidine-HCl and 50 mM EDTA in order to collect the insoluble proteins which may have precipitated onto the column (peak 2/3, arrowed). This material was refolded by

overnight dialysis into 20 mM Tris-HCl (pH 7.8). After dialysis, proteins still insoluble were removed by centrifugation. SDS-PAGE and Coomassie staining showed that this insoluble material contained predominantly multimeric VWF115-A3 (Fig. 3.13, right panel, lane 3), while the soluble fraction contained a large amount of highly pure VWF115-A3 monomers of predicted 38.6 kDa molecular weight (Fig. 3.13, right panel, lane 2) and could thus be used in the following experiments.

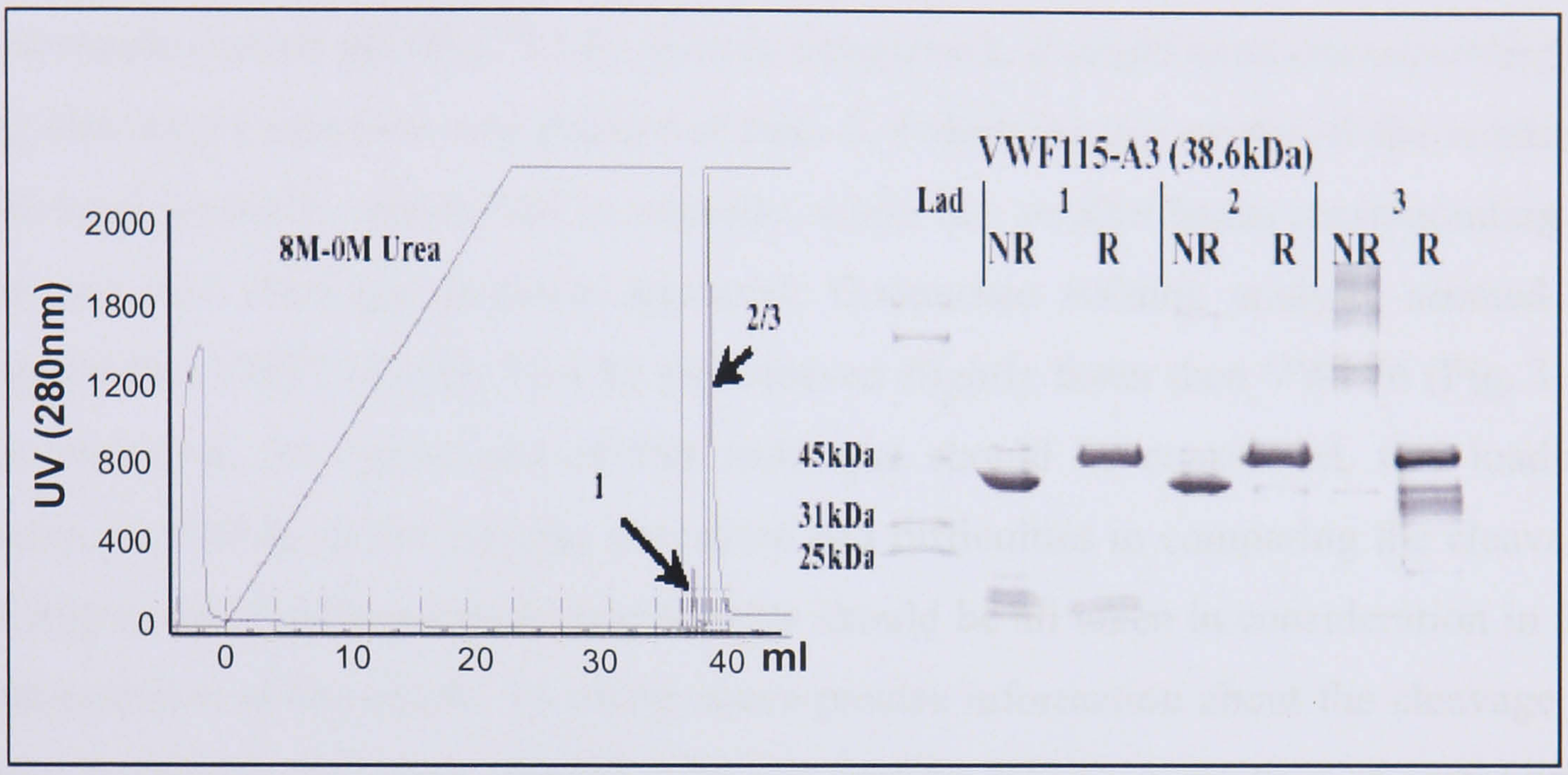


Fig. 3.13 Purification and refolding of VWF115-A3 from inclusion bodies. Inclusion bodies were solubilised in a buffer containing 8 M urea, 20 mM Tris-HCl (pH 7.8), 500 mM NaCl and 20 mM imidazole and refolded on the column, using an 8M-0M urea linear gradient. A chromatogram of VWF115-A3 purification is shown (left panel). The peak (1) eluted with 20 mM Tris-HCl (pH 7.8), 500 mM NaCl and 500 mM imidazole and the peak (2/3) stripped with 20 mM Tris-HCl (pH 7.8), 500 mM NaCl, 6 M guanidine-HCl and 50 mM EDTA are highlighted by a corresponding arrow. The eluted peak (1), the soluble (2) and the insoluble (3) stripped fractions were analysed by 4-15% Tris-HCl SDS-PAGE, under reducing (R) and non-reducing (NR) conditions, and Coomassie stained (right panel). VWF115-A3 was visualised as a single 38.6 kDa band (lane 1 and 2). The presence of the disulphide bond in the A3 domain was confirmed by the mobility shift between R and NR. The insoluble stripped fraction contained predominantly VWF115-A3 polymers and it was discarded (lane 3). Lad: ladder of protein molecular weight markers.

3.2.4 Proteolysis of VWF76, VWF115, VWF115-A3 by ADAMTS13

3.2.4.1 Qualitative analysis of cleavage

In order to provide preliminary information on the capability of ADAMTS13 to cleave each of the recombinant VWF A2/A3 domain substrates, a time course cleavage reaction was set up for each fragment. Purified recombinant ADAMTS13 (5.5 nM)

was pre-incubated without the recombinant VWF fragments at 37°C for 30 minutes in reaction buffer (20 mM Tris-HCl (pH 7.8), 150 mM NaCl and 5 mM $CaCl_2$). The pre-incubation was required to allow the optimal association with calcium, which has been demonstrated to be critical for the normal function and activity of the enzyme [147,196]. The cleavage reaction was initiated by the addition of 6 μM of each substrate and stopped by adding EDTA to sub-samples at different time points (0-6 hours). High substrate concentration was required to visualise the cleavage reactions on a Coomassie stained gel (Fig. 3.14). In each experiment, a single band corresponding to the full-length substrate was present at time 0. Following the course of the reaction, this band gradually diminished in intensity, while two smaller bands corresponding to the expected cleavage products appeared. Coomassie staining analysis seemed to suggest that VWF115 (Fig. 3.14 B) was cleaved slightly faster then VWF76 (Fig. 3.14 A). However, the limitations of this technique should be considered. Gel loading issues, variability in the staining procedure and difficulties in comparing the cleavage of fragments of different molecular weights should be all taken in consideration in the interpretation of the result. To obtain more precise information about the cleavage of these fragments, the same samples were analysed by HPLC. A gradient of acetonitrile allowed the resolution of the full-length substrate from the two cleavage products (Fig. 3.14, see peaks 1 and 2 in corresponding "VWF Cleavage Products" panel). To identify each peak, the peak fractions were collected and analysed by mass spectrometry (data not shown). In each case, peak 1 corresponded to the N-terminal cleavage product and peak 2 corresponded to the C-terminal fragment. Mass spectrometry analysis also confirmed that proteolysis occurred between the expected Y1605-M1606 bond. To estimate the efficiency of the cleavage for each fragment, the appearance of each peak 1 (N-terminal tagged cleavage product) was monitored over time and represented as a percentage of total substrate proteolysis. Results are shown graphically in Fig. 3.14 (A, B and C), as "% Substrate Cleavage". The rate of proteolysis of VWF115 and VWF115-A3 was quite similar, whereas VWF76 was cleaved slightly slower. These preliminary data were not used to accurately calculate the catalytic constants for the three fragments, as the experiments were performed using high substrate concentrations (very possibly > than the K_m for the reactions) (see below).

As previously mentioned, full-length VWF can be cleaved by ADAMTS13 *in vitro* in the presence of denaturants which are able to unfold the molecule and expose the cleavage site [149,196]. In recent studies, it was shown that also the intact VWF A2

domain requires denaturing conditions to be effectively proteolysed by ADAMTS13 [186,256]. In my experiments, VWF76, VWF115 and VWF115-A3 were readily cleaved by ADAMTS13 in the absence of denaturants, suggesting they were already in a permissive conformation. However, to test if denaturants can further improve the cleavage, the experiments described above were repeated in the presence of 1 M urea. The rates of proteolysis were comparable to those in the absence of urea (data not shown). This confirmed that the fragments in the absence of denaturants were already in a permissive conformation for cleavage. It also showed that 1 M urea does not significantly influence ADAMTS13 function against these short substrates.

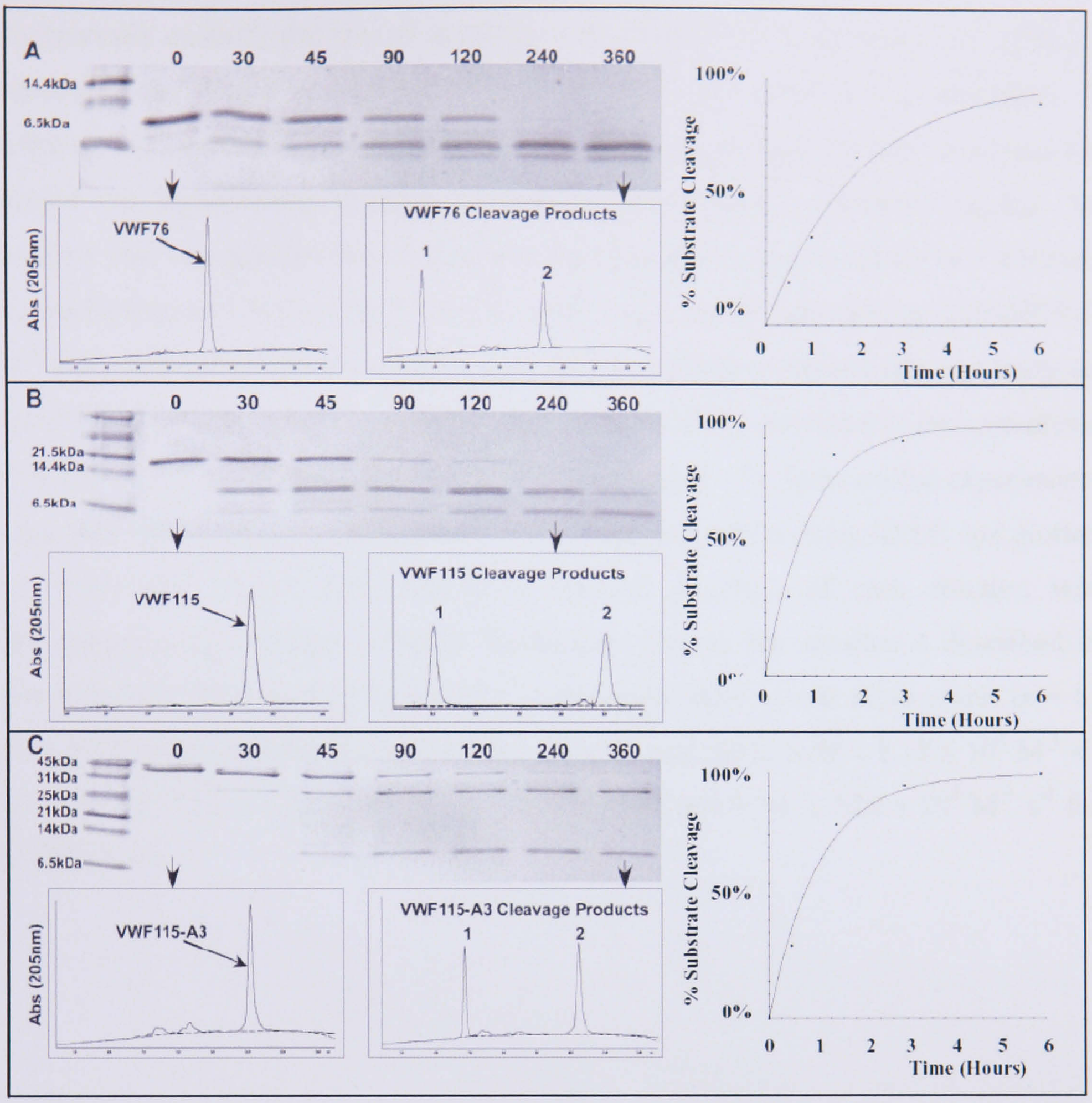


Fig. 3.14 VWF76, VWF115, VWF115-A3 cleavage by ADAMTS13. 6 μM of VWF76 (A), VWF115 (B) and VWF115-A3 (C) were incubated with 5.5 nM ADAMTS13, in reaction buffer (20 mM Tris-HCl (pH 7.8), 150 mM NaCl and 5 mM $CaCl_2$). Sub-samples were stopped with EDTA at different time points (0-6 hours) and analysed by Coomassie staining on a 16.5 % Tris-Tricine gel and by HPLC. For each fragment, a single band corresponding to the full-length substrate at time 0 was visible on the gel. Following the course of the reaction, this band gradually diminished in intensity, while two smaller bands corresponding to the expected cleavage products appeared. Using the HPLC, a gradient of acetonitrile allowed the resolution of the full-length substrate from the two cleavage products. HPLC peaks were collected and analysed by mass spectrometry to confirm their identity: the full-length substrate is highlighted by an arrow, while the two cleavage products are numbered 1 and 2, the N-terminal and the C-terminal cleaved fragments, respectively. In each case, the rate of cleavage was determined monitoring the appearance of cleavage product peak 1. The results are shown graphically on the right hand side of each of the corresponding figures. In each graph, the percentage of substrate cleavage was plotted against time.

3.2.4.2 Quantitative analysis of cleavage

To precisely quantify the rate of cleavage of the three VWF fragments, low substrate concentrations should be used to conform to pseudo-first order kinetic conditions. If substrate concentration is much lower than K_m, changing the substrate concentration should not significantly change the value of the catalytic efficiency k_{cat}/K_m. To confirm this, two parallel time course experiments were set up in which two different concentrations of VWF115 (0.25 and 0.5 μM) were used as substrate for ADAMTS13 (8.5 nM). Sub-samples were stopped with EDTA at different time points and analysed by HPLC. The rate of cleavage plotted against time clearly showed that the proteolysis of the two amounts of substrate was comparable (Fig. 3.15). Time course experiments were then set up using 0.5 μM of each VWF fragment, analysed by HPLC and plotted as before (Fig. 3.16). The specificity constant (k_{cat}/K_m) of each reaction was determined using Enzfitter software, fitting the curve to the equation 1 described in Materials and Methods (see Section 2.3.3). Repeated time course experiments (n = 8) allowed a robust determination of k_{cat}/K_m for each fragment: 6.39 ± 1.18 x 10^4 M^{-1} s^{-1} for VWF76, 7.83 ± 1.18 x 10^4 M^{-1} s^{-1} for VWF115 and 6.70 ± 2.78 x 10^4 M^{-1} s^{-1} for VWF115-A3.

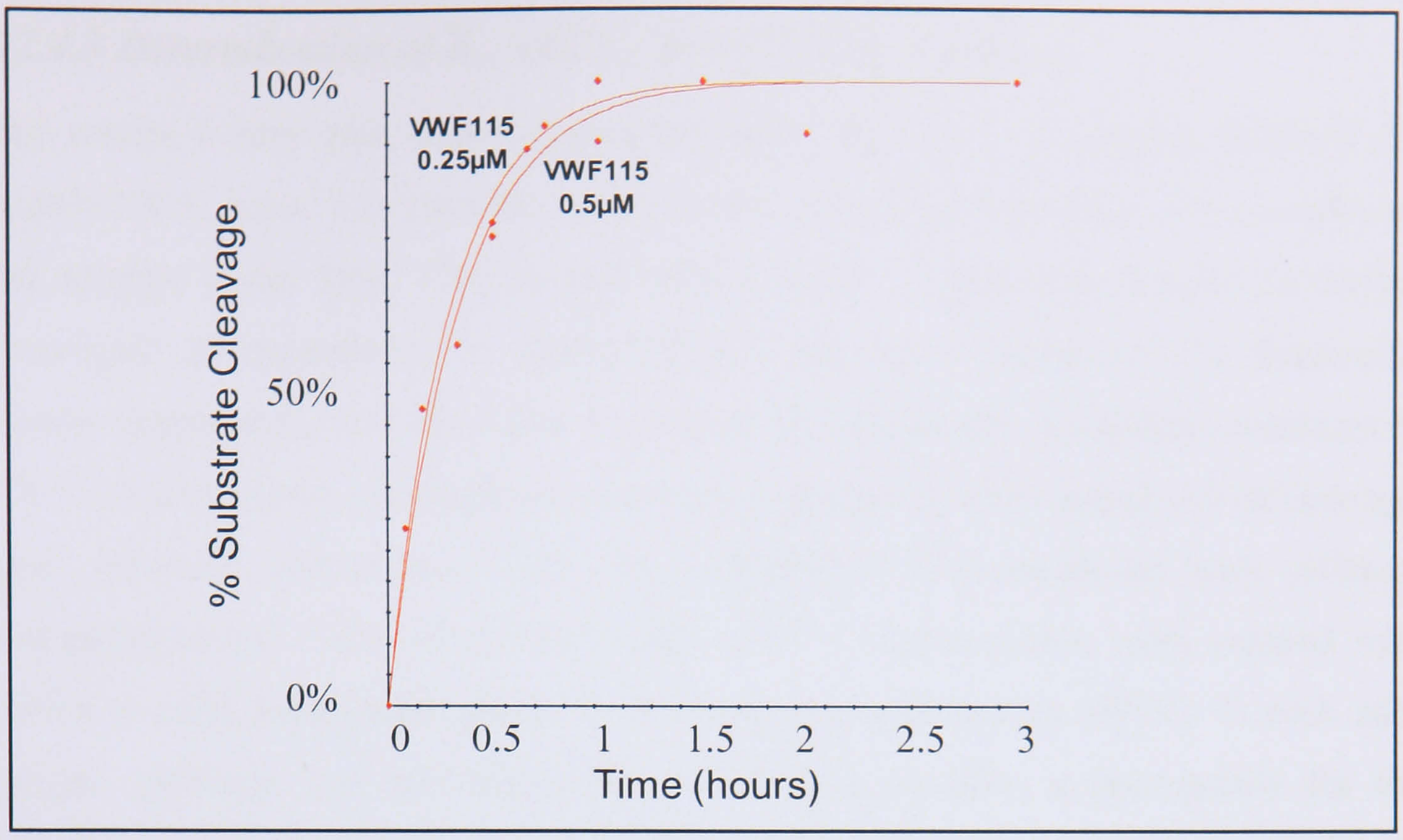
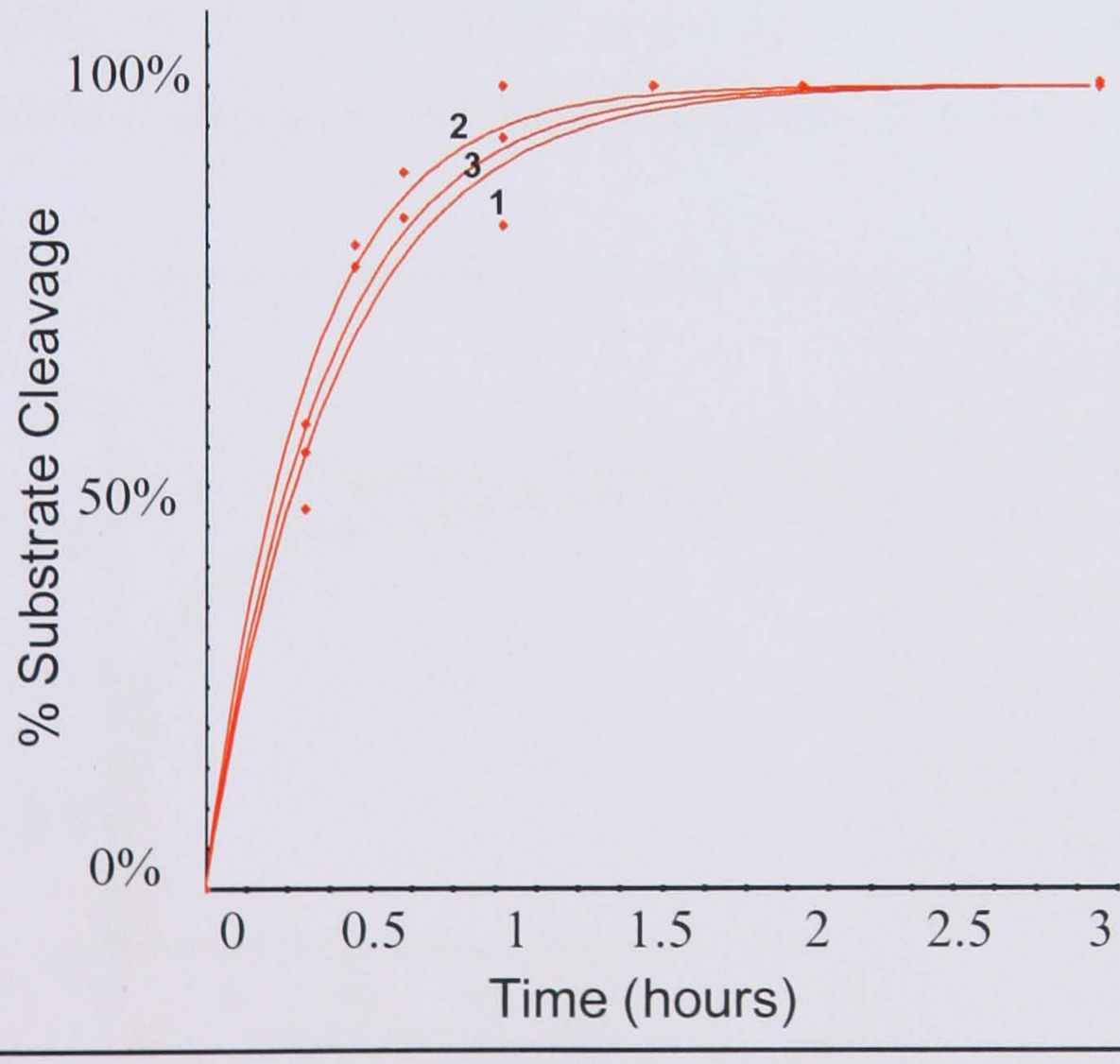


Fig. 3.15 Proteolysis of VWF115 is independent of its concentration. 0.25 and 0.5 μM of VWF115 were incubated with 8.5 nM of ADAMTS13 in two parallel experiments, in reaction buffer (20 mM Tris-HCl (pH 7.8), 150 mM NaCl and 5 mM $CaCl_2$). Sub-samples were taken at specific time points, stopped with EDTA and analysed by HPLC. The graph clearly shows that the different amounts of substrate were cleaved at a similar rate.



VWF substrate	k_{cat}/K_m (x 10^4 M^{-1} s^{-1})
1. VWF76	6.39± 1.18
2. VWF115	7.83± 1.18
3. VWF115-A3	6.70 ± 2.78

Fig. 3.16 Proteolysis of VWF76, VWF115 and VWF115-A3 by ADAMTS13 under low substrate concentrations. 0.5 μM of each substrate was incubated with 8.5 nM of ADAMTS13, in reaction buffer (20 mM Tris-HCl (pH 7.8), 150 mM NaCl and 5 mM $CaCl_2$). The reaction was stopped with EDTA at specific time points and sub-samples analysed by HPLC. The percentage of substrate cleavage was plotted against time. k_{cat}/K_m value (± S.E.) for each substrate was calculated and is shown in the table (*n* = 8).

3.2.4.3 Determination of K_m and k_{cat} for VWF115 cleavage

The results I have just shown suggested that VWF115 is a suitable substrate for ADAMTS13, since it is cleaved readily under normal physiological ionic conditions and slightly faster than VWF76 and VWF115-A3. I therefore decided to further investigate its proteolysis by ADAMTS13. I set out to determine the *Michaelis-Menten* constant K_m and the turnover number k_{cat}. Estimates of catalytic constants of VWF115 proteolysis were obtained from the dependence of the initial rate of cleavage upon substrate concentration. 8.5 nM ADAMTS13 was incubated with different concentrations of VWF115 (0.25-25 μM) at 37°C. Sub-samples were stopped with EDTA at early time points (0, 5, 10 minutes) and analysed by HPLC. In each sub-sample, cleavage was less than 15% of the total possible, a prerequisite for the calculation of first-order kinetic parameters, since substrate proteolysis is essentially linear during this phase. The initial velocity (nM/sec) of cleavage was plotted against substrate concentration and the data were fitted to the *Michaelis-Menten* equation (see equation 2 in Section 2.3.4) (Fig. 3.17). Values for K_m and V_{max} were derived. The parameter k_{cat} was calculated from the ratio $V_{max}/[E]$. Separate experiments (n=4) gave a mean value of 1.61 ± 0.47 μM for K_m, and 0.14 ± 0.06 s^{-1} for k_{cat}, from which k_{cat}/K_m of 8.70 x 10^4 $M^{-1}s^{-1}$ could again be calculated. This was compatible with the previous estimation of catalytic efficiency (see Section 3.2.4.2).

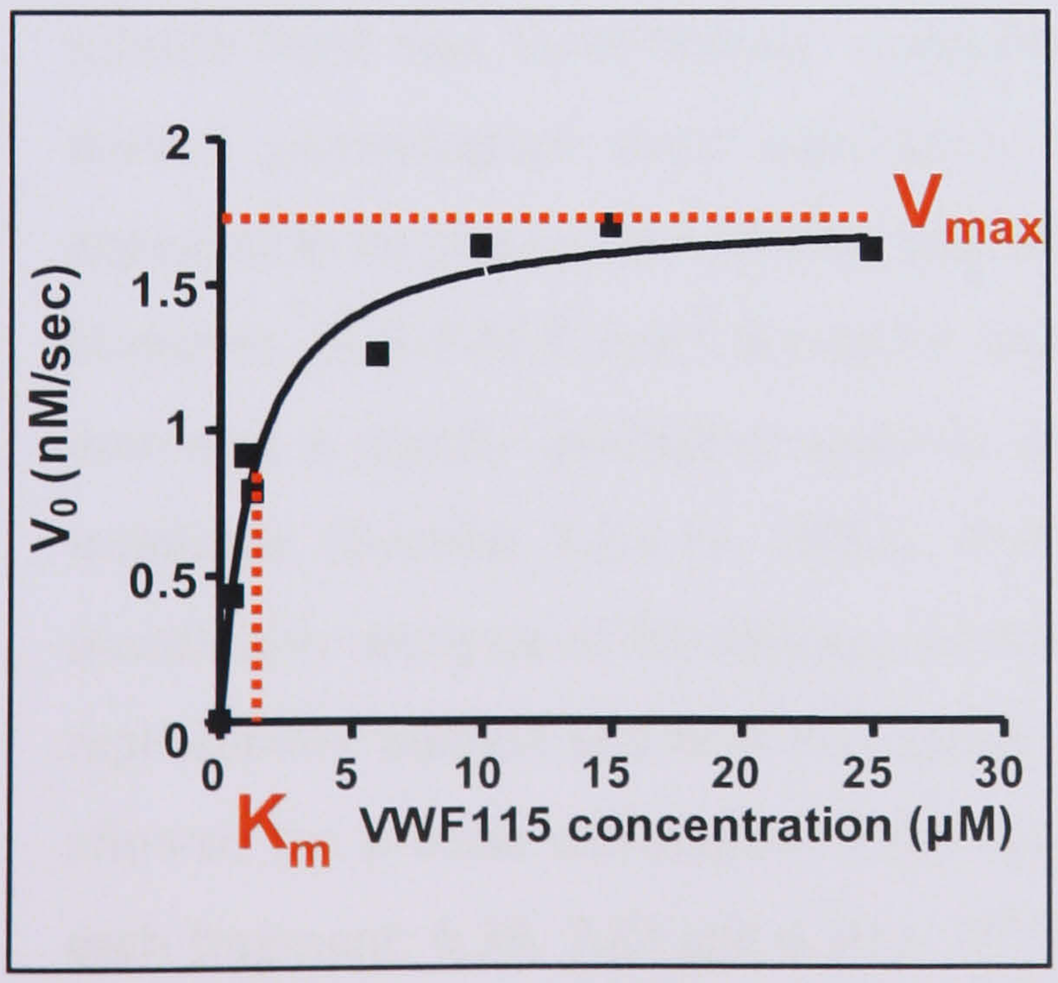


Fig. 3.17 *Michaelis-Menten* plot of VWF115 cleavage by ADAMTS13. 8.5 nM ADAMTS13 was incubated with different concentrations of VWF115 (0.25-25 μM) in reaction buffer (20 mM Tris-HCl (pH 7.8), 150 mM NaCl and 5 mM $CaCl_2$). The reactions were stopped at early time points (0, 5, 10 min). Initial velocity (V_0) was plotted against substrate concentration. Data were fitted to *Michaelis-Menten* equation, using Graph Pad Prism 4 software. The experiment shown gave a value of 1.31 μM for K_m and 1.75 nM/sec for V_{max}, from which k_{cat} was calculated to be 0.20 s^{-1}.

3.2.5 Discussion

ADAMTS13 cleaves the peptidyl bond Y1605-M1606 in the A2 domain of VWF [106]. regulating its plasma multimeric size. *In vivo,* ADAMTS13 activity seems to be shear-dependent [149]. *In vitro*, it can only cleave VWF in the presence of denaturants (guanidine-HCl or urea) and extended incubation times [196]. This suggests that the conformation of VWF is a critical determinant of its susceptibility to ADAMTS13 proteolysis. In recent studies, it has been reported that the isolated intact VWFA2 domain is also not readily cleaved by ADAMTS13 [186,256] (see also Section 3.6). This can be attributed to the folded conformation of the A2 domain with its cleavage site buried in the centre of the molecule (see Fig. 1.10 in Section 1.3.5.1).

I expressed recombinant VWF fragments, spanning different regions of A2 and A3 domains: VWF76 (1593-1668), VWF115 (1554-1668), VWF115-A3 (1554-1874). The expression of these fragments in bacteria was successful (Section 3.2.3). Particularly, the on-column refolding technique of miss-folded proteins from inclusion bodies allowed the recovering of a large amount of protein (up to 50 mg per litre of culture), free from bacterial contaminants. Apart of the high yield, other advantages of bacterial over mammalian expression are the rapid time of growth and requirement of simple nutriments. Subsequently, the cleavage of the three fragments by ADAMTS13 was investigated. Coomassie staining analysis (Fig. 3.14) showed that they were all readily proteolysed by ADAMTS13 in the absence of denaturants, suggesting that the scissile bond was constitutively accessible, allowing the analysis of cleavage under normal physiological ionic conditions. Furthermore, VWF115 and VWF115-A3 appeared to be cleaved at a similar rate, whereas VWF76 was cleaved slightly slower. However, SDS-PAGE and Coomassie staining do not allow a quantitative analysis and moreover a merely qualitative analysis can be confounded by the limitations of this technique (Section 3.2.4.1). HPLC analysis was optimised to allow an accurate quantitative analysis of the kinetics of the cleavage. It was found to be a precise and reproducible method and relatively quick, after shortening the acetonitrile gradient. It allowed the precise calculation of the catalytic efficiency k_{cat}/K_m for the cleavage of each fragment: 6.39, 7.83 and 6.70 x 10^4 M^{-1} s^{-1} for VWF76, VWF115 and VWF115-A3, respectively (Fig. 3.16). These results suggest that the presence of A3 domain does not influence the rate of A2 domain proteolysis, despite a binding site for ADAMTS13 having been recently reported in the A3 domain [107] (see Chapters 5 and 6 for further discussion). VWF76 was cleaved slightly slower than VWF115, suggesting

that residues between 1554 and 1592 in the A2 domain might not be essential for its cleavage. Furthermore, the k_{cat}/K_m value gives an idea of the overall efficiency of the enzyme. From the absolute value calculated, it appears that ADAMTS13 is not a very efficient enzyme (see Chapter 5 for further discussion). VWF115 proteolysis was further investigated by monitoring the initial rates of cleavage at different substrate concentrations (Fig. 3.17). k_{cat} and K_m were calculated to be 0.14 s^{-1} and 1.61 μM, respectively. k_{cat}/K_m could again be calculated, giving a value of 8.70 x 10^4 $M^{-1}s^{-1}$, which is in good agreement with the estimate of catalytic efficiency derived from the time course experiment.

3.3 CHARACTERISATION OF ADAMTS13 RECOGNITION OF VWF115

3.3.1 Introduction

In the previous Section, I have shown that a shorter VWF A2 fragment, VWF115, is readily cleaved by ADAMTS13 in the absence of denaturants. I fully characterised the kinetics of its cleavage, deriving values for k_{cat}/K_m and k_{cat} and K_m individually. The K_m value is known to be an approximation of the binding affinity of enzyme and substrate. In order to study the VWF115 binding interaction with ADAMTS13 and to calculate the equilibrium dissociation constant K_D, I optimised two different techniques, SPR and an equilibrium plate-based binding assay. The two approaches are described in this Section, along with their advantages and limitations.

3.3.2 Characterisation of ADAMTS13 binding to VWF115 by SPR

The interaction between VWF115 and ADAMTS13 was initially studied using a dual flowcell BIAcore X biosensor system utilising SPR (see Section 2.4.1). This technique allows monitoring the binding between molecules in real time. Both association and dissociation phases are visualised. Furthermore, the BIAcore system includes the BIAevaluation software, which provides various models (based on different types of interactions) to which the binding curves can be fitted (see Section 2.4.2). This software enables the determination of the association and dissociation rate constants (k_a and k_d, respectively) and the equilibrium dissociation constant K_D.

3.3.2.1 Immobilisation of ADAMTS13 or VWF115 on a CM5 chip using monoclonal antibodies

Various attempts were made using specific monoclonal antibodies to immobilise either ADAMTS13 or VWF115 onto a CM5 chip surface. Antibodies offer a number of advantages for capturing biomolecules over the sensor chip. They can be readily and easily immobilised on the sensor surface using amine coupling, without compromising their antigen-binding capacity. Furthermore, their high selectivity for specific antigens allows the capture of ligands from impure sample. Finally, capture of the ligand is in a controlled orientation, allowing the exposure of the particular domains which need to be investigated.

An early attempt using a monoclonal anti-ADAMTS13 CUB domain antibody is depicted in Fig. 3.18. After surface activation with NHS/EDC (see Section 2.4.1.2).

100 µl of anti-CUB antibody (50 µg/ml) was injected over both flow cell 1 and 2 of a CM5 sensor chip. Free reactive surface groups were blocked, by injecting ethanolamine-HCl. ~ 16000 RU of the antibody was covalently immobilised over both flow cells (Fig. 3.18 A). 100 µl of ADAMTS13 (2 µM) was passed over flow cell 2 only and ~ 4200 RU was immobilised (Fig. 3.18 B). Flow cell 1 was used as a reference cell. Different concentrations of VWF115 were injected over both the active and the control flow cells, in the absence of $CaCl_2$. Calcium was omitted in order to limit proteolysis, which might confound evaluation. A binding response could be detected in flow cell 2, none in flow cell 1, suggesting a specific interaction between VWF115 and ADAMTS13. Different regeneration conditions were tested: glycine-HCl (pH 2) seemed to completely strip ADAMTS13 from the anti-CUB antibody, without damaging the antibody-coated surface (Fig. 3.18 B). Unfortunately, ADAMTS13 dissociated quite rapidly from the anti-CUB antibody (Fig. 3.18 B), making comprehensive analysis impractical since SPR relies of the reproducibility of ligand coupling and repeating injections of the analyte. Furthermore, a drifting base-line often represents a major problem during the fitting of the curves. Two other available monoclonal antibodies, directed to epitopes myc-tag and disintegrin-like domain, respectively, and a polyclonal antibody anti TSR (2-4) domain were subsequently tested. However, they all showed a similar problem of fast dissociation from ADAMTS13 (data not shown).

Two separate attempts were made to immobilise VWF115 on the chip. This would have been the best option, practically, since it required less materials to be used (both ligand and analyte). This is because the SPR response is proportional to the molecular weight of the molecule which is used as the analyte (see Section 2.4.1.3). After surface activation, ~ 6000 RU of an anti-N terminal His-tag antibody, anti-His G antibody, was immobilised on both flow cells of a CM5 sensor chip (Fig 3.19 A). This antibody was designed to specifically bind to the N-terminal His-tag, uniquely recognising a glycine residue close to the histidines. VWF115 was passed over flow cell 2 and ~1400 RU were immobilised (Fig 3.19 B). However, when ADAMTS13 was injected over both flow cells, a non specific binding was detected in flow cell 1, suggesting ADAMTS13 C-terminal His-tag may have interacted with the antibody (Fig 3.19 B). A second attempt to immobilise VWF115 used an anti-Xpress antibody, recognising the Xpress epitope contained on the VWF115. Unfortunately, this strategy was also unsuccessful due to the fast off-rate of VWF115 from the antibody (data not shown).

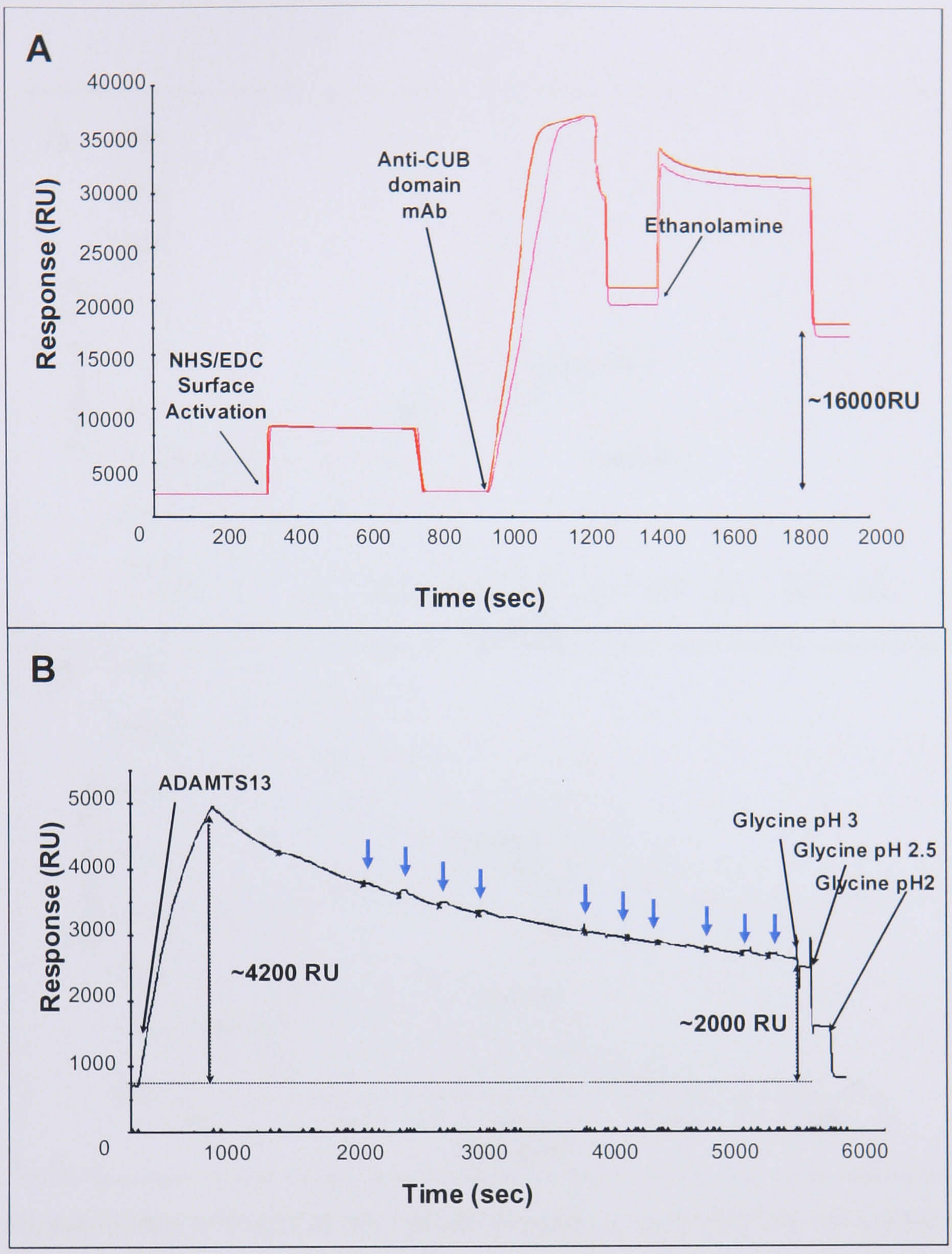


Fig. 3.18 Immobilisation of ADAMTS13 via an anti-CUB antibody and VWF115-ADAMTS13 binding. **(A)** The anti-CUB antibody was immobilised on both flow cell 1 (red line) and 2 (pink line). The chip surface was activated injecting 50 µl of 0.4 M EDC/ 0.1 M NHS. Immediately after, 100 µl of anti-CUB antibody (50 µg/ml) in acetate buffer (pH 5.0) was injected in order to be covalently bound onto the chip. All free reactive surface groups were then blocked with 35 µl of 1 M ethanolamine-HCl (pH 8.5). Following this procedure, ~16000 RU of anti-CUB antibody could be immobilised on the chip. **(B)** 100 µl of ADAMTS13 (2 µM) in HBS-P buffer was injected over flow cell 2 only. ~ 4200 RU of ADAMTS13 was bound to the anti-CUB antibody. 30 µl of different concentrations of VWF 115 in HBS-P buffer were injected (blue arrows), giving a specific binding response (not shown). However, ADAMTS13 appeared to dissociate quite fast from the antibody: after less than 10 minutes, only ~2000 RU were still bound to it. Different regeneration conditions [glycine-HCl (pH 3), glycine-HCl (pH 2.5) and glycine-HCl (pH 2)] were also tested: glycine-HCl (pH 2) completely removed ADAMTS13 from the antibody.

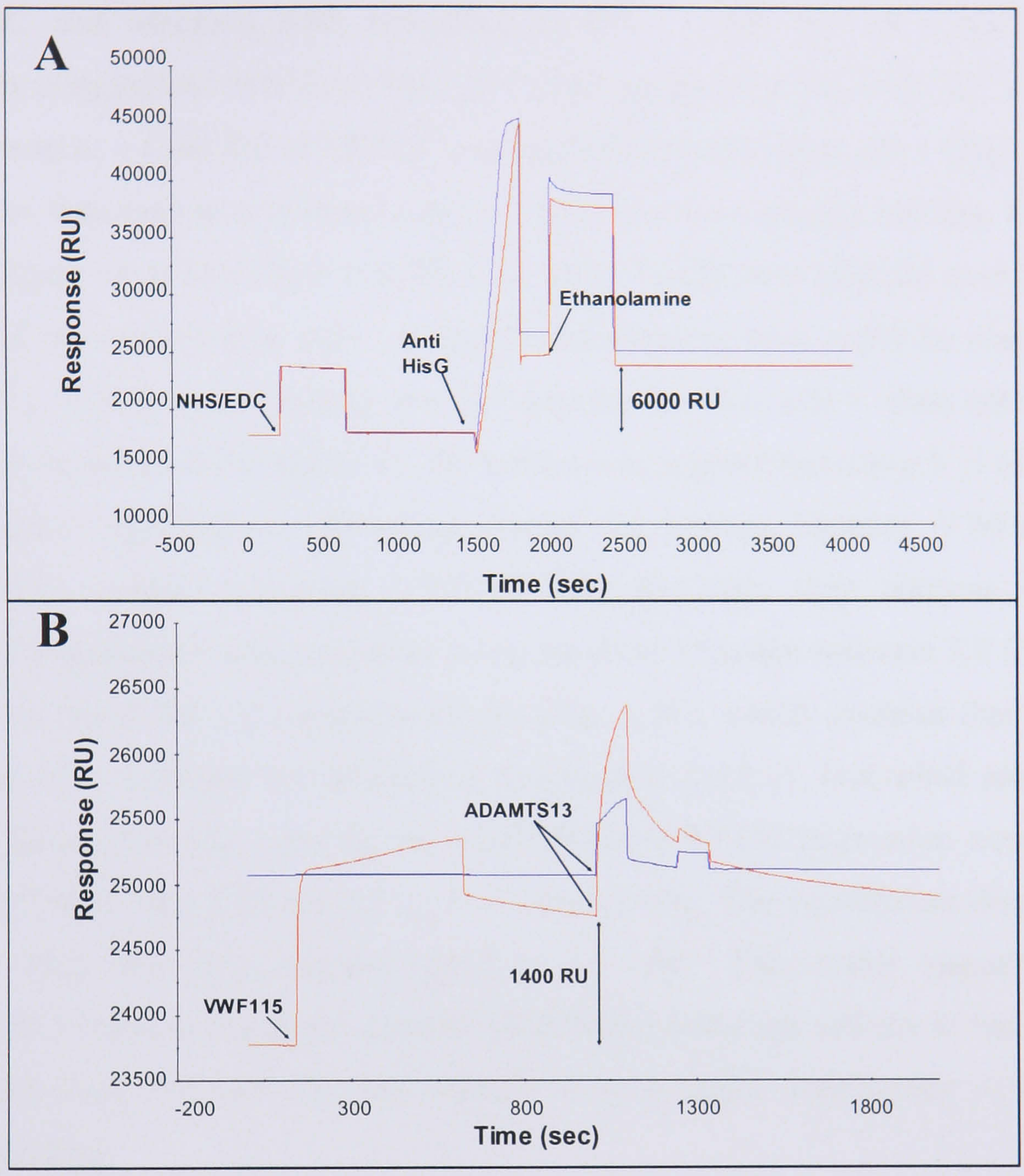


Fig. 3.19 Immobilisation of VWF115 via Anti-His G antibody and VWF115-ADAMTS13 binding. **(A)** Anti-His G antibody was immobilised on both flow cell 1 (blue line) and 2 (red line). After surface activation, 50 µl of 30 µg/ml anti-His G antibody in acetate buffer (pH 5.0) was injected. Following ethanolamine-HCl injection, ~ 6000 RU of anti-His G antibody could be immobilised on the chip. **(B)** 80 µl of 300 µg/ml VWF115 in HBS-P buffer was injected over flow cell 2 only. ~1400 RU of VWF115 was bound to the anti-His G antibody. 30 µl of 1 µM ADAMTS13 in HBS-P buffer was injected over both flow cells. A specific binding response was detected on flow cell 2 (red line). However, non specific binding was detected on flow cell 1 (blue line), suggesting ADAMTS13 interacted with the antibody.

3.3.2.2 Direct immobilisation of VWF115 on a CM5 chip

In the absence of a successful antibody capturing method, I directly immobilised VWF115 on the sensor surface by amine coupling. After surface activation with NHS/EDC and blocking with ethanolamine-HCl, ~ 600 RU of VWF115 was covalently immobilised over flow cell 2 of a CM5 sensor chip (Fig. 3.20 A). Using the same approach, ~ 1500 RU of hEPCR was immobilised over flow cell 1 (Fig. 3.20 B), which then was used as a reference cell to control for non-specific binding. Different concentrations of ADAMTS13 (10, 20, 27.5 and 55 nM) were injected over both the active and the control flow cells. A specific binding response could be observed in flow cell 2. Non-specific binding was not detected on flow cell 1 (data not shown). After each injection of ADAMTS13, the surface was regenerated using 5 µl of 10 mM NaOH, which appeared to effectively disrupt the binding between VWF115 and ADAMTS13, without removing VWF115 from the chip. Data analysis of three individual experiments was performed using the BIAevaluation software 3.0 fitting the binding curves to the 1:1 Langmuir model (Fig. 3.21), which assumes that the two molecules have a simple 1:1 interaction (see Section 2.4.2.1). Individual association (k_a) and dissociation (k_d) rates for the ADAMTS13-VWF115 interaction were 10.1 ± 3.35 x 10^4 $M^{-1}s^{-1}$ and 1.72 ± 0.29 x 10^3 s^{-1} respectively. The equilibrium dissociation constant (K_D) was also derived (20.0 ± 5.8 nM). This result suggested that ADAMTS13 binds to the short substrate (VWF115) with high affinity in the absence of calcium ions. The slow off-rate seemed to be a major determinant of the high affinity binding.

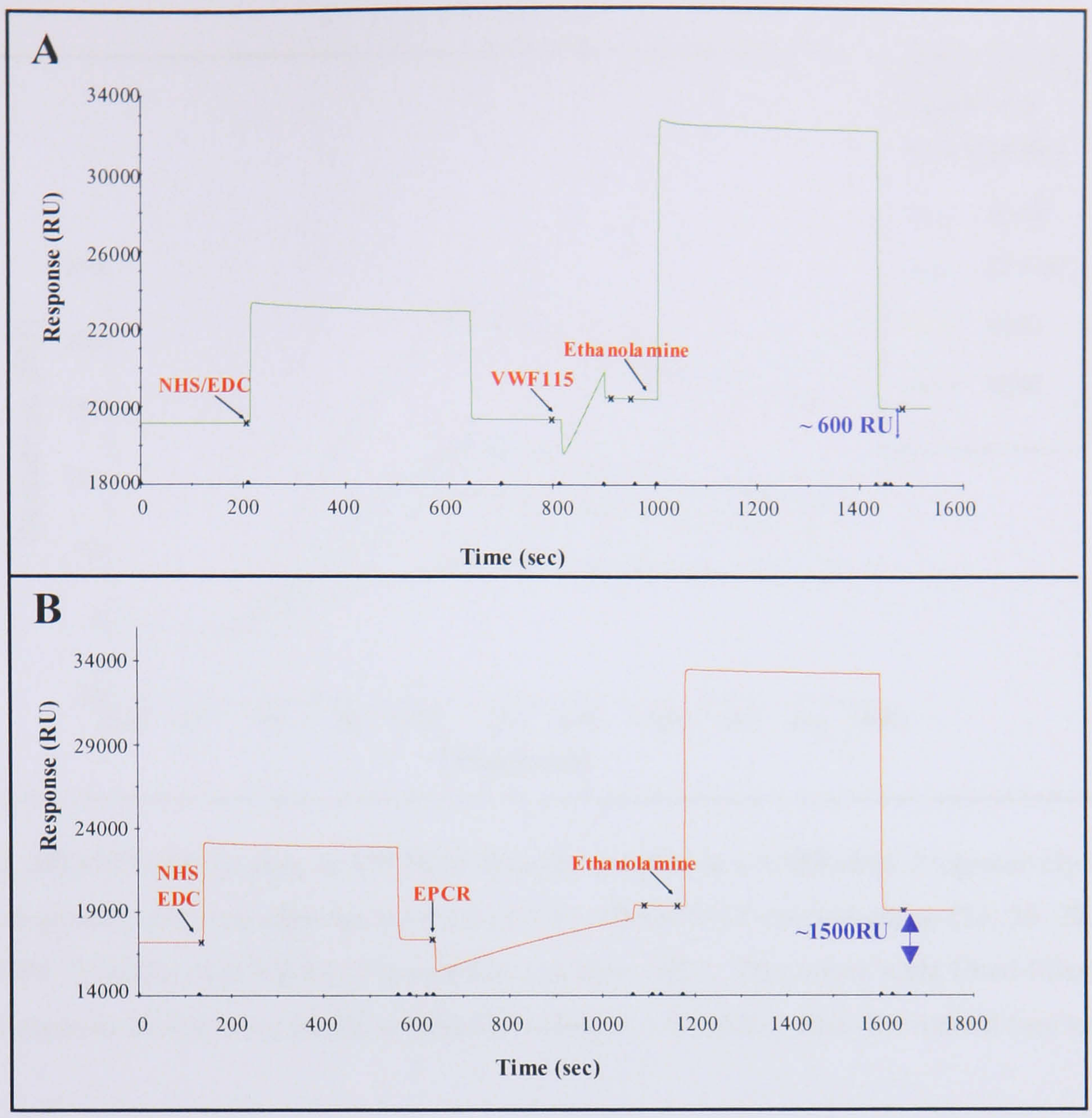


Fig. 3.20 Immobilisation of VWF115 and hEPCR. (A) VWF115 immobilisation over flow cell 2. The chip surface was activated with NHS/EDC. Immediately after, 10 µl of 0.6 µM VWF115 in acetate buffer (pH 5.0) was injected in order to covalently bind it to the chip. All free reactive surface groups were blocked with ethanolamine-HCl (pH 8.5). Following this procedure, ~600 RU of VWF115 could be immobilised on the chip. **(B)** hEPCR immobilisation on flow cell 1. After activating the surface with NHS/EDC, 50 µl of 2.5 µM hEPCR in acetate buffer (pH 5.0) was injected over flow cell 1. Free reactive surface groups were blocked with ethanolamine-HCl (pH 8.5). Finally, ~1500 RU of hEPCR could be immobilised.

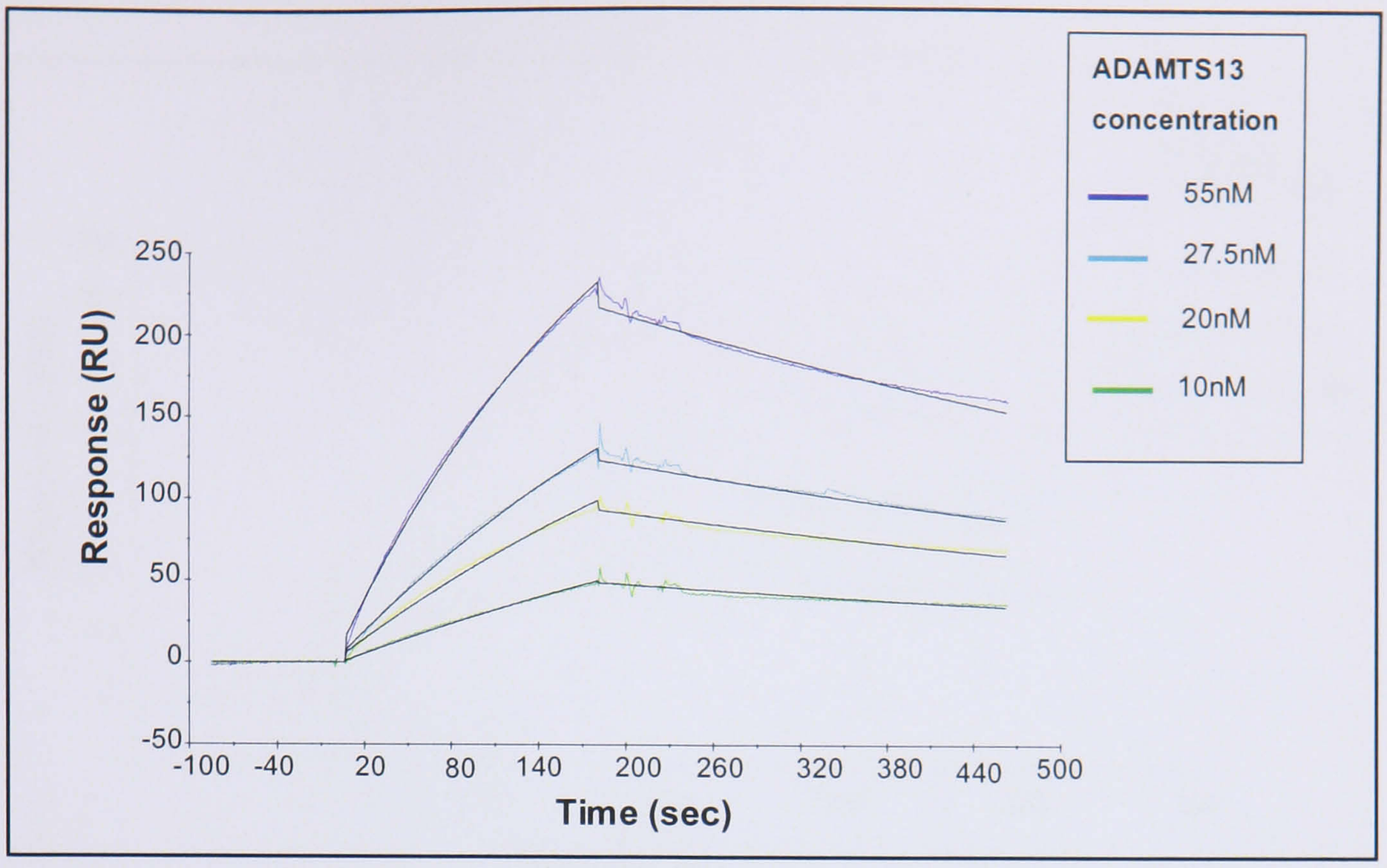


Fig. 3.21 ADAMTS13 binding to VWF115 directly coupled to a CM5 chip. Progressively increased binding responses observed after the injection of four ADAMTS13 concentrations (10, 20, 27.5 and 55 nM) in HBS-P buffer over VWF115 immobilised in flow cell 2. The curves were fitted (black line) to the 1:1 Langmuir model using the BIAevaluation software 3.0 and K_D value determined (see text).

3.3.2.3 Direct immobilisation of ADAMTS13 on a CM5 chip

To obtain further support for a high affinity binding interaction between ADAMTS13 and VWF115, the same strategy of amine coupling was used to immobilise ADAMTS13 on the sensor chip. ~ 8000 RU of ADAMTS13 was covalently immobilised over flow cell 2 and ~ 6000 RU of RCR-2 antibody was immobilised over flow cell 1 as a control (not shown). Different concentrations of VWF115 (62.5, 125 and 250 nM) were injected over both the active and the control flow cells. A binding response could be observed in flow cell 2, whereas none in flow cell 1, suggesting a specific interaction (Fig. 3.22). However, the binding curves differed from the one previously observed when VWF115 was immobilised on the chip (Fig. 3.21). The data could not be fitted to a 1:1 Langmuir model, but fitted best to a heterogeneous ligand model, which supposes the presence of different binding sites (see Section 2.4.2.2). Two K_D values were derived: 13.4 nM and 233 nM. The high affinity binding was in the same range of the one found when VWF115 was immobilised on the chip. Whether the low affinity binding reflects binding complexity or an artefact has still to be clarified (see Section 3.3.4).

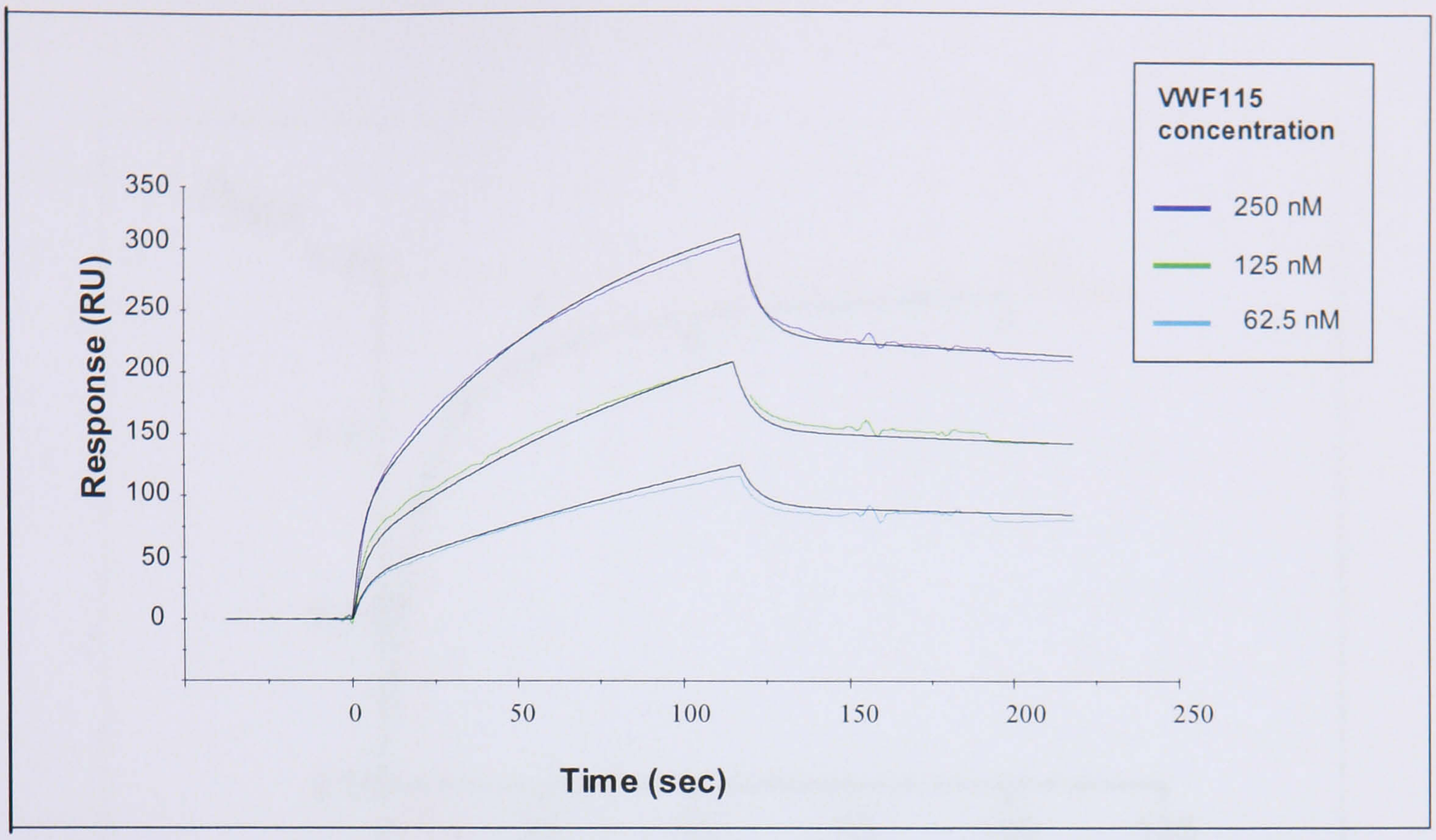


Fig. 3.22 VWF115 binding to ADAMTS13 directly coupled to a CM5 chip. Progressively increased binding responses observed after the injection of three VWF115 concentrations (62.5, 125 and 250 nM) in HBS-P buffer over ADAMTS13 immobilised over flow cell 2. The curves were fitted (black line) to the heterogenous ligand model using the BIAevaluation software 3.0 and two values for K_D determined (see text).

3.3.3 Characterisation of ADAMTS13 binding to VWF115 using a microtiter plate-based immunoassay

The above two SPR approaches suggested ADAMTS13 and VWF115 interact with each other with high affinity. A microtiter plate-based immunoassay was employed as an alternative approach to confirm this result. In contrast to the BIAcore technique, this method studies the binding in equilibrium conditions. In my assay, 100 µl of 140 nM VWF115 was used to coat a 96 well microtiter plate. Different ADAMTS13 concentrations (1.56-100 nM) were applied to the wells and incubated at 37°C for 3 hours. Biotinylated anti-TSR (2-4) pAb was used to detect bound ADAMTS13. Subsequently, Streptavidin-HRP was applied to the wells and OPD added to allow the developing of the colour, as described in Materials and Methods (see Section 2.4.4). The absorbance readings at 492 nm were plotted against the ADAMTS13 concentration (Fig. 3.23) and data fitted to the one binding site model (see equation 5 in Section 2.4.4). Separate experiments (n=6) gave a mean value of 16.2 ± 1.5 nM for the K_D. When the same experiment was repeated in the presence of 50 mM EDTA to

inhibit any proteolysis by ADAMTS13, it gave a K_D mean value of 8.0 ± 1.0 nM (n=7).

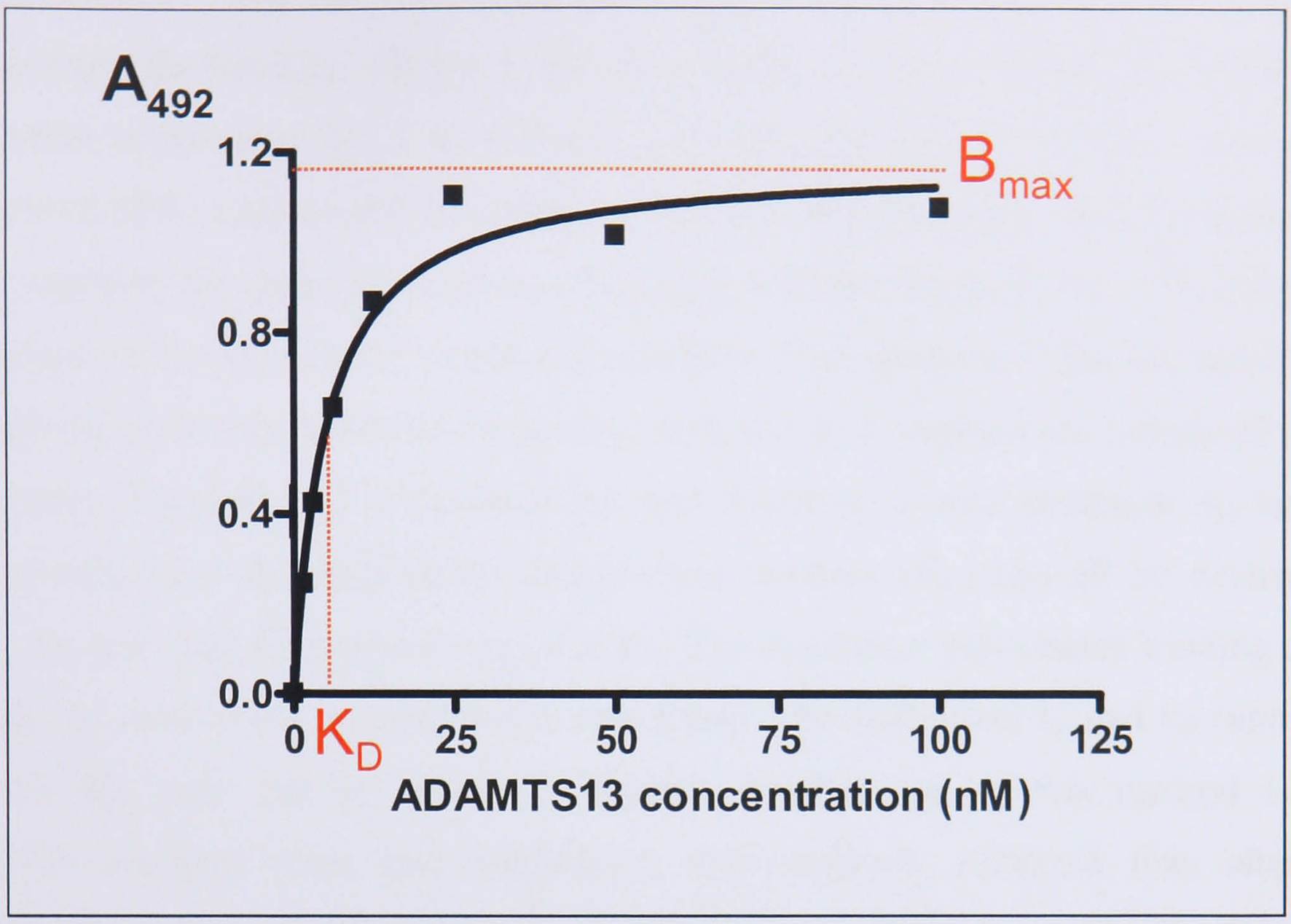


Fig. 3.23 VWF115-ADAMTS13 binding (plate-based binding assay). 140 nM of VWF115 in 50 mM sodium carbonate buffer (pH 9.6) was coated into a 96 well microtiter plate. Different ADAMTS13 concentrations (1.56-100 nM) in dilution buffer (PBS-1% BSA) and 50 mM EDTA were applied and incubated at 37°C for 3 hours. Biotinylated anti-TSR (2-4) pAb was applied for 90 minutes and, subsequently, Streptavidin-HRP for 1 hour. The HRP substrate, OPD, was added to develop the colour. The absorbance was read at 492 nm and plotted against ADAMTS13 concentration. The curve was fitted to the one binding site model, using Graph Pad Prism 4 software. The experiment shown gave a value of 8.5 nM for the K_D (highlighted in red). The maximal binding (B_{max}) is also highlighted in red.

3.3.4 Discussion

In the previous Section, I have fully characterised the kinetics of cleavage of VWF115 by ADAMTS13. The K_m was found to be 1.61 μM. Since this value is thought to approximate the binding affinity, it seems to suggest a quite low affinity interaction. To further investigate this, I have directly studied ADAMTS13-VWF115 interaction using both SPR analysis and microtiter plate-based immunoassay. The two techniques allow studying the same phenomenon from two different perspectives. SPR offers the advantage of monitoring the binding in real time. The progress of the interaction can be followed over time and both association and dissociation phase are visualised in the sensogram. Furthermore, the association and dissociation rate constants (k_a and k_d, respectively) and the equilibrium dissociation constant (K_D) can all be determined using the provided BIAevaluation software. The microtiter plate-based binding assay studies the interaction in equilibrium conditions. The individual k_a and k_d cannot be derived. K_D only can be obtained. Another disadvantage of this method is that repetitive washing steps and incubations with antibody solutions may alter the equilibrium condition, favouring dissociation. However, it has been recently shown [258] that the dissociation of ADAMTS13 from VWF was slow (half-time ~ 4 hours). The slow off-rate was also evident in the SPR experiments I have performed (Fig. 3.21 and 3.22). Therefore, measuring the binding by an ELISA-based colorimetric detection method should be feasible. The advantages of the plate-based equilibrium binding assay consist in lower costs and the possibility of multiple comparisons, analysing different samples or using different buffer conditions (i.e. presence and absence of urea) on the same plate (see Section 3.6.7 and 3.6.8).

Initially, different attempts were made with SPR using specific monoclonal antibodies to immobilise either ADAMTS13 or VWF115 on the surface of a CM5 sensor chip. The high specificity of monoclonal antibodies would have allowed the immobilisation of the specific ligand even when present in non purified solutions. Furthermore, the immobilisation of the ligand would have been in a specific controlled orientation. Unfortunately, all the attempts using monoclonal antibodies failed (Section 3.3.2.1). The alternative strategy adopted consisted of immobilising the ligand directly on the CM5 sensor chip by amine coupling. The disadvantage of this technique is that the immobilisation of the ligand occurs randomly, since free amino groups are widely distributed in most proteins. This can result in a heterogeneous population of immobilised ligands in which the binding site may be or be not completely exposed

and thus available for the interaction to occur. Either VWF115 or ADAMTS13 were directly immobilised on a CM5 sensor chip. When VWF115 was immobilised (Section 3.3.2.2), a 1:1 binding response could be observed when ADAMTS13 was passed over it. Data analysis of the VWF115-ADAMTS13 interaction from three separate experiments gave a value of 20.0 nM for K_D (Fig. 3.21). This high affinity binding seemed to be conferred by a slow dissociation rate. When ADAMTS13 was bound to the chip (Section 3.3.2.3), a lower affinity component was also apparent suggesting heterogeneity of binding (Fig. 3.22). This low affinity interaction may represent an actual secondary binding site for VWF115 on ADAMTS13. One molecule of immobilised ADAMTS13 may bind to two molecules of VWF115, with high and low affinity respectively. SPR thus detects two populations of VWF115 fragments, which interact with ADAMTS13 with different association and dissociation rates. The two binding sites could not be detected when VWF115 was immobilised onto the chip, because one molecule of ADAMTS13 may bind to two immobilised VWF115, leading to a single association-dissociation mode which is the result of the contribution of the two binding sites. Alternatively, the observed heterogeneous binding may be due to a limitation of the amine coupling technique, resulting in a heterogeneous population of immobilised ligands in which the binding site may be or be not completely exposed. This problem may be solved if ADAMTS13 could be immobilised on the chip in a precise orientated way. One possibility may be to immobilise ADAMTS13 via its His-tag on a NTA sensor chip. This chip has a dextran surface matrix with immobilised nitrilotriacetic acid which chelates metal ions, such as Ni^{2+}, and thus it can bind His-tag of recombinant proteins. To avoid binding of His-tag VWF115 to the surface, before passing it over ADAMTS13, the surface would have to be blocked with another His-tag protein (which is known not to interact with ADAMTS13 and VWF).

The equilibrium binding approach using a microtiter plate confirmed high affinity binding (Fig. 3.23), giving mean values for K_D of 16.2 nM and 8.0 nM, in the absence and presence of EDTA, respectively. The reduced binding (~ 2 fold) in the absence of EDTA suggested that some cleavage of the substrate may occur during the incubation with ADAMTS13, but alternative explanations are conceivable. For example, it is possible that the presence of Zn^{2+} in the active site may modify the binding affinity of ADAMTS13 for the substrate. The addition of EDTA was not required for SPR experiments because the short contact time between VWF115 and ADAMTS13 did not allow any cleavage to occur, as shown by a stable baseline after each binding experiment.

It should be noticed the discrepancy between the K_m and the K_D, suggesting that binding and cleavage may not be directly related. This aspect is discussed in more details in the final discussion (see Chapter 5).

3.4 TYPE 2A VWD MUTATIONS AND VWF115 PROTEOLYSIS

3.4.1 Introduction

As discussed in Section 1.2.9, VWD is the most common human congenital bleeding disorder, caused by a quantitative or qualitative defect in VWF. The most common qualitative VWD is type 2A VWD, which is characterised by the absence of large and intermediate molecular weight VWF multimers. A subgroup of type 2A VWD (group II) is caused by mutations mainly clustered in the A1 and A2 domains. Individuals with these mutations have normal synthesis and secretion of VWF multimers but increased susceptibility to proteolysis by ADAMTS13 and this diminishes the high molecular weight VWF pool. This is thought to be because of structural changes that lead to the exposure of the A2 domain cleavage site [183-185]. As a first step to identify important residues in the VWF A2 domain which may influence its proteolysis by ADAMTS13, I introduced six type 2A VWD mutations into VWF115. As previously discussed, VWF115 is efficiently cleaved by ADAMTS13 in the absence of denaturants, probably because of its permissive conformation. Thus, any influence of specific type 2A VWD mutations upon VWF115 proteolysis could be studied in physiological ionic conditions. The effect of specific mutations upon substrate specificity, rather than upon the overall A2 domain structure, could be investigated. I studied the cleavage of the mutants by HPLC, using the conditions previously optimised, and I compared their rates of proteolysis with that calculated for the wild type VWF115.

3.4.2 Site-directed mutagenesis of type 2A VWD mutations

Six type 2A VWD mutations (R1597Q, R1597W, D1614G, I1628T, G1629R and E1638K) were selected (see http://www.vwf.group.shef.ac.uk/vwd.html) and introduced into the VWF115 construct by site-directed mutagenesis. They were chosen because all were located within the A2 domain and they were thought to belong to type 2A group II. The expression of four of them (R1597Q [183], R1597W [182,183,328], I1628T [329] and E1638K [330]) has been studied *in vitro* in COS cells and it was shown that these mutations do not affect VWF multimerisation and secretion process of VWF. Furthermore, analysis of platelet lysates from patients with these particular mutations revealed that they contained intact high molecular weight multimers. All this suggests that the anomalous multimeric pattern observed in plasma may be the result of increased proteolysis by ADAMTS13. It has indeed been demonstrated that

recombinant full-length VWF mutants R1597Q and R1597W were spontaneously cleaved by ADAMTS13, in the absence of denaturants [183]. The position of the six mutations on the linear sequence of VWF115 is shown in Fig. 3.24 A. Their location is also shown on a predicted model of VWF A2 domain (Fig. 3.24 B). This model was generated with the PDB model viewer (http://www.expasy.org/spdbv/), using the crystal structure of A3 domain as a template [172] (PDB number: 1ATZ), since A2 and A3 domains are predicted to be structurally homologous.

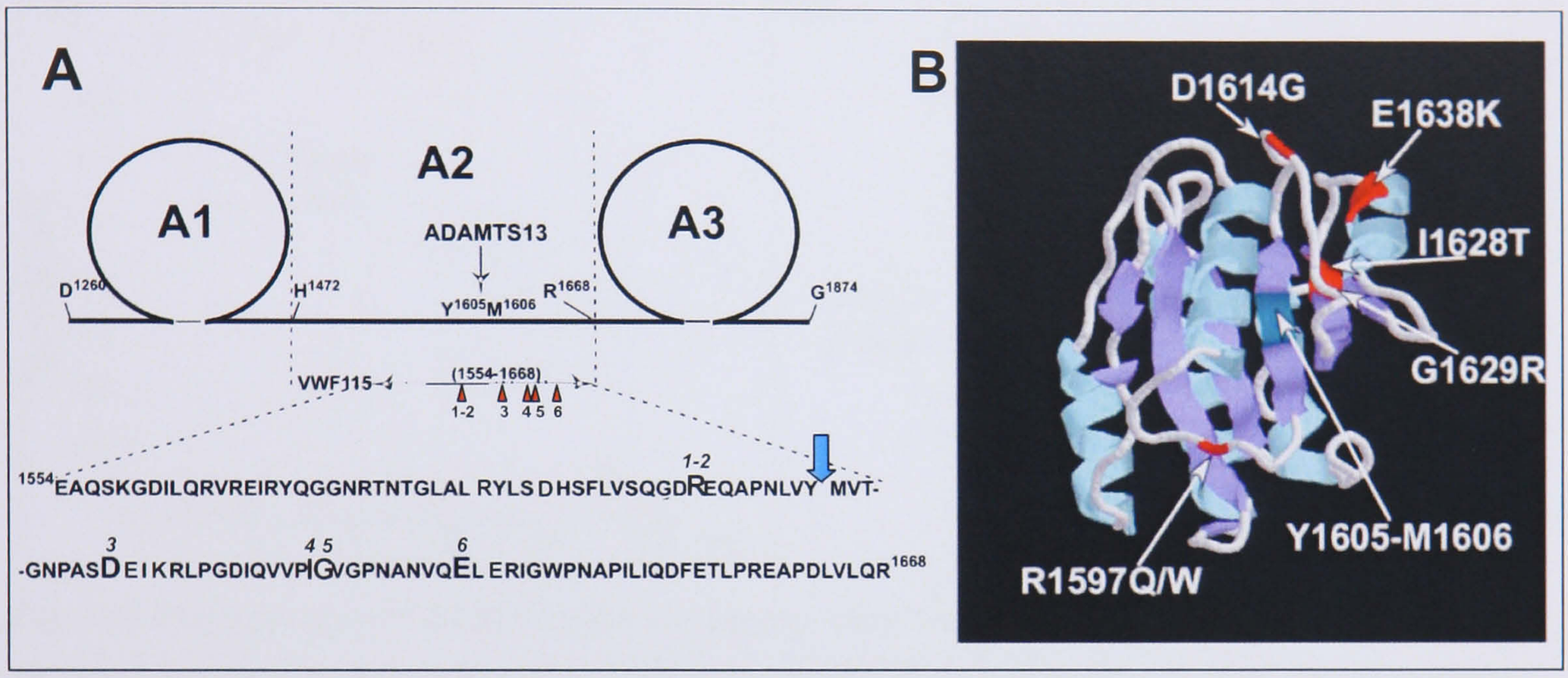


Fig. 3.24 VWF115 type 2A (II) mutants. A) VWF115 fragment is shown beneath the diagram of the VWF A1A2A3 domains. The amino acid sequence of VWF115 is given in full beneath. The ADAMTS13 cleavage site is marked with a blue arrow. The six type 2A (II) VWD mutations are numbered (1-6): R1597W (1), R1597Q (2), D1614G (3), I1628T (4), G1629R (5) and E1638K (6). Their positions are highlighted above VWF115 sequence. **B)** Predicted model of VWF A2 domain. The cleavage site (Y1605-M1606) is highlighted in green within the centre of the A2 domain. The positions of the six type 2A mutations are highlighted in red.

3.4.3 Expression and purification of type 2A VWD mutants

As has been described for wild type VWF115, the type 2A VWD mutants were expressed in Rosetta *E. coli* cells and purified from the inclusion bodies, using an 8M-0M urea linear gradient on a nickel-chelating column (Fig. 3.25 A). The eluted fractions were analysed by SDS-PAGE and Coomassie staining and visualised on the gel as single 16.9 kDa bands, in the absence of any major contaminants (Fig. 3.25 B).

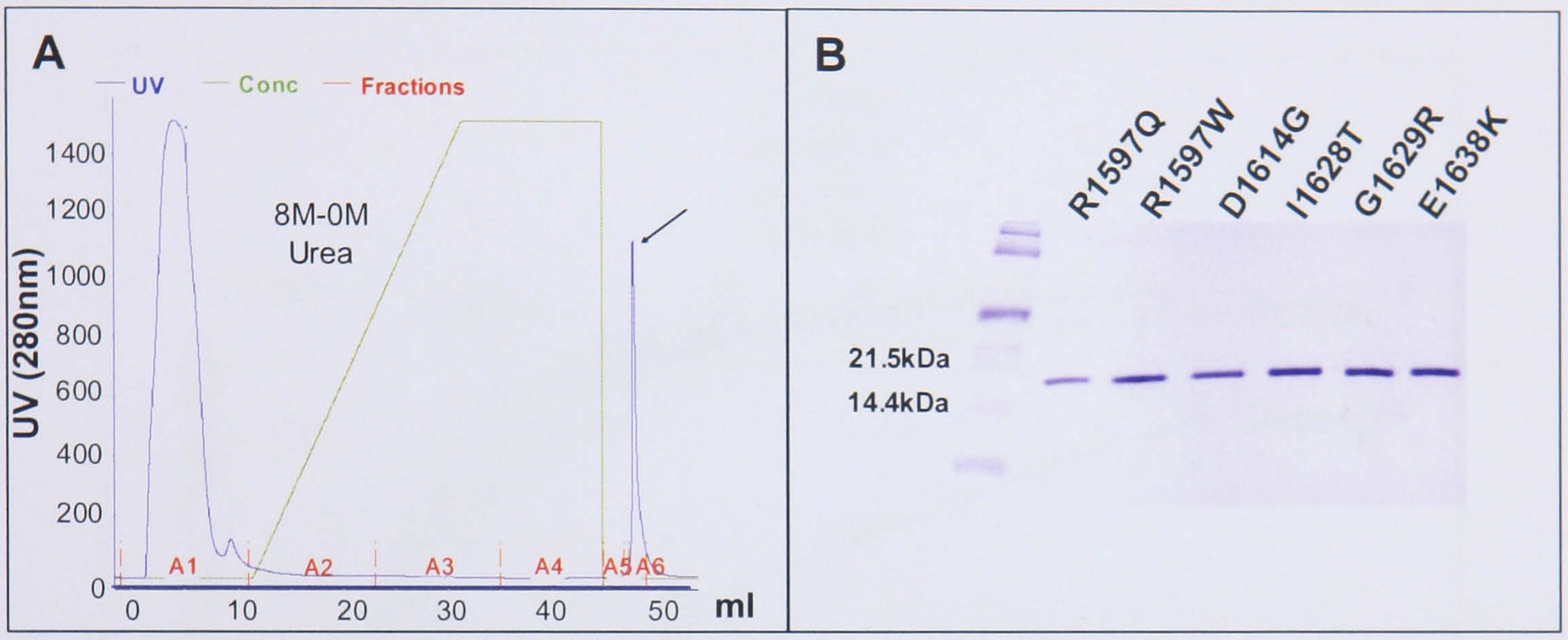


Fig. 3.25 Purification of VWF115 type 2A mutants. (A) Purification and refolding of VWF115 type 2A mutants from inclusion bodies. The chromatogram of R1597Q purification is shown as an example. Inclusion bodies were solubilised in a buffer containing 8 M urea, 20 mM Tris-HCl (pH 7.8), 500 mM NaCl and 20 mM imidazole and refolded using an 8M-0M urea linear gradient. Bound proteins were eluted using 20 mM Tris-HCl (pH 7.8), 500 mM NaCl and 500 mM imidazole. The eluted peak is highlighted by an arrow. **(B)** The eluted fractions of all the mutants were analysed by Coomassie staining on a 16.5% Tris-Tricine gel and they all migrated as a major band of the expected mass of 16.9 kDa.

3.4.4 Influence of type 2A VWD mutations on ADAMTS13 proteolysis

To assess the influence of the introduced type 2A VWD mutations upon VWF115 proteolysis, time course experiments were set up as previously described for wild type VWF115. HPLC analysis showed that most of these mutations (R1597Q, R1597W, D1614G, I1628T and G1629R) had no significant effect upon VWF115 proteolysis (Fig. 3.26). However, E1638K mutant appeared to be cleaved slightly slower than the wild type VWF115. Intriguingly, cleavage of D1614G mutant was markedly slower.

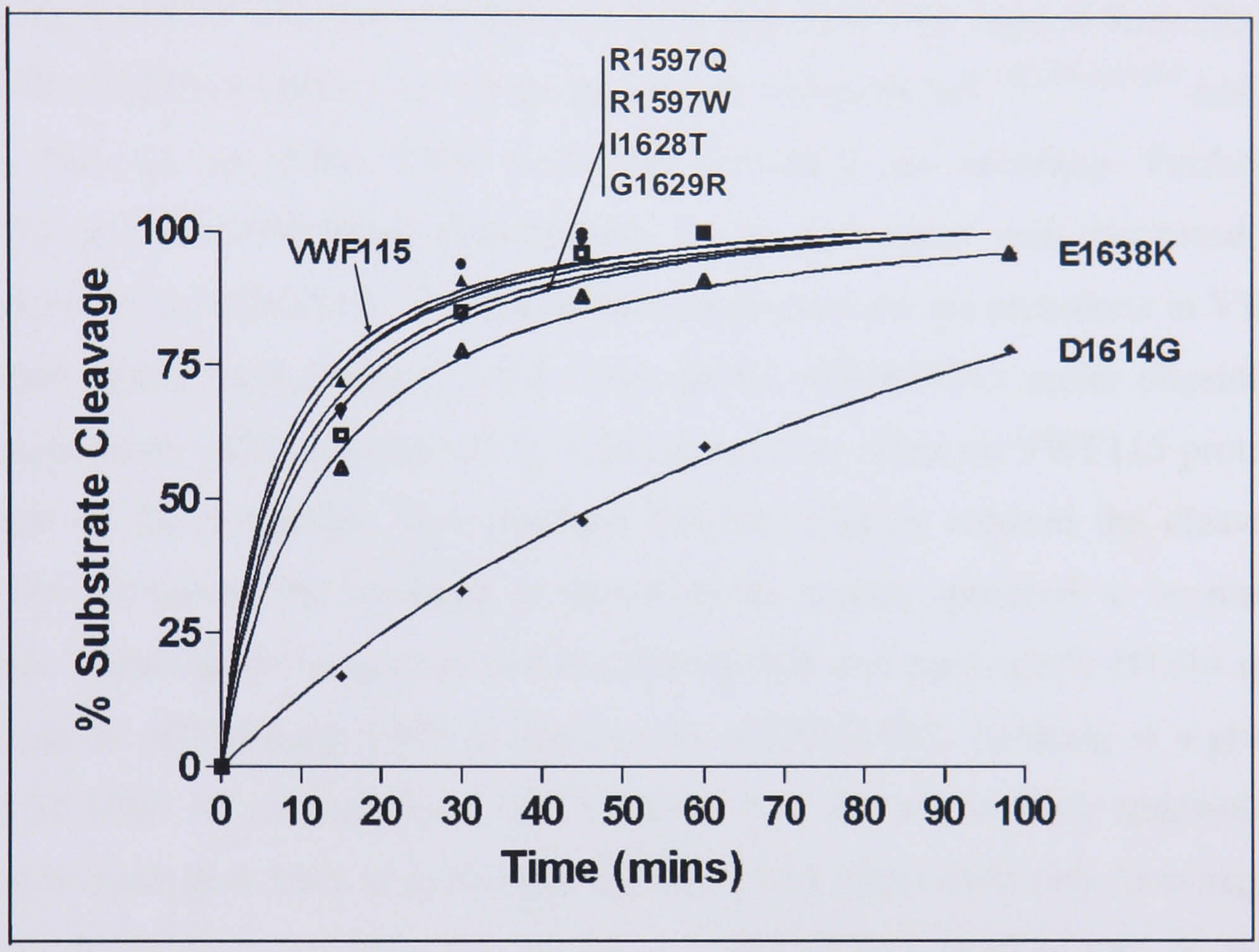


Fig. 3.26 HPLC analysis of proteolysis of VWF115 type 2A mutants. 0.5 μM VWF115 type 2A mutants and wild type VWF115 were incubated with 10 nM of ADAMTS13 in reaction buffer (20 mM Tris-HCl (pH 7.8), 150 mM NaCl and 5 mM $CaCl_2$). The reaction was stopped with EDTA at different time points and sub-samples analysed by HPLC. The percentage of substrate cleavage was plotted against time. R1597Q, R1597W, I1628T and G1629R were proteolysed at a similar rate as the wild type VWF115. E1638K was cleaved slightly slower. The rate of cleavage for D1614G appeared to be appreciably decreased.

3.4.5 Discussion

It has been shown that most type 2A (group II) VWD mutations are located in the A2 domain [183-185]. They are generally associated with normal VWF multimerisation and secretion but increased susceptibility to ADAMTS13 proteolysis. This leads to the loss of high and intermediate molecular weight multimers and ultimately to the bleeding clinical phenotype, as high molecular weight multimers are the most haemostatically active. I selected some type 2A VWD mutations all clustered in the A2 domain (R1597Q, R1597W, D1614G, I1628T, G1629R and E1638K). Four of them (R1597Q, R1597W, I1628T, E1638K) have been previously characterised [182,183,328-330] and it was shown they do not affect VWF multimers formation and secretion. Furthermore, R1597Q and R1597W were demonstrated to be associated with increased VWF proteolysis by ADAMTS13 [183]. I individually expressed the six mutations in VWF115 and investigated their influence upon cleavage by ADAMTS13 under physiological ionic conditions. HPLC analysis (Fig. 3.26) showed no effect on VWF115 proteolysis for most of the mutations. The mutation E1638K slightly reduced the cleavage of VWF115. However, the cleavage of the D1614G mutant appeared to be markedly reduced. These results suggested that residues E1638 and particularly D1614 may be important in determining VWF proteolysis by ADAMTS13. Looking at a predicted model of VWF A2 domain (Fig. 3.24 B), these two charged residues appeared to be located in close proximity to each other on the surface of the molecule. This suggested the hypothesis that they may be part of an ADAMTS13 binding site. In order to understand how these mutations might generate a type 2A VWD phenotype, which is after all characterised by enhanced cleavage, their influence would have to be investigated upon the cleavage of a whole A2 fragment, A1-A2-A3 fragment and the full-length multimeric VWF. If these mutants do infer a type 2A VWD phenotype, it is likely they do this by unfolding the A1-A2-A3 region. In a recent study [331], 13 type 2A VWD mutations have been expressed both in the full-length VWF and in a fragment spanning the VWF A1 through to the A3 domain. Amongst these mutations, two are the same as I introduced in VWF115, I1628T and E1638K. Another one involves the residues G1629, but with a different amino acid substitution (E). The cleavage of the 13 variants by ADAMTS13 was analysed and most of them, including G1629E and E1638K, appeared to increase the rate of proteolysis. Particularly, G1629E markedly increased the proteolysis of full-length VWF and allowed the fragment A1-A2-A3 to be cleaved even in the absence of denaturing conditions. This suggests that this

mutation may induce a structural change that causes the A2 domain to unfold, leading to its rapid proteolysis. In another recent study [186], the mutation R1597Q has been introduced in VWFA2 and VWFA1A2A3 fragments. The two substrates were cleaved readily even in the absence of urea, differently from fragments containing wild type A2 domain.

In summary, I conclude that residue D1614 might be important in controlling direct cleavage of VWF115. I must emphasise that VWF115 cleavage does not appear to be controlled by conformational changes that govern access to the scissile bond. If D1614 is a determinant of direct cleavage, then residues surrounding it must also be important in this respect. This will be considered further in the following Sections.

3.5 IDENTIFICATION OF CHARGED RESIDUES IN VWF115 INVOLVED IN ADAMTS13 BINDING

3.5.1 Introduction

In Sections 3.2.4 and 3.3, I demonstrated that a short fragment of the A2 domain (VWF115) could be cleaved efficiently by ADAMTS13 in the absence of denaturants (see Fig. 3.16) and it could bind to ADAMTS13 with high affinity (see Fig. 3.21, 3.22 and 3.23). Together, these findings suggested that crucial residues for cleavage and/or binding by ADAMTS13 are present in VWF115. Moreover, I also identified two type 2A VWD mutations (D1614G and E1638K) that appeared to reduce VWF115 proteolysis by ADAMTS13 (see Section 3.4 and Fig. 3.26). Both these residues are negatively charged and they are predicted to be located in close proximity to each other on the surface of the VWF A2 domain model (Fig. 3.24 B). I therefore hypothesised that these residues might be part of an ADAMTS13 docking site and I sought other charged residues predicted to lie on the surface of the A2 domain and in proximity to D1614 and E1638. In what follows, I identified 7 charged residues which I individually mutated to alanine in VWF115 by site-directed mutagenesis. The cleavage of the mutants by ADAMTS13 was analysed by Coomassie staining and HPLC analysis. Furthermore, for the mutants exhibiting decreased rate of cleavage, their binding to ADAMTS13 was tested by SPR.

3.5.2 Site-directed mutagenesis of surface charged residues in VWF115

Certain basic and acidic residues were identified on the surface of the predicted model of VWF A2 domain (Fig. 3.27 B). Seven charged residues (R1583, D1587, D1614, E1615, K1617, E1638, E1640) were selected to be mutated into alanine in the VWF115 substrate. Their location in the VWF115 linear sequence is shown in Fig. 3.27 A. The majority of them were located in the C-terminal part of the molecule (in respect of the cleavage site), whereas R1583 and D1587 were in the N-terminal region. Site-directed mutagenesis was performed as described in Materials and Methods (see Section 2.1.3.1). PCR products were analysed on a 1% agarose gel (Fig. 3.28), before proceeding to the transformation of XL-10 Gold *E.coli* cells.

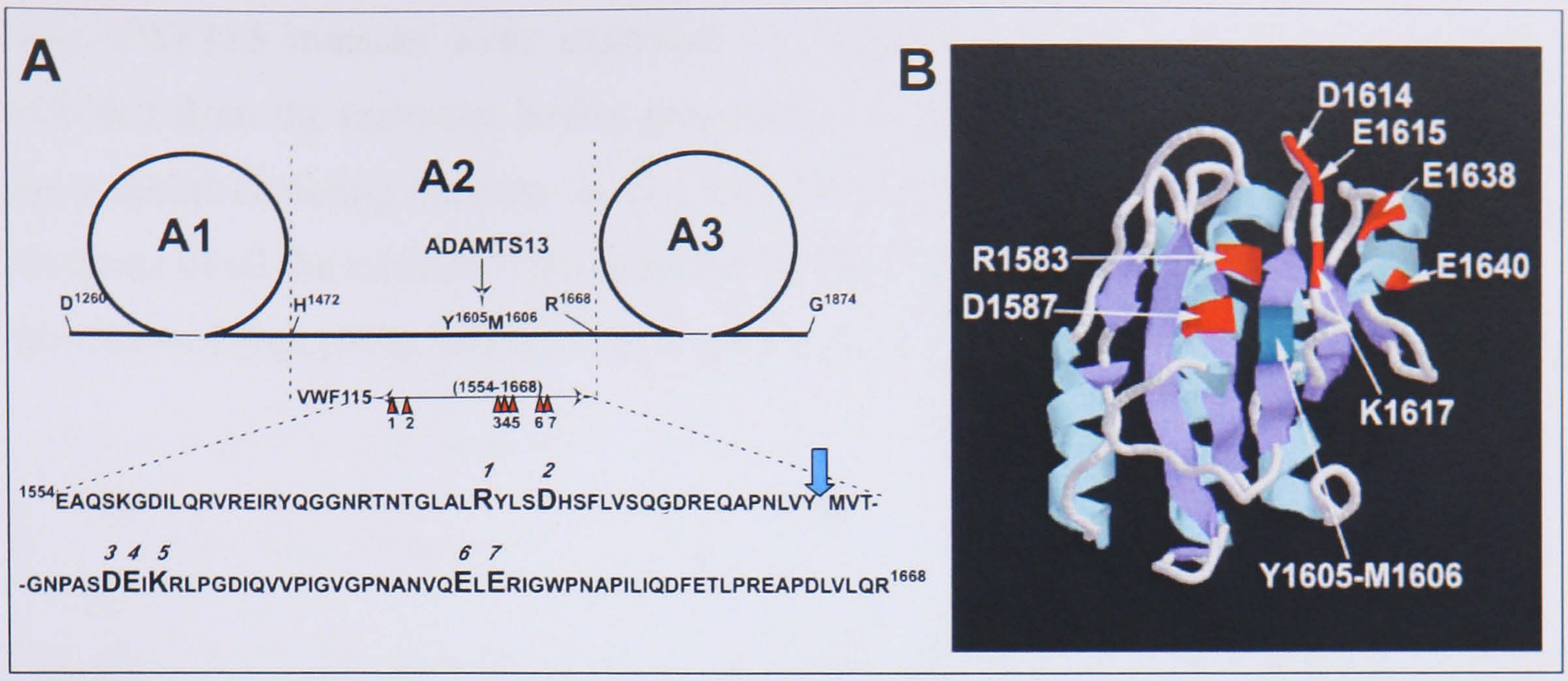


Fig. 3.27 VWF115 charged mutants. A) VWF115 fragment is shown beneath the diagram of the VWF A1A2A3 domains. The amino acid sequence of VWF115 is given. The ADAMTS13 cleavage site is marked with a blue arrow. The seven charged mutations are numbered (1-7): R1583A (1), D1587A (2), D1614A (3), E1615A (4), K1617A (5), E1638A (6) and E1640A (7). Their positions are highlighted above the VWF115 sequence. **B)** Predicted model of VWF A2 domain. The cleavage site (Y1605-M1606) is highlighted in green within the centre of the A2 domain. The position of the acidic and basic amino acids mutated to alanine and predicted to form a charged patch on the surface of the A2 domain are highlighted in red.

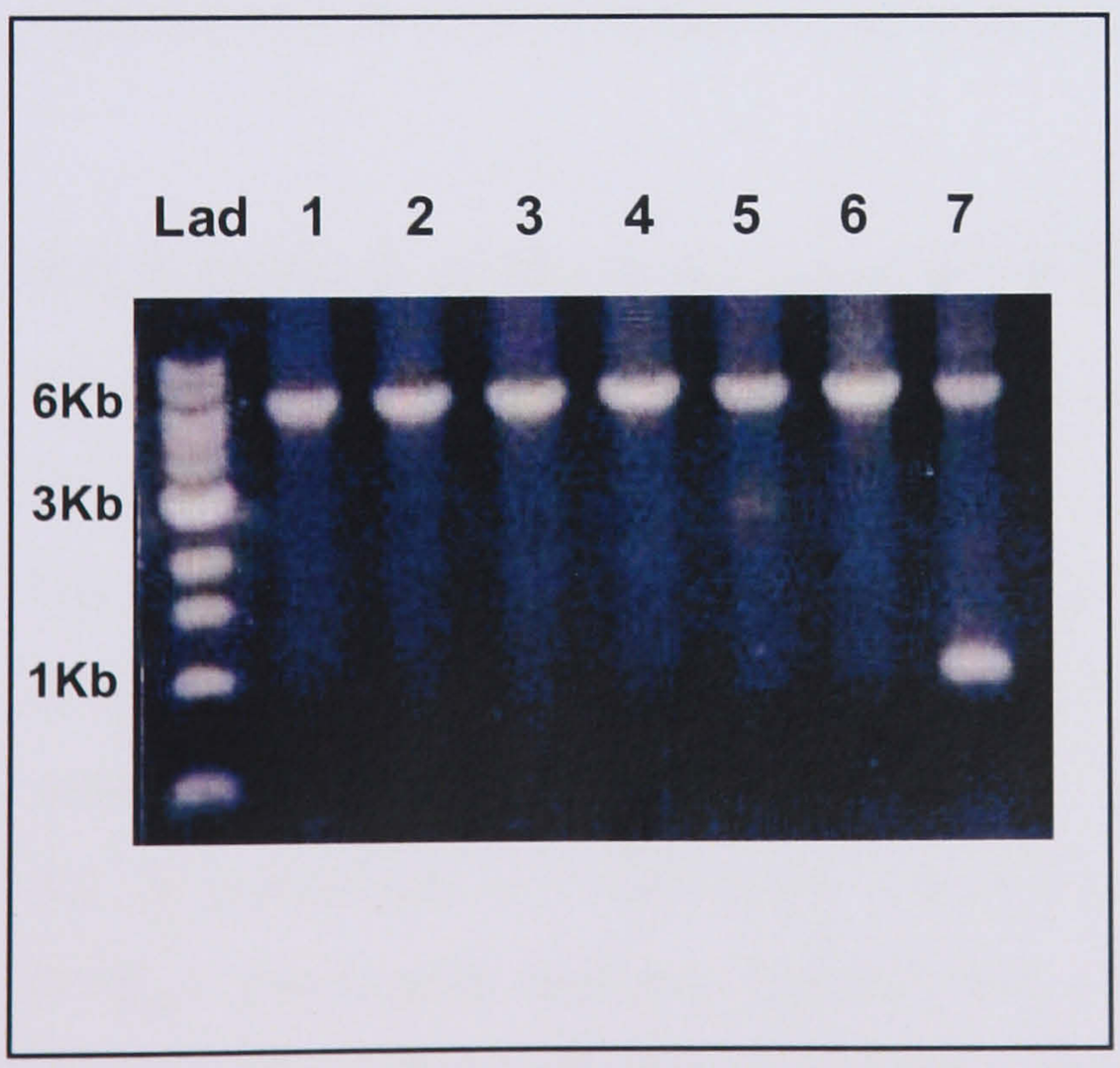


Fig. 3.28 Gel electrophoresis following PCR reaction. After site-directed mutagenesis, PCR products were analysed on a 1% agarose gel (running conditions: 70 V, 60 minutes). The following mutations were introduced in VWF115 pET100 vector: R1583A (lane 1), D1587A (lane 2), D1614A (lane 3), E1615A (lane 4), K1617A (lane 5), E1638A (lane 6) and E1640A (lane 7). Non-specific products were detected in sample 5 and 7. The two bands of 5764 bp of these samples were subsequently purified from gel. 1kb Ladder (Lad) was used to assess the size of the fragments.

3.5.3 Expression and purification of VWF115 charged mutants

The VWF115 mutants were expressed in Rosetta *E. coli* cells and purified and refolded from the inclusion bodies preparation, using an 8M-0M urea linear gradient on a nickel-chelating column, as for wild type VWF115 (Fig. 3.29 A). The eluted fractions of all the mutants were analysed by SDS-PAGE and Coomassie staining, and this showed high purity bands of the expected size of 16.9 kDa (Fig. 3.29 B).

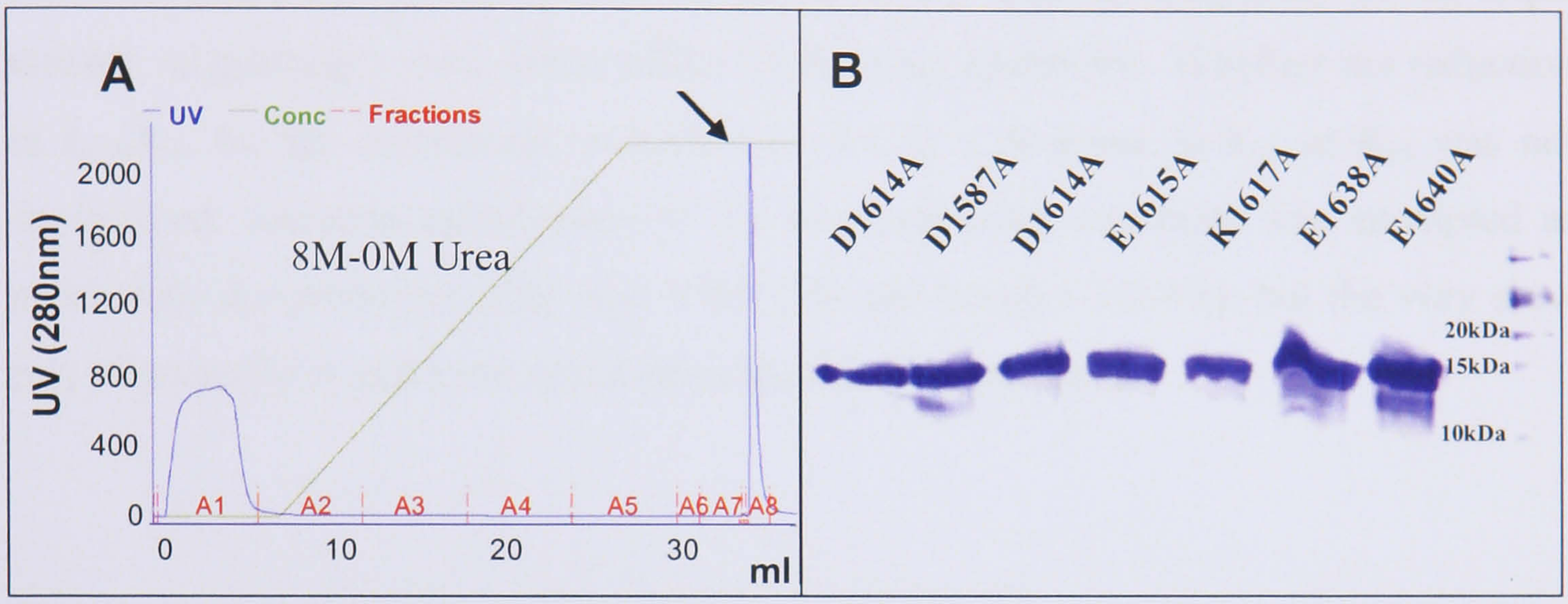
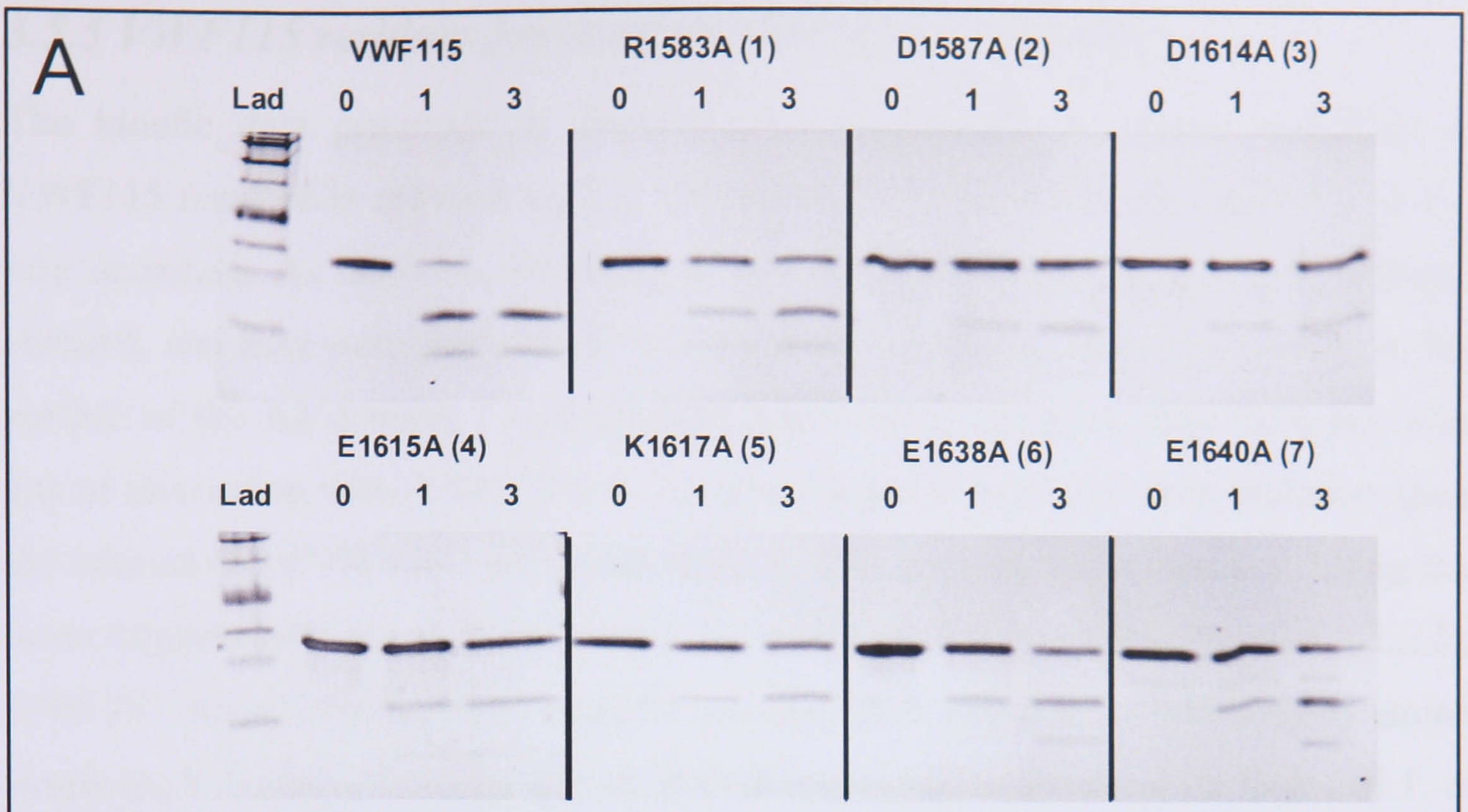


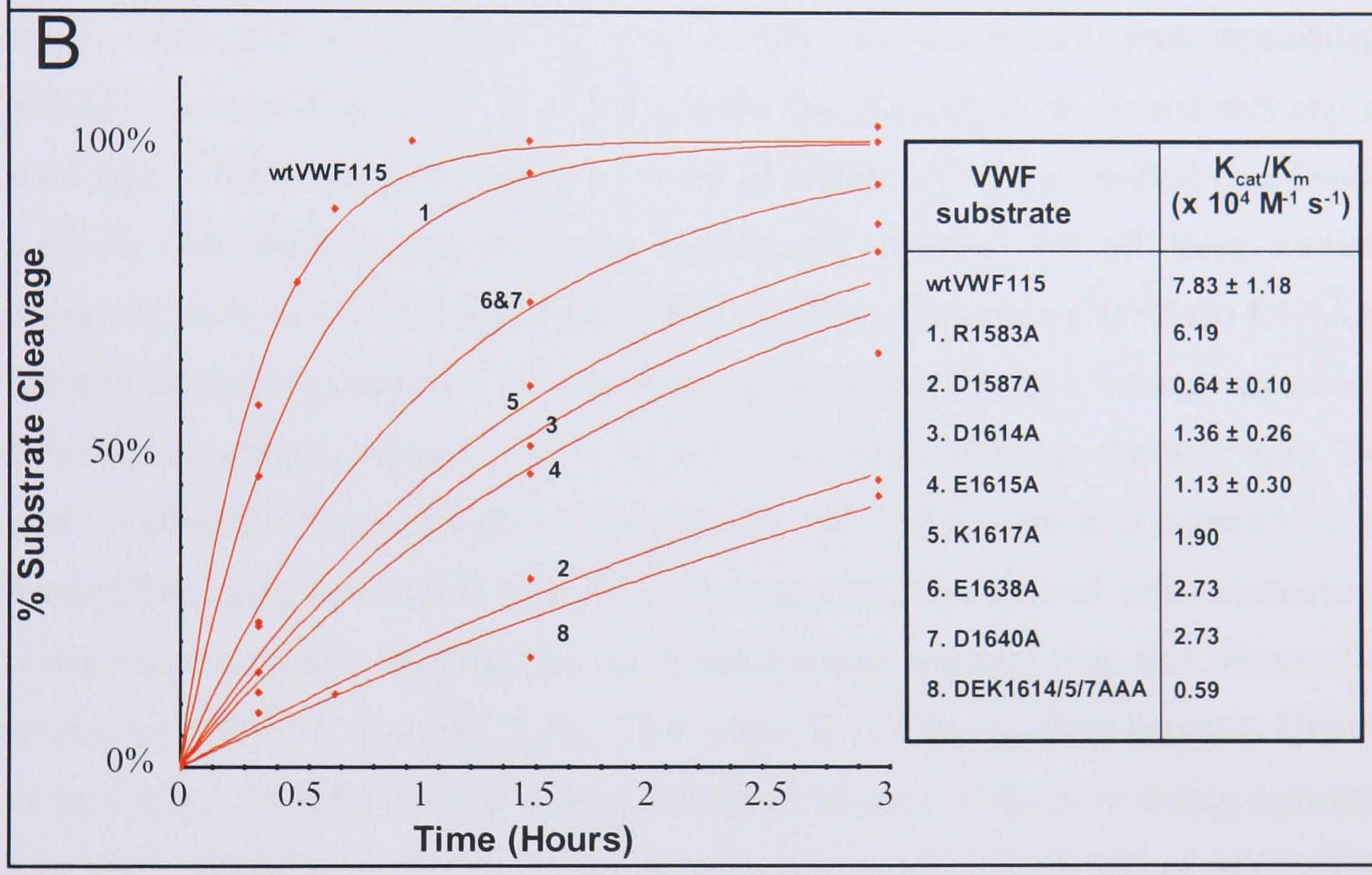
Fig. 3.29 Purification of VWF115 charged mutants. (A) Purification and refolding of VWF115 mutants from inclusion bodies. A chromatogram of D1614A VWF115 purification is shown as an example. Inclusion bodies were solubilised in a buffer containing 8 M urea, 20 mM Tris-HCl (pH 7.8), 500 mM NaCl and 20 mM imidazole and refolded using an 8M-0M urea linear gradient. The elution was performed using 20 mM Tris-HCl (pH 7.8), 500 mM NaCl and 500 mM imidazole. The eluted peak is highlighted by an arrow. **(B)** The eluted fractions from all the mutants were analysed by Coomassie staining on a 16.5% Tris-Tricine gel, showing a major band of 16.9 kDa.

3.5.4 Analysis of the cleavage of VWF115 charged mutants

To investigate the influence of the mutations introduced in VWF115 upon proteolysis by ADAMTS13, time course experiments were performed as described for the wild type VWF115. Initially, 6 μM of each substrate was incubated with 5.5 nM of ADAMTS13 and sub-samples analysed by SDS-PAGE followed by Coomassie staining. All the variants were cleaved slower than the wild type VWF115 (Fig. 3.30 A). Visualisation by Coomassie staining required high substrate concentrations (>>K_m). For kinetic analysis, repeated time course experiments, using low substrate concentrations (0.5 μM), were performed and analysed by HPLC (Fig. 3.30 B). The catalytic efficiency of all the VWF115 mutants was determined (see table in Fig. 3.30 B). The rate of proteolysis of the R1583A mutant was not significantly different from that of the wild type VWF115. The rate of cleavage of E1638A and E1640A variants

was slightly reduced (2-3 fold). The most affected mutant was D1587A. showing a 12-fold reduction in the catalytic efficiency. Individual mutations of K1617. D1614 and E1615 residues, which are predicted to lie on the same loop on the surface of A2 domain, induced a significant reduction in the rate of cleavage (4, 6 and 7 fold, respectively). These results suggested that this loop may play a crucial role in the cleavage reaction by ADAMTS13. Consequently, a VWF115 fragment containing all the three mutations (DEK1614/5/7AAA) was generated and its cleavage analysed. The HPLC analysis revealed a 13-fold reduction in the catalytic efficiency of the triple mutant, suggesting a cumulative effect of the three mutations. Whether the reduction in k_{cat}/K_m for the mentioned mutants was due to a decrease in k_{cat} or K_m was not determined. Accurate calculations of the two individual constants was attempted as previously described for wild type VWF115 (see Section 3.2.4.3), but the very slow rate of proteolysis make the initial rate calculation impractical.





VWF substrate	K_{cat}/K_m (x 10^4 M^{-1} s^{-1})
wtVWF115	7.83 ± 1.18
1. R1583A	6.19
2. D1587A	0.64 ± 0.10
3. D1614A	1.36 ± 0.26
4. E1615A	1.13 ± 0.30
5. K1617A	1.90
6. E1638A	2.73
7. D1640A	2.73
8. DEK1614/5/7AAA	0.59

Fig. 3.30 Proteolysis of VWF115 charged mutants by ADAMTS13. (A) SDS-PAGE and Coomassie staining of wild type and mutant VWF115 substrate proteolysis. 6 μM of each substrate was incubated with 5.5 nM of ADAMTS13 in reaction buffer (20 mM Tris-HCl (pH 7.8), 150 mM NaCl and 5 mM $CaCl_2$). The reaction was stopped with EDTA at different time points and sub-samples analysed on a 16.5% Tris-Tricine gel stained by Coomassie Blue. All the mutants appeared to be cleaved slower than the wild type VWF115. Lad: ladder of protein molecular weight markers. **(B)** HPLC analysis of wild type and mutant VWF115 substrate proteolysis. 0.5 μM of each substrate was incubated with 8.5 nM of ADAMTS13 in reaction buffer (20 mM Tris-HCl (pH 7.8), 150 mM NaCl and 5 mM $CaCl_2$). The reaction was stopped with EDTA at different time points and sub-samples analysed by HPLC. The percentage of substrate cleavage plotted against time confirmed the decreased rate of cleavage for all the mutants. In the table, the catalytic efficiency (k_{cat}/K_m) value for each substrate is given (± S.E). For VWF115, $n = 8$. For the most affected single mutants (D1587A, D1614A and E1615A), $n = 3$. For the least affected variants (R1583A, E1638A, D1640A and K1617A) and the triple mutant (DEK1614/5/7AAA), $n = 1$.

3.5.5 VWF115 residues involved in ADAMTS13 binding

The kinetic data presented in Section 3.5.4 suggested that certain mutations in VWF115 resulted in reduced $k_{cat}/K_{m.}$. Whether these mutations influenced k_{cat} or K_m was uncertain. As D1587A, D1614A, E1615A and K1617A were the most affected variants, and they were predicted to be located in close proximity to each other on the surface of the A2 domain, I hypothesised that these amino acids may form part of a site of interaction with ADAMTS13. To measure the influence of each mutation upon the interaction of VWF115 with ADAMTS13, SPR analysis was employed. Using the same experimental protocol developed for wild type VWF115 (see Section 3.3.2.2), ~600 RU of each mutant were immobilised over flow cell 2 of a CM5 chip by amine coupling. In each case, ~1500 RU of hEPCR were used as a control on flow cell 1. A single concentration of ADAMTS13 (27.5 nM) was passed over each immobilised VWF115 mutant (Fig. 3.31). The shape of the binding curves of the mutants and the wild type VWF115 were the same as obtained before, using this method (see Section 3.3.2.2). The binding response was significantly reduced for all three mutants, compared with that of the wild type VWF115. The triple mutant DEK1614/5/7AAA showed no binding response. Of the single mutants, the D1614A variant appeared to be the most affected variant, with a response ~10 times less than the wild type. Two other ADAMTS13 concentrations (55 nM and 137.5 nM) were also passed over the immobilised D1614A mutant (Fig. 3.32). As expected, this showed some evidence for a stepwise increase in binding, but still a much lower response than that observed for wild type VWF115 (see Fig. 3.21). The actual K_D of the binding between D1614A variant and ADAMTS13 could not be calculated because of the poor fitting associated with the low binding response. A second approach, in which 8083 RU of ADAMTS13 was covalently bound to flow cell 2 of a CM5 sensor chip was employed (see Section 3.3.2.3). 6068 RU of RCR-2 antibody was immobilised on flow cell 1 as a control. 500 nM of each mutant was passed over the chip. The shape of the binding curves of the mutants and the wild type VWF115 were the same as obtained before, using this method (see Section 3.3.2.3). Even with this method, an accurate K_D could not be derived for the VWF115 mutants. However, it was clear that the binding of each variant to ADAMTS13 was significantly compromised. Taken together, both the two SPR approaches confirmed the importance of D1587, D1614, E1615 and K1617 residues in binding to ADAMTS13.

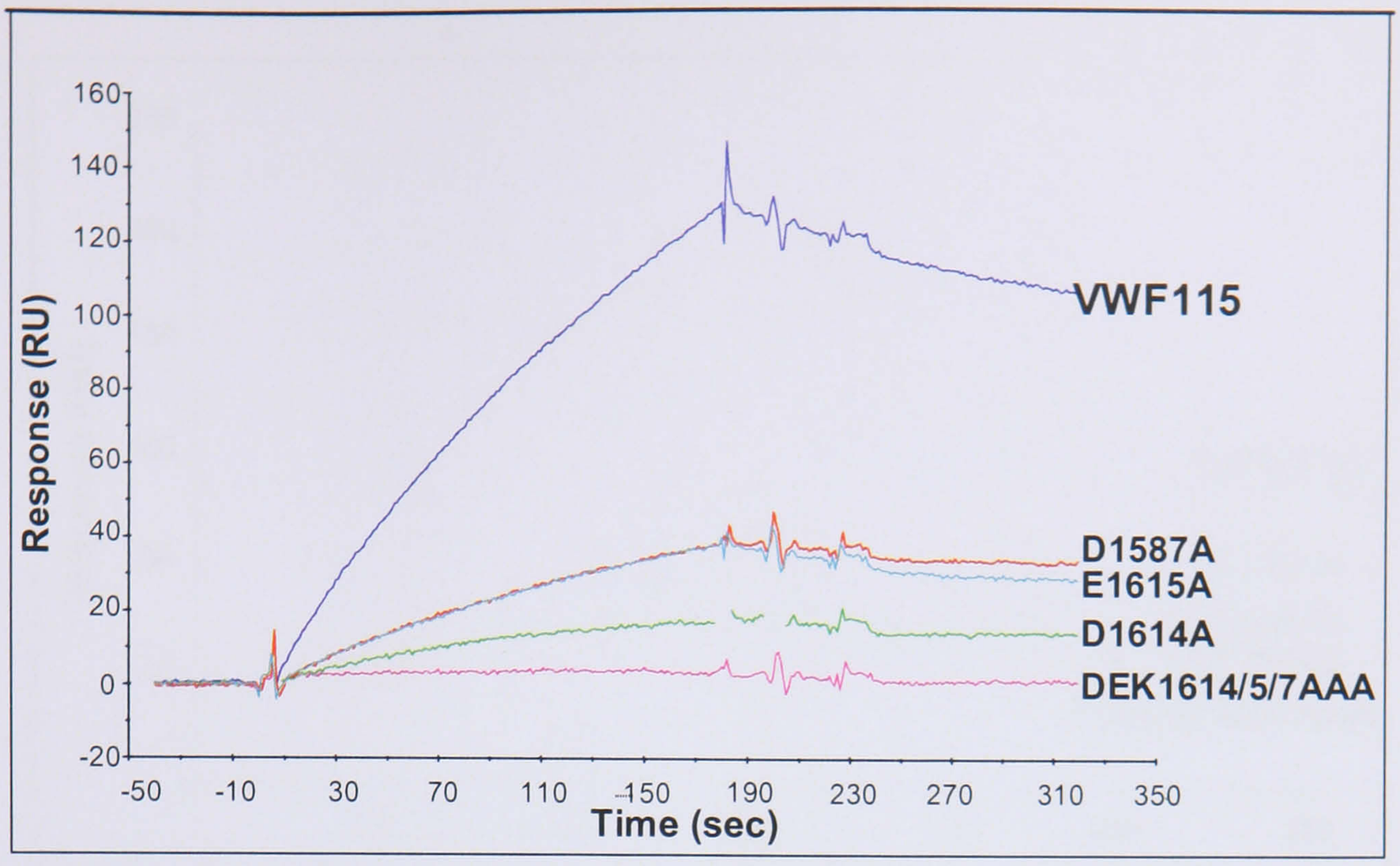


Fig. 3.31 Binding between ADAMTS13 and immobilised wild type VWF115 and D1587A, D1614A, E1615A and DEK1614/5/7AAA variants. After surface activation, ~600 RU of wild type and mutant VWF115 fragments was immobilised on the CM5 chip. The difference in binding response following 27.5 nM ADAMTS13 injection over wild type VWF115 and each of the mutant is graphically represented above. All the VWF115 variants appeared to bind weakly to ADAMTS13. D1614A was the single mutation that most markedly affected the binding between VWF115 and ADAMTS13. No binding response was detected for DEK1614/5/7AAA.

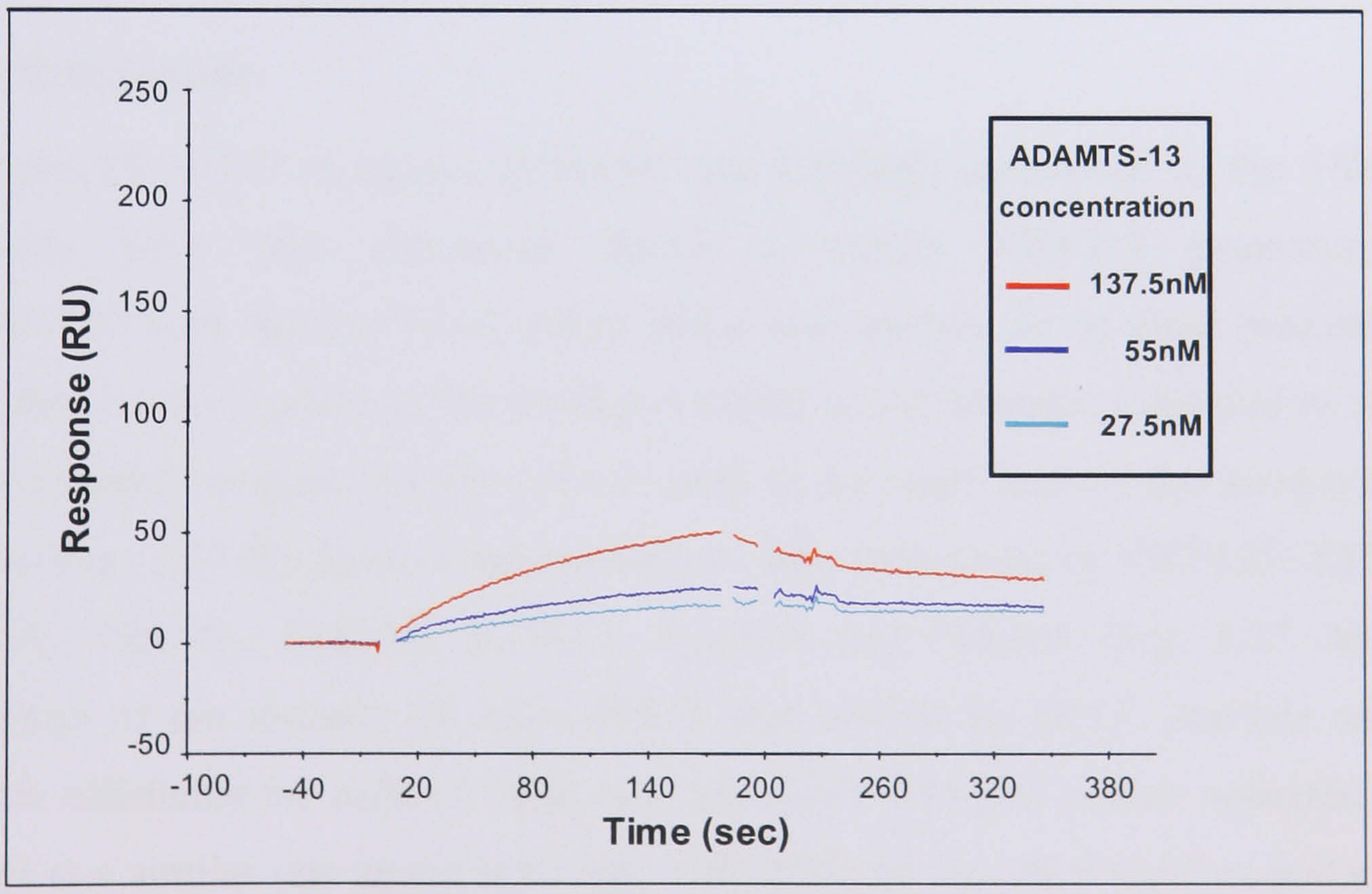


Fig. 3.32 Binding between ADAMTS13 and immobilised D1614A mutant. After surface activation, ~600 RU of D1614A variant was immobilised on the CM5 chip. Binding response following the injection of three ADAMTS13 concentrations (27.5, 55 and 137.5 nM) over the immobilised D1614A mutant is shown. The binding between D1614A variant and ADAMTS13 appeared to be markedly decreased, comparing with the wild type response. However, the curves could not be fitted because of the small size of the response and consequently the K_D value could not be calculated.

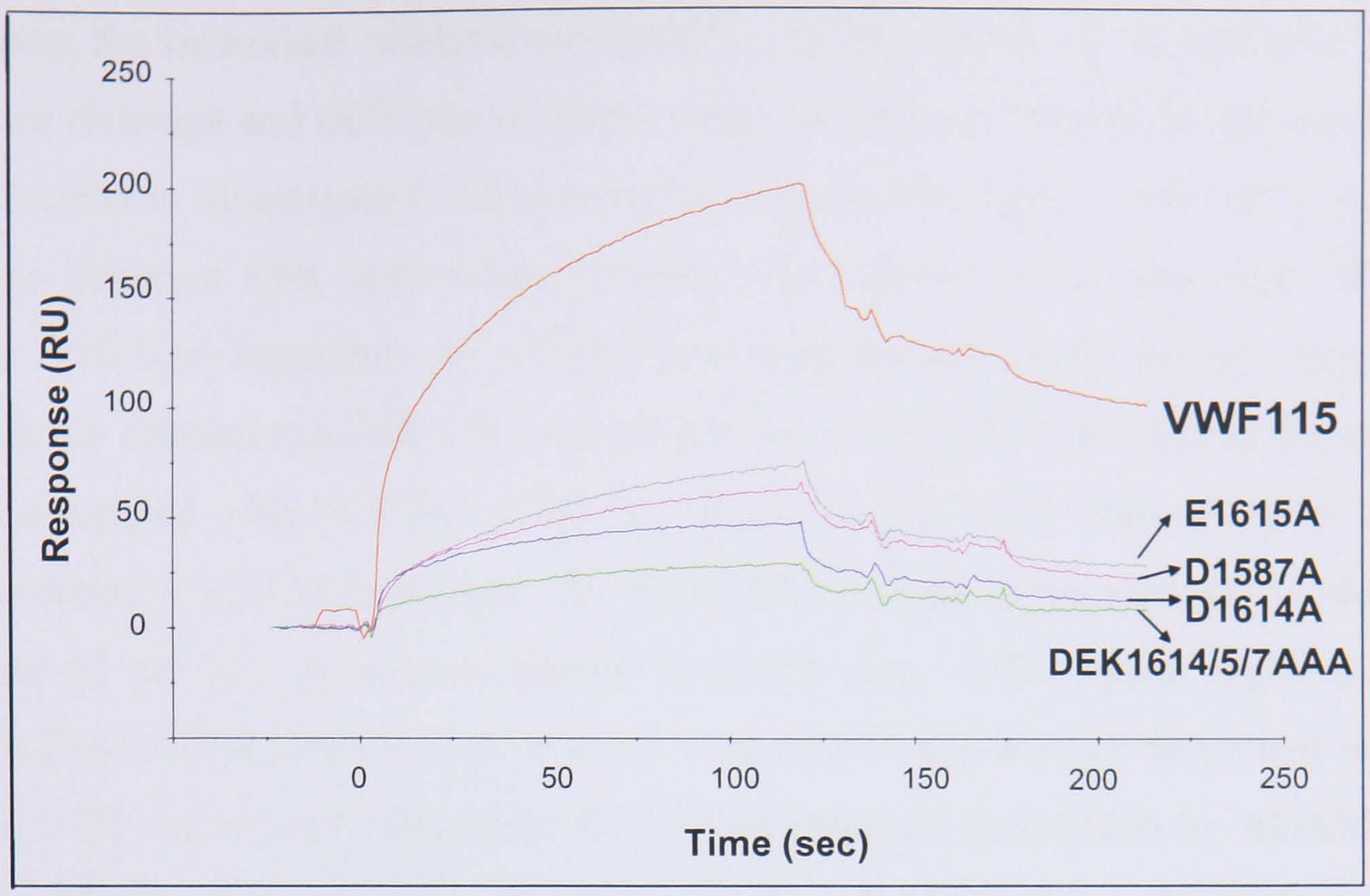


Fig. 3.33 Binding between wild type and mutant VWF115 fragments and immobilised ADAMTS13. After surface activation, ~8083 RU of ADAMTS13 was immobilised on the CM5 chip. Difference in binding response was observed following 500 nM injection of each VWF115 mutant over ADAMTS13. All the VWF115 variants appeared to bind weaker to ADAMTS13 than wild type VWF115.

3.5.6 Discussion

Two type 2A VWD mutations (D1614G and E1638K) introduced in the VWF115 fragments have been previously shown to reduce VWF115 proteolysis by ADAMTS13 (see Section 3.4.4). Since these two residues lie in close proximity to each other on the surface of the predicted model of A2 domain, I decided to mutate further charged residues thought to be located in the same area on the surface of A2 domain (Fig. 3.27 B). Seven single mutations were introduced in VWF115: R1583A, D1587A, D1614A, E1615A, K1617A, E1638A and E1640A (Fig. 3.27 A). The proteolysis of the mutants by ADAMTS13 was studied by HPLC analysis and the catalytic efficiency for each of them was calculated. R1583A mutant appeared to be cleaved at a similar rate as the wild type VWF115. All the other mutants had clearly reduced cleavage rates (Fig. 3.30 B). The most affected variant was D1587A with a ~12 fold reduction in the rate of cleavage. The catalytic efficiency for K1617A, D1614A and E1615A was 4-7 fold reduced. Since these three residues are predicted to lie on the same loop of the A2 domain, a triple mutant (DEK1614/5/7AAA) was generated. Its catalytic efficiency was 13 fold less than VWF115, implying that the

amino acid in this charged loop may act together in binding and/or proteolysis. However, the individual catalytic constants k_{cat} and K_m could not be calculated due to the poor cleavage and difficulty of determining an accurate initial rate of proteolysis. I thus decided to investigate if these mutations impaired binding to ADAMTS13, using the two different SPR approaches previously described for the wild type VWF115 (either VWF115 fragments or ADAMTS13 immobilised on the sensor chip). Both approaches showed markedly reduced affinity for ADAMTS13 for each of the mutants when compared with wild type VWF115 (Fig. 3.31 and 3.33). Unfortunately, the K_D for the interaction of each mutant with ADAMTS13 could not be accurately calculated because of the low binding responses observed (Fig. 3.32). Taken together, these results showed that D1587, D1614, E1615 and K1617 appeared to be critical residues within VWF A2 domain, important for both binding and proteolysis by ADAMTS13. They probably form part of a docking site for ADAMTS13 on the surface of A2 domain. Additional charged residues on the surface of the A2 domain and domains in VWF other than A2 may also be involved in ADAMTS13 binding and their role will also be investigated (see Sections 4.1.1 and 4.1.3).

3.6 BINDING AND PROTEOLYSIS OF VWF A2 DOMAIN BY ADAMTS13

3.6.1 Introduction

It has been reported that *in vitro* cleavage of the intact VWF A2 domain requires denaturants [186,332]. The denaturants are assumed to induce conformational changes that probably expose the cleavage site, or an ADAMTS13 binding site, or both. To test whether the influence on cleavage of the charged mutations described in Section 3.5.4 was maintained in a fully folded A2 domain, I introduced the most affected mutations (D1587A, D1614A, E1615A) into a whole A2 domain fragment. This approach was also useful to ascertain whether these mutations would alter the conformation of the A2 domain, leading to a more readily exposed scissile bond easily cleaved by ADAMTS13 in the absence of denaturants. The cleavage of wild type and mutant VWFA2 fragments by ADAMTS13 was studied both in the absence and presence of 1 M urea and analysed both by Coomassie staining and HPLC analysis. Furthermore, ADAMTS13-VWFA2 interaction was studied using the plate-based equilibrium binding assay, previously described for VWF115. Inhibition binding experiments were also performed to ascertain whether the binding site is exposed or hidden in the folded A2 domain and to determine whether additional residues important for binding are located in VWFA2 but not in VWF115.

3.6.2 Bacterial expression of VWFA2

Wild type VWFA2 was initially cloned into pET101/D-TOPO vector and then sub-cloned into pTrcHisA vector (see Section 2.1.2.1). The resulting fragment depicted in Fig. 3.34 had two polyhistidine tags, one at each terminus. Subsequently, I expressed this fragment in Rosetta *E. coli* cells and recovered it from the inclusion body preparation, after bacterial lysis. It was refolded and purified by nickel-chelating column affinity chromatography, using an 8M-0M urea linear gradient (Fig. 3.35 A). Both the eluted fraction and the fraction stripped with 6 M guanidine-HCl and 50 mM EDTA were dialysed into 20 mM Tris-HCl (pH 7.8) and analysed by Coomassie staining. The majority of the protein was recovered in the stripped fraction and it appeared as a single 26.9 kDa band (Fig. 3.35 B).

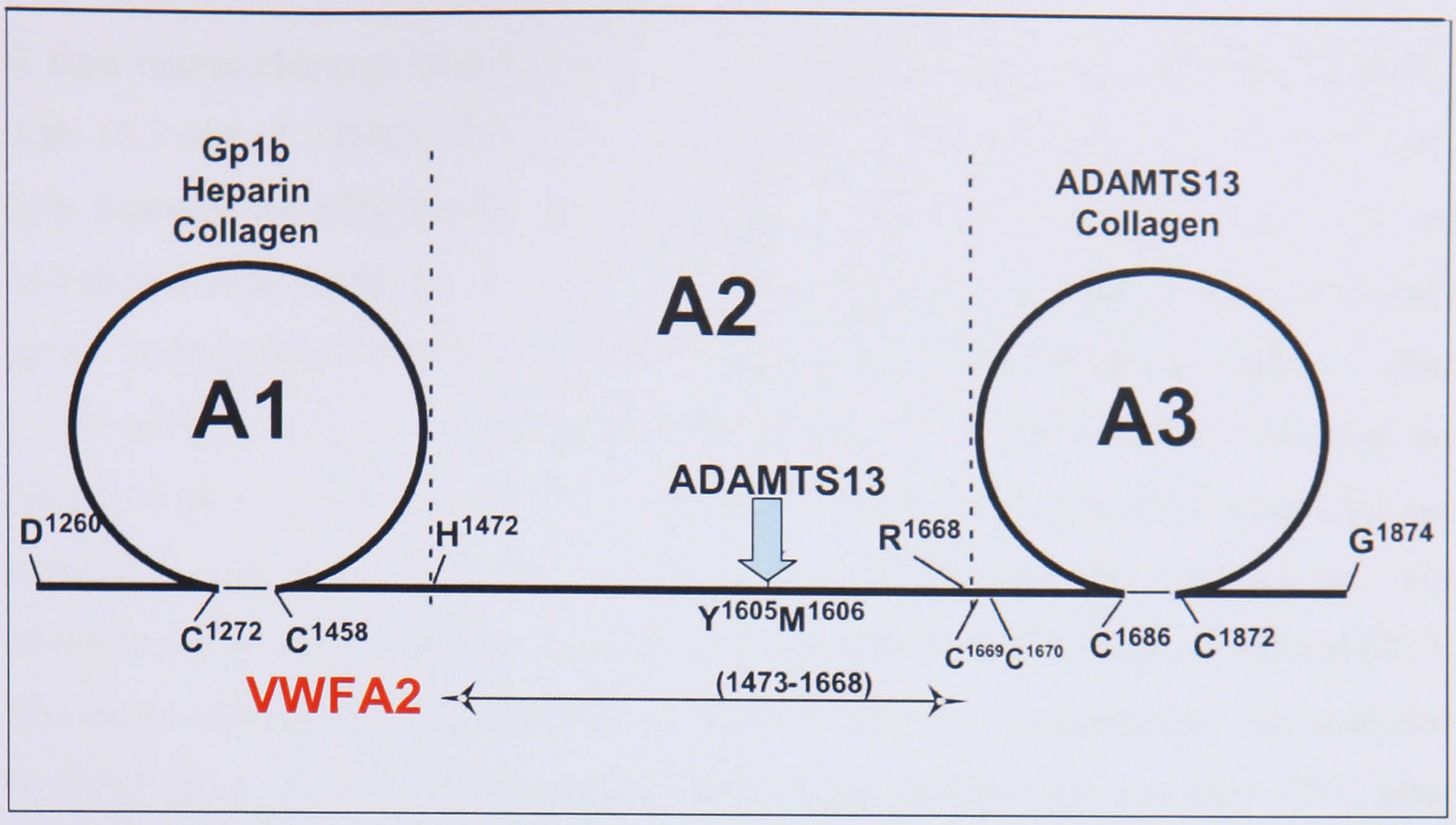


Fig. 3.34 Recombinant VWFA2 fragment. Recombinant VWFA2 is shown beneath the diagram of the VWFA1A2A3 domains. The ADAMTS13 cleavage site (Y1605-M1606) and major ligands for each domain are highlighted above. The residues which VWFA2 spans are given in brackets.

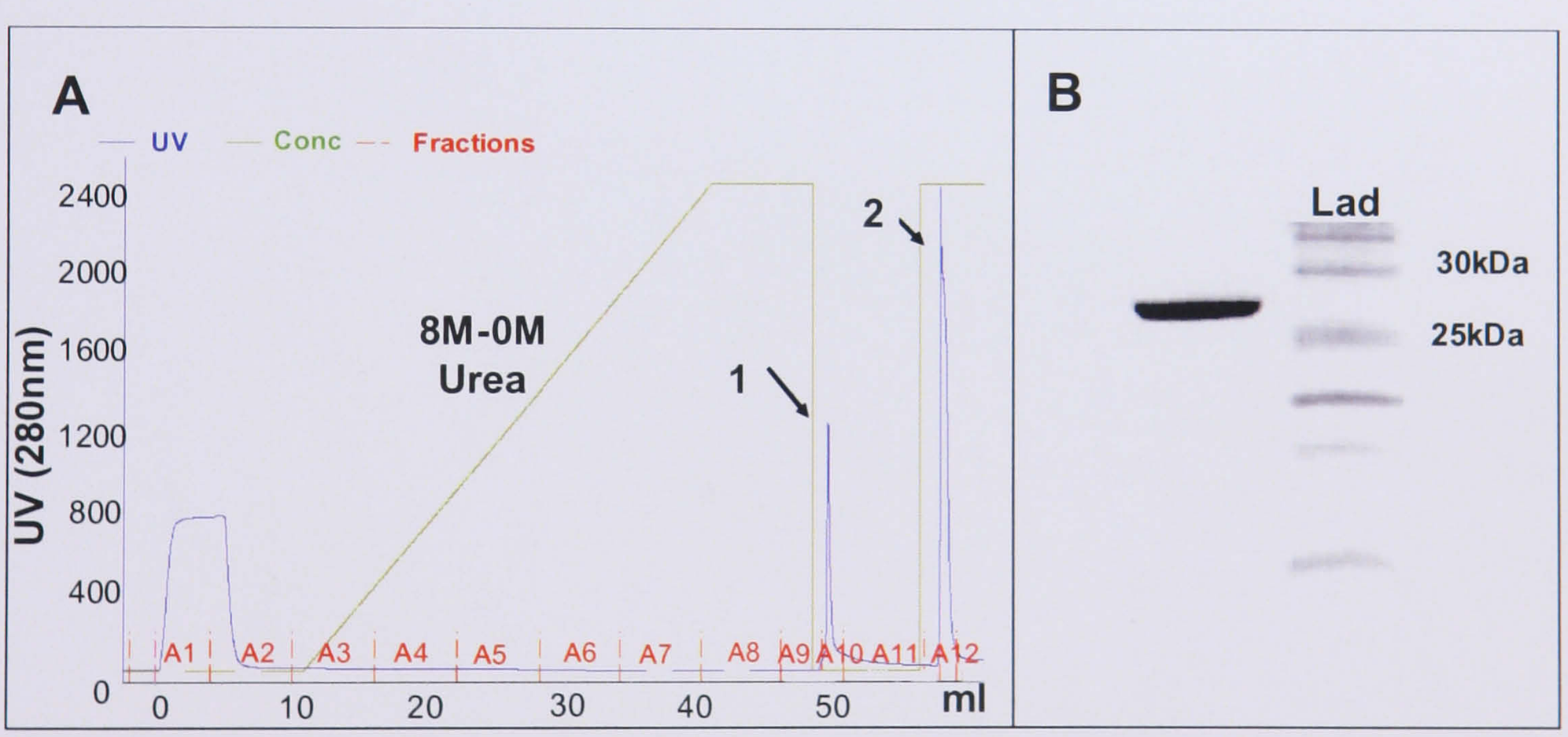


Fig. 3.35 Purification of wild type VWFA2. (A) Purification and refolding of wild type VWFA2 from inclusion bodies. Inclusion bodies were solubilised in a buffer containing 8 M urea, 20 mM Tris-HCl (pH 7.8), 500 mM NaCl and 20 mM imidazole and refolded using an 8M-0M urea linear gradient. The proteins eluted with 20 mM Tris-HCl (pH 7.8), 500 mM NaCl and 500 mM imidazole (peak 1) and the proteins stripped with 20 mM Tris-HCl (pH 7.8), 500 mM NaCl 6 M guanidine-HCl and 50 mM EDTA, (peak 2) are highlighted by arrows. **(B)** Wild type VWFA2 stripped fraction was analysed on a 16.5 % Tris-Tricine gel stained by Coomassie Blue. The purified VWFA2 was visualised as a 26.9 kDa band. Lad: ladder of protein molecular weight markers.

3.6.3 Denaturants enhance VWFA2 proteolysis

A time course cleavage experiment was set up incubating 6 μM of wild type VWFA2 with 16.5 nM of ADAMTS13, both in the absence and in the presence of 1 M urea. The analysis by SDS-PAGE and Coomassie staining is shown in Fig. 3.36. In accordance with previous studies [186,332], VWFA2 fragment was proteolysed extremely slowly in the absence of urea, and the N-terminal cleavage product was slightly visible on the gel even after 3 hours incubation time (Fig. 3.36 A). The fragment was cleaved visibly faster in the presence of 1 M urea (Fig. 3.36 B). However, the reaction did not proceed as rapidly as for VWF115 (see Fig. 3.14 B), since the cleavage was not completed even after 3 hours, despite using increased concentration of ADAMTS13. The same experiment was performed using low substrate concentration and analysed by HPLC (Fig. 3.37). In the absence of denaturants, the cleavage was only ~28% after 5 hours. In the presence of 1 M urea, although VWFA2 was cleaved faster, it still did not reach completion even if the reaction seemed to have reached a plateau (~50-60% after 5 hours).

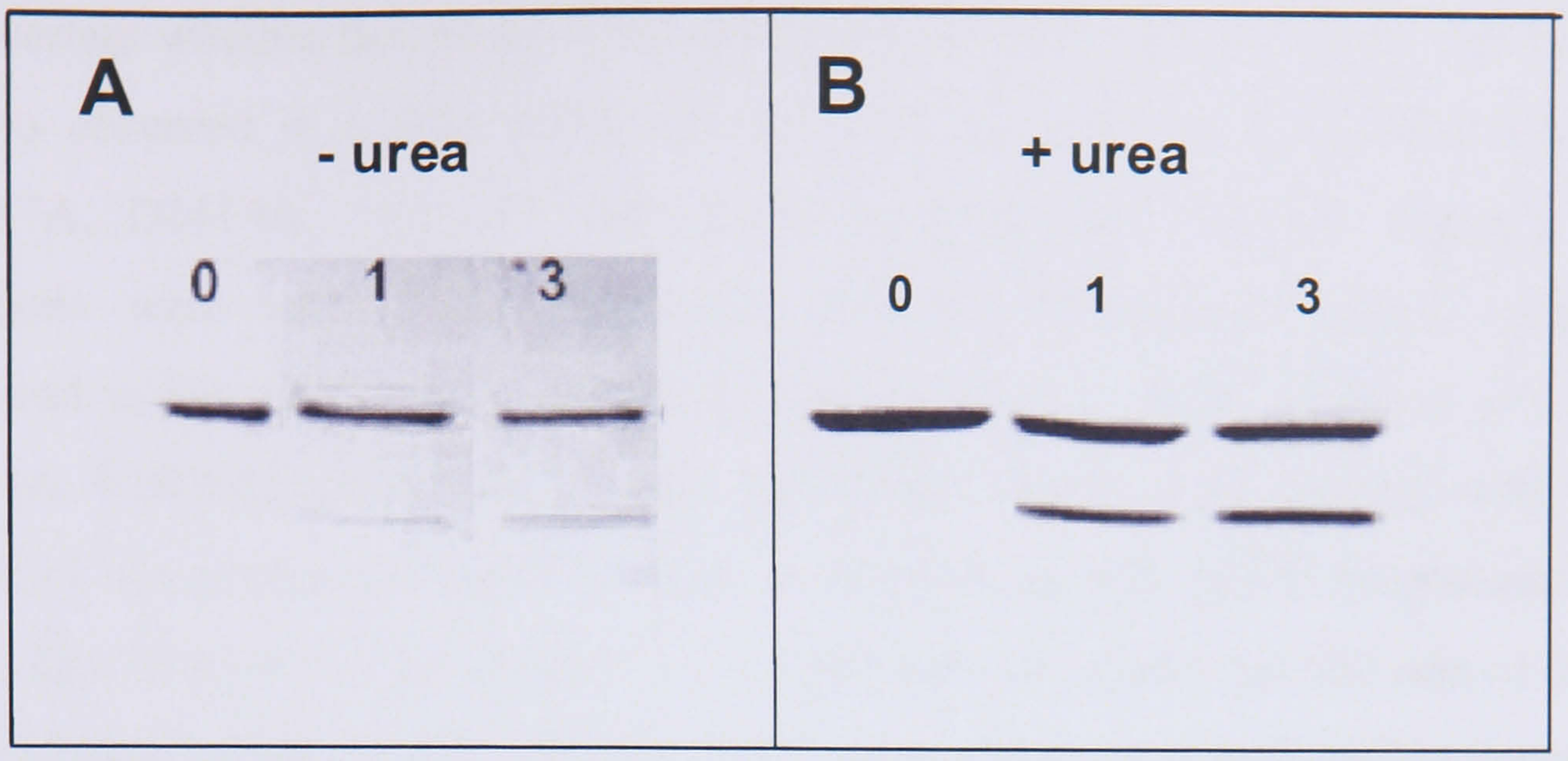


Fig. 3.36 Wild type VWFA2 proteolysis followed by SDS-PAGE and Coomassie staining. 6 μM of wild type VWFA2 was incubated with 16.5 nM ADAMTS13 in 20 mM Tris-HCl (pH 7.8), 150 mM NaCl and 5 mM $CaCl_2$, in the absence (panel A) and presence (panel B) of 1 M urea. Sub-samples were taken at different time points (0, 1, 3 hours) and analysed by SDS-PAGE (16.5% Tris-Tricine gel) and Coomassie staining. The larger N-terminal cleavage product is evident, whereas the smaller C-terminal fragment could not be readily visualised. In the presence of denaturants, the cleavage appeared to be faster, even if it still did not go to completion after 3 hours.

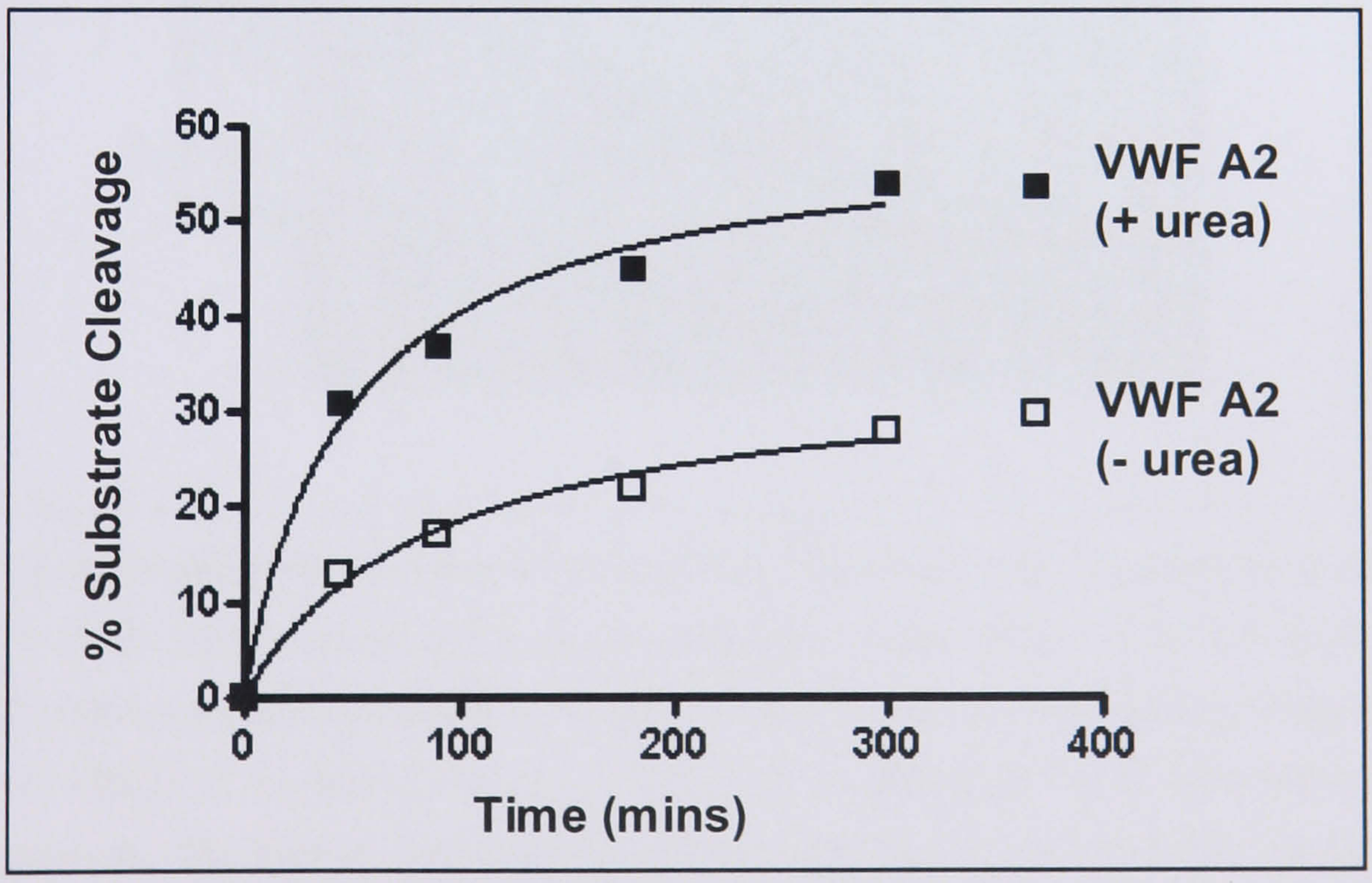


Fig. 3.37 Wild type VWFA2 proteolysis followed by HPLC. 0.5 μM of wild type VWF A2 was incubated with 16.5 nM of ADAMTS13 in reaction buffer (20 mM Tris-HCl (pH 7.8), 150 mM NaCl and 5 mM $CaCl_2$), in the presence or absence of 1 M urea. Each time point was analysed using HPLC and the rate of cleavage plotted against time. The cleavage reaction was much faster in the presence of denaturants. However, it seemed to plateau at ~50-60% cleavage after 5 hours.

3.6.4 Sub-cloning of D1587A, D1614A and E1615A in VWF A2 domain

To ascertain whether the effect of the mutations in VWF115 (see Section 3.5.4) could be also observed in a fully folded A2 domain, the three most affected mutations (D1587A, D1614A, E1615A) were introduced into the VWFA2 fragment. The mutations were individually sub-cloned into the VWFA2 pTrcHisA vector as described in Materials and Methods (see Section 2.1.4.1). After VWF115 (D1587A, D1614A, E1615A) pET100 and VWFA2 pTrcHisA vectors were digested with Kpn I and Pvu I, the products of digestion were assessed by agarose gel electrophoresis (Fig. 3.38). The band of 3.6 kb (from VWFA2 pET100 digestion) and the one of 1.2 kb (from mutated VWF115 pET100 digestion) were gel extracted and used as vector and insert respectively in the subsequent ligation step. The ligation reactions were then used to transform DH5α cells as described in Section 2.1.4.2. The success of the ligation step was confirmed by sequencing the purified plasmid preparations.

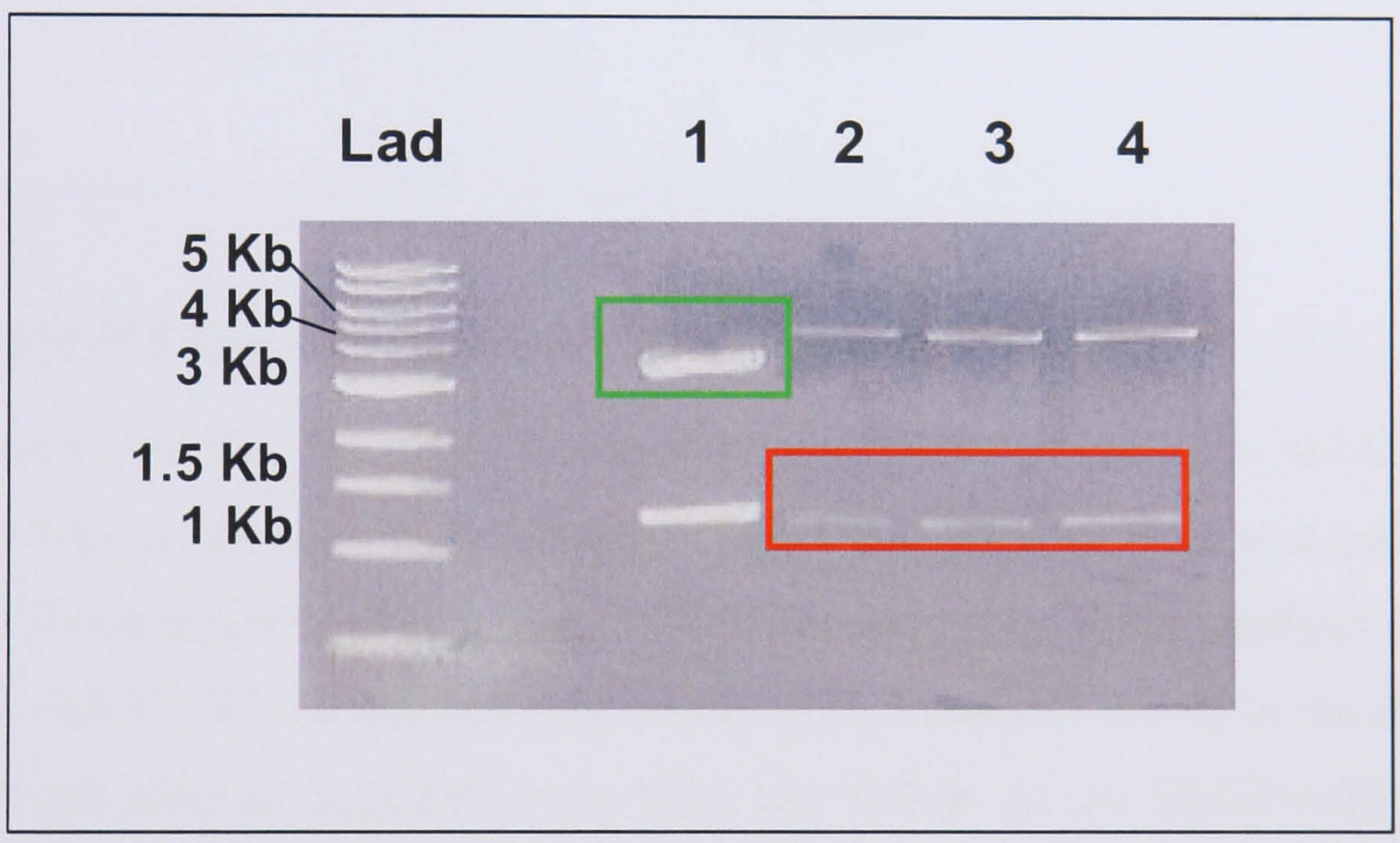


Fig. 3.38 Gel electrophoresis following Kpn I and Pvu I digestion. After digesting the vectors with Kpn I and Pvu I, the cleaved products were analysed on a 0.8 % agarose gel. The digestion of wild type VWFA2 pTrcHisA generated two bands of 3.6 and 1.4 kb, respectively. The digestion of the mutated VWF115 pET100 (D1587A, lane 2; D1614A, lane 3; E1615A, lane 4) produced two bands of 4.9 and 1.2 kb, respectively. The band of 3.6 kb highlighted by a green box (in lane 1) and the bands of 1.2 kb highlighted by a red box (in lanes 2-4) were gel-extracted and subsequently used as vector and inserts respectively in the ligation step. Lad: ladder of molecular weight marker.

3.6.5 Expression and purification of VWFA2 mutants

As described above for wild type VWFA2, VWFA2 variants were expressed in Rosetta *E. coli* cells. They were refolded and purified by nickel-chelating column affinity chromatography, with an 8M-0M urea linear gradient (not shown). The majority of the protein was recovered in the stripped fraction. This material was analysed by SDS-PAGE and Coomassie staining and it appeared as a single 23 kDa band (Fig. 3.39).

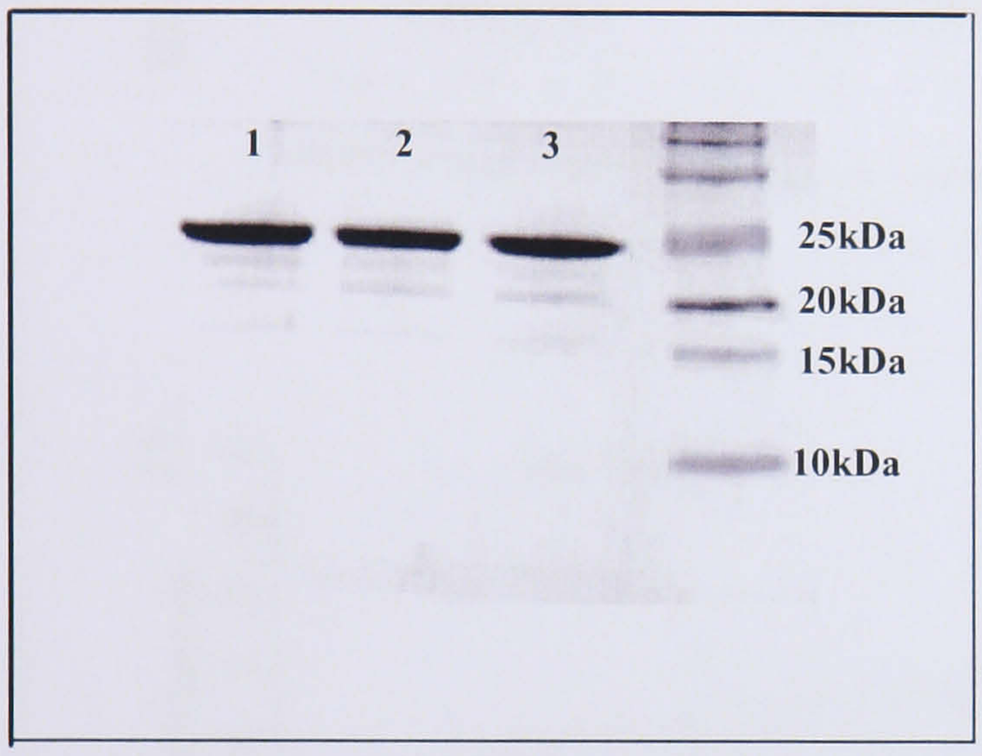


Fig. 3.39 VWFA2 mutants examined with SDS-PAGE and Coomassie staining. The stripped fractions from VWFA2 variants were analysed on a 16.5 % Tris-Tricine gel followed by Coomassie staining. D1587A (lane 1), D1614A (lane 2) and E1615A (lane 3) VWFA2 mutants appeared as 23 kDa bands.

3.6.6 ADAMTS13 cleavage of VWFA2 variants

Time course cleavage reactions were set up for VWFA2 variants (D1587A, D1614A and E1615A), as previously described for wild type VWFA2, and analysed both by SDS-PAGE/Coomassie staining (Fig. 3.40 A and B) and by HPLC analysis (Fig. 3.40 C and D). All VWFA2 fragments were proteolysed extremely slowly in the absence of urea, and the cleaved fragments were only just visible on the SDS-PAGE gel even after 3 hours incubation time (Fig. 3.40 A). Due to the small amount of proteolysis, it was not possible to accurately compare the cleavage of the fragments with each other. All the fragments were cleaved visibly faster in the presence of 1 M urea (Fig. 3.40 B), suggesting that the mutations do not cause gross structural changes that alter the cleavage, as observed for type 2A group II VWD mutations. Comparing wild type VWFA2 with the three mutants, it seemed that the latter are cleaved slower (Fig. 3.40 B). The result was confirmed by HPLC analysis, where the mutants were generally cleaved slower than wild type VWFA2, both in the absence (Fig. 3.40 C) and in the presence of urea (Fig. 3.40 D). Taken together, these results confirmed that the mutated residues (D1587A, D1614A and D1615A) not only affect the cleavage of the

short substrate VWF115 but also when introduced into a complete domain (VWFA2), highlighting the importance of these three amino acids in recognition and cleavage of the VWFA2 domain by ADAMTS13.

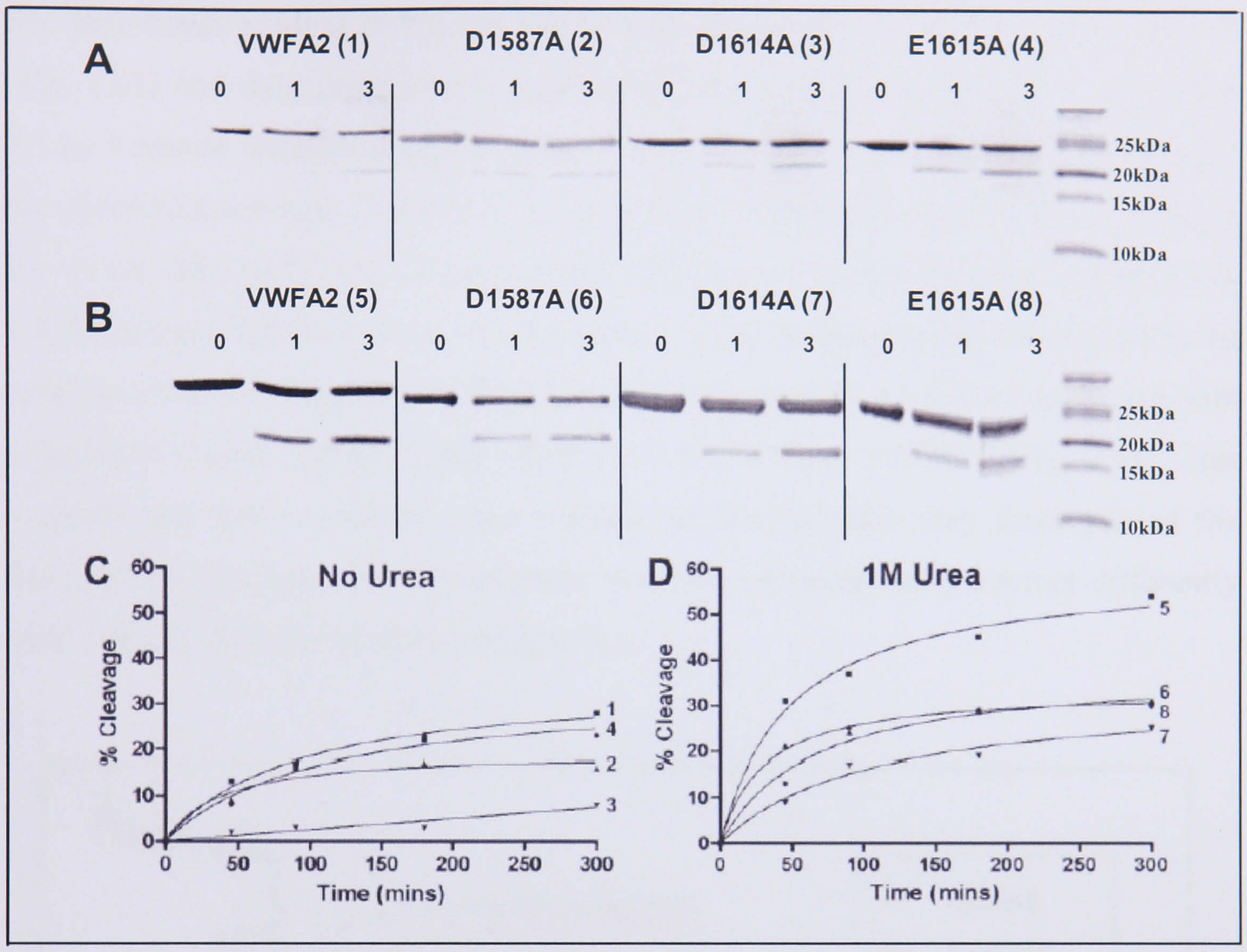


Fig. 3.40 Proteolysis of wild type and mutant VWFA2 fragments. A) 6 μM of wild type VWFA2 (1) or VWFA2 mutants (2-4) was incubated with 16.5 nM ADAMTS13 in 20 mM Tris-HCl (pH 7.8), 150 mM NaCl and 5 mM $CaCl_2$, in the absence of denaturants. Sub-samples were taken at 0, 1, 3 hours and analysed by SDS-PAGE followed by Coomassie staining. Uncleaved fragment was detected as a band of 26 kDa and 23 kDa, for wild type VWFA2 and mutants, respectively. Only the larger N-terminal cleavage product was evident, whereas the smaller C-terminal fragment could not be visualised. **B)** 6 μM of mutant VWFA2 fragments was incubated with 16.5 nM ADAMTS13 (in the same buffer as in A), in the presence of 1 M urea and analysed as before. **C)** HPLC analyses of time course reactions containing 0.5 μM of each substrate and 16.5 nM ADAMTS13 in the absence of urea. **D)** HPLC analyses of time course reactions containing 0.5 μM of each substrate and 16.5 nM of ADAMTS13 in the presence of 1 M urea.

3.6.7 Wild type VWFA2 binding to ADAMTS13

The binding of ADAMTS13 to VWFA2 was studied by microtiter plate-based equilibrium binding assay, as previously described for VWF115 (see Section 3.3.3). The absorbance reading at 492 nm was plotted against the ADAMTS13 concentration (Fig. 3.41) and data fitted to the one binding site model (see equation 5 in Section 2.4.4). Separate experiments (n=6) gave a mean value of 10.9 ± 0.8 nM for the K_D of the interaction between ADAMTS13 and VWFA2, in the absence of EDTA. A K_D of 3.1 ± 0.8 nM (n=4) was obtained when EDTA was added. In some experiments, VWF115 was immobilised on the same plate to allow a direct comparison between the binding of the two fragments to ADAMTS13. It appeared that VWFA2 interacted with ADAMTS13 with slightly higher affinity (~2-3 fold) than VWF115 (Fig. 3.41). This suggests that there could be other residues in VWFA2 that may form part of the ADAMTS13 binding site. Alternatively, the two molecules may interact differently with ADAMTS13 due to their conformation.

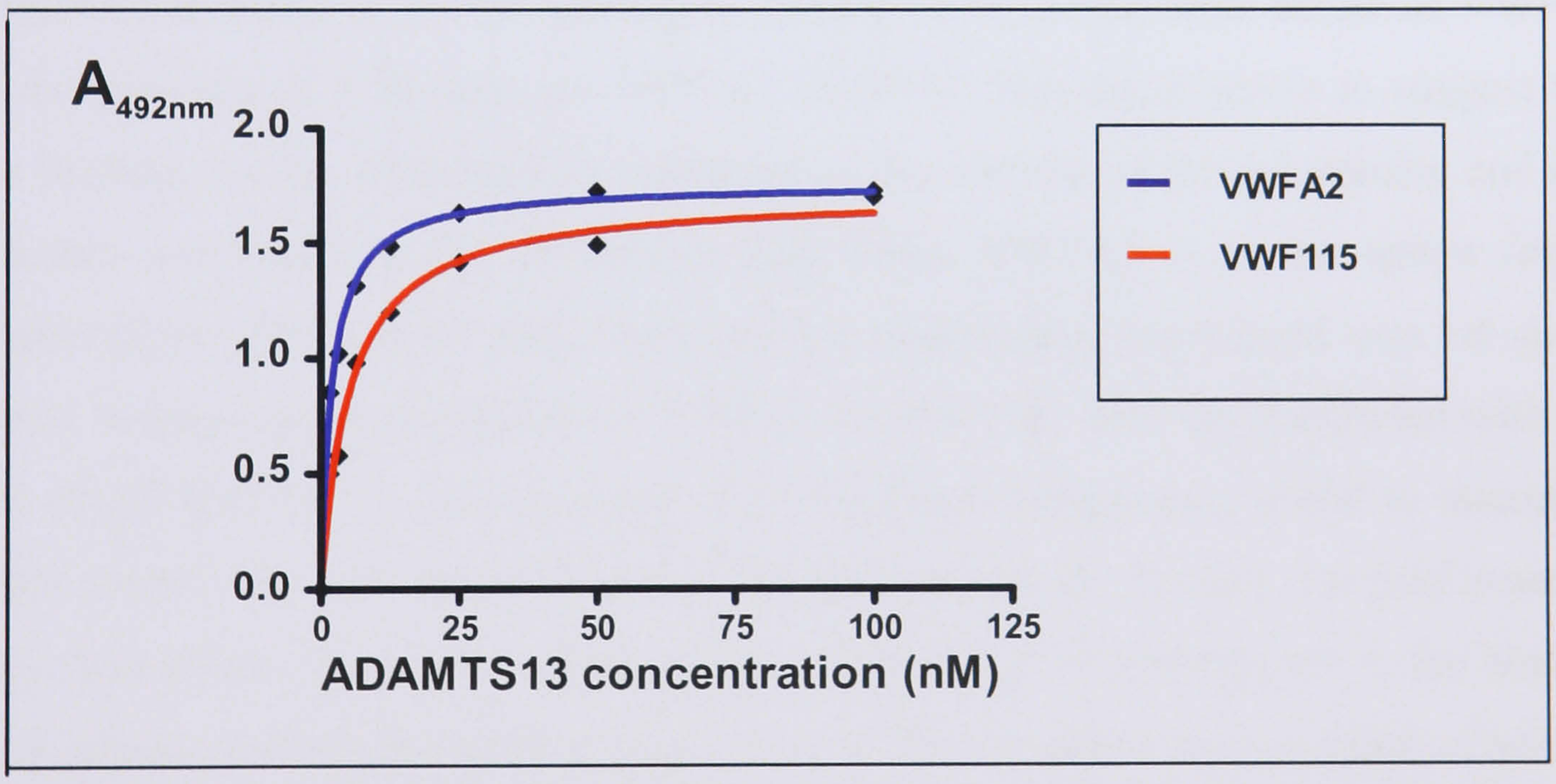


Fig. 3.41 VWFA2-ADAMTS13 binding. Direct comparison of ADAMTS13 binding to VWF115 and VWFA2. 140 nM of either VWF115 or VWFA2 in 50 mM sodium carbonate buffer (pH 9.6) was coated into a 96 well microtiter plate. Different ADAMTS13 concentrations (1.56-100 nM) in PBS-1% BSA and 50 mM EDTA were applied and incubated at 37°C for 3 hours. Biotinylated anti-TSR (2-4) pAb was applied for 90 minutes and subsequently, Streptavidin-HRP for 1 hour. The HRP substrate, OPD, was added to develop the colour. The absorbance was read at 492 nm and plotted against ADAMTS13 concentration. The binding curves for VWFA2 and for VWF115 are depicted in blue and red, respectively. The curves were fitted to the one binding site model, giving values for K_D. In the shown example, the calculated K_D was 5.4 and 2.0 nM, for VWF115 and VWFA2, respectively.

3.6.8 Soluble and plate-bound VWFA2: competition experiments

The above result showed high affinity binding between ADAMTS13 and VWFA2. However, this may be not representative of what occurs in solution, since it has been previously shown [258] that the conformation of full-length VWF changed significantly on its binding to the surface of a microtiter plate. This probably induced an "unfolding" of the molecule similar to the one caused by denaturants. In order to investigate the binding between VWFA2 and ADAMTS13 in solution, a competition experiment was set up. 140 nM of VWFA2 was immobilised into the wells of a microtiter plate. ADAMTS13 (concentration range 1.56-100 nM), in the presence of EDTA, was pre-incubated with 1400 nM of either VWFA2, or VWFA2 in the presence of 1 M urea, or VWFA2 R1597Q variant, before being added to VWFA2-coated wells. The mutation R1597Q causes VWD type 2A and it has been previously reported to allow the cleavage of both full-length VWF and VWFA2 in the absence of denaturants or fluid shear stress [183,186]. The detection of the binding was performed as described in Section 3.3.3. As shown in Fig. 3.42, VWFA2 in solution competed with immobilised VWFA2 for the binding to ADAMTS13, to the same extent as VWFA2 in the presence of 1 M urea and VWFA2 R1597Q. This result seems to suggest that the binding site for ADAMTS13 is located on the surface on the A2 domain and it is exposed and available for interaction even when VWFA2 is in the native folded conformation. To confirm this result, another competition experiment was set up, in which increasing concentrations of VWFA2 (0-560 nM) were pre-incubated with 6.5 nM of ADAMTS13 (in the presence of EDTA) and subsequently added to microtiter wells coated with 140 nM of VWFA2. The detection of the binding was performed as described above. The result was plotted as a percentage of binding (where the binding in the absence of soluble VWFA2 was taken as 100%) against the logarithm of soluble VWFA2 concentration (Fig. 3.43). The data from 9 separate experiments were fitted to the equation described in Materials and Methods (see equation 6 in Section 2.4.5.3) and this gave a mean value of 73.8 ± 11.7 nM for IC50. The K_i could be calculated from IC50, using the equation 7 in Section 2.4.5.3, giving a value of 1.60 ± 0.25 nM. This value is comparable with the K_D of 3.1 nM found for ADAMTS13 interaction with immobilised VWFA2 in the presence of EDTA (see Section 3.6.7). This experiment confirmed that soluble VWFA2 can indeed compete with immobilised VWFA2 for binding to ADAMTS13, in the absence of denaturants.

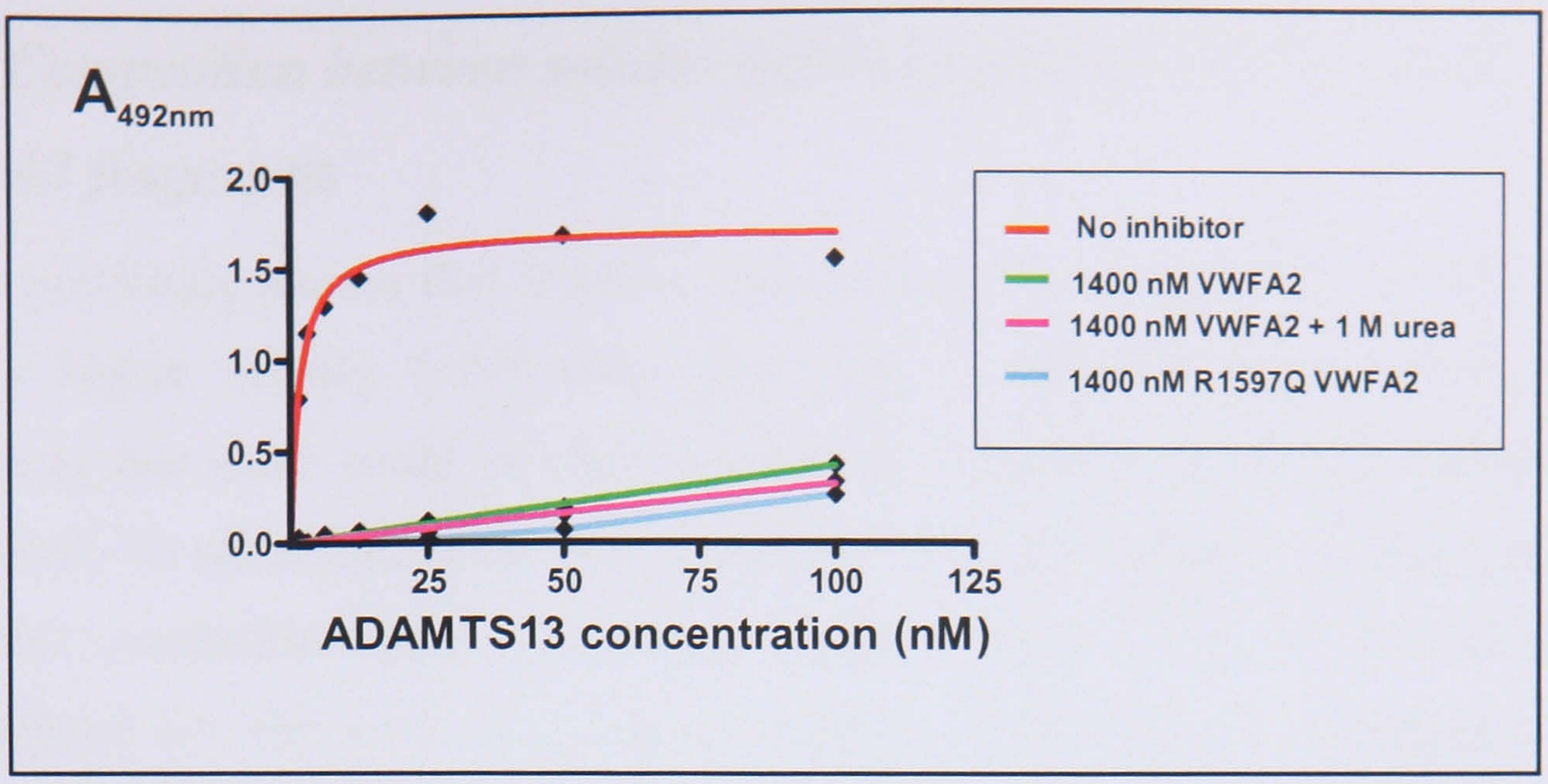


Fig. 3.42 Soluble and plate-bound VWFA2 competition. 140 nM of VWFA2 in 50 mM sodium carbonate buffer (pH 9.6) was coated into the wells of a microtiter plate. ADAMTS13 (1.56-100 nM) in PBS-1% BSA and 50 mM EDTA was pre-incubated with 1400 nM of alternatively VWFA2 (in the presence and absence of 1 M urea) or VWF A2 R1594Q and added to the wells. Bound ADAMTS13 was detected with biotinylated anti-TSR (2-4) pAb followed by Streptavidin-HRP, as previously described. Absorbance at 492 nm was plotted against ADAMTS13 concentration. The red curve represents ADAMTS13 binding to immobilised VWFA2, in the absence of any inhibitor. Inhibition of the binding occurred in a similar way when ADAMTS13 was pre-incubated with soluble VWFA2 (green), with soluble VWFA2 in the presence of 1 M urea (pink) or with R1597Q VWFA2 (light blue).

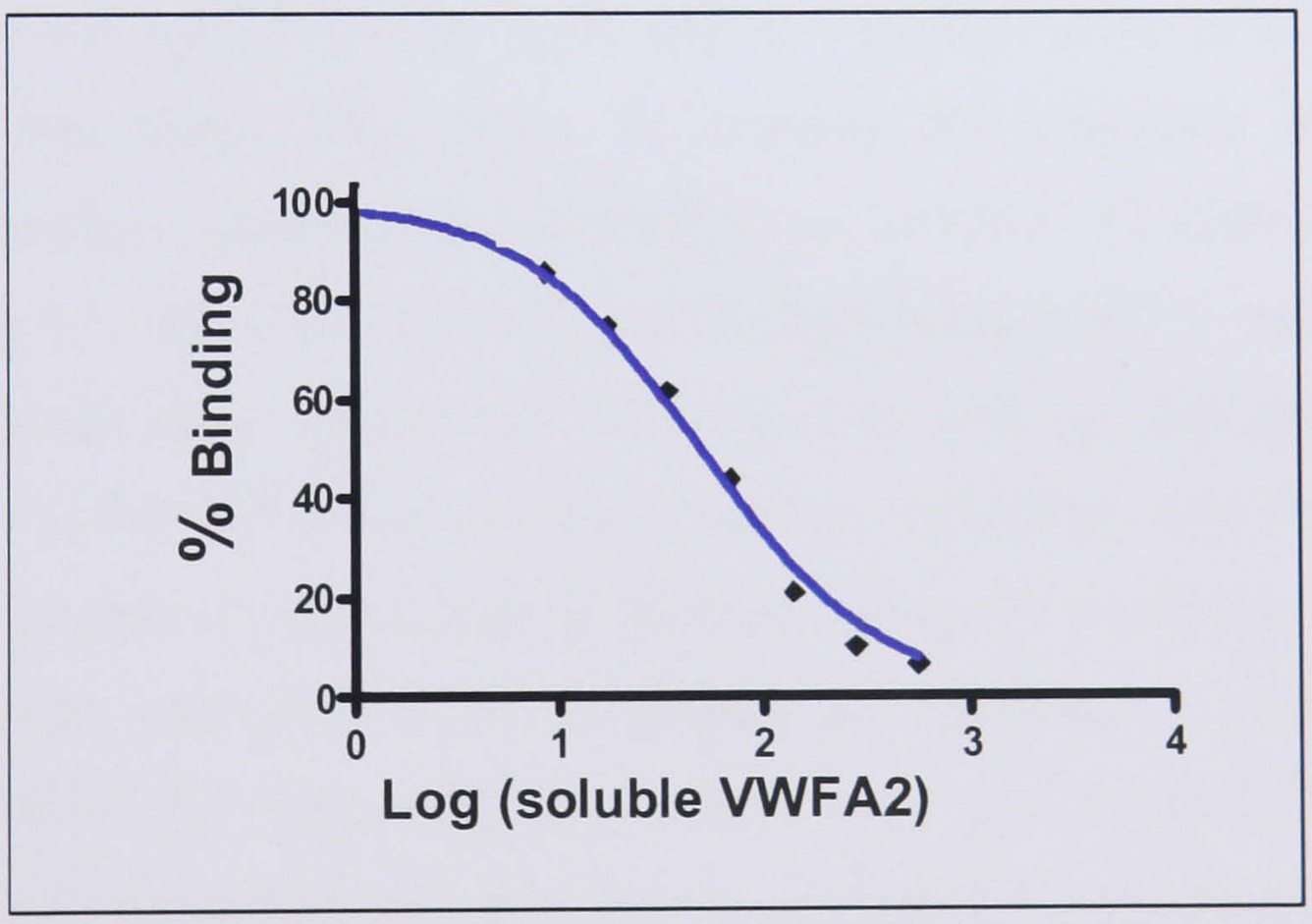


Fig. 3.43 Competition for ADAMTS13 binding between immobilised and soluble VWFA2. 140 nM of VWFA2 in 50 mM sodium carbonate buffer (pH 9.6) was coated into the wells of a microtiter plate. 6.5 μM of ADAMTS13 in PBS-1% BSA and 50 mM EDTA was pre-incubated with increasing concentrations of VWFA2 (0-560 nM) and added to the wells. ADAMTS13 binding was detected using biotinylated anti-TSR (2-4) pAb. The result was plotted as a percentage of the total binding observed in the absence of any soluble VWFA2 against the logarithm of soluble VWFA2 concentration. The curve was fitted to the one site competition equation using Graph Pad Prism 4 software, giving an estimate of the IC50 (see text).

3.6.9 Competition between soluble and immobilised VWF115 and VWFA2 fragments

I have previously shown that VWFA2 seemed to interact with ADAMTS13 with a slightly higher affinity (~2-3 fold) than that of VWF115 (see Section 3.6.7), suggesting that there could be other residues in VWFA2 involved in ADAMTS13 interaction. To understand if the difference in the K_D between the two fragments was important, competition experiments were set up as follows. 140 nM of VWFA2 was immobilised into the wells of a microtiter plate. ADAMTS13 (concentration range 1.56-100 nM), in the presence of EDTA, was pre-incubated with three different concentrations of soluble VWF A2 or soluble VWF115 (140, 700 and 1400 nM). The detection of the binding was performed as described above and in each case the absorbance at 492 nm was plotted against ADAMTS13 concentration. Comparing the two graphs in Fig. 3.44, it is evident that soluble VWF115 (Fig. 3.44 A) did not compete with immobilised VWFA2 as well as soluble VWFA2 (Fig. 3.44 B) for the binding to ADAMTS13. This further suggests the presence of other important residues present in VWFA2 which may contribute to the binding. A similar result was obtained when VWF115 was coated onto the wells and the inhibitory effect of soluble VWF115 and VWFA2 was tested (Fig. 3.45). To quantify the inhibition effect for each fragment, increasing concentrations of VWFA2 or VWF115 (0-2240 nM) were pre-incubated with 6.5 nM of ADAMTS13, in the presence of EDTA, and subsequently added to microtiter wells coated with VWFA2 (Fig. 3.46 A). The same experiment was performed with VWF115 immobilised onto the wells (Fig. 3.46 B). In each case, the result was plotted as a percentage of binding (where the binding in the absence of soluble competitor was taken as 100%) against the logarithm of soluble competitor concentration. IC50 for each competition experiment was obtained from fitting the curves to the one site competition equation (see equation 6 in Section 2.4.5.3) and K_i could be calculated (see equation 7 in Section 2.4.5.3). IC50 and K_i values are listed in the table on the right of each graph. K_i calculated using soluble VWF115 as a competitor was always higher (~ 6-7 fold) than the one found when soluble VWFA2 was used, both in the case VWF115 or VWFA2 was immobilised on the plate.

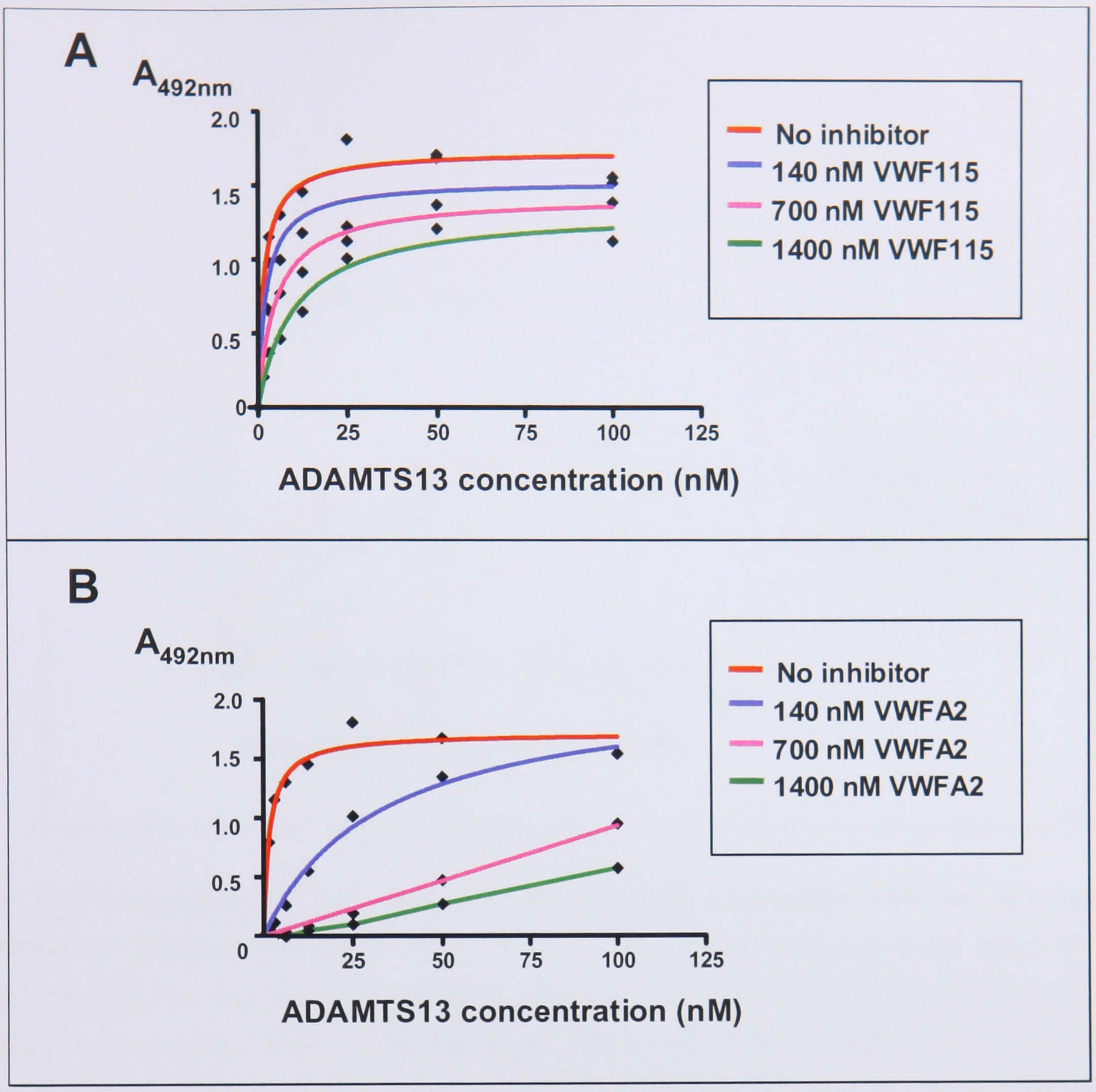


Fig. 3.44 Competition for ADAMTS13 binding between immobilised VWFA2 and soluble VWF115 or VWFA2. 140 nM of VWFA2 in 50 mM sodium carbonate buffer (pH 9.6) was immobilised into the well of a microtiter plate (in both A and B). ADAMTS13 (1.56-100 nM) in PBS-1% BSA and 50 mM EDTA was pre-incubated with increasing concentrations (140, 700 and 1400 nM) of soluble VWF115 (in A) or VWFA2 (in B) and added to the wells. In both A and B, increasing amounts of the competitor resulted in a reduction in immobilised VWFA2-ADAMTS13 interaction. However, the inhibition is markedly more effective using soluble VWFA2.

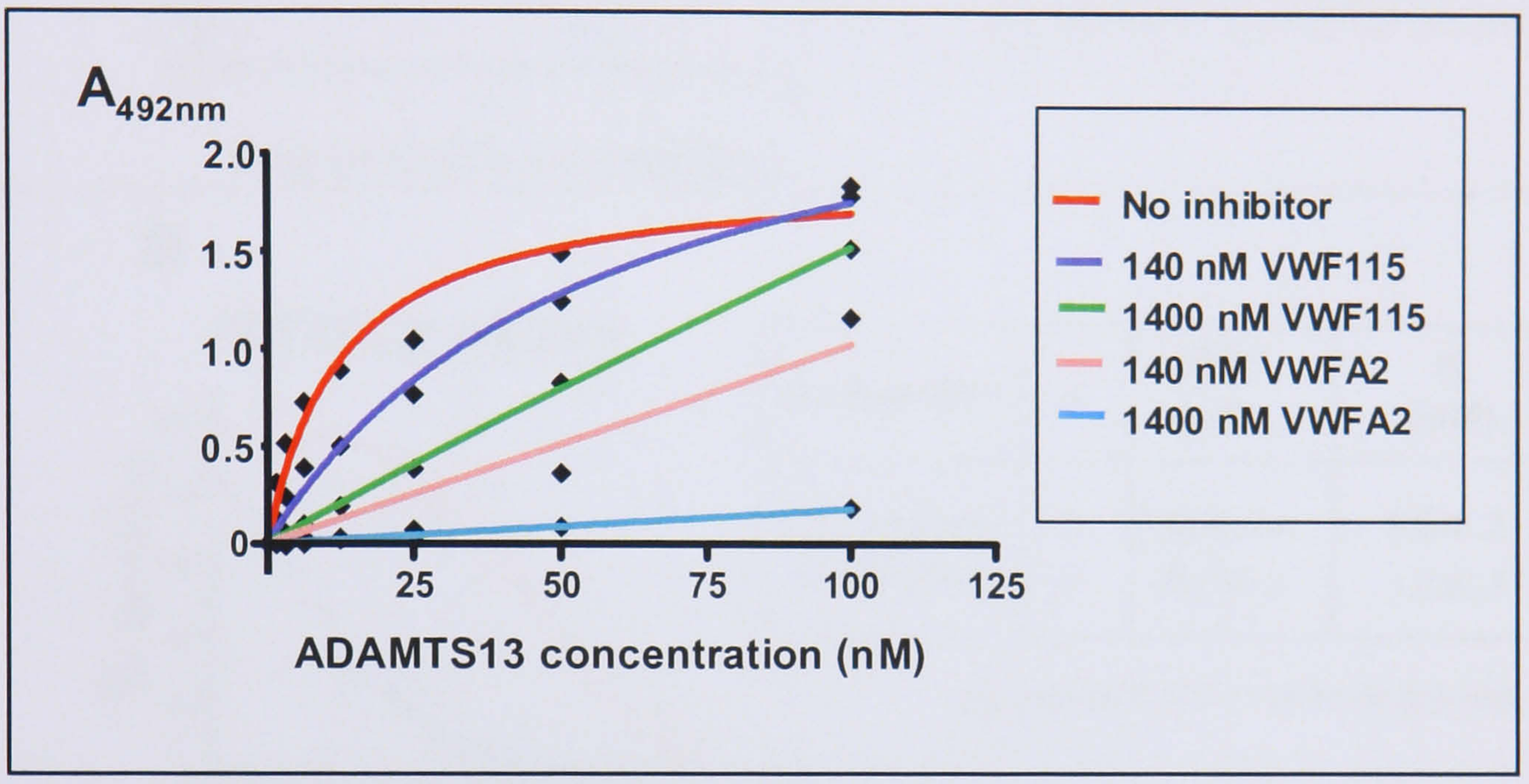


Fig. 3.45 Competition for ADAMTS13 binding between immobilised VWF115 and soluble VWF115 or VWFA2. 140 nM of VWF115 in 50 mM sodium carbonate buffer (pH 9.6) was immobilised into the well of a microtiter plate. ADAMTS13 (1.56-100 nM) in PBS-1% BSA, 50 mM EDTA was pre-incubated with two concentrations (140 and 1400 nM) of soluble VWFA2 or VWF115 and added to the wells. The graph clearly shows that soluble VWFA2 competed better than soluble VWF115 for immobilised VWF115-ADAMTS13 binding.

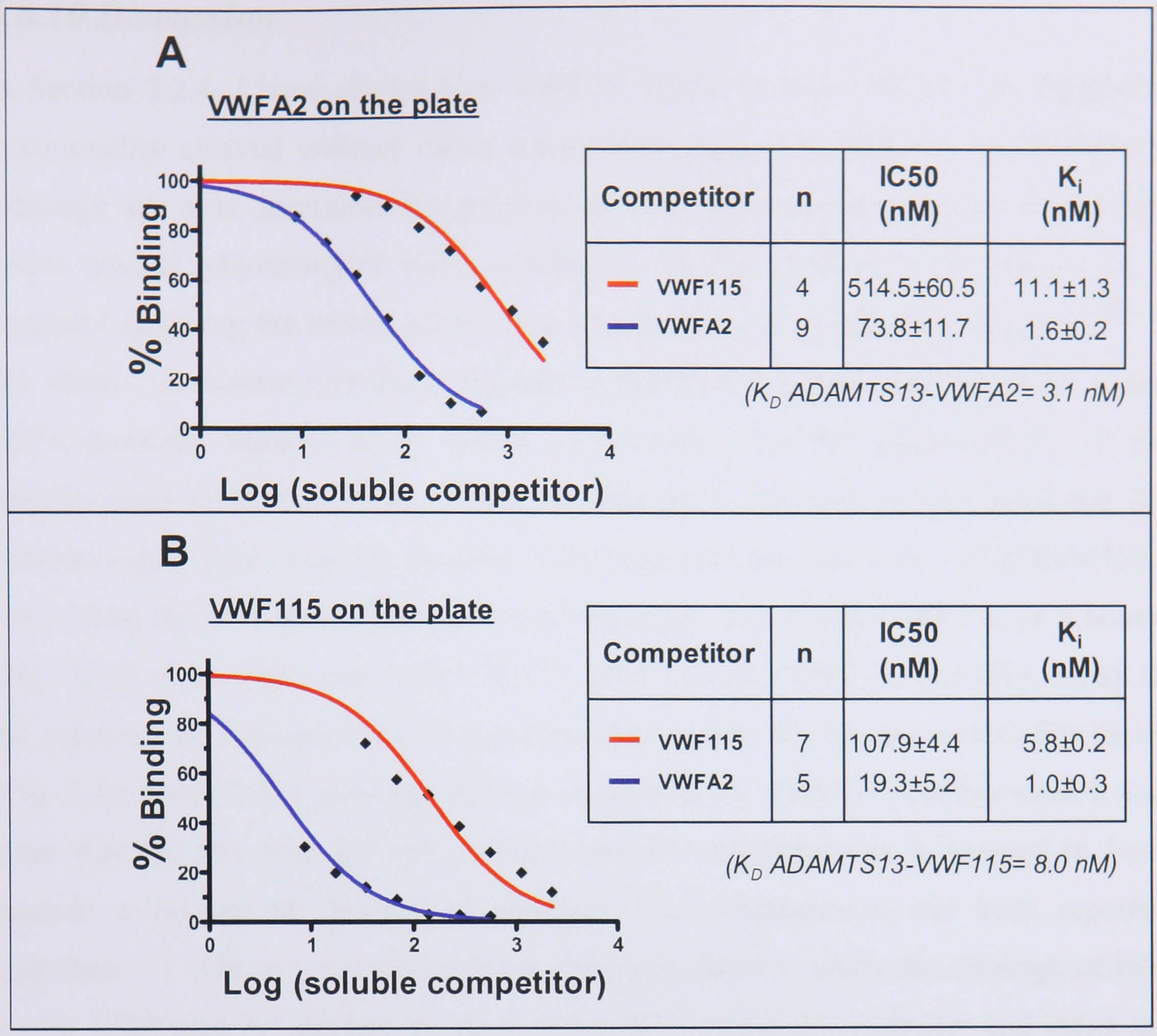


Fig. 3.46 IC50 and K_i values for the inhibition of ADAMTS13 binding to immobilised VWFA2 or VWF115, using soluble VWF115 or VWFA2 as competitors. 140 nm of VWFA2 (panel A) or VWF115 (panel B) in 50 mM sodium carbonate buffer (pH 9.6) were immobilised into the wells. 6.5 nM of ADAMTS13 in PBS-1% BSA and 50 mM EDTA was pre-incubated with increasing concentrations (0-2240 nM) of soluble VWFA2 (blue curves) or VWF115 (red curves), and then added to the wells. ADAMTS13 bound to the immobilised substrate is plotted as a percentage of total binding (in the absence of any competitor) against the logarithm of soluble competitor concentration. The curves were fitted to the one site competition equation, giving values for IC50. K_i values could be calculated using the equation 7 in Section 2.4.5.3. In the table on the right of each graph, values for total number of experiments (n), IC50 and K_i are reported. The K_D for the binding of ADAMTS13 to the immobilised substrate, in the absence of any inhibition, is given in brackets below each table. Both the two graphs (panel A and panel B) and the comparison of K_i values clearly show that soluble VWFA2 competes better than soluble VWF115 for the binding between ADAMTS13 and the immobilised substrate.

3.6.10 Discussion

In Section 3.2.4, I have shown how VWF76, VWF115 and VWF115-A3 fragments were readily cleaved without using denaturants, suggesting that the Y1605-M1606 cleavage site was accessible for proteolysis. This allowed the analysis of cleavage under normal physiological ionic conditions. In this Section, the cleavage of a fragment spanning the whole A2 domain was analysed. As previously reported [186,332], the whole A2 domain was quite resistant to ADAMTS13 cleavage (Fig. 3.36 A and 3.37), probably because of its folded conformation and the inaccessibility of the scissile bond (Y1605-M1606), which lies buried in the core of the predicted A2 domain model (Fig. 1.10 B). Despite using increased concentrations of ADAMTS13 (16.5 nM), the wild type VWFA2 was proteolysed very slowly (~28% after 5 hours) (Fig. 3.37) when compared with VWF76, VWF115 and VWF115-A3 (Fig. 3.16). In the presence of denaturants (1 M urea) the cleavage of A2 domain was visibly faster (Fig. 3.36 B and 3.37), although still not as rapid as for VWF115. Furthermore, it was clear that the reaction did not proceed towards completion as it seemed to have reached a plateau at 50-60% of cleavage. This phenomenon has been reported elsewhere [186]. The use of denaturant conditions is useful to study the cleavage of full-length VWF and A2 domain *in vitro*, since they unfold the molecule and make the cleavage site accessible by ADAMTS13. However, it should be considered that this does not represent a physiological condition and, furthermore, it is not known how similar is the VWF unravelling caused by denaturants to that induced by high shear stress *in vivo*. The use of mild denaturant conditions (i.e 1 M urea) may be not so effective in stably denaturing the VWF substrate. However, increased concentration of urea cannot be used, because they could significantly affect ADAMTS13 activity. It may be possible, that some VWFA2 molecules previously denatured can gradually regain their native conformation. This may explain why the cleavage reaction of VWFA2 does not go to completion, whereas a VWFA2 with the type 2A (group II) mutation (R1597Q) can fully be proteolysed in the absence of urea [186]. However, preliminary experiments performed by my colleague Dr. James Crawley showed that the percentage of cleavage reached at plateau increased by using higher concentrations of ADAMTS13. This suggests that the proteolysis of VWF may not go to completion because some inhibition by cleavage products occurred (see Section 4.3).

In Section 3.5.4 and 3.5.5, I have shown that three mutations (D1587A, D1614A and E1615A) individually introduced in VWF115 affected its cleavage and binding to

ADAMTS13. In order to assess that this effect was not merely a feature of that particular substrate, the same mutations were introduced into the whole VWFA2 domain. All the mutants appeared to be cleaved visibly faster in the presence of 1 M urea than in its absence (Fig. 3.40 A and B), demonstrating that the mutations do not cause structural changes that alter the cleavage of the A2 domain, a property that has been reported for several type 2A VWD mutations. The cleavage of the three individual variants was slowed when compared to wild type A2 fragment (Fig. 3.40 C and D), confirming the importance of these amino acids on the surface of A2 domain in determining VWF cleavage by ADAMTS13.

As already stated, wild type VWFA2 is quite resistant to proteolysis in the absence of denaturants or shear stress. However, whether these conditions induce conformational changes that expose the cleavage site or a cryptic ADAMTS13 binding site has not been clarified yet. To have a better understanding of ADAMTS13 binding to VWFA2 domain, different binding experiments were set up using the microtiter plate-based equilibrium binding method. Initially, VWFA2 was immobilised on the plate and the binding to ADAMTS13 tested as previously described for VWF115. The result showed a high affinity binding (K_D~ 10.9 nM and 3.1 nM, in the absence and presence of EDTA respectively) (Fig. 3.41). However, it has been previously demonstrated that the immobilisation of full-length VWF on the plate surface probably causes a conformational change similar to that caused by urea. Immobilised VWF could bind ADAMTS13 with high affinity (K_D ~ 14 nM), but soluble VWF could only compete with the immobilised VWF for ADAMTS13 binding when 1 M urea was added [258]. A similar experiment was performed, competing the binding between immobilised VWFA2 and ADAMTS13 with soluble VWFA2 in the absence and presence of 1 M urea. A type 2A VWFA2 variant (R1597Q) was also used as a competitor in a parallel experiment. It has been previously reported that this mutation increased the rate of both full-length VWF and VWFA2 proteolysis, even in the absence of urea, probably interfering with the normal folding of the domain [183,333]. Both soluble VWFA2 in the absence and presence of urea and R1597Q VWFA2 could effectively inhibit ADAMTS13 binding to immobilised VWFA2 (Fig. 3.42), suggesting that the binding site on the A2 domain is exposed even when the molecule is in solution in a globular conformation. To confirm this result, the inhibition of immobilised VWFA2-ADAMTS13 interaction was investigated using increased concentrations of soluble VWFA2 (Fig. 3.43). The K_i was calculated to be 1.60 nM, confirming soluble VWFA2 could indeed effectively compete for the binding to ADAMTS13. Overall,

these results suggest that even if globular VWFA2 can bind to ADAMTS13 with high affinity, its cleavage is significantly impaired probably because the cleavage site is hidden in the core of the molecule.

Furthermore, since the K_D for VWFA2 binding to ADAMTS13 was reproducibly found to be ~ 2-3 times lower than the one for VWF115, the possibility of other residues in the VWFA2 being part of ADAMTS13 docking site was further investigated. A series of competition experiments were performed, immobilising alternatively VWFA2 (Fig. 3.44 and 3.46 A) or VWF115 (Fig. 3.45 and 3.46 B) on the plate and inhibiting the binding to ADAMTS13 using soluble VWFA2 or VWF115. In both situations, it was clear that VWFA2 was a better competitor, suggesting other amino acids involved in ADAMTS13 binding are probably located in the N-terminal region of VWFA2 lacking in VWF 115 (residues 1473-1554) (see Section 4.1.1).

4. ON-GOING AND FUTURE WORK

4.1 INVESTIGATION OF OTHER VWF REGIONS IMPORTANT FOR ITS CLEAVAGE/BINDING BY ADAMTS13

In the work described in this thesis I have shown that a short VWF A2 fragment (VWF115) interacts with ADAMTS13 with high affinity (see Section 3.3) and I have identified four charged amino acids (D1587, D1614, E1615 and K1617) in this region that are important for both ADAMTS13 proteolysis and binding (see Section 3.5). These residues are predicted to be located in proximity to each other and they are probably part of a docking site on the surface of the folded A2 domain (see Fig.3.27 B in Section 3.5.2). In order to investigate other regions important for VWF cleavage by ADAMTS13 and to fully map the ADAMTS13 docking site on VWF, further site-directed mutagenesis of selected residues in VWF 115 and VWFA2 is planned. Furthermore, binding studies using ADAMTS13 truncated fragments suggested that different ADAMTS13 domains contribute to VWF interaction [238,258]. It is likely that a corresponding number of distinct sites of interaction are present on VWF. To investigate this possibility, I will study the binding of ADAMTS13 to additional fragments of VWF spanning domains other than the A2 domain.

4.1.1 Site-directed mutagenesis of charged residues in VWFA2 N-terminal region

Amongst the previously studied residues, only one (D1587A) of those showing a slower cleavage and impaired binding was located in the N-terminal part of the VWF115 fragment. However, I have recently found that the VWFA2 N-terminal cleavage product (residues 1473-1605) still maintains quite high affinity for ADAMTS13 (see Section 4.3). Furthermore, I have previously demonstrated that VWFA2 binds to ADAMTS13 with slightly higher affinity than VWF115 (see Sections 3.6.7 and 3.6.9), suggesting that other residues involved in the interaction with ADAMTS13 may be located in the region 1473-1554. Using the same model of the A2 domain previously described, another 23 charged residues predicted to be located on the surface have been identified in the region 1473-1605 (see Fig. 4.1 A and B): 12 are located in the N-terminal region present both in VWFA2 and in VWF115 (residues 1554-1605) (Fig. 4.1 A) and 11 are in the region present in VWFA2 and not

in VWF115 (residues 1473-1553) (Fig.4.1 B). Most of these residues appeared to be located on the opposite side on the A2 model, in respect to D1587, D1614, E1615 and K1617. They may form another ADAMTS13 docking site on the A2 domain surface or be part of the same binding site when the VWF molecule is in the unfolded conformation. The plan is to mutate the mentioned residues variously in VWF115 and in VWFA2 and then analyse their influence upon VWF recognition and proteolysis by ADAMTS13.

Of the all above residues, four have been already mutated into glycine or alanine in VWF115 construct, generating the two following mutants: R1575A and DRE1596/7/8AGA. The mutants were expressed in Rosetta *E. coli* cells and purified from inclusion bodies, as described for wild type VWF115. The analysis of their cleavage by ADAMTS13 using HPLC showed a significant reduction in cleavage compared with the wild type VWF115. Their influence upon ADAMTS13 binding still needs to be investigated.

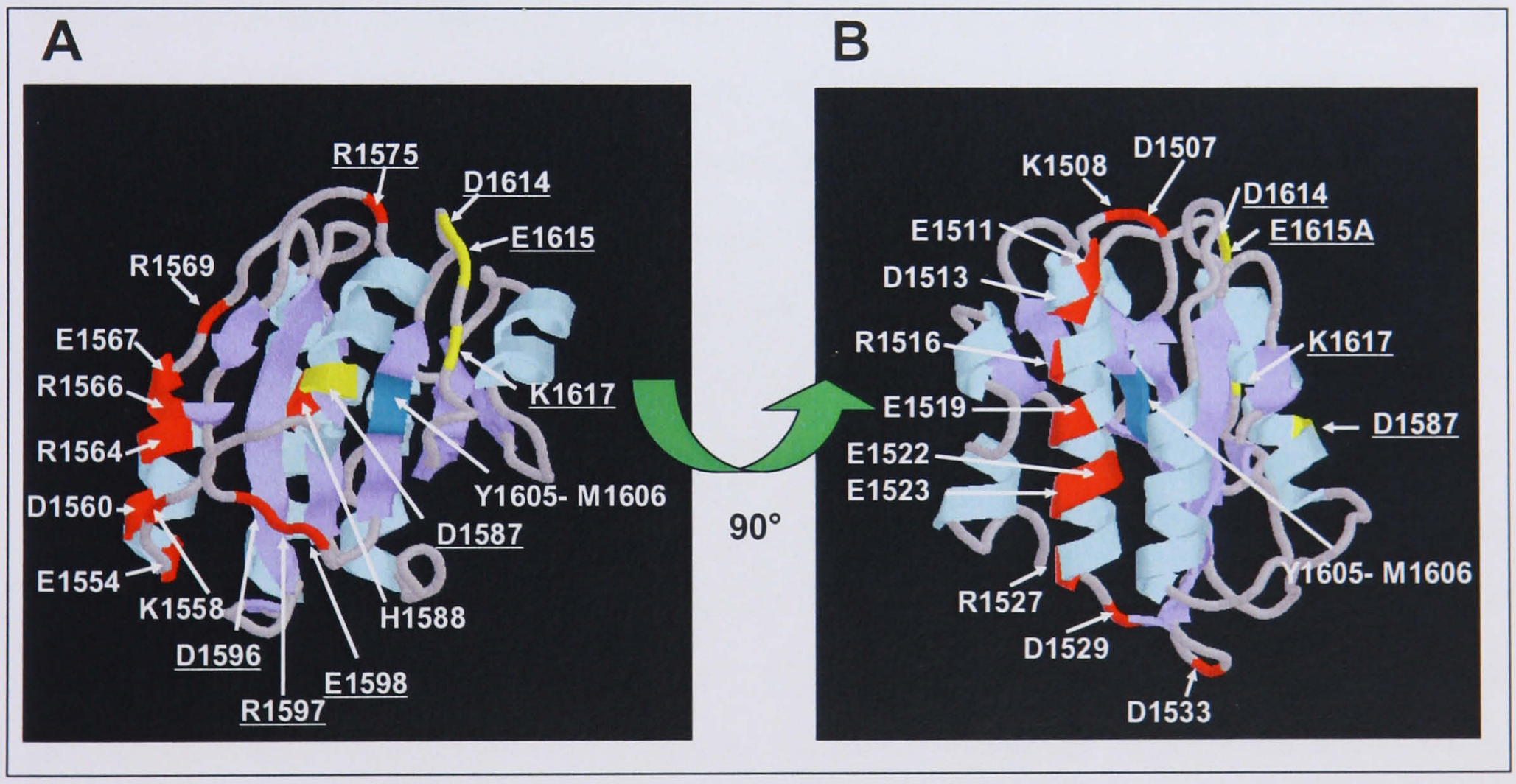


Fig. 4.1 Location of 23 charged residues on the surface of A2 domain. The predicted model of VWFA2 domain is shown in panel A and panel B in two different orientations. In both A and B, the cleavage site (Y1605-M1606) is highlighted in green in the core of A2 domain. The four residues (D1587, D1614, E1615 and K1617) previously identified to be important for ADAMTS13 binding are indicated in yellow and underlined. **A)** 12 identified charged residues are located in the N-terminal part of VWF115 and are highlighted in red. The residues underlined represent amino acids already mutated. **B)** 11 identified charged residues are located in the region which is present in VWFA2 but not in VWF115 and are highlighted in red.

4.1.2 Site-directed mutagenesis of VWF cleavage site and surrounding residues

ADAMTS13 substrate specificity for VWF is probably conferred by a specific and regulated interaction between the two molecules. However, what precisely confers the specificity for the cleavage of the Y1605-M1606 bond is unclear. To identify determinants for cleavage specificity I will investigate the role of the residues of the cleavage site (Y1605 and M1606) and surrounding residues (L1603, V1604, V1607 and T1608) (Fig. 4.2). It has been reported that the cleavage site residues in the substrate of serine proteases are critical for proteolysis. A noted example is represented by the cleavage of activated coagulation factor V (FVa) by APC. APC inactivates FVa via proteolytic cleavage at residues R306 and R506 [334]. A mutation in one of the cleavage site in FVa (R506Q) leads to a prothrombotic condition known as factor V Leiden, where the rate of cleavage of FVa is markedly decreased, with cleavage only occurring at R306 [335]. To investigate the importance of the cleavage site residues in VWF, Y1605 and M1606 has been mutated into alanine residues in VWF115, individually (Y1605A and M1606A) and in a double mutant (YM1605/6AA). The fragments have been expressed in Rosetta *E. coli* and purified from inclusion bodies, as for wild type VWF115. A preliminary analysis of the cleavage of the YM1605/6AA using 20 nM of ADAMTS13 showed no proteolysis occurred even after 5 hours incubation. Furthermore, the binding of YM1605/6AA to ADAMTS13 has been investigated by SPR. YM1605/6AA was covalently coupled to a CM5 sensor chip as described for wild type VWF115 (see Section 3.3.2.2). When the same concentration of ADAMTS13 (20 nM) was passed over both immobilised YM1605/6AA and wild type VWF115, a comparable binding response was detected for both the fragments (Fig. 4.3). A similar result was obtained when ADAMTS13 was immobilised onto the sensor chip surface and wild type VWF115 and YM1605/6AA passed over it (not shown). These preliminary results seem to suggest that the cleavage site residues are crucial in determining VWF proteolysis, but they are not directly involved in the binding to ADAMTS13. The role of these residues still needs to be analysed in more details, altogether with that of the residues surrounding the cleavage site (L1603, V1604, V1607 and T1608), in order to clarify if there is an amino acid consensus sequence recognised by ADAMTS13 responsible of giving specificity to the cleavage.



Fig. 4.2 Residues surrounding the cleavage site. The predicted model of A2 domain is shown above and the cleavage site (Y1605-M1606) is highlighted in green. The residues of the cleavage site have been mutated to alanines, individually and in a double mutant. Also the four residues (two at each site of the cleavage site) highlighted in red will be mutated alternatively to alanine or glycine.

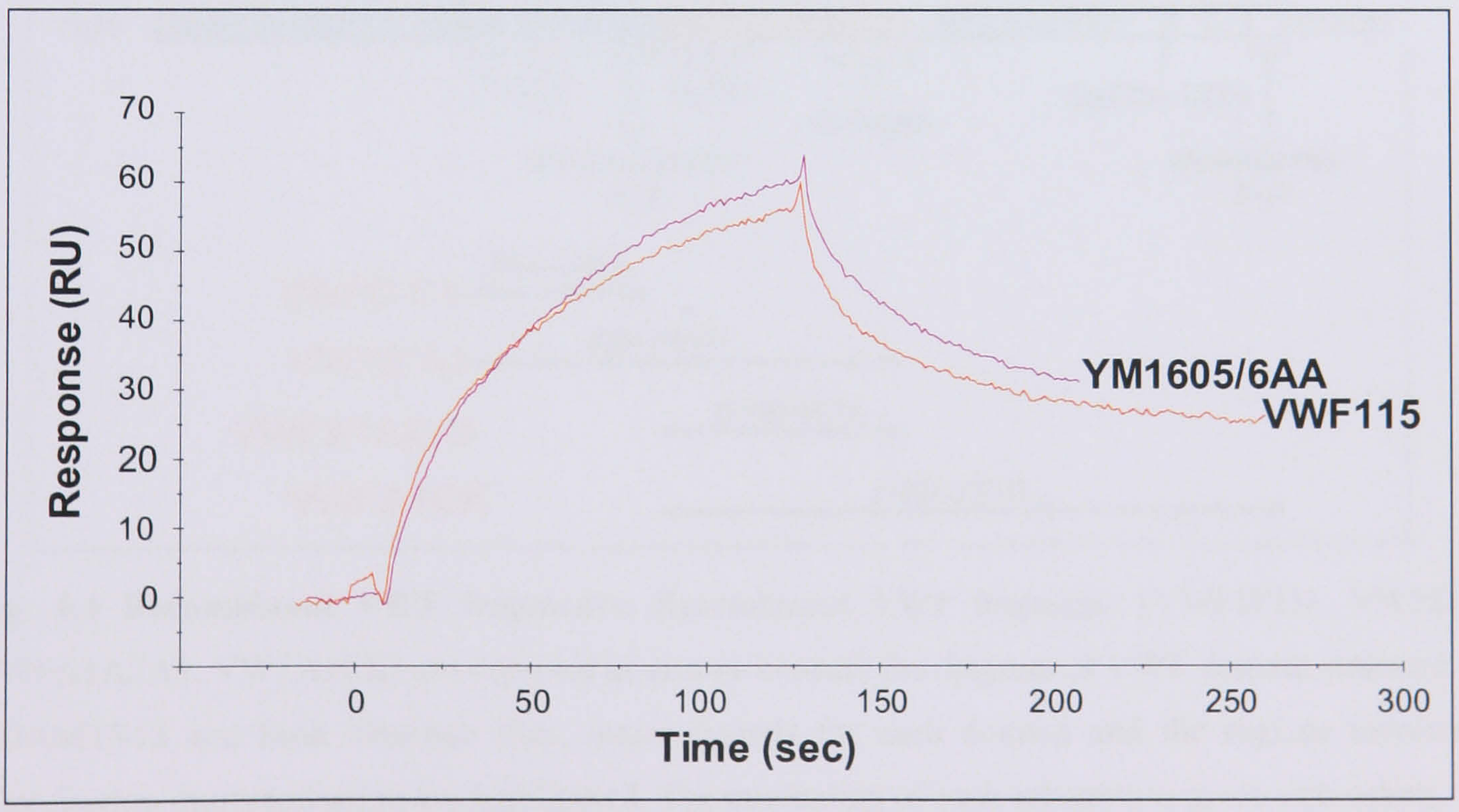


Fig. 4.3 SPR analysis of binding between ADAMTS13 and immobilised wild type VWF115 and YM1605/6AA variant. After surface activation, ~600 RU of wild type VWF115 or YM1605/6AA was immobilised onto a CM5 sensor chip and 20 nM of ADAMTS13 was passed over the two fragments. The two binding responses were overlaid and no major difference could be noticed.

4.1.3 Characterisation of ADAMTS13 binding to VWFD'D3, VWFA1A2A3, VWFD'A3 AND VWFA1CK

The charged residues I have identified to be important for ADAMTS13 binding (see Section 3.5) and the further residues I am planning to mutate (see Section 4.1.1) are all located in the A2 domain. However, VWF is a large and complex molecule and it is likely that other residues elsewhere may play a role in establishing and/or modulating the interaction with ADAMTS13 [107] [258]. Some VWF fragments expressed in mammalian cells (a kind gift from Dr. Peter Lenting, University of Utrecht) are depicted in Fig. 4.4: VWFD'D3 (764-1247), VWFD'A3 (764-1874), VWFA1A2A3 (1260-1874), and VWFA1CK (1260-2813). Their interaction with ADAMTS13 will be studied using the plate-based immunoassay, as described for VWF115 (see Section 3.3.3). A comparison of the K_D values of each fragment should allow the identification of additional ADAMTS13 binding sites on VWF. The effects of urea may also be investigated in each case. Inhibition studies may eventually be taken in consideration to further clarify the role of particular domains.

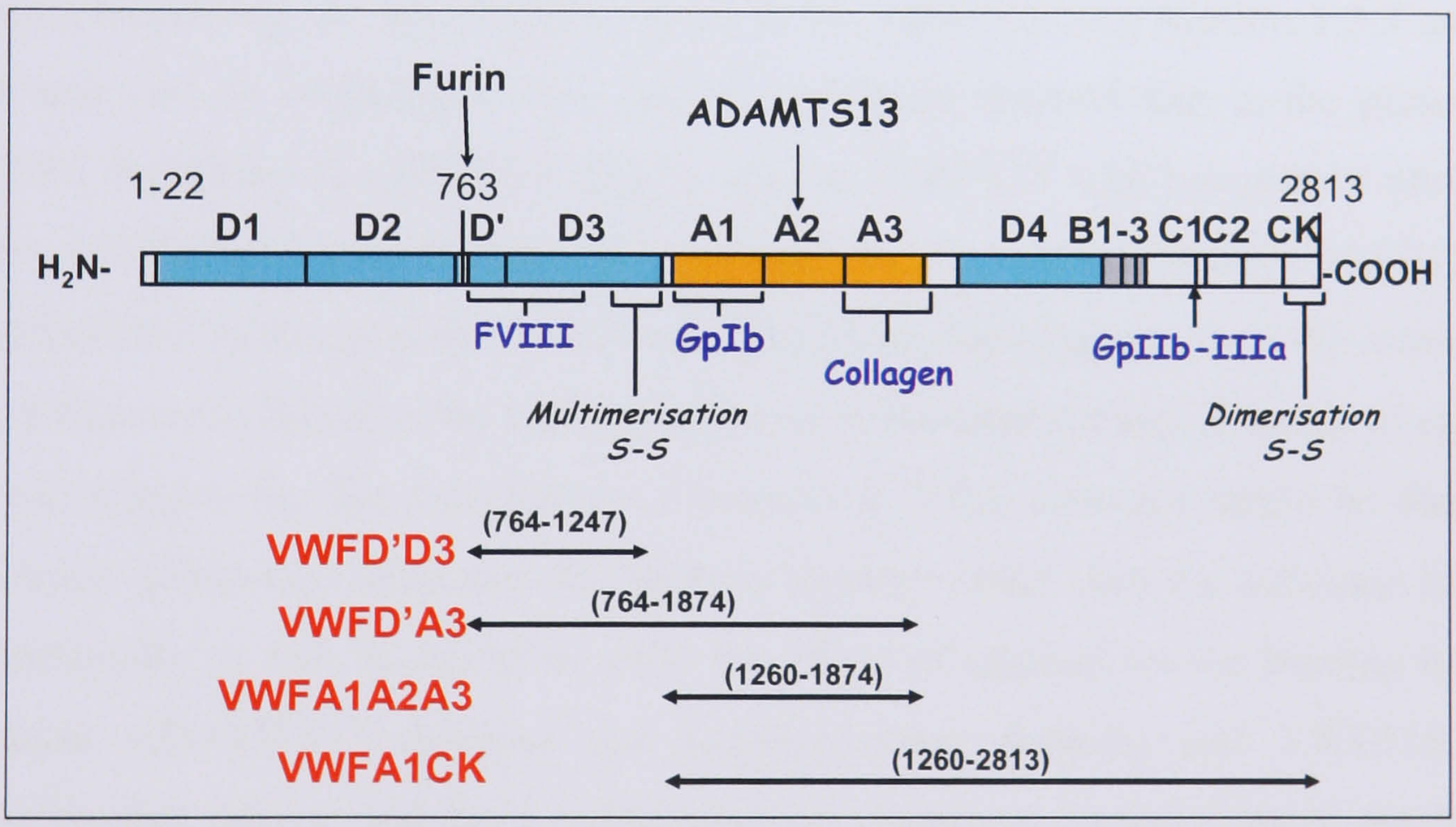


Fig. 4.4 Recombinant VWF fragments. Recombinant VWF fragments (VWFD'D3, VWFD'A3, VWFA1A2A3, VWFA1CK) are depicted as arrows beneath the diagram of VWF domain structure. The ADAMTS13 and furin cleavage sites, major ligands for each domain and the regions involved in dimerisation/multimerisation are highlighted. The numbering of each substrate is given in brackets.

4.2 ROLE OF CALCIUM IONS IN VWF-ADAMTS13 BINDING

The importance of calcium ions in VWF proteolysis by ADAMTS13 has been previously reported [147,196]. The proteolysis of VWF is markedly slowed in the absence of Ca^{2+}. However, if this is due to impairment of the binding or of the cleavage has not been investigated.

All the binding experiments (SPR and plate-based equilibrium binding assay) I have presented in my study were performed in the absence of calcium ions. I have shown (see Sections 3.3.2.2, 3.3.2.3, 3.3.3 and 3.6.7) that both VWF115 and VWFA2 bound to ADAMTS13 with high affinity, suggesting that Ca^{2+} is not an absolute requirement for binding. However, more investigations will be necessary to assess if the presence of Ca^{2+} may in some way modulate the binding. I have recently generated an active site ADAMTS13 mutant (E225A), which has been expressed in HEK293 cells and purified as described for the wild type ADAMTS13 (see Section 3.1). The residue E225 is conserved in all the members of the family of metzincins family. It is a catalytic residue which is important to establish the initial binding to a molecule of water, supporting the nucleophilic attack to the substrate (see Section 1.3.3 and Fig. 1.8 and 1.9). A preliminary time course experiment showed that in the presence of E225A mutation, ADAMTS13 activity against VWF115 was completely abolished. This ADAMTS13 mutant will allow the study of the binding between VWF115 and ADAMTS13 in the presence of calcium, without any interference from the cleavage. If no difference is found in the binding response in the absence and presence of calcium, it will suggest that the importance of calcium in VWF cleavage might be due to an allosteric effect that influences the enzyme activity rather than the substrate binding. Additionally, it will be useful to study the effect of calcium on the binding between isolated ADAMTS13 domains (i.e metalloprotease domain) and VWF115. It is possible that calcium induces a conformational change in the metalloprotease domain, making it able to interact with VWF115. The substrate can thus fit in the enzyme pocket and be readily cleaved.

4.3 INHIBITION OF VWFA2 PROTEOLYSIS BY ITS CLEAVAGE PRODUCTS

In Section 3.6.3, I have shown how VWFA2 was proteolysed extremely slowly in the absence of denaturant. In the presence of 1 M urea, the fragment was cleaved markedly faster. However, the reaction seemed not to reach completion (see Fig. 3.37) and to plateau at a percentage of total cleavage which varied according to the amount of enzyme used. This may be explained by an inhibitory effect by the cleavage products. If one or both the two cleavage products still maintain quite high affinity for the enzyme, they might effectively compete with the intact VWFA2 for the binding to ADAMTS13. The more the cleavage reaction proceeds, the more the inhibition effect may be evident. To investigate this possibility, I will express in *E. coli* the two VWFA2 cleavage products (Fig. 4.5) and study their inhibition upon VWFA2 binding and cleavage by ADAMTS13. I have decided to generate the N-terminal cleavage (VWF NCleav) product with an N-terminal His-tag and the C-terminal cleavage product (VWF CCleav) with a C-terminal His-tag. VWF NCleav has been already generated and its interaction with ADAMTS13 tested using a plate-based binding assay (Fig. 4.6). The fragment still binds to ADAMTS13 with quite high affinity (K_D ~40 nM), supporting the possibility of an inhibition of VWFA2 proteolysis by its cleavage products. Further experiments will be required to investigate this possibility, setting up competition experiments both upon binding and cleavage of VWFA2.

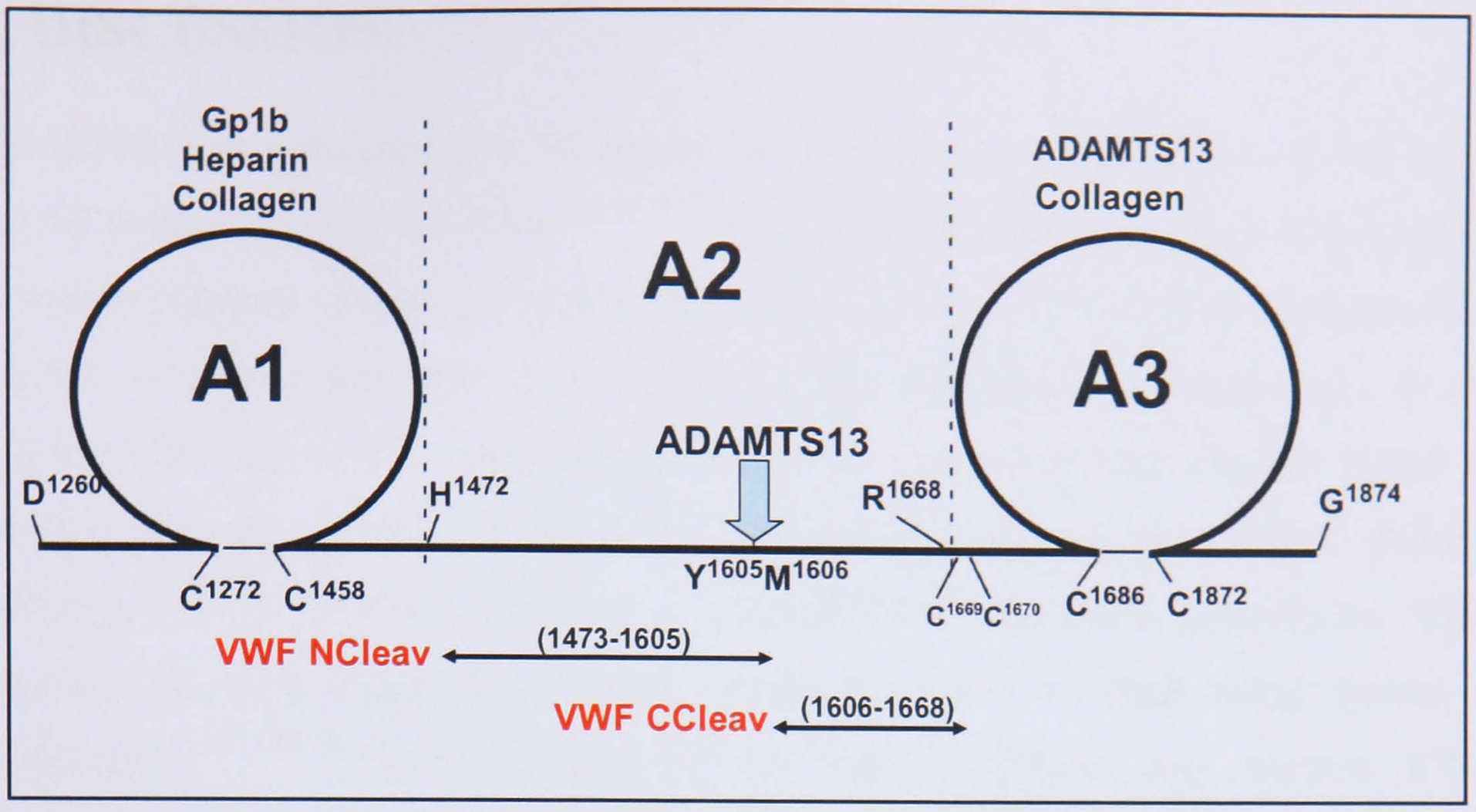


Fig. 4.5 VWF A2 domain cleavage products. VWF A2 N-terminal cleavage product (VWF NCleav) and C-terminal cleavage product (VWF CCleav) are shown as arrows beneath the diagram of the A1A2A3 domains. The ADAMTS13 cleavage site and major ligands of each domain are highlighted above. The numbering of each fragment is given in brackets. VWF NCleav has a N-terminal His-tag, whereas VWF CCleav has a C-terminal His-tag.

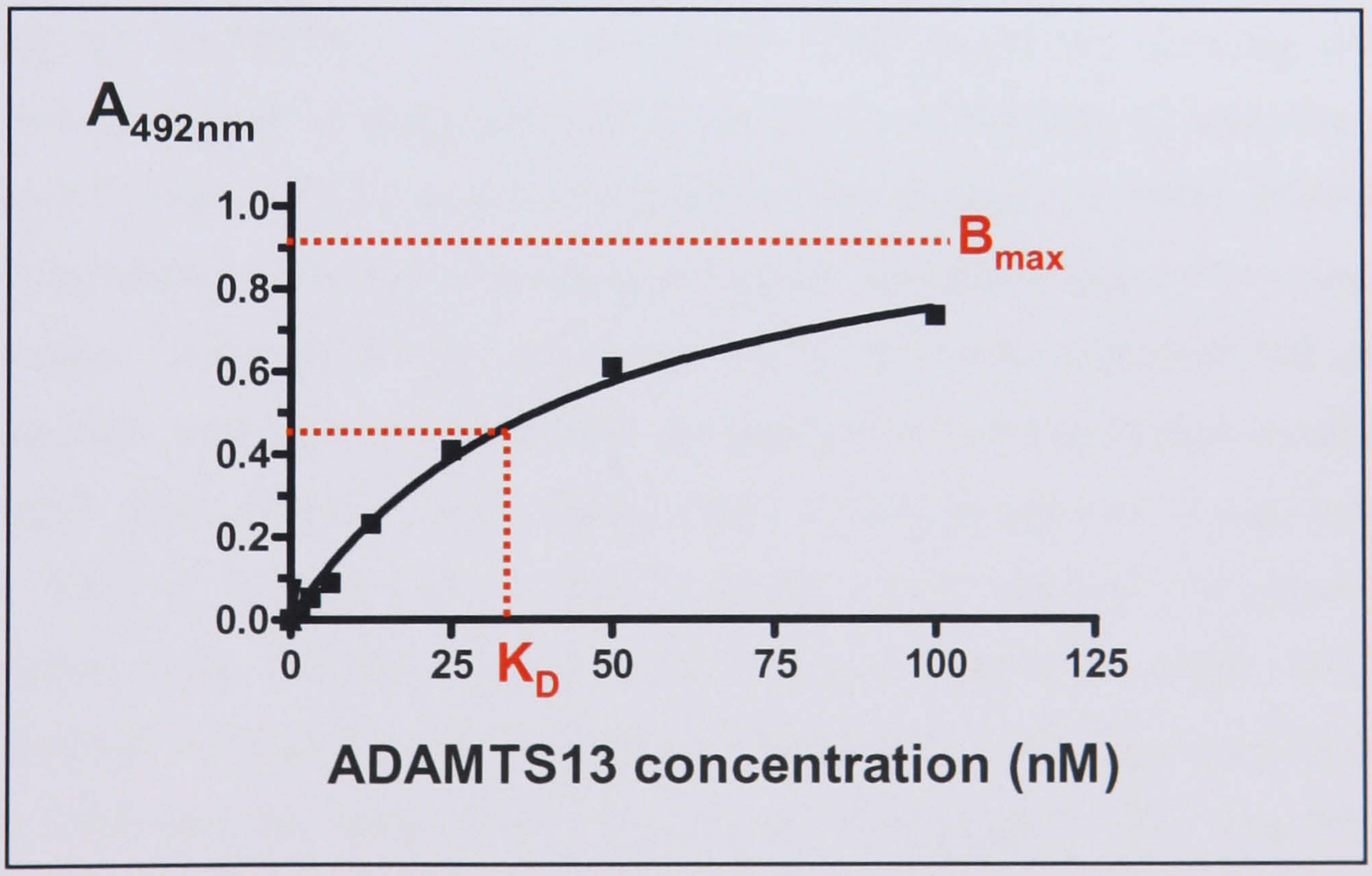


Fig. 4.6 Binding of VWF NCleav to ADAMTS13. 140 nM of VWF NCleav in 50 mM sodium carbonate buffer (pH 9.6) was immobilised into a 96 well microtiter plate. Different ADAMTS13 concentrations (1.56-100 nM) in a buffer containing PBS, Tween (0.1%), 1% BSA and 50 mM EDTA were applied and incubated for three hours. ADAMTS13 bound was detected using biotinylated anti-TSR (2-4) pAb as previously described. The absorbance at 492 nm was plotted against ADAMTS13 concentration and the curve was fitted to the one binding site model, using Graph Pad Prism 4 Software. The experiment gave a K_D value of 40 nM.

5. DISCUSSION

ADAMTS13 is a plasma zinc-dependent metalloprotease which cleaves VWF within the A2 domain (Y1605-M1606) [106,147,196], regulating its multimeric size and its ability to recruit platelets at sites of vessel injury (see Section 1.3). At the beginning of my project, very little was known about the precise mechanism of proteolysis. It was hypothesised that VWF conformation played an important role. Studies based on electron microscopy showed that VWF circulates in plasma as a folded globular molecule [145,146], relatively resistant to ADAMTS13 dependent proteolysis. VWF cleavage *in vitro* required particular conditions, such as high shear forces or denaturants [149,196,327]. It was suggested that these conditions may unravel VWF, exposing the ADAMTS13 cleavage site or its binding site (see Section 1.3.5.1). Furthermore, it was known that calcium ions were required for an efficient VWF proteolysis [147,196]. However, no information was available about how VWF and ADAMTS13 interact with each other.

In order to elucidate which elements in VWF are important for its recognition and cleavage by ADAMTS13, I expressed certain VWF fragments, spanning different region of the A2 and A3 domain (VWF76, VWF115 and VWF115-A3) (see Fig. 3.6 in Section 3.2.1) in *E. coli*. The use of these short VWF fragments to study ADAMTS13 proteolysis offers numerous advantages, compared with full-length VWF or an entire A2 domain. Firstly, short VWF fragments can be efficiently expressed and purified from bacteria, leading to the generation of large amounts of highly pure proteins in a reasonably short period of time, using simple culture procedures. In contrast, full-length VWF is a large and complex molecule which needs to be expressed in mammalian cells. Secondly, the cleavage of these fragments can be studied in physiological conditions in the absence of denaturants, contrasting again from full-length VWF and the intact VWF A2 domain. This suggests they may be in an unfolded conformation in which the cleavage site is constitutively exposed. Finally, the cleavage of small VWF fragments can be accurately quantified by HPLC analysis, where the release of a short cleavage product can be readily monitored. However, use of the short substrates generated in bacteria does have limitations. First of all, the kinetic constants I obtained from the proteolysis of VWF115 should be carefully evaluated as this cannot necessarily be extrapolated to the full-length VWF, since

VWF115 may lack some domains important in modulating VWF proteolysis. Furthermore, the expression in bacteria does not include post-translational modifications of proteins, such as glycosylation. It is known that ABO groups influence VWF plasma levels [90,91]. Furthermore it has been recently shown that they also influence VWF proteolysis by ADAMTS13 [92,93]. The influence of glycosylation upon cleavage and binding to ADAMTS13 can not be studied using the VWF fragments I have generated in bacteria.

HPLC analysis was found to be a reliable method to obtain kinetic constants of the cleavage of short VWF fragments by ADAMTS13. VWF115 proteolysis was fully characterised from the kinetic point of view and I derived values for k_{cat}/K_m (7.83 x 10^4 M^{-1} s^{-1}), k_{cat} (0.14 s^{-1}) and K_m (1.61 μM) (see Sections 3.2.4.2 and 3.2.4.3). The catalytic efficiency value suggests that ADAMTS13 is not a very efficient enzyme. For example, the catalytic efficiency for the activation of FV by thrombin is 3.26 x 10^6 M^{-1} s^{-1} [336]. The low catalytic efficiency of ADAMTS13 may not be important, as only a few cleavages in full-length VWF are sufficient to drastically reduce its haemostatic potential. Alternatively, it remains possible that other plasma cofactors can markedly improve the efficiency of proteolysis, as it has been reported for different enzymes involved in haemostasis [58,337]. If so, these plasma cofactors remain to be identified.

The k_{cat}/K_m value calculated for VWF115 proteolysis appeared to be comparable to that recently reported for the full-length VWF, in the presence of denaturants and under conditions of low ionic strength (3.4 x 10^4 M^{-1} s^{-1}) [262]. However, in this study the catalytic efficiency was estimated indirectly using a CBA assay, without the advantage of accurately quantifying the rate of cleavage monitoring a released peptide. In contrast, the findings differ in another recent study, where the k_{cat}/K_m for the cleavage of full-length VWF was calculated to be 92 x 10^4 M^{-1} s^{-1} [1234], more than 10 fold higher than the value I calculated for VWF115. The latter experiments were performed in denaturing conditions, monitoring the appearance of the 350 kDa VWF product band by densitometry. In the same study, K_m and k_{cat} for the cleavage of full-length VWF were estimated to be 15 nM and 0.0138 s^{-1}, respectively. The 100 fold difference between the K_m of VWF115 and that of full-length VWF suggests that VWF115 probably lacks exosites that in the full-length VWF may be required for substrate recognition or, alternatively, the tertiary structure required for an efficient cleavage. The 10 fold decrease in the k_{cat} for the full-length VWF in respect to that of VWF115 may be explained by the different size and structure of the two molecules. It

is possible that, in saturation conditions, the enzyme cleaves a smaller molecule, such as VWF115, faster than a complex molecule, such as full-length VWF, in which more steric hindrance is probably present. Furthermore, the dissociation of the cleavage products from the enzyme may be slower for the cleavage of full-length VWF than for that of VWF115. Alternatively, the discrepancy in k_{cat} between VWF115 and full-length VWF may be explained by differences in the cleavage conditions or in the sensitivity of the detection methods. In that same study, the catalytic constants for the cleavage of FRETS-VWF73 were derived using a fluorimetric assay. The results were 3.2 μM for the K_m and 0.97 s^{-1} for the k_{cat}. The K_m appeared to be in agreement with the one we calculated for VWF115. The discrepancy in the k_{cat} between VWF73 and VWF115 could once again be explained by the different sizes of the two fragments or, alternatively, by differences arising from the employed assays.

Since VWF115 was readily cleaved by ADAMTS13, I decided to study the interaction between the two molecules by both SPR analysis and plate-based immunoassay. Both approaches demonstrated that ADAMTS13 binds to VWF115 with high affinity. The equilibrium dissociation constant K_D was calculated to be ~20.0 nM, using SPR (see Section 3.3.2.2), and 16.2 nM and 8.0 nM using the plate-based immunoassay, in the absence and presence of EDTA, respectively (see Section 3.3.3). These results suggested that critical VWF residues involved in ADAMTS13 interaction are located within VWF115 (1554-1668). I found that the binding to ADAMTS13 of four VWF115 variants (D1587A, D1614, E1615A and K1617A) was markedly reduced (see Section 3.5.5), suggesting that residues D1587, D1614, E1615 and K1617 may be part of a charged ADAMTS13 docking site on the surface of the A2 domain (see Fig. 3.27 in Section 3.5.2). The cleavage of the above variants by ADAMTS13 was also significantly affected (see Section 3.5.4), suggesting that a reduction in the binding indeed impaired proteolysis. However, different findings suggest that high affinity binding is necessary but may be not sufficient to obtain an efficient cleavage. The discrepancy between K_m and K_D values I observed for VWF115 (1.61 μM and 8-20 nM, respectively) suggests that the tight interaction between VWF115 and ADAMTS13 does not necessarily produce efficient cleavage. Other VWF regions may be important for its recognition and cleavage by ADAMTS13 (see below). A binding site in the A3 domain (K_D 58.7 nM) has been reported, using both SPR and a flow chamber system [107]. However, my results, in agreement with those by Nishio *et al* [186], showed that the addition of A3 domain to the A2 domain fragments did not affect the

cleavage. It is therefore likely that, even if there is a binding site in the VWFA3 domain it is not functional in terms of cleavage (see below). My study of binding and cleavage of the intact VWF A2 domain corroborates the contention that binding and cleavage need not be directly related. VWFA2 immobilised on a microtiter plate bound to ADAMTS13 with high affinity (K_D ~10.9 nM and 3.1 nM, in the absence and presence of EDTA, respectively) (see Section 3.6.7). Furthermore, soluble VWFA2 in the absence or presence of 1 M urea could compete equally with immobilised VWFA2 for ADAMTS13 binding (see Section 3.6.8). These results suggest that the ADAMTS13 docking site is exposed even when the A2 domain is in a folded globular conformation. However, VWFA2 cannot be effectively cleaved by ADAMTS13 in the absence of denaturants, as shown in Section 3.6.3 and in accordance with previous studies [186,332]. This suggests that, although soluble VWFA2 can interact with ADAMTS13 with high affinity, it cannot be effectively cleaved, possibly because of the inaccessibility of the cleavage site. The 81 amino acids in the amino-terminus of the intact A2 domain (which are not present in VWF115) may be responsible for masking the scissile bond. Furthermore, the high affinity binding between VWF115/VWFA2 and ADAMTS13 was found in the absence of calcium, suggesting that Ca^{2+} is not an absolute requirement for binding. However, it is necessary for effective cleavage [147,196]. It is possible that calcium may cause an allosteric effect that influences the enzyme activity (see below). This again demonstrates that high affinity binding does not necessarily lead to efficient proteolysis.

In addition to D1587, D1614, E1617 and K1617, other residues in the A2 domain may be part of the ADAMTS13 binding site. I have identified an additional 23 charged residues on the surface of the A2 domain which could also be involved in binding to ADAMTS13 (see Section 4.1.1). They are all located in the N-terminal part of VWF A2 domain (residues 1473-1605), some in the region present both in VWF115 and VWFA2 (residues 1554-1605) and the remainder in the region present only in VWFA2 and not in VWF115 (residues 1473-1553). Looking at the predicted model of A2 domain (see Fig. 4.1 A and B, in Section 4.1.1), some of these residues appeared to be located close to D1587, D1614, E1615 and K1617. They may thus be part of the same ADAMTS13 docking site. However, most of the new identified residues are on the opposite site on the A2 model and they may form another ADAMTS13 exosite. Whether there are two distinct exosites is uncertain, as there is no means of predicting

how VWF conformation may be affected by its unravelling from globular to unfolded forms. In a recent study, it has been found that a deletion of the last nine C-terminal residues from VWF73 resulted in a fragment that was resistant to cleavage [332], suggesting that residues from E1660 to R1668 are essential for proteolysis. It is possible that these residues may also contribute to ADAMTS13 interaction.

The limits of the approach I used to select the residues to be mutated should be taken in consideration. In the absence of a crystal structure of the A2 domain, the use of a model is useful to predict the location of residues. However, it is possible that some residues identified as being on the surface of the A2 domain may not actually be exposed and, on the other hand, some residues hidden in the model may indeed be on the surface. Only a crystal structure of the A2 domain will definitely clarify the exact location of all the residues. The difficulty in crystallising the A2 domain is probably due to an unstable conformation that naturally unravells. This may be explained by the absence of a disulphide bridge which stabilise the corresponding loops within the A1 and A3 domains. The two residues that in the A2 domain correspond to the cysteines involved in the formation of the disulphide bond in the A3 domain have been mutated to cysteines by my colleague Dr. James Crawley and a VWFA2 domain with a disulphide bond has been generated. This mutated A2 molecule may assist crystallisation attempts.

Based on the above considerations, I conclude that I have identified a high affinity binding site in the VWFA2 domain, which seems to be the major docking site for ADAMTS13. Other residues located in other domains of VWF may also be involved in the binding between VWF and ADAMTS13, stabilising and modulating this interaction.

As mentioned above, a lower affinity binding site has been reported in the A3 domain [107] and it may have a role in the initial contact between VWF and ADAMTS13 (see below). Furthermore, it was reported that the presence of A1 domain markedly decreased the rate of substrate cleavage [333], suggesting that it may shield the ADAMTS13 cleavage site and/or binding site on the adjacent A2 domain. In order to investigate the role of VWF regions other than the A2 domain, I am currently studying the binding to ADAMTS13 of larger VWF fragments [(VWFD'D3 (764-1247), VWFD'A3 (764-1874), VWFA1A2A3 (1260-1874), and VWFA1CK (1260-2813)] (see Section 4.1.3).

From what is discussed above, the VWF interaction with ADAMTS13 and substrate proteolysis appear to be complex. I have reported a high affinity binding site in the A2 domain. Additional domains in VWF seem to play an important role in the modulation of binding. This complexity extents to the metalloprotease. A number of distinct sites in ADAMTS13 appear to be involved. Binding studies using truncated forms of ADAMTS13 have demonstrated that several domains contribute to the interaction with VWF [238,258]. The Cys-rich and spacer domains appear to have a crucial role in binding VWF, although other domains, i.e. TSRs and CUB domains, may also be involved (see Section 1.3.4). It seems likely that the two molecules interact with multiple contact sites. I will now attempt to integrate the results derived from my work and other studies, by proposing a model of VWF proteolysis by ADAMTS13.

VWF is normally present in plasma in a globular and condensed conformation [145,146], which cannot interact with platelets or collagen. This conformation appears to be resistant to ADAMTS13 dependent proteolysis [149,196,327], probably because the cleavage site is hidden in the core of the molecule. It is possible that also a mayor ADAMTS13 binding site is not exposed. This is supported by the finding that soluble VWF cannot compete for the binding of plate-coated VWF with ADAMTS13 [258] (plate-coated VWF is almost certainly in an unfolded conformation). Circulating globular VWF may not bind to ADAMTS13 or, alternatively, the two molecules may interact to form a low-affinity complex. Preliminary results obtained by my colleague Tom McKinnon support the latter hypothesis. A binding site on the A3 domain may be constitutively exposed on circulating VWF and weakly interact with ADAMTS13, without inducing proteolysis. The complementary binding site in ADAMTS13 may be the CUB domains or one of other C-terminal domains, such as TSRs (Fig. 5.1 A). In the presence of high shear stress, VWF is induced to unravel, exposing both a high affinity ADAMTS13 docking site and the cleavage site. The unfolding is probably a progressive process in which VWF binding sites and cleavage site are slowly revealed, and each interaction may in turn contribute to the exposure of additional interacting domains. Two studies have suggested that the contribution of the CUB-domain may be important in flowing conditions [259,260], as a mechanism of initial tethering to VWF (possibly interacting with the A3 domain) (Fig. 5.1 B). This initial low-affinity interaction may further favour the unfolding of VWF molecule under high shear and lead to the exposure of a second binding site present in the A2 domain, which interacts

with high affinity with its complementary region of ADAMTS13. A likely candidate for the latter is the spacer domain [238,258] (Fig. 5.1 B). I have shown that although the intact folded VWFA2 domain can bind to ADAMTS13 with high affinity, it is resistant to proteolysis in the absence of denaturants (see Section 3.6). This suggests that complex interactions and the rheological forces may act in synergy to lead finally to the exposure of the cleavage site. Furthermore, the presence of calcium ions is required to induce substrate proteolysis. It is likely that binding of Ca^{2+} induces a conformational change in the protease domain, leading to enzyme activation (Fig. 5.1 C). ADAMTS13 is then able to cleave VWF within the A2 domain (Y1605-M1606). It finally dissociates from the two VWF cleavage products (Fig. 5.1 D).

This proposed mechanism of ADAMTS13-VWF interaction is a tentative model, based on the available literature and my own results reported in this thesis. Undoubtedly, our understanding of the ADAMTS13-VWF interaction is in its infancy and in the near future additional studies, perhaps involving crystallisation, are likely to lead to a more refined model.

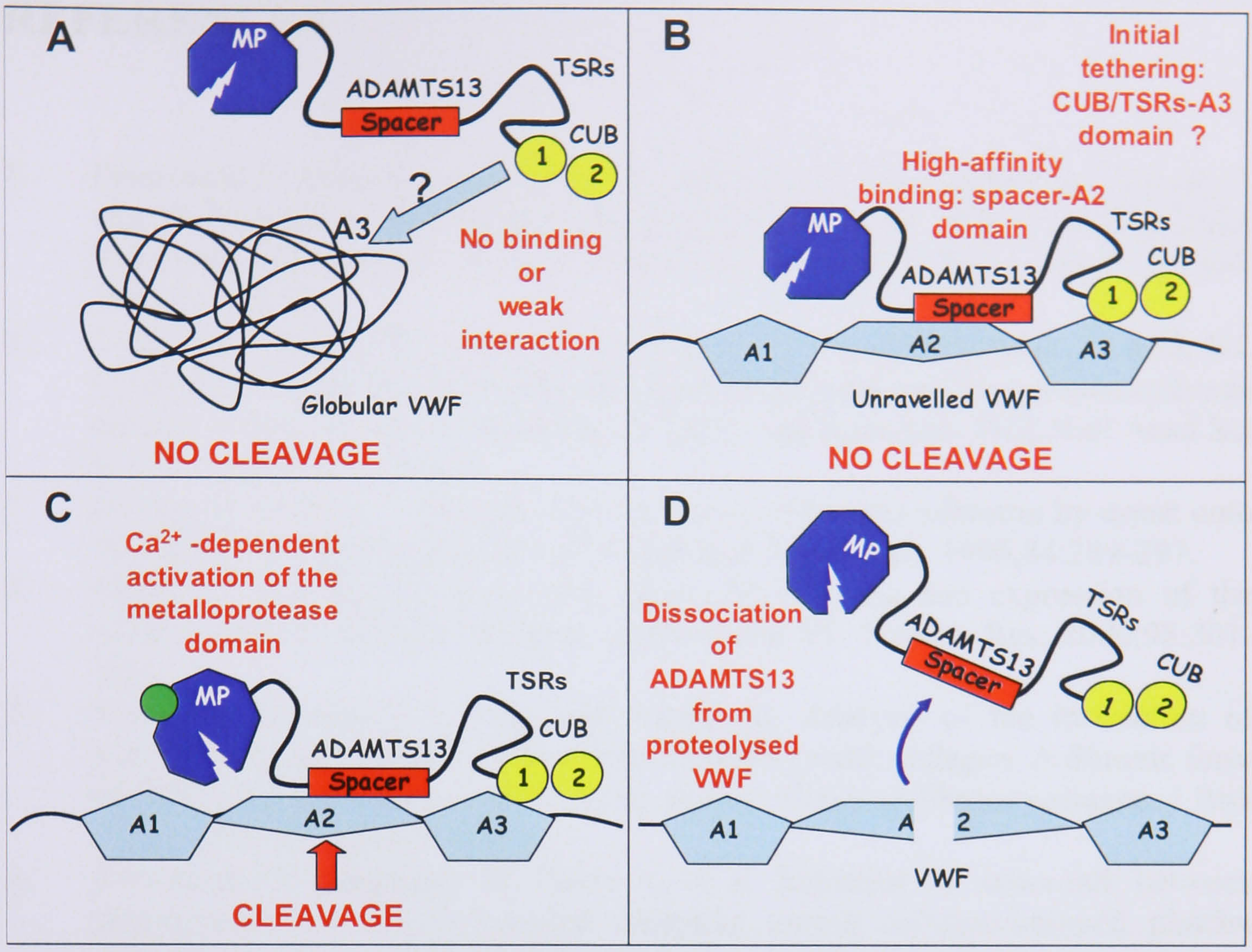


Fig. 5.1 A proposed mechanism for VWF binding to and proteolysis by ADAMTS13. A) VWF circulates in plasma in a globular conformation, which cannot be cleaved by ADAMTS13, as its A2 domain cleavage site is hidden. In this conformation, VWF does not interact with ADAMTS13 with high affinity. The CUB domains or TSRs may constitutively bind to VWF with low affinity (possibly to the A3 domain), without inducing any proteolysis. **B)** In the presence of high shear stress, VWF gradually unfolds. The CUB domains/TSRs interacting with VWF A3 domain (or other exposed VWF regions) may represent an initial tethering mechanism between the two molecules. This initial contact may then favour the establishing of a high-affinity interaction, possibly between the VWF A2 domain and ADAMTS13 spacer domain. These multiple interactions and shear stress together completely unfold VWF and expose the scissile bond. **C)** In order to have an efficient proteolysis, calcium ions (depicted as a green sphere) are required. They probably bind to the protease domain, inducing a conformational change, which in turn activates ADAMTS13. D) VWF is finally cleaved within the A2 domain. The two cleavage products have a lower affinity for ADAMTS13 and are then released.

REFERENCES

1. Fressinaud E, Baruch D, Girma JP, Sakariassen KS, Baumgartner HR, Meyer D. von Willebrand factor-mediated platelet adhesion to collagen involves platelet membrane glycoprotein IIb-IIIa as well as glycoprotein Ib. J Lab Clin Med. 1988;112:58-67.
2. Lopez JA, Chung DW, Fujikawa K, Hagen FS, Papayannopoulou T, Roth GJ. Cloning of the alpha chain of human platelet glycoprotein Ib: a transmembrane protein with homology to leucine-rich alpha 2-glycoprotein. Proc Natl Acad Sci U S A. 1987;84:5615-5619.
3. Savage B, Saldivar E, Ruggeri ZM. Initiation of platelet adhesion by arrest onto fibrinogen or translocation on von Willebrand factor. Cell. 1996;84:289-297.
4. Miura Y, Ohnuma M, Jung SM, Moroi M. Cloning and expression of the platelet-specific collagen receptor glycoprotein VI. Thromb Res. 2000;98:301-309.
5. Miura Y, Takahashi T, Jung SM, Moroi M. Analysis of the interaction of platelet collagen receptor glycoprotein VI (GPVI) with collagen. A dimeric form of GPVI, but not the monomeric form, shows affinity to fibrous collagen. J Biol Chem. 2002;277:46197-46204.
6. Nieswandt B, Bergmeier W, Eckly A, et al. Evidence for cross-talk between glycoprotein VI and Gi-coupled receptors during collagen-induced platelet aggregation. Blood. 2001;97:3829-3835.
7. Knight CG, Morton LF, Onley DJ, et al. Identification in collagen type I of an integrin alpha2 beta1-binding site containing an essential GER sequence. J Biol Chem. 1998;273:33287-33294.
8. Verkleij MW, MJ IJ, Heijnen-Snyder GJ, et al. Adhesive domains in the collagen III fragment alpha1(III)CB4 that support alpha2beta1- and von Willebrand factor-mediated platelet adhesion under flow conditions. Thromb Haemost. 1999;82:1137-1144.
9. Offermanns S, Toombs CF, Hu YH, Simon MI. Defective platelet activation in G alpha(q)-deficient mice. Nature. 1997;389:183-186.
10. Wu Y, Suzuki-Inoue K, Satoh K, et al. Role of Fc receptor gamma-chain in platelet glycoprotein Ib-mediated signaling. Blood. 2001;97:3836-3845.
11. Inoue O, Suzuki-Inoue K, Dean WL, Frampton J, Watson SP. Integrin alpha2beta1 mediates outside-in regulation of platelet spreading on collagen through activation of Src kinases and PLCgamma2. J Cell Biol. 2003;160:769-780.
12. Marshall SJ, Senis YA, Auger JM, et al. GPIb-dependent platelet activation is dependent on Src kinases but not MAP kinase or cGMP-dependent kinase. Blood. 2004;103:2601-2609.
13. Arthur JF, Gardiner EE, Matzaris M, et al. Glycoprotein VI is associated with GPIb-IX-V on the membrane of resting and activated platelets. Thromb Haemost. 2005;93:716-723.
14. Vu TK, Wheaton VI, Hung DT, Charo I, Coughlin SR. Domains specifying thrombin-receptor interaction. Nature. 1991;353:674-677.
15. Vu TK, Hung DT, Wheaton VI, Coughlin SR. Molecular cloning of a functional thrombin receptor reveals a novel proteolytic mechanism of receptor activation. Cell. 1991;64:1057-1068.

16. Chen YH, Pouyssegur J, Courtneidge SA, Van Obberghen-Schilling E. Activation of Src family kinase activity by the G protein-coupled thrombin receptor in growth-responsive fibroblasts. J Biol Chem. 1994;269:27372-27377.
17. Jin J, Kunapuli SP. Coactivation of two different G protein-coupled receptors is essential for ADP-induced platelet aggregation. Proc Natl Acad Sci U S A. 1998;95:8070-8074.
18. Dangelmaier C, Jin J, Smith JB, Kunapuli SP. Potentiation of thromboxane A2-induced platelet secretion by Gi signaling through the phosphoinositide-3 kinase pathway. Thromb Haemost. 2001;85:341-348.
19. Bevers EM, Tilly RH, Senden JM, Comfurius P, Zwaal RF. Exposure of endogenous phosphatidylserine at the outer surface of stimulated platelets is reversed by restoration of aminophospholipid translocase activity. Biochemistry. 1989;28:2382-2387.
20. Sune A, Bette-Bobillo P, Bienvenue A, Fellmann P, Devaux PF. Selective outside-inside translocation of aminophospholipids in human platelets. Biochemistry. 1987;26:2972-2978.
21. Zwaal RF, Schroit AJ. Pathophysiologic implications of membrane phospholipid asymmetry in blood cells. Blood. 1997;89:1121-1132.
22. Diaz C, Schroit AJ. Role of translocases in the generation of phosphatidylserine asymmetry. J Membr Biol. 1996;151:1-9.
23. Dorsam RT, Kim S, Murugappan S, et al. Differential requirements for calcium and Src family kinases in platelet GPIIb/IIIa activation and thromboxane generation downstream of different G-protein pathways. Blood. 2005;105:2749-2756.
24. Ni H, Denis CV, Subbarao S, et al. Persistence of platelet thrombus formation in arterioles of mice lacking both von Willebrand factor and fibrinogen. J Clin Invest. 2000;106:385-392.
25. Ni H, Yuen PS, Papalia JM, et al. Plasma fibronectin promotes thrombus growth and stability in injured arterioles. Proc Natl Acad Sci U S A. 2003;100:2415-2419.
26. Dixit VM, Haverstick DM, O'Rourke KM, et al. A monoclonal antibody against human thrombospondin inhibits platelet aggregation. Proc Natl Acad Sci U S A. 1985;82:3472-3476.
27. Chung J, Gao AG, Frazier WA. Thrombspondin acts via integrin-associated protein to activate the platelet integrin alphaIIbbeta3. J Biol Chem. 1997;272:14740-14746.
28. Chung J, Wang XQ, Lindberg FP, Frazier WA. Thrombospondin-1 acts via IAP/CD47 to synergize with collagen in alpha2beta1-mediated platelet activation. Blood. 1999;94:642-648.
29. Trumel C, Plantavid M, Levy-Toledano S, et al. Platelet aggregation induced by the C-terminal peptide of thrombospondin-1 requires the docking protein LAT but is largely independent of alphaIIb/beta3. J Thromb Haemost. 2003;1:320-329.
30. Bonnefoy A, Daenens K, Feys HB, et al. Thrombospondin-1 controls vascular platelet recruitment and thrombus adherence in mice by protecting (sub)endothelial VWF from cleavage by ADAMTS13. Blood. 2006;107:955-964.
31. Asch E, Podack E. Vitronectin binds to activated human platelets and plays a role in platelet aggregation. J Clin Invest. 1990;85:1372-1378.
32. Plow EF. Vitronectin: back into the spotlight. J Thromb Haemost. 2005;3:873-874.

33. Reheman A, Gross P, Yang H, et al. Vitronectin stabilizes thrombi and vessel occlusion but plays a dual role in platelet aggregation. J Thromb Haemost. 2005;3:875-883.
34. Fay WP, Parker AC, Ansari MN, Zheng X, Ginsburg D. Vitronectin inhibits the thrombotic response to arterial injury in mice. Blood. 1999;93:1825-1830.
35. Daniel JL, Dangelmaier C, Jin J, Ashby B, Smith JB, Kunapuli SP. Molecular basis for ADP-induced platelet activation. I. Evidence for three distinct ADP receptors on human platelets. J Biol Chem. 1998;273:2024-2029.
36. Hollopeter G, Jantzen HM, Vincent D, et al. Identification of the platelet ADP receptor targeted by antithrombotic drugs. Nature. 2001;409:202-207.
37. Leon C, Ravanat C, Freund M, Cazenave JP, Gachet C. Differential involvement of the P2Y1 and P2Y12 receptors in platelet procoagulant activity. Arterioscler Thromb Vasc Biol. 2003;23:1941-1947.
38. Raychowdhury MK, Yukawa M, Collins LJ, McGrail SH, Kent KC, Ware JA. Alternative splicing produces a divergent cytoplasmic tail in the human endothelial thromboxane A2 receptor. J Biol Chem. 1994;269:19256-19261.
39. Offermanns S, Laugwitz KL, Spicher K, Schultz G. G proteins of the G12 family are activated via thromboxane A2 and thrombin receptors in human platelets. Proc Natl Acad Sci U S A. 1994;91:504-508.
40. Paul BZ, Jin J, Kunapuli SP. Molecular mechanism of thromboxane A(2)-induced platelet aggregation. Essential role for p2t(ac) and alpha(2a) receptors. J Biol Chem. 1999;274:29108-29114.
41. Ohkubo S, Nakahata N, Ohizumi Y. Thromboxane A2-mediated shape change: independent of Gq-phospholipase C--Ca2+ pathway in rabbit platelets. Br J Pharmacol. 1996;117:1095-1104.
42. Dorsam RT, Kim S, Jin J, Kunapuli SP. Coordinated signaling through both G12/13 and G(i) pathways is sufficient to activate GPIIb/IIIa in human platelets. J Biol Chem. 2002;277:47588-47595.
43. Cleator JH, Zhu WQ, Vaughan DE, Hamm HE. Differential regulation of endothelial exocytosis of P-selectin and von Willebrand factor by protease-activated receptors and cAMP. Blood. 2006;107:2736-2744.
44. Andrieux A, Hudry-Clergeon G, Ryckewaert JJ, et al. Amino acid sequences in fibrinogen mediating its interaction with its platelet receptor, GPIIbIIIa. J Biol Chem. 1989;264:9258-9265.
45. Bodary SC, Napier MA, McLean JW. Expression of recombinant platelet glycoprotein IIbIIIa results in a functional fibrinogen-binding complex. J Biol Chem. 1989;264:18859-18862.
46. Moake JL, Turner NA, Stathopoulos NA, Nolasco LH, Hellums JD. Involvement of large plasma von Willebrand factor (vWF) multimers and unusually large vWF forms derived from endothelial cells in shear stress-induced platelet aggregation. J Clin Invest. 1986;78:1456-1461.
47. Goto S, Ikeda Y, Saldivar E, Ruggeri ZM. Distinct mechanisms of platelet aggregation as a consequence of different shearing flow conditions. J Clin Invest. 1998;101:479-486.
48. Romo GM, Dong JF, Schade AJ, et al. The glycoprotein Ib-IX-V complex is a platelet counterreceptor for P-selectin. J Exp Med. 1999;190:803-814.
49. Nemerson Y. Tissue factor and hemostasis. Blood. 1988;71:1-8.
50. Weiss HJ, Turitto VT, Baumgartner HR, Nemerson Y, Hoffmann T. Evidence for the presence of tissue factor activity on subendothelium. Blood. 1989;73:968-975.
51. Zwaal RF, Comfurius P, Bevers EM. Lipid-protein interactions in blood coagulation. Biochim Biophys Acta. 1998;1376:433-453.

52. Brummel KE, Paradis SG, Butenas S, Mann KG. Thrombin functions during tissue factor-induced blood coagulation. Blood. 2002;100:148-152.
53. Miletich JP, Jackson CM, Majerus PW. Properties of the factor Xa binding site on human platelets. J Biol Chem. 1978;253:6908-6916.
54. Lorand L. Factor XIII: structure, activation, and interactions with fibrinogen and fibrin. Ann N Y Acad Sci. 2001;936:291-311.
55. Broze GJ, Jr., Warren LA, Novotny WF, Higuchi DA, Girard JJ, Miletich JP. The lipoprotein-associated coagulation inhibitor that inhibits the factor VII-tissue factor complex also inhibits factor Xa: insight into its possible mechanism of action. Blood. 1988;71:335-343.
56. Rosenberg RD, Rosenberg JS. Natural anticoagulant mechanisms. J Clin Invest. 1984;74:1-6.
57. Esmon CT, Owen WG. Identification of an endothelial cell cofactor for thrombin-catalyzed activation of protein C. Proc Natl Acad Sci U S A. 1981;78:2249-2252.
58. Esmon CT. Molecular events that control the protein C anticoagulant pathway. Thromb Haemost. 1993;70:29-35.
59. Walker FJ. Regulation of activated protein C by protein S. The role of phospholipid in factor Va inactivation. J Biol Chem. 1981;256:11128-11131.
60. Vlot AJ, Koppelman SJ, van den Berg MH, Bouma BN, Sixma JJ. The affinity and stoichiometry of binding of human factor VIII to von Willebrand factor. Blood. 1995;85:3150-3157.
61. Nogami K, Shima M, Nishiya K, et al. A novel mechanism of factor VIII protection by von Willebrand factor from activated protein C-catalyzed inactivation. Blood. 2002;99:3993-3998.
62. Saenko EL, Yakhyaev AV, Mikhailenko I, Strickland DK, Sarafanov AG. Role of the low density lipoprotein-related protein receptor in mediation of factor VIII catabolism. J Biol Chem. 1999;274:37685-37692.
63. Mancuso DJ, Tuley EA, Westfield LA, et al. Structure of the gene for human von Willebrand factor. J Biol Chem. 1989;264:19514-19527.
64. Bonthron D, Orkin SH. The human von Willebrand factor gene. Structure of the 5' region. Eur J Biochem. 1988;171:51-57.
65. Patracchini P, Calzolari E, Aiello V, et al. Sublocalization of von Willebrand factor pseudogene to 22q11.22-q11.23 by in situ hybridization in a 46,X,t(X;22)(pter;q11.21) translocation. Hum Genet. 1989;83:264-266.
66. Marchetti G, Patracchini P, Volinia S, et al. Characterization of the pseudogenic and genic homologous regions of von Willebrand factor. Br J Haematol. 1991;78:71-79.
67. Friedman AD. Transcriptional regulation of granulocyte and monocyte development. Oncogene. 2002;21:3377-3390.
68. Cantor AB, Orkin SH. Transcriptional regulation of erythropoiesis: an affair involving multiple partners. Oncogene. 2002;21:3368-3376.
69. Raich N, Romeo PH. Erythroid regulatory elements. Stem Cells. 1993;11:95-104.
70. Cowan PJ, Tsang D, Pedic CM, et al. The human ICAM-2 promoter is endothelial cell-specific in vitro and in vivo and contains critical Sp1 and GATA binding sites. J Biol Chem. 1998;273:11737-11744.
71. Zhang R, Min W, Sessa WC. Functional analysis of the human endothelial nitric oxide synthase promoter. Sp1 and GATA factors are necessary for basal transcription in endothelial cells. J Biol Chem. 1995;270:15320-15326.

72. Mollica LR, Crawley JT, Liu K, et al. Role of a 5'-enhancer in the transcriptional regulation of the human endothelial cell protein C receptor gene. Blood. 2006;108:1251-1259.
73. Jahroudi N, Lynch DC. Endothelial-cell-specific regulation of von Willebrand factor gene expression. Mol Cell Biol. 1994;14:999-1008.
74. Aird WC, Jahroudi N, Weiler-Guettler H, Rayburn HB, Rosenberg RD. Human von Willebrand factor gene sequences target expression to a subpopulation of endothelial cells in transgenic mice. Proc Natl Acad Sci U S A. 1995;92:4567-4571.
75. Jahroudi N, Ardekani AM, Greenberger JS. An NF1-like protein functions as a repressor of the von Willebrand factor promoter. J Biol Chem. 1996;271:21413-21421.
76. Ardekani AM, Greenberger JS, Jahroudi N. Two repressor elements inhibit expression of the von Willebrand factor gene promoter in vitro. Thromb Haemost. 1998;80:488-494.
77. Peng Y, Jahroudi N. The NFY transcription factor functions as a repressor and activator of the von Willebrand factor promoter. Blood. 2002;99:2408-2417.
78. Rand JH, Badimon L, Gordon RE, Uson RR, Fuster V. Distribution of von Willebrand factor in porcine intima varies with blood vessel type and location. Arteriosclerosis. 1987;7:287-291.
79. Wu QY, Bahnak BR, Coulombel L, et al. Analysis of von Willebrand factor mRNA from the lung of pigs with severe von Willebrand disease by using a human cDNA probe. Blood. 1988;71:1341-1346.
80. Bahnak BR, Wu QY, Coulombel L, et al. Expression of von Willebrand factor in porcine vessels: heterogeneity at the level of von Willebrand factor mRNA. J Cell Physiol. 1989;138:305-310.
81. Smith JM, Meinkoth JH, Hochstatter T, Meyers KM. Differential distribution of von Willebrand factor in canine vascular endothelium. Am J Vet Res. 1996;57:750-755.
82. Coffin JD, Harrison J, Schwartz S, Heimark R. Angioblast differentiation and morphogenesis of the vascular endothelium in the mouse embryo. Dev Biol. 1991;148:51-62.
83. Yamamoto K, de Waard V, Fearns C, Loskutoff DJ. Tissue distribution and regulation of murine von Willebrand factor gene expression in vivo. Blood. 1998;92:2791-2801.
84. Zanetta L, Marcus SG, Vasile J, et al. Expression of Von Willebrand factor, an endothelial cell marker, is up-regulated by angiogenesis factors: a potential method for objective assessment of tumor angiogenesis. Int J Cancer. 2000;85:281-288.
85. Katsumi A, Tuley EA, Bodo I, Sadler JE. Localization of disulfide bonds in the cystine knot domain of human von Willebrand factor. J Biol Chem. 2000;275:25585-25594.
86. Titani K, Kumar S, Takio K, et al. Amino acid sequence of human von Willebrand factor. Biochemistry. 1986;25:3171-3184.
87. Marti T, Rosselet SJ, Titani K, Walsh KA. Identification of disulfide-bridged substructures within human von Willebrand factor. Biochemistry. 1987;26:8099-8109.
88. Matsui T, Titani K, Mizuochi T. Structures of the asparagine-linked oligosaccharide chains of human von Willebrand factor. Occurrence of blood group A, B, and H(O) structures. J Biol Chem. 1992;267:8723-8731.
89. Matsui T, Fujimura Y, Nishida S, Titani K. Human plasma alpha 2-macroglobulin and von Willebrand factor possess covalently linked ABO(H)

blood group antigens in subjects with corresponding ABO phenotype. Blood. 1993;82:663-668.
90. Shima M, Fujimura Y, Nishiyama T, et al. ABO blood group genotype and plasma von Willebrand factor in normal individuals. Vox Sang. 1995;68:236-240.
91. Gill JC, Endres-Brooks J, Bauer PJ, Marks WJ, Jr., Montgomery RR. The effect of ABO blood group on the diagnosis of von Willebrand disease. Blood. 1987;69:1691-1695.
92. Bowen DJ. An influence of ABO blood group on the rate of proteolysis of von Willebrand factor by ADAMTS13. J Thromb Haemost. 2003;1:33-40.
93. O'Donnell J S, McKinnon TA, Crawley JT, Lane DA, Laffan MA. Bombay phenotype is associated with reduced plasma-VWF levels and an increased susceptibility to ADAMTS13 proteolysis. Blood. 2005;106:1988-1991.
94. Voorberg J, Fontijn R, van Mourik JA, Pannekoek H. Domains involved in multimer assembly of von willebrand factor (vWF): multimerization is independent of dimerization. Embo J. 1990;9:797-803.
95. Ruggeri ZM. Structure of von Willebrand factor and its function in platelet adhesion and thrombus formation. Best Pract Res Clin Haematol. 2001;14:257-279.
96. Pietu G, Ribba AS, Meulien P, Meyer D. Localization within the 106 N-terminal amino acids of von Willebrand factor (vWF) of the epitope corresponding to a monoclonal antibody which inhibits vWF binding to factor VIII. Biochem Biophys Res Commun. 1989;163:618-626.
97. Sobel M, Soler DF, Kermode JC, Harris RB. Localization and characterization of a heparin binding domain peptide of human von Willebrand factor. J Biol Chem. 1992;267:8857-8862.
98. Colombatti A, Bonaldo P. The superfamily of proteins with von Willebrand factor type A-like domains: one theme common to components of extracellular matrix, hemostasis, cellular adhesion, and defense mechanisms. Blood. 1991;77:2305-2315.
99. Sadler JE. Biomedicine. Contact--how platelets touch von Willebrand factor. Science. 2002;297:1128-1129.
100. Huizinga EG, Tsuji S, Romijn RA, et al. Structures of glycoprotein Ibalpha and its complex with von Willebrand factor A1 domain. Science. 2002;297:1176-1179.
101. Mohri H, Yoshioka A, Zimmerman TS, Ruggeri ZM. Isolation of the von Willebrand factor domain interacting with platelet glycoprotein Ib, heparin, and collagen and characterization of its three distinct functional sites. J Biol Chem. 1989;264:17361-17367.
102. Maita N, Nishio K, Nishimoto E, et al. Crystal structure of von Willebrand factor A1 domain complexed with snake venom, bitiscetin: insight into glycoprotein Ibalpha binding mechanism induced by snake venom proteins. J Biol Chem. 2003;278:37777-37781.
103. Pareti FI, Niiya K, McPherson JM, Ruggeri ZM. Isolation and characterization of two domains of human von Willebrand factor that interact with fibrillar collagen types I and III. J Biol Chem. 1987;262:13835-13841.
104. Hoylaerts MF, Yamamoto H, Nuyts K, Vreys I, Deckmyn H, Vermylen J. von Willebrand factor binds to native collagen VI primarily via its A1 domain. Biochem J. 1997;324 (Pt 1):185-191.
105. Mazzucato M, Spessotto P, Masotti A, et al. Identification of domains responsible for von Willebrand factor type VI collagen interaction mediating platelet adhesion under high flow. J Biol Chem. 1999;274:3033-3041.

106. Dent JA, Berkowitz SD, Ware J, Kasper CK, Ruggeri ZM. Identification of a cleavage site directing the immunochemical detection of molecular abnormalities in type IIA von Willebrand factor. Proc Natl Acad Sci U S A. 1990;87:6306-6310.
107. Dong JF, Moake JL, Bernardo A, et al. ADAMTS-13 metalloprotease interacts with the endothelial cell-derived ultra-large von Willebrand factor. J Biol Chem. 2003;278:29633-29639.
108. Beacham DA, Wise RJ, Turci SM, Handin RI. Selective inactivation of the Arg-Gly-Asp-Ser (RGDS) binding site in von Willebrand factor by site-directed mutagenesis. J Biol Chem. 1992;267:3409-3415.
109. Hubbard SC, Robbins PW. Synthesis of the N-linked oligosaccharides of glycoproteins. Assembly of the lipid-linked precursor oligosaccharide and its relation to protein synthesis in vivo. J Biol Chem. 1980;255:11782-11793.
110. Hubbard SC, Ivatt RJ. Synthesis and processing of asparagine-linked oligosaccharides. Annu Rev Biochem. 1981;50:555-583.
111. Wagner DD, Mayadas T, Marder VJ. Initial glycosylation and acidic pH in the Golgi apparatus are required for multimerization of von Willebrand factor. J Cell Biol. 1986;102:1320-1324.
112. Fujimura Y, Titani K, Holland LZ, et al. A heparin-binding domain of human von Willebrand factor. Characterization and localization to a tryptic fragment extending from amino acid residue Val-449 to Lys-728. J Biol Chem. 1987;262:1734-1739.
113. Dong Z, Thoma RS, Crimmins DL, McCourt DW, Tuley EA, Sadler JE. Disulfide bonds required to assemble functional von Willebrand factor multimers. J Biol Chem. 1994;269:6753-6758.
114. Verweij CL, Hart M, Pannekoek H. Expression of variant von Willebrand factor (vWF) cDNA in heterologous cells: requirement of the pro-polypeptide in vWF multimer formation. Embo J. 1987;6:2885-2890.
115. Mayadas TN, Wagner DD. Vicinal cysteines in the prosequence play a role in von Willebrand factor multimer assembly. Proc Natl Acad Sci U S A. 1992;89:3531-3535.
116. Rosenberg JB, Haberichter SL, Jozwiak MA, et al. The role of the D1 domain of the von Willebrand factor propeptide in multimerization of VWF. Blood. 2002;100:1699-1706.
117. Purvis AR, Sadler JE. A covalent oxidoreductase intermediate in propeptide-dependent von Willebrand factor multimerization. J Biol Chem. 2004;279:49982-49988.
118. Wise RJ, Pittman DD, Handin RI, Kaufman RJ, Orkin SH. The propeptide of von Willebrand factor independently mediates the assembly of von Willebrand multimers. Cell. 1988;52:229-236.
119. Verweij CL, Hart M, Pannekoek H. Proteolytic cleavage of the precursor of von Willebrand factor is not essential for multimer formation. J Biol Chem. 1988;263:7921-7924.
120. Vischer UM, Wagner DD. von Willebrand factor proteolytic processing and multimerization precede the formation of Weibel-Palade bodies. Blood. 1994;83:3536-3544.
121. Wagner DD, Olmsted JB, Marder VJ. Immunolocalization of von Willebrand protein in Weibel-Palade bodies of human endothelial cells. J Cell Biol. 1982;95:355-360.
122. Cramer EM, Meyer D, le Menn R, Breton-Gorius J. Eccentric localization of von Willebrand factor in an internal structure of platelet alpha-granule resembling that of Weibel-Palade bodies. Blood. 1985;66:710-713.

123. Wagner DD, Saffaripour S, Bonfanti R, et al. Induction of specific storage organelles by von Willebrand factor propolypeptide. Cell. 1991;64:403-413.
124. Voorberg J, Fontijn R, Calafat J, Janssen H, van Mourik JA, Pannekoek H. Biogenesis of von Willebrand factor-containing organelles in heterologous transfected CV-1 cells. Embo J. 1993;12:749-758.
125. Hop C, Fontijn R, van Mourik JA, Pannekoek H. Polarity of constitutive and regulated von Willebrand factor secretion by transfected MDCK-II cells. Exp Cell Res. 1997;230:352-361.
126. Haberichter SL, Fahs SA, Montgomery RR. von Willebrand factor storage and multimerization: 2 independent intracellular processes. Blood. 2000;96:1808-1815.
127. Schick PK, Walker J, Profeta B, Denisova L, Bennett V. Synthesis and secretion of von Willebrand factor and fibronectin in megakaryocytes at different phases of maturation. Arterioscler Thromb Vasc Biol. 1997;17:797-801.
128. Sporn LA, Marder VJ, Wagner DD. Inducible secretion of large, biologically potent von Willebrand factor multimers. Cell. 1986;46:185-190.
129. Kaufmann JE, Oksche A, Wollheim CB, Gunther G, Rosenthal W, Vischer UM. Vasopressin-induced von Willebrand factor secretion from endothelial cells involves V2 receptors and cAMP. J Clin Invest. 2000;106:107-116.
130. Brass LF. Thrombin and platelet activation. Chest. 2003;124:18S-25S.
131. Wagner DD, Fay PJ, Sporn LA, Sinha S, Lawrence SO, Marder VJ. Divergent fates of von Willebrand factor and its propolypeptide (von Willebrand antigen II) after secretion from endothelial cells. Proc Natl Acad Sci U S A. 1987;84:1955-1959.
132. Borchiellini A, Fijnvandraat K, ten Cate JW, et al. Quantitative analysis of von Willebrand factor propeptide release in vivo: effect of experimental endotoxemia and administration of 1-deamino-8-D-arginine vasopressin in humans. Blood. 1996;88:2951-2958.
133. Meriane F, Zerhouni L, Djeha N, Goudemand M, Mazurier C. Biological effects of a S/D-treated, very high purity, von Willebrand factor concentrate in five patients with severe von Willebrand disease. Blood Coagul Fibrinolysis. 1993;4:1023-1029.
134. Mayadas TN, Wagner DD. von Willebrand factor biosynthesis and processing. Ann N Y Acad Sci. 1991;614:153-166.
135. Lenting PJ, Westein E, Terraube V, et al. An experimental model to study the in vivo survival of von Willebrand factor. Basic aspects and application to the R1205H mutation. J Biol Chem. 2004;279:12102-12109.
136. Stoddart JH, Jr., Andersen J, Lynch DC. Clearance of normal and type 2A von Willebrand factor in the rat. Blood. 1996;88:1692-1699.
137. Turecek PL, Gritsch H, Pichler L, et al. In vivo characterization of recombinant von Willebrand factor in dogs with von Willebrand disease. Blood. 1997;90:3555-3567.
138. Mohlke KL, Purkayastha AA, Westrick RJ, et al. Mvwf, a dominant modifier of murine von Willebrand factor, results from altered lineage-specific expression of a glycosyltransferase. Cell. 1999;96:111-120.
139. Ellies LG, Ditto D, Levy GG, et al. Sialyltransferase ST3Gal-IV operates as a dominant modifier of hemostasis by concealing asialoglycoprotein receptor ligands. Proc Natl Acad Sci U S A. 2002;99:10042-10047.
140. Schooten CJ, Tjernberg P, Westein E, et al. Cysteine-mutations in von Willebrand factor associated with increased clearance. J Thromb Haemost. 2005;3:2228-2237.

141. Gavazova S, Gill JC, Scott JP, et al. A mutation in the D4 domain of von Willebrand factor (VWF) results in a variant of type I von Willebrand disease with accelerated in vivo VWF clearance. blood. 2002;100:476.
142. Studt JD, Budde U, Schneppenheim R, et al. Quantification and facilitated comparison of von Willebrand factor multimer patterns by densitometry. Am J Clin Pathol. 2001;116:567-574.
143. Krizek DR, Rick ME. A rapid method to visualize von willebrand factor multimers by using agarose gel electrophoresis, immunolocalization and luminographic detection. Thromb Res. 2000;97:457-462.
144. Baillod P, Affolter B, Kurt GH, Pflugshaupt R. Multimeric analysis of von Willebrand factor by vertical sodium dodecyl sulphate agarose gel electrophoresis, vacuum blotting technology and sensitive visualization by alkaline phosphatase anti-alkaline phosphatase complex. Thromb Res. 1992;66:745-755.
145. Fowler WE, Fretto LJ, Hamilton KK, Erickson HP, McKee PA. Substructure of human von Willebrand factor. J Clin Invest. 1985;76:1491-1500.
146. Fretto LJ, Fowler WE, McCaslin DR, Erickson HP, McKee PA. Substructure of human von Willebrand factor. Proteolysis by V8 and characterization of two functional domains. J Biol Chem. 1986;261:15679-15689.
147. Furlan M, Robles R, Lamie B. Partial purification and characterization of a protease from human plasma cleaving von Willebrand factor to fragments produced by in vivo proteolysis. Blood. 1996;87:4223-4234.
148. Federici AB, Bader R, Pagani S, Colibretti ML, De Marco L, Mannucci PM. Binding of von Willebrand factor to glycoproteins Ib and IIb/IIIa complex: affinity is related to multimeric size. Br J Haematol. 1989;73:93-99.
149. Siedlecki CA, Lestini BJ, Kottke-Marchant KK, Eppell SJ, Wilson DL, Marchant RE. Shear-dependent changes in the three-dimensional structure of human von Willebrand factor. Blood. 1996;88:2939-2950.
150. Furlan M. Von Willebrand factor: molecular size and functional activity. Ann Hematol. 1996;72:341-348.
151. Tangelder GJ, Slaaf DW, Arts T, Reneman RS. Wall shear rate in arterioles in vivo: least estimates from platelet velocity profiles. Am J Physiol. 1988;254:H1059-1064.
152. Wootton DM, Ku DN. Fluid mechanics of vascular systems, diseases, and thrombosis. Annu Rev Biomed Eng. 1999;1:299-329.
153. Maalej N, Holden JE, Folts JD. Effect of Shear Stress on Acute Platelet Thrombus Formation in Canine Stenosed Carotid Arteries: An In Vivo Quantitative Study. J Thromb Thrombolysis. 1998;5:231-238.
154. Vlot AJ, Koppelman SJ, Meijers JC, et al. Kinetics of factor VIII-von Willebrand factor association. Blood. 1996;87:1809-1816.
155. Bahou WF, Ginsburg D, Sikkink R, Litwiller R, Fass DN. A monoclonal antibody to von Willebrand factor (vWF) inhibits factor VIII binding. Localization of its antigenic determinant to a nonadecapeptide at the amino terminus of the mature vWF polypeptide. J Clin Invest. 1989;84:56-61.
156. Ginsburg D, Bockenstedt PL, Allen EA, et al. Fine mapping of monoclonal antibody epitopes on human von Willebrand factor using a recombinant peptide library. Thromb Haemost. 1992;67:166-171.
157. Foster PA, Fulcher CA, Marti T, Titani K, Zimmerman TS. A major factor VIII binding domain resides within the amino-terminal 272 amino acid residues of von Willebrand factor. J Biol Chem. 1987;262:8443-8446.

158. Saenko EL, Shima M, Rajalakshmi KJ, Scandella D. A role for the C2 domain of factor VIII in binding to von Willebrand factor. J Biol Chem. 1994;269:11601-11605.
159. Saenko EL, Scandella D. The acidic region of the factor VIII light chain and the C2 domain together form the high affinity binding site for von willebrand factor. J Biol Chem. 1997;272:18007-18014.
160. Shima M, Yoshioka A, Nakajima M, Nakai H, Fukui H. A monoclonal antibody (NMC-VIII/10) to factor VIII light chain recognizing Glu1675-Glu1684 inhibits factor VIII binding to endogenous von Willebrand factor in human umbilical vein endothelial cells. Br J Haematol. 1992;81:533-538.
161. Shima M, Scandella D, Yoshioka A, et al. A factor VIII neutralizing monoclonal antibody and a human inhibitor alloantibody recognizing epitopes in the C2 domain inhibit factor VIII binding to von Willebrand factor and to phosphatidylserine. Thromb Haemost. 1993;69:240-246.
162. Nogami K, Shima M, Giddings JC, et al. Circulating factor VIII immune complexes in patients with type 2 acquired hemophilia A and protection from activated protein C-mediated proteolysis. Blood. 2001;97:669-677.
163. Eaton D, Rodriguez H, Vehar GA. Proteolytic processing of human factor VIII. Correlation of specific cleavages by thrombin, factor Xa, and activated protein C with activation and inactivation of factor VIII coagulant activity. Biochemistry. 1986;25:505-512.
164. Hill-Eubanks DC, Parker CG, Lollar P. Differential proteolytic activation of factor VIII-von Willebrand factor complex by thrombin. Proc Natl Acad Sci U S A. 1989;86:6508-6512.
165. Myles T, Yun TH, Leung LL. Structural requirements for the activation of human factor VIII by thrombin. Blood. 2002;100:2820-2826.
166. Precup JW, Kline BC, Fass DN. A monoclonal antibody to factor VIII inhibits von Willebrand factor binding and thrombin cleavage. Blood. 1991;77:1929-1936.
167. Nyman D. Collagen-induced platelet aggregation: evidence of several mechanisms for the induction of platelet release by collagen. Thromb Res. 1977;10:743-751.
168. Santoro SA, Cowan JF. Adsorption of von Willebrand factor by fibrillar collagen--implications concerning the adhesion of platelets to collagen. Coll Relat Res. 1982;2:31-43.
169. Bockenstedt P, McDonagh J, Handin RI. Binding and covalent cross-linking of purified von Willebrand factor to native monomeric collagen. J Clin Invest. 1986;78:551-556.
170. Roth GJ, Titani K, Hoyer LW, Hickey MJ. Localization of binding sites within human von Willebrand factor for monomeric type III collagen. Biochemistry. 1986;25:8357-8361.
171. Rand JH, Patel ND, Schwartz E, Zhou SL, Potter BJ. 150-kD von Willebrand factor binding protein extracted from human vascular subendothelium is type VI collagen. J Clin Invest. 1991;88:253-259.
172. Huizinga EG, Martijn van der Plas R, Kroon J, Sixma JJ, Gros P. Crystal structure of the A3 domain of human von Willebrand factor: implications for collagen binding. Structure. 1997;5:1147-1156.
173. Romijn RA, Bouma B, Wuyster W, et al. Identification of the collagen-binding site of the von Willebrand factor A3-domain. J Biol Chem. 2001;276:9985-9991.
174. Romijn RA, Westein E, Bouma B, et al. Mapping the collagen-binding site in the von Willebrand factor-A3 domain. J Biol Chem. 2003;278:15035-15039.

175. Cruz MA, Yuan H, Lee JR, Wise RJ, Handin RI. Interaction of the von Willebrand factor (vWF) with collagen. Localization of the primary collagen-binding site by analysis of recombinant vWF A domain polypeptides. J Biol Chem. 1995;270:19668.
176. Celikel R, Ruggeri ZM, Varughese KI. von Willebrand factor conformation and adhesive function is modulated by an internalized water molecule. Nat Struct Biol. 2000;7:881-884.
177. Matsushita T, Meyer D, Sadler JE. Localization of von willebrand factor-binding sites for platelet glycoprotein Ib and botrocetin by charged-to-alanine scanning mutagenesis. J Biol Chem. 2000;275:11044-11049.
178. Holmberg L, Nilsson IM. von Willebrand's disease. Eur J Haematol. 1992;48:127-141.
179. Rodeghiero F, Castaman G, Dini E. Epidemiological investigation of the prevalence of von Willebrand's disease. Blood. 1987;69:454-459.
180. Keeney S, Cumming AM. The molecular biology of von Willebrand disease. Clin Lab Haematol. 2001;23:209-230.
181. Ginsburg D, Bowie EJ. Molecular genetics of von Willebrand disease. Blood. 1992;79:2507-2519.
182. Lyons SE, Bruck ME, Bowie EJ, Ginsburg D. Impaired intracellular transport produced by a subset of type IIA von Willebrand disease mutations. J Biol Chem. 1992;267:4424-4430.
183. Tsai HM, Sussman, II, Ginsburg D, Lankhof H, Sixma JJ, Nagel RL. Proteolytic cleavage of recombinant type 2A von Willebrand factor mutants R834W and R834Q: inhibition by doxycycline and by monoclonal antibody VP-1. Blood. 1997;89:1954-1962.
184. Tsai HM. Type 2 A (group II) von Willebrand disease mutations increase the susceptibility of VWF to ADAMTS-13. J Thromb Haemost. 2004;2:2057.
185. O'Brien LA, Sutherland JJ, Hegadorn C, et al. A novel type 2A (Group II) von Willebrand disease mutation (L1503Q) associated with loss of the highest molecular weight von Willebrand factor multimers. J Thromb Haemost. 2004;2:1135-1142.
186. Nishio K, Anderson PJ, Zheng XL, Sadler JE. Binding of platelet glycoprotein Ibalpha to von Willebrand factor domain A1 stimulates the cleavage of the adjacent domain A2 by ADAMTS13. Proc Natl Acad Sci U S A. 2004;101:10578-10583.
187. Ginsburg D, Sadler JE. von Willebrand disease: a database of point mutations, insertions, and deletions. For the Consortium on von Willebrand Factor Mutations and Polymorphisms, and the Subcommittee on von Willebrand Factor of the Scientific and Standardization Committee of the International Society on Thrombosis and Haemostasis. Thromb Haemost. 1993;69:177-184.
188. Holmberg L, Dent JA, Schneppenheim R, Budde U, Ware J, Ruggeri ZM. von Willebrand factor mutation enhancing interaction with platelets in patients with normal multimeric structure. J Clin Invest. 1993;91:2169-2177.
189. Mancuso DJ, Kroner PA, Christopherson PA, Vokac EA, Gill JC, Montgomery RR. Type 2M:Milwaukee-1 von Willebrand disease: an in-frame deletion in the Cys509-Cys695 loop of the von Willebrand factor A1 domain causes deficient binding of von Willebrand factor to platelets. Blood. 1996;88:2559-2568.
190. Nishino M, Nishino S, Sugimoto M, Shibata M, Tsuji S, Yoshioka A. Changes in factor VIII binding capacity of von Willebrand factor and factor VIII coagulant activity in two patients with type 2N von Willebrand disease after hemostatic treatment and during pregnancy. Int J Hematol. 1996;64:127-134.

191. Fressinaud E, Mazurier C, Meyer D. Molecular genetics of type 2 von Willebrand disease. Int J Hematol. 2002;75:9-18.
192. Sadler JE. Biochemistry and genetics of von Willebrand factor. Annu Rev Biochem. 1998;67:395-424.
193. Furlan M, Robles R, Morselli B, Sandoz P, Lammle B. Recovery and half-life of von Willebrand factor-cleaving protease after plasma therapy in patients with thrombotic thrombocytopenic purpura. Thromb Haemost. 1999;81:8-13.
194. Gerritsen HE, Robles R, Lammle B, Furlan M. Partial amino acid sequence of purified von Willebrand factor-cleaving protease. Blood. 2001;98:1654-1661.
195. Zheng X, Chung D, Takayama TK, Majerus EM, Sadler JE, Fujikawa K. Structure of von Willebrand factor-cleaving protease (ADAMTS13), a metalloprotease involved in thrombotic thrombocytopenic purpura. J Biol Chem. 2001;276:41059-41063.
196. Tsai HM. Physiologic cleavage of von Willebrand factor by a plasma protease is dependent on its conformation and requires calcium ion. Blood. 1996;87:4235-4244.
197. Levy GG, Nichols WC, Lian EC, et al. Mutations in a member of the ADAMTS gene family cause thrombotic thrombocytopenic purpura. Nature. 2001;413:488-494.
198. Plaimauer B, Zimmermann K, Volkel D, et al. Cloning, expression, and functional characterization of the von Willebrand factor-cleaving protease (ADAMTS13). Blood. 2002;100:3626-3632.
199. Kuno K, Kanada N, Nakashima E, Fujiki F, Ichimura F, Matsushima K. Molecular cloning of a gene encoding a new type of metalloproteinase-disintegrin family protein with thrombospondin motifs as an inflammation associated gene. J Biol Chem. 1997;272:556-562.
200. Fernandes RJ, Hirohata S, Engle JM, et al. Procollagen II amino propeptide processing by ADAMTS-3. Insights on dermatosparaxis. J Biol Chem. 2001;276:31502-31509.
201. Colige A, Vandenberghe I, Thiry M, et al. Cloning and characterization of ADAMTS-14, a novel ADAMTS displaying high homology with ADAMTS-2 and ADAMTS-3. J Biol Chem. 2002;277:5756-5766.
202. Kuno K, Okada Y, Kawashima H, et al. ADAMTS-1 cleaves a cartilage proteoglycan, aggrecan. FEBS Lett. 2000;478:241-245.
203. Tortorella M, Pratta M, Liu RQ, et al. The thrombospondin motif of aggrecanase-1 (ADAMTS-4) is critical for aggrecan substrate recognition and cleavage. J Biol Chem. 2000;275:25791-25797.
204. Tortorella MD, Liu RQ, Burn T, Newton RC, Arner E. Characterization of human aggrecanase 2 (ADAM-TS5): substrate specificity studies and comparison with aggrecanase 1 (ADAM-TS4). Matrix Biol. 2002;21:499-511.
205. Collins-Racie LA, Flannery CR, Zeng W, et al. ADAMTS-8 exhibits aggrecanase activity and is expressed in human articular cartilage. Matrix Biol. 2004;23:219-230.
206. Somerville RP, Longpre JM, Jungers KA, et al. Characterization of ADAMTS-9 and ADAMTS-20 as a distinct ADAMTS subfamily related to Caenorhabditis elegans GON-1. J Biol Chem. 2003;278:9503-9513.
207. Kevorkian L, Young DA, Darrah C, et al. Expression profiling of metalloproteinases and their inhibitors in cartilage. Arthritis Rheum. 2004;50:131-141.
208. Vazquez F, Hastings G, Ortega MA, et al. METH-1, a human ortholog of ADAMTS-1, and METH-2 are members of a new family of proteins with angio-inhibitory activity. J Biol Chem. 1999;274:23349-23357.

209. Luque A, Carpizo DR, Iruela-Arispe ML. ADAMTS1/METH1 inhibits endothelial cell proliferation by direct binding and sequestration of VEGF165. J Biol Chem. 2003;278:23656-23665.
210. Shindo T, Kurihara H, Kuno K, et al. ADAMTS-1: a metalloproteinase-disintegrin essential for normal growth, fertility, and organ morphology and function. J Clin Invest. 2000;105:1345-1352.
211. Masui T, Hosotani R, Tsuji S, et al. Expression of METH-1 and METH-2 in pancreatic cancer. Clin Cancer Res. 2001;7:3437-3443.
212. Porter S, Scott SD, Sassoon EM, et al. Dysregulated expression of adamalysin-thrombospondin genes in human breast carcinoma. Clin Cancer Res. 2004;10:2429-2440.
213. Bode W, Gomis-Ruth FX, Stockler W. Astacins, serralysins, snake venom and matrix metalloproteinases exhibit identical zinc-binding environments (HEXXHXXGXXH and Met-turn) and topologies and should be grouped into a common family, the 'metzincins'. FEBS Lett. 1993;331:134-140.
214. Stocker W, Grams F, Baumann U, et al. The metzincins--topological and sequential relations between the astacins, adamalysins, serralysins, and matrixins (collagenases) define a superfamily of zinc-peptidases. Protein Sci. 1995;4:823-840.
215. Kuno K, Matsushima K. ADAMTS-1 protein anchors at the extracellular matrix through the thrombospondin type I motifs and its spacing region. J Biol Chem. 1998;273:13912-13917.
216. Rodriguez-Manzaneque JC, Milchanowski AB, Dufour EK, Leduc R, Iruela-Arispe ML. Characterization of METH-1/ADAMTS1 processing reveals two distinct active forms. J Biol Chem. 2000;275:33471-33479.
217. Flannery CR, Zeng W, Corcoran C, et al. Autocatalytic cleavage of ADAMTS-4 (Aggrecanase-1) reveals multiple glycosaminoglycan-binding sites. J Biol Chem. 2002;277:42775-42780.
218. Cal S, Arguelles JM, Fernandez PL, Lopez-Otin C. Identification, characterization, and intracellular processing of ADAM-TS12, a novel human disintegrin with a complex structural organization involving multiple thrombospondin-1 repeats. J Biol Chem. 2001;276:17932-17940.
219. Maskos K, Fernandez-Catalan C, Huber R, et al. Crystal structure of the catalytic domain of human tumor necrosis factor-alpha-converting enzyme. Proc Natl Acad Sci U S A. 1998;95:3408-3412.
220. Orth P, Reichert P, Wang W, et al. Crystal structure of the catalytic domain of human ADAM33. J Mol Biol. 2004;335:129-137.
221. Andreini C, Banci L, Bertini I, Elmi S, Rosato A. Comparative analysis of the ADAM and ADAMTS families. J Proteome Res. 2005;4:881-888.
222. Bode W, Kress LF, Meyer EF, Gomis-Ruth FX. The crystal structure of adamalysin II, a zinc-endopeptidase from the snake venom of the eastern diamondback rattlesnake Crotalus adamanteus. Braz J Med Biol Res. 1994;27:2049-2068.
223. Levy GG, Motto DG, Ginsburg D. ADAMTS13 turns 3. Blood. 2005;106:11-17.
224. Fujikawa K, Suzuki H, McMullen B, Chung D. Purification of human von Willebrand factor-cleaving protease and its identification as a new member of the metalloproteinase family. Blood. 2001;98:1662-1666.
225. Kokame K, Matsumoto M, Soejima K, et al. Mutations and common polymorphisms in ADAMTS13 gene responsible for von Willebrand factor-cleaving protease activity. Proc Natl Acad Sci U S A. 2002;99:11902-11907.
226. Zhou W, Inada M, Lee TP, et al. ADAMTS13 is expressed in hepatic stellate cells. Lab Invest. 2005;85:780-788.

227. Uemura M, Tatsumi K, Matsumoto M, et al. Localization of ADAMTS13 to the stellate cells of human liver. Blood. 2005;106:922-924.
228. Suzuki M, Murata M, Matsubara Y, et al. Detection of von Willebrand factor-cleaving protease (ADAMTS-13) in human platelets. Biochem Biophys Res Commun. 2004;313:212-216.
229. Turner N, Nolasco L, Tao Z, Dong JF, Moake J. Human endothelial cells synthesize and release ADAMTS-13. J Thromb Haemost. 2006;4:1396-1404.
230. Van Wart HE, Birkedal-Hansen H. The cysteine switch: a principle of regulation of metalloproteinase activity with potential applicability to the entire matrix metalloproteinase gene family. Proc Natl Acad Sci U S A. 1990;87:5578-5582.
231. Majerus EM, Zheng X, Tuley EA, Sadler JE. Cleavage of the ADAMTS13 propeptide is not required for protease activity. J Biol Chem. 2003;278:46643-46648.
232. Yiallouros I, Grosse Berkhoff E, Stocker W. The roles of Glu93 and Tyr149 in astacin-like zinc peptidases. FEBS Lett. 2000;484:224-228.
233. Bode W, Fernandez-Catalan C, Tschesche H, Grams F, Nagase H, Maskos K. Structural properties of matrix metalloproteinases. Cell Mol Life Sci. 1999;55:639-652.
234. Anderson PJ, Kokame K, Sadler JE. Zinc and calcium ions cooperatively modulate ADAMTS13 activity. J Biol Chem. 2006;281:850-857.
235. Auld DS. Removal and replacement of metal ions in metallopeptidases. Methods Enzymol. 1995;248:228-242.
236. Zheng X, Nishio K, Majerus EM, Sadler JE. Cleavage of von Willebrand factor requires the spacer domain of the metalloprotease ADAMTS13. J Biol Chem. 2003;278:30136-30141.
237. Soejima K, Matsumoto M, Kokame K, et al. ADAMTS-13 cysteine-rich/spacer domains are functionally essential for von Willebrand factor cleavage. Blood. 2003;102:3232-3237.
238. Ai J, Smith P, Wang S, Zhang P, Zheng XL. The proximal carboxyl-terminal domains of ADAMTS13 determine substrate specificity and are all required for cleavage of von Willebrand factor. J Biol Chem. 2005;280:29428-29434.
239. Christianson DW, David PR, Lipscomb WN. Mechanism of carboxypeptidase A: hydration of a ketonic substrate analogue. Proc Natl Acad Sci U S A. 1987;84:1512-1515.
240. Schneppenheim R, Budde U, Oyen F, et al. von Willebrand factor cleaving protease and ADAMTS13 mutations in childhood TTP. Blood. 2003;101:1845-1850.
241. Serrano SM, Jia LG, Wang D, Shannon JD, Fox JW. Function of the cysteine-rich domain of the haemorrhagic metalloproteinase atrolysin A: targeting adhesion proteins collagen I and von Willebrand factor. Biochem J. 2005;391:69-76.
242. Assink K, Schiphorst R, Allford S, et al. Mutation analysis and clinical implications of von Willebrand factor-cleaving protease deficiency. Kidney Int. 2003;63:1995-1999.
243. Klaus C, Plaimauer B, Studt JD, et al. Epitope mapping of ADAMTS13 autoantibodies in acquired thrombotic thrombocytopenic purpura. Blood. 2004.
244. Soejima K, Nakamura H, Hirashima M, Morikawa W, Nozaki C, Nakagaki T. Analysis on the Molecular Species and Concentration of Circulating ADAMTS13 in Blood. J Biochem (Tokyo). 2006;139:147-154.
245. Adams JC, Tucker RP. The thrombospondin type 1 repeat (TSR) superfamily: diverse proteins with related roles in neuronal development. Dev Dyn. 2000;218:280-299.

246. Tan K, Duquette M, Liu JH, et al. Crystal structure of the TSP-1 type 1 repeats: a novel layered fold and its biological implication. J Cell Biol. 2002;159:373-382.
247. Dawson DW, Pearce SF, Zhong R, Silverstein RL, Frazier WA, Bouck NP. CD36 mediates the In vitro inhibitory effects of thrombospondin-1 on endothelial cells. J Cell Biol. 1997;138:707-717.
248. Asch AS, Silbiger S, Heimer E, Nachman RL. Thrombospondin sequence motif (CSVTCG) is responsible for CD36 binding. Biochem Biophys Res Commun. 1992;182:1208-1217.
249. Tandon NN, Rock G, Jamieson GA. Anti-CD36 antibodies in thrombotic thrombocytopenic purpura. Br J Haematol. 1994;88:816-825.
250. Schultz DR, Arnold PI, Jy W, et al. Anti-CD36 autoantibodies in thrombotic thrombocytopenic purpura and other thrombotic disorders: identification of an 85 kD form of CD36 as a target antigen. Br J Haematol. 1998;103:849-857.
251. Dong JF BA, Nolasco L, Padilla A, Moake J, Lopez J. ADAMTS-13 proteolysis of ultralarge von willebrand factor multimers on the endothelial surface requires protease docking and is inhibited by thrombospondin-1 (abstract). Blood. 2003.
252. Xie L, Chesterman CN, Hogg PJ. Control of von Willebrand factor multimer size by thrombospondin-1. J Exp Med. 2001;193:1341-1349.
253. Pimanda JE, Ganderton T, Maekawa A, et al. Role of thrombospondin-1 in control of von Willebrand factor multimer size in mice. J Biol Chem. 2004;279:21439-21448.
254. Bork P, Beckmann G. The CUB domain. A widespread module in developmentally regulated proteins. J Mol Biol. 1993;231:539-545.
255. Tao Z, Wang Y, Choi H, et al. Cleavage of ultralarge multimers of von Willebrand factor by C-terminal-truncated mutants of ADAMTS-13 under flow. Blood. 2005;106:141-143.
256. Banno F, Kaminaka K, Soejima K, Kokame K, Miyata T. Identification of strain-specific variants of mouse Adamts13 gene encoding von Willebrand factor-cleaving protease. J Biol Chem. 2004.
257. Pimanda JE, Maekawa A, Wind T, Paxton J, Chesterman CN, Hogg PJ. Congenital thrombotic thrombocytopenic purpura in association with a mutation in the second CUB domain of ADAMTS13. Blood. 2004;103:627-629.
258. Majerus EM, Anderson PJ, Sadler JE. Binding of ADAMTS13 to von Willebrand factor. J Biol Chem. 2005.
259. Tao Z, Peng Y, Nolasco L, et al. Recombinant CUB-1 domain polypeptide inhibits the cleavage of ULVWF strings by ADAMTS13 under flow conditions. Blood. 2005;106:4139-4145.
260. Zhang W. MD, Ginsburg, D. ADAMTS13 Binds VWF Via its C-Terminal CUB2 Domain. Blood. 2004;104:126.
261. Nolasco LH, Turner NA, Bernardo A, et al. Hemolytic uremic syndrome-associated Shiga toxins promote endothelial-cell secretion and impair ADAMTS13 cleavage of unusually large von Willebrand factor multimers. Blood. 2005;106:4199-4209.
262. De Cristofaro R, Peyvandi F, Palla R, et al. Role of chloride ions in modulation of the interaction between von Willebrand factor and ADAMTS-13. J Biol Chem. 2005;280:23295-23302.
263. Dong JF, Moake JL, Nolasco L, et al. ADAMTS-13 rapidly cleaves newly secreted ultralarge von Willebrand factor multimers on the endothelial surface under flowing conditions. Blood. 2002;100:4033-4039.

264. Arya M, Anvari B, Romo GM, et al. Ultralarge multimers of von Willebrand factor form spontaneous high-strength bonds with the platelet glycoprotein Ib-IX complex: studies using optical tweezers. Blood. 2002;99:3971-3977.
265. Padilla A, Moake JL, Bernardo A, et al. P-selectin anchors newly released ultralarge von Willebrand factor multimers to the endothelial cell surface. Blood. 2004;103:2150-2156.
266. Crawley JT, Lam JK, Rance JB, Mollica LR, O'Donnell JS, Lane DA. Proteolytic inactivation of ADAMTS13 by thrombin and plasmin. Blood. 2005;105:1085-1093.
267. Sadler JE. Thrombomodulin structure and function. Thromb Haemost. 1997;78:392-395.
268. Bernardo A, Ball C, Nolasco L, Moake JF, Dong JF. Effects of inflammatory cytokines on the release and cleavage of the endothelial cell-derived ultralarge von Willebrand factor multimers under flow. Blood. 2004;104:100-106.
269. Studt JD, Hovinga JA, Antoine G, et al. Fatal congenital thrombotic thrombocytopenic purpura with apparent ADAMTS13 inhibitor: in vitro inhibition of ADAMTS13 activity by hemoglobin. Blood. 2005;105:542-544.
270. Moschcowitz E. Hyaline thrombosis of the terminal arterioles and capillaries: a hitherto underscribed disease. Proc N Y Pathol Soc. 1924;24:21-24.
271. Schulman I, Pierce M, Lukens A, Currimbhoy Z. Studies on thrombopoiesis. I. A factor in normal human plasma required for platelet production; chronic thrombocytopenia due to its deficiency. Blood. 1960;16:943-957.
272. Upshaw JD, Jr. Congenital deficiency of a factor in normal plasma that reverses microangiopathic hemolysis and thrombocytopenia. N Engl J Med. 1978;298:1350-1352.
273. Moake JL, Rudy CK, Troll JH, et al. Unusually large plasma factor VIII:von Willebrand factor multimers in chronic relapsing thrombotic thrombocytopenic purpura. N Engl J Med. 1982;307:1432-1435.
274. Rock G, Porta C, Bobbio-Pallavicini E. Thrombotic thrombocytopenic purpura treatment in year 2000. Haematologica. 2000;85:410-419.
275. Torok TJ, Holman RC, Chorba TL. Increasing mortality from thrombotic thrombocytopenic purpura in the United States--analysis of national mortality data, 1968-1991. Am J Hematol. 1995;50:84-90.
276. Furlan M, Lammle B. von Willebrand factor in thrombotic thrombocytopenic purpura. Thromb Haemost. 1999;82:592-600.
277. Rock GA, Shumak KH, Buskard NA, et al. Comparison of plasma exchange with plasma infusion in the treatment of thrombotic thrombocytopenic purpura. Canadian Apheresis Study Group. N Engl J Med. 1991;325:393-397.
278. Wallace DC, Lovric A, Clubb JS, Carseldine DB. Thrombotic thrombocytopenic purpura in four siblings. Am J Med. 1975;58:724-734.
279. Shinohara T, Miyamura S, Suzuki E, Kobayashi K. Congenital microangiopathic hemolytic anemia: report of a Japanese girl. Eur J Pediatr. 1982;138:191-193.
280. Wiznitzer A, Mazor M, Leiberman JR, Bar-Levie Y, Gurman G, Glezerman M. Familial occurrence of thrombotic thrombocytopenic purpura in two sisters during pregnancy. Am J Obstet Gynecol. 1992;166:20-21.
281. Saitoh H, Murakami H, Mori C. Upshaw-Schulman syndrome in two siblings. Acta Paediatr Jpn. 1990;32:373-376.
282. Barbot J, Costa E, Guerra M, et al. Ten years of prophylactic treatment with fresh-frozen plasma in a child with chronic relapsing thrombotic thrombocytopenic purpura as a result of a congenital deficiency of von Willebrand factor-cleaving protease. Br J Haematol. 2001;113:649-651.

283. George JN. How I treat patients with thrombotic thrombocytopenic purpura-hemolytic uremic syndrome. Blood. 2000;96:1223-1229.
284. Furlan M, Lammle B. Aetiology and pathogenesis of thrombotic thrombocytopenic purpura and haemolytic uraemic syndrome: the role of von Willebrand factor-cleaving protease. Best Pract Res Clin Haematol. 2001;14:437-454.
285. Savasan S, Lee SK, Ginsburg D, Tsai HM. ADAMTS13 gene mutation in congenital thrombotic thrombocytopenic purpura with previously reported normal VWF cleaving protease activity. Blood. 2003;101:4449-4451.
286. Matsumoto M, Kokame K, Soejima K, et al. Molecular characterization of ADAMTS13 gene mutations in Japanese patients with Upshaw-Schulman syndrome. Blood. 2004;103:1305-1310.
287. Uchida T, Wada H, Mizutani M, et al. Identification of novel mutations in ADAMTS13 in an adult patient with congenital thrombotic thrombocytopenic purpura. Blood. 2004.
288. Veyradier A, Lavergne JM, Ribba AS, et al. Ten candidate ADAMTS13 mutations in six French families with congenital thrombotic thrombocytopenic purpura (Upshaw-Schulman syndrome). J Thromb Haemost. 2004;2:424-429.
289. Licht C, Stapenhorst L, Simon T, Budde U, Schneppenheim R, Hoppe B. Two novel ADAMTS13 gene mutations in thrombotic thrombocytopenic purpura/hemolytic-uremic syndrome (TTP/HUS). Kidney Int. 2004;66:955-958.
290. Moake JL. Thrombotic microangiopathies. N Engl J Med. 2002;347:589-600.
291. Tsai MH, Tsai SL, Chen TC, Liaw YF. Ticlopidine-induced cholestatic hepatitis with anti-nuclear antibody in serum. J Formos Med Assoc. 2000;99:866-869.
292. Bennett CL, Connors JM, Carwile JM, et al. Thrombotic Thrombocytopenic Purpura Associated with Clopidogrel. N Engl J Med. 2000;342:1773-1777.
293. Furlan M, Robles R, Solenthaler M, Lammle B. Acquired Deficiency of von Willebrand Factor-Cleaving Protease in a Patient With Thrombotic Thrombocytopenic Purpura. Blood. 1998;91:2839-2846.
294. Tsai H-M, Lian EC-Y. Antibodies to von Willebrand Factor-Cleaving Protease in Acute Thrombotic Thrombocytopenic Purpura. N Engl J Med. 1998;339:1585-1594.
295. Veyradier A, Obert B, Houllier A, Meyer D, Girma JP. Specific von Willebrand factor-cleaving protease in thrombotic microangiopathies: a study of 111 cases. Blood. 2001;98:1765-1772.
296. Studt JD, Kremer Hovinga JA, Alberio L, Bianchi V, Lammle B. Von Willebrand factor-cleaving protease (ADAMTS-13) activity in thrombotic microangiopathies: diagnostic experience 2001/2002 of a single research laboratory. Swiss Med Wkly. 2003;133:325-332.
297. Vesely SK, George JN, Lammle B, et al. ADAMTS13 activity in thrombotic thrombocytopenic purpura-hemolytic uremic syndrome: relation to presenting features and clinical outcomes in a prospective cohort of 142 patients. Blood. 2003;102:60-68.
298. Scheiflinger F, Knobl P, Trattner B, et al. Nonneutralizing IgM and IgG antibodies to von Willebrand factor-cleaving protease (ADAMTS-13) in a patient with thrombotic thrombocytopenic purpura. Blood. 2003;102:3241-3243.
299. Studt JD, Hovinga JA, Radonic R, et al. Familial acquired thrombotic thrombocytopenic purpura: ADAMTS13 inhibitory autoantibodies in identical twins. Blood. 2004;103:4195-4197.
300. Rarick MU, Espina B, Mocharnuk R, Trilling Y, Levine AM. Thrombotic thrombocytopenic purpura in patients with human immunodeficiency virus

infection: a report of three cases and review of the literature. Am J Hematol. 1992;40:103-109.
301. Roy V, Rizvi MA, Vesely SK, George JN. Thrombotic thrombocytopenic purpura-like syndromes following bone marrow transplantation: an analysis of associated conditions and clinical outcomes. Bone Marrow Transplant. 2001;27:641-646.
302. Moake JL, Byrnes JJ. Thrombotic microangiopathies associated with drugs and bone marrow transplantation. Hematol Oncol Clin North Am. 1996;10:485-497.
303. George JN. The association of pregnancy with thrombotic thrombocytopenic purpura-hemolytic uremic syndrome. Curr Opin Hematol. 2003;10:339-344.
304. Caramaschi P, Riccetti MM, Pasini AF, Savarin T, Biasi D, Todeschini G. Systemic lupus erythematosus and thrombotic thrombocytopenic purpura. Report of three cases and review of the literature. Lupus. 1998;7:37-41.
305. Fontana S, Gerritsen HE, Kremer Hovinga J, Furlan M, Lammle B. Microangiopathic haemolytic anaemia in metastasizing malignant tumours is not associated with a severe deficiency of the von Willebrand factor-cleaving protease. Br J Haematol. 2001;113:100-102.
306. Mannucci PM, Karimi M, Mosalaei A, Canciani MT, Peyvandi F. Patients with localized and disseminated tumors have reduced but measurable levels of ADAMTS-13 (von Willebrand factor cleaving protease). Haematologica. 2003;88:454-458.
307. Mannucci PM, Canciani MT, Forza I, Lussana F, Lattuada A, Rossi E. Changes in health and disease of the metalloprotease that cleaves von Willebrand factor. Blood. 2001;98:2730-2735.
308. Loof AH, van Vliet HH, Kappers-Klunne MC. Low activity of von Willebrand factor-cleaving protease is not restricted to patients suffering from thrombotic thrombocytopenic purpura. Br J Haematol. 2001;112:1087-1088.
309. Moore JC, Hayward CP, Warkentin TE, Kelton JG. Decreased von Willebrand factor protease activity associated with thrombocytopenic disorders. Blood. 2001;98:1842-1846.
310. Remuzzi G, Galbusera M, Noris M, et al. von Willebrand factor cleaving protease (ADAMTS13) is deficient in recurrent and familial thrombotic thrombocytopenic purpura and hemolytic uremic syndrome. Blood. 2002;100:778-785.
311. Veyradier A, Obert B, Haddad E, et al. Severe deficiency of the specific von Willebrand factor-cleaving protease (ADAMTS 13) activity in a subgroup of children with atypical hemolytic uremic syndrome. J Pediatr. 2003;142:310-317.
312. Ono T, Mimuro J, Madoiwa S, et al. Severe secondary deficiency of von Willebrand factor-cleaving protease (ADAMTS13) in patients with sepsis-induced disseminated intravascular coagulation: its correlation with development of renal failure. Blood. 2006;107:528-534.
313. Bianchi V, Robles R, Alberio L, Furlan M, Lammle B. Von Willebrand factor-cleaving protease (ADAMTS13) in thrombocytopenic disorders: a severely deficient activity is specific for thrombotic thrombocytopenic purpura. Blood. 2002;100:710-713.
314. Matsumoto M, Yagi H, Ishizashi H, Wada H, Fujimura Y. The Japanese experience with thrombotic thrombocytopenic purpura-hemolytic uremic syndrome. Semin Hematol. 2004;41:68-74.
315. Studt JD, Bohm M, Budde U, Girma JP, Varadi K, Lammle B. Measurement of von Willebrand factor-cleaving protease (ADAMTS-13) activity in plasma: a multicenter comparison of different assay methods. J Thromb Haemost. 2003;1:1882-1887.

316. Tripodi A, Chantarangkul V, Bohm M, et al. Measurement of von Willebrand factor cleaving protease (ADAMTS-13): results of an international collaborative study involving 11 methods testing the same set of coded plasmas. J Thromb Haemost. 2004;2:1601-1609.
317. Favaloro EJ. Von Willebrand factor collagen-binding (activity) assay in the diagnosis of von Willebrand disease: a 15-year journey. Semin Thromb Hemost. 2002;28:191-202.
318. Furlan M, Lammle B. Assays of von Willebrand factor-cleaving protease: a test for diagnosis of familial and acquired thrombotic thrombocytopenic purpura. Semin Thromb Hemost. 2002;28:167-172.
319. Gerritsen HE, Turecek PL, Schwarz HP, Lammle B, Furlan M. Assay of von Willebrand factor (vWF)-cleaving protease based on decreased collagen binding affinity of degraded vWF: a tool for the diagnosis of thrombotic thrombocytopenic purpura (TTP). Thromb Haemost. 1999;82:1386-1389.
320. Pimanda JE, Chesterman CN, Hogg PJ. A perspective on the measurement of ADAMTS13 in thrombotic thrombocytopaenic purpura. Eur J Haematol. 2003;70:257-262.
321. Bohm M, Vigh T, Scharrer I. Evaluation and clinical application of a new method for measuring activity of von Willebrand factor-cleaving metalloprotease (ADAMTS13). Ann Hematol. 2002;81:430-435.
322. Kokame K, Nobe Y, Kokubo Y, Okayama A, Miyata T. FRETS-VWF73, a first fluorogenic substrate for ADAMTS13 assay. Br J Haematol. 2005;129:93-100.
323. Motto DG, Chauhan AK, Zhu G, et al. Shigatoxin triggers thrombotic thrombocytopenic purpura in genetically susceptible ADAMTS13-deficient mice. J Clin Invest. 2005;115:2752-2761.
324. Banno F, Kokame K, Okuda T, et al. Complete deficiency in ADAMTS13 is prothrombotic, but it alone is not sufficient to cause thrombotic thrombocytopenic purpura. Blood. 2006;107:3161-3166.
325. Chauhan AK, Motto DG, Lamb CB, et al. Systemic antithrombotic effects of ADAMTS13. J Exp Med. 2006;203:767-776.
326. Chion CK, Doggen CJ, Crawley JT, Lane DA, Rosendaal FR. ADAMTS13 and von Willebrand Factor and the risk of myocardial infarction in men. Blood. 2006.
327. Tsai HM, Sussman, II, Nagel RL. Shear stress enhances the proteolysis of von Willebrand factor in normal plasma. Blood. 1994;83:2171-2179.
328. Ginsburg D, Konkle BA, Gill JC, et al. Molecular basis of human von Willebrand disease: analysis of platelet von Willebrand factor mRNA. Proc Natl Acad Sci U S A. 1989;86:3723-3727.
329. Lyons SE, Cooney KA, Bockenstedt P, Ginsburg D. Characterization of Leu777Pro and Ile865Thr type IIA von Willebrand disease mutations. Blood. 1994;83:1551-1557.
330. Ribba AS, Voorberg J, Meyer D, Pannekoek H, Pietu G. Characterization of recombinant von Willebrand factor corresponding to mutations in type IIA and type IIB von Willebrand disease. J Biol Chem. 1992;267:23209-23215.
331. Hassenpflug WA, Budde U, Obser T, et al. Impact of mutations in the von Willebrand factor A2 domain on ADAMTS13-dependent proteolysis. Blood. 2006;107:2339-2345.
332. Kokame K, Matsumoto M, Fujimura Y, Miyata T. VWF73, a region from D1596 to R1668 of von Willebrand factor, provides a minimal substrate for ADAMTS-13. Blood. 2004;103:607-612.

333. Nishio K. Recombinant von Willebrand factor A1A2A3 domains and fragments thereof as substrates for ADAMTS-13 in healty controls and patients with thrombotic thrombocytopenic purpura (abstract). blood. 2003;102.
334. Kalafatis M, Rand MD, Mann KG. The mechanism of inactivation of human factor V and human factor Va by activated protein C. J Biol Chem. 1994;269:31869-31880.
335. Bertina RM, Koeleman BP, Koster T, et al. Mutation in blood coagulation factor V associated with resistance to activated protein C. Nature. 1994;369:64-67.
336. Monkovic DD, Tracy PB. Activation of human factor V by factor Xa and thrombin. Biochemistry. 1990;29:1118-1128.
337. Griffith MJ. The heparin-enhanced antithrombin III/thrombin reaction is saturable with respect to both thrombin and antithrombin III. J Biol Chem. 1982;257:13899-13302.

APPENDICES

APPENDIX I-OLIGONUCLEOTIDE PRIMERS

Table 1. Primers used for PCR amplification

	Primer forward	*Primer reverse*	*Ta (° C)*
VWF76	5' CACCAGCCAGGGTGACCGGGAGC 3'	5' CCTCTGCAGCACCAGGTCAGG 3'	55
VWF115	5' CACCGAGGCACAGTCCCAAAGGGGACAT 3'	5' CCTCTGCAGCACCAGGTCAGG 3'	60
VWF115-A3	5' CACCGAGGCACAGTCCCAAAGGGGACAT 3'	5' CTATCCAGAGCACAGTTTGTG 3'	62
VWFA2	5' CTTCTTGGTCAGCCAGGGTG 3'	5' CCTCGCAGCACCAGGTCAGG 3'	61

Table 2. Primers used for site-directed mutagenesis

	Primer forward	*Primer reverse*	*Ta (°C)*
R1583A	5' CACTGGGCTGGCCCTG**GC**GTACCTCTCTGACCAC 3'	5' GTGGTCAGAGAGGTAC**GC**CAGGGCCAGCCCAGTG 3'	60
D1587A	5' CCTGCGGTACCTCTCT**GC**CCACAGCTTCTTGGTCAG 3'	5' GCTGACCAAGAAGCTGTGG**GC**AGAGAGGTACCGCAGG 3'	60
D1614A	5' CGGAAATCCTGCCTCTG**C**TGAGATCAAGAGGCTGC 3'	5' GCAGCCTCTTGATCTCA**G**CAGAGGCAGGATTTCCG 3'	60
E1615A	5' GGAAATCCTGCCTCTGATG**C**GATCAAGAGGCTGCC 3'	5' GGAAATCCTGCCTCTGATG**C**GATCAAGAGGCTGCC 3'	60
E1617A	5' CCTGCCTCTGATGAGATC**GC**GAGGCTGCCTGGAGAC 3'	5' GTCTCCAGGCAGCCTC**GC**GATCTCATCAGAGGCAGG 3'	60
E1638A	5' CCCTAATGCCAACGTGCAGG**C**GCTGGAGAGGATTG 3'	5' CAATCCTCTCCAGC**G**CCTGCACGTTGGCATTAGGG 3'	60
E1640A	5' CCAACGTGCAGGAGCTGG**C**GAGGATTGGCTGG 3'	5' CCAGCCAATCCTC**G**CCAGCTCCTGCACGTTGG 3'	60
VWF115-A3 **	5' GGTGCTGCAGAGG**GC**C**GC**CTCCGGAGAGGGG 3'	5' CCCCTCTCCGGAG**GC**G**GC**CCTCTGCAGCAC 3'	60
R1597Q	5' CAGCCAGGGTGA**CCA**GGAGCAGGCGC 3'	5' GCGCCTGCTCC**TGG**TCACCCTGGCTG 3'	60
R1597W	5' CAGCCAGGGTGA**CTG**GGAGCAGGCGC 3'	5' GCGCCTGCTCC**CAG**TCACCCTGGCTG 3'	60
D1614G	5' GGAAATCCTGCCTCT**GGT**GAGATCAAGAGGCTG 3'	5' CAGCCTCTTGATCTC**ACC**AGAGGCAGGATTTCC 3'	60
I1628T	5' GGTGGTGCCC**ACT**GGAGTGGGCC 3'	5' GGCCCACTCC**AGT**GGGCACCACC 3'	60
G1629A	5' GGTGGTGCCCATT**CGA**GTGGGCCCTAATG 3'	5'-CATTAGGGCCCAC**TCG**AATGGGCACCACC-3'	60
E1638K	5'-GCCAACGTGCAG**AAG**CTGGAGAGGATTGG-3'	5'-CCAATCCTCTCCAG**CTT**CTGCACGTTGGC-3'	60

Table 3. Primers used for sequencing

	Primer forward	*Primer reverse*
T7	5' TAATACGACTCACTATAGGG 3'	5' TAGTTATTGCTCAGCGGTGG 3'

APPENDIX II-COMPOSITION OF BUFFERS

10 X DNA loading buffer

0.125% (w/v) xilene cyanol, 0.125% (w/v) bromophenol blue, 0.625% SDS (w/v), 20% (v/v) glycerol

10 X TBE buffer

0.89 M Tris-borate (pH 8.3), 20 mM EDTA. Prior to use, this was diluted to 1 x TBE buffer with purified water.

TE buffer

10 mM Tris (pH 8.0), 1 mM EDTA

SDS-PAGE Electrophoresis buffer

25 mM Tris-HCl (pH 8.3) 192 mM glycine and 0.1% (w/v) SDS

2 x Protein Loading buffer

150 mM Tris-HCl (pH 6.8), 20% (v/v) glycerol, 4% (w/v) SDS, 0.125% (w/v) bromophenol blue

Transfer buffer

25 mM Tris-HCl (pH 8.3), 192 mM glycine, 20% (v/v) methanol

PBS buffer

Dissolve 5 PBS tablets (Sigma) to 1 litre of distilled H_2O

APPENDIX III-BROTH AND AGAR

LB (Luria-Bertani) broth

1% (w/v) bacto-tryptone, 0.5% (w/v) bacto-yeast extract, 1% (w/v) NaCl

LB agar

1% (w/v) bacto-tryptone, 0.5% (w/v) bacto-yeast extract, 1% (w/v) NaCl, 1.5% bacto-agar

SOC medium

2% (w/v) bacto-tryptone, 0.5% (w/v) bacto-yeast extract, 10 mM NaCl, 2.5 mM KCl, 10 mM $MgCl_2$, 10 mM $MgSO_4$, 20 mM Glucose

2X YT broth

1.6% (w/v) bacto-tryptone, 1% (w/v) bacto-yeast extract and 0.5% (w/v) NaCl

The components of each medium are dissolved in ultra-pure water and autoclaved.

COPY OF THE PUBLICATION ARISING FROM THE WORK IN THIS THESIS

THE JOURNAL OF BIOLOGICAL CHEMISTRY VOL. 281, NO. 3, pp. 1555–1563, January 20, 2006
© 2006 by The American Society for Biochemistry and Molecular Biology, Inc. Printed in the U.S.A.

ADAMTS13 Substrate Recognition of von Willebrand Factor A2 Domain*

Received for publication, July 29, 2005, and in revised form, September 22, 2005 Published, JBC Papers in Press, October 12, 2005, DOI 10.1074/jbc.M508316200

Sara Zanardelli, James T. B. Crawley[1], Chan K. N. Chan Kwo Chion, Jonathan K. Lam, Roger J. S. Preston, and David A. Lane

From the Department of Haematology, Imperial College London, London W12 ONN, United Kingdom

ADAMTS13 controls the multimeric size of circulating von Willebrand factor (VWF) by cleaving the Tyr^{1605}–Met^{1606} bond in the A2 domain. To examine substrate recognition, we expressed in bacteria and purified three A2 (VWF76-(1593–1668), VWF115-(1554–1668), VWFA2-(1473–1668)) and one A2-A3 (VWF115-A3-(1554–1874)) domain fragments. Using high pressure liquid chromatography analysis, the initial rates of VWF115 cleavage by ADAMTS13 at different substrate concentrations were determined, and from this the kinetic constants were derived (K_m 1.61 μM; k_{cat} 0.14 s^{-1}), from which the specificity constant k_{cat}/K_m was calculated, 8.70×10^4 M^{-1} s^{-1}. Similar values of the specificity constant were obtained for VWF76 and VWF115-A3. To identify residues important for recognition and proteolysis of VWF115, we introduced certain type 2A von Willebrand disease mutations by site-directed mutagenesis. Although most were cleaved normally, one (D1614G) was cleaved ~8-fold slower. Mutagenesis of additional charged residues predicted to be in close proximity to Asp^{1614} on the surface of the A2 domain (R1583A, D1587A, D1614A, E1615A, K1617A, E1638A, E1640A) revealed up to 13-fold reduction in k_{cat}/K_m for D1587A, D1614A, E1615A, and K1617A mutants. When introduced into the intact VWFA2 domain, proteolysis of the D1587A, D1614A, and E1615A mutants was also slowed, particularly in the presence of urea. Surface plasmon resonance demonstrated appreciable reduction in binding affinity between ADAMTS13 and VWF115 mutants (K_D up to ~1.3 μM), compared with VWF115 (K_D 20 nM). These results demonstrate an important role for Asp^{1614} and surrounding charged residues in the binding and cleavage of the VWFA2 domain by ADAMTS13.

Von Willebrand factor (VWF)[2] is a large multimeric plasma glycoprotein that mediates tethering and adhesion of circulating platelets at sites of vascular injury (1). Following endothelial damage, plasma VWF binds to the exposed sub-endothelial collagen (2). Once immobilized, the shear forces of the flowing blood induce a conformational transition that unravels the VWF molecule (3). This in turn exposes the binding sites for glycoprotein (Gp)Ibα, part of the GpIb-IX-V receptor on the surface of circulating platelets that confer platelet-tethering function (4). Once tethered, platelets become activated and subsequently present GpIIb/IIIa on their surface, which makes a tighter, more stable interaction with both VWF and fibrinogen. Activated platelets provide the phosphatidylserine-rich surface critical for the assembly of the procoagulant enzyme complexes that lead to the generation of thrombin (5).

VWF is expressed by endothelial cells and megakaryocytes (6). It is synthesized as 250-kDa monomers, which undergo intracellular processing-glycosylation, multimerization, and propeptide removal-that leads to formation of mature VWF multimers (7). Although much of endothelial VWF is constitutively secreted into the blood as multimers of varying size, a proportion is stored either within Weibel-Palade bodies in endothelial cells or within α-granules in platelets (8). These stored pools, which can be released upon specific stimulation, contain predominantly hyper-reactive "ultra-large" VWF that can exceed 2×10^4 kDa.

A wide range of VWF multimers (500–20,000 kDa) are found in normal plasma that differ only by the number of constituent VWF units. The largest VWF multimers unravel more readily in response to shear forces and contain more platelet binding sites. These species therefore confer the greatest hemostatic potential. The size of plasma VWF, and thus its platelet-tethering function, is regulated to prevent aberrant/spontaneous platelet-rich thrombus formation. VWF multimeric size is modulated by the plasma metalloproteinase ADAMTS13, which cleaves at a single site in the VWF A2 domain between Tyr^{1605} and Met^{1606} (9). This proteolysis can only proceed once VWF has been unraveled, either by rheological forces or *in vitro* in the presence of denaturants, both of which induce the exposure of the A2 domain scissile bond (10). Physiologically, this occurs upon VWF secretion from endothelial cells, limiting the thrombogenic potential of newly secreted ultra-large VWF by converting it into smaller multimeric forms (11). The nature of ADAMTS13 recognition of the A2 domain is poorly understood. In part, this is because of complex folding and interdependence of the A1-A2-A3 domains. This has been illustrated by proteolysis studies conducted with isolated domain fragments and certain VWF mutations that confer type 2A (group II) von Willebrand disease (VWD) (12–14). The latter are proximate or within the A2 domain and manifest enhanced ADAMTS13-dependent VWF proteolysis. This is thought to be because of structural changes that lead to constitutive/enhanced exposure of the A2 domain cleavage site (15).

Because of the uncertainty surrounding A2 domain recognition mechanisms by ADAMTS13, we have prepared both wild-type and variant A2 domain fragments that span the Tyr^{1605}-Met^{1606} cleavage site. For the first time, the cleavage of these by ADAMTS13 has been evaluated kinetically under normal physiological ionic conditions. We show that critical residues in the vicinity of the cleavage site are required for optimum cleavage and form part of an ADAMTS13 docking site within the A2 domain.

EXPERIMENTAL PROCEDURES

Expression and Purification of Recombinant ADAMTS13 and VWF Fragments—Recombinant human ADAMTS13 with a C-terminal Myc/His_6 tag was expressed and purified as previously described (16). For

* This work was supported by British Heart Foundation grants (to D. A. L. and J. T. B. C.). The costs of publication of this article were defrayed in part by the payment of page charges. This article must therefore be hereby marked "*advertisement*" in accordance with 18 U.S.C. Section 1734 solely to indicate this fact.

[1] To whom correspondence should be addressed: Dept. of Haematology, Faculty of Medicine, Imperial College London, 5th Floor, Commonwealth Bldg., Hammersmith Hospital Campus, Du Cane Rd., London W12 0NN, UK. Tel.: 44-20-8383-2297; Fax: 44-20-8383-2296; E-mail: j.crawley@imperial.ac.uk.

[2] The abbreviations used are: VWF, von Willebrand factor; HPLC, high pressure liquid chromatography; VWD, von Willebrand disease; Gp, glycoprotein; SPR, surface plasmon resonance; Tricine, *N*-[2-hydroxy-1,1-bis(hydroxymethyl)ethyl]glycine.

Downloaded from www.jbc.org at Imperial College London on November 2, 2006

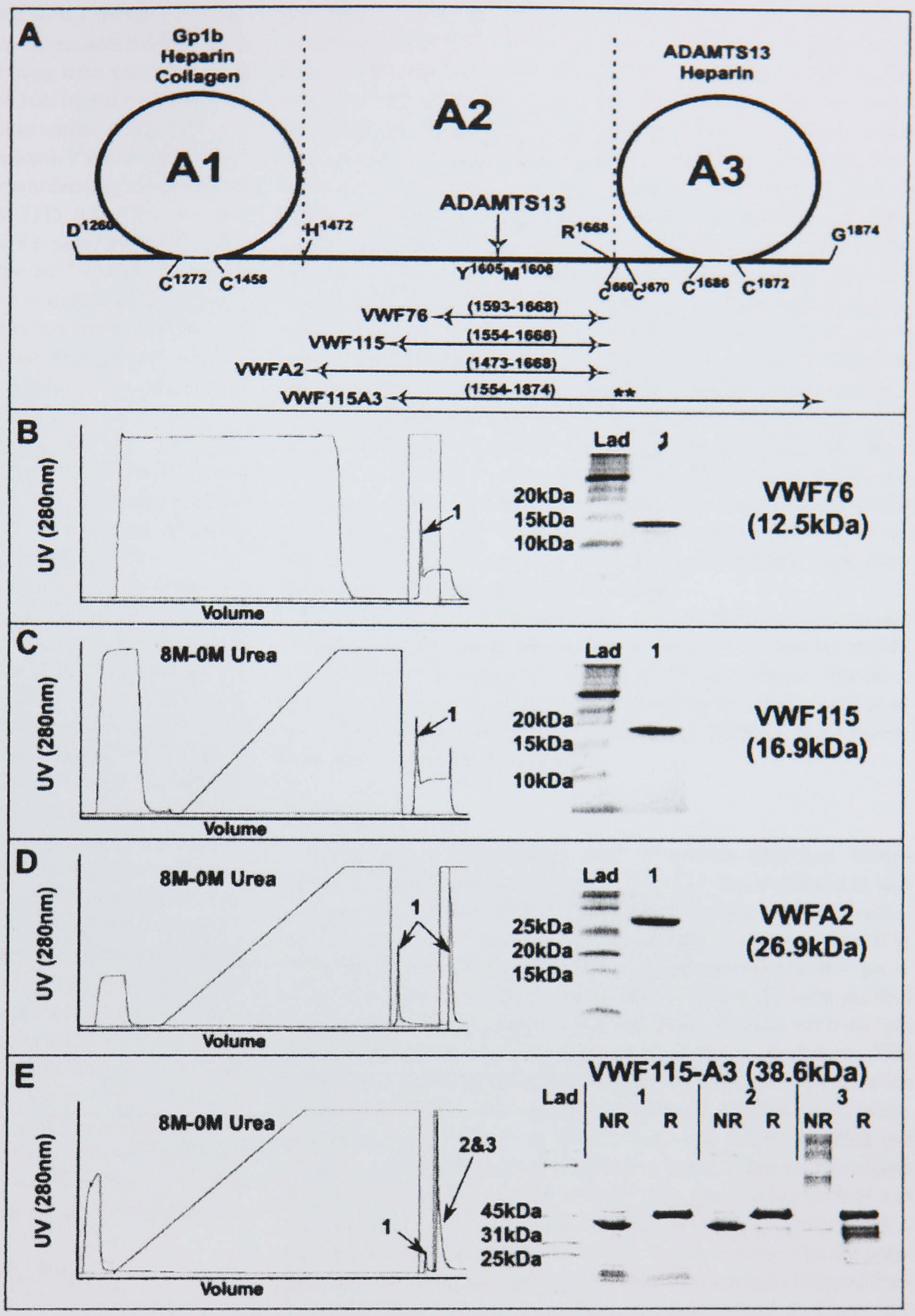


FIGURE 1. **Purification of recombinant VWF76, VWF115, VWFA2, and VWF115-A3.** *A*, diagram of the VWF A1A2A3 domains. A1 and A3 each contain paired cysteines, which are marked as are the amino acids at the boundary of each domain. Major ligands for each domain are highlighted. The ADAMTS13 cleavage site (Y^{1605}-M^{1606}) lies in the middle of the A2 domain. *Labeled arrows* represent the recombinant VWF fragments (*VWF76*, *VWF115*, *VWFA2*, and *VWF115-A3*) expressed in *E. coli*. All had an N-terminal polyhistidine/Xpress epitope tag. The VWF numbering of each substrate is given. In VWF115-A3, the 2 adjacent cysteine residues at 1669 and 1670 (**) were mutated to alanine. *B*, purification of VWF76 from cytoplasmic fraction extracted from transformed Rosetta *E. coli*. Chromatogram of VWF76 purification is shown. The eluted peak (*1*) was analyzed by SDS-PAGE and Coomassie staining. VWF76 was visualized as a single 12.5-kDa band, corresponding to its predicted mass. *C*, purification and refolding of VWF115 from inclusion body fraction extracted from transformed Rosetta *E. coli*. Inclusion bodies were solubilized with 8 M urea and refolded on a nickel-chelating column using an 8–0 M urea linear gradient. Chromatogram of VWF115 purification is shown. The eluted peak (*1*) was analyzed by SDS-PAGE and Coomassie staining. VWF115 migrated as a single 16.9-kDa band corresponding to its predicted mass. *D*, purification and refolding of VWFA2 from bacterial inclusion bodies. Inclusion bodies were solubilized with 8 M urea and refolded as for VWF115. Chromatogram of VWFA2 purification is shown. The eluted peak and stripped peaks (*1*) were dialysed and soluble material combined and analyzed by SDS-PAGE and Coomassie staining. As predicted, VWFA2 migrated as a 26.9-kDa band. *E*, purification and refolding of VWF115-A3 from Rosetta-Gami *E. coli* inclusion bodies. Insoluble material was solubilized and purified as for VWF115 and VWFA2. The eluted peak (*1*) and peaks stripped with 6 M guanidine/EDTA (2/3) were dialysed into 20 mM Tris (pH 7.8). The eluted peak (*1*), soluble stripped fraction (*2*), and insoluble precipitate after dialysis (*3*) were analyzed by reducing (*R*) and non-reducing (*NR*) SDS-PAGE and Coomassie staining. Under non-reducing conditions, soluble VWF115-A3 in *1* and *2* was visualized as a single 38.6-kDa band corresponding to its predicted mass. Correctly folded, monomeric VWF115-A3 was obtained within *fractions 1* and *2*. The presence of the disulfide bond was demonstrated by the band shift seen under reducing conditions. The insoluble precipitate contained predominantly VWF115-A3 polymers of higher molecular mass (*3-NR*).

surface plasmon resonance (SPR) and kinetic analysis experiments, an additional gel filtration step, using a Sephadex 26/10 column (Amersham Biosciences), was employed to obtain higher purity ADAMTS13.

The coding regions for different VWF A domain fragments (VWF76, Ser^{1593}-Arg^{1668}; VWF115, Glu^{1554}-Arg^{1668}; VWF115-A3, Glu^{1554}-Glu^{1874}; VWFA2, Met^{1473}-Arg^{1668}) were PCR amplified from the human VWF cDNA using *Pfx* high fidelity DNA polymerase (Invitrogen) according to the manufacturer's instructions. Fragments were cloned into the bacterial expression vector pET100/D-TOPO (Invitrogen), which fuses a His_6 and Xpress epitope tag to the N terminus of cloned sequences. As the VWF A3 domain contains two disulfide bonds, the adjacent paired cysteines at positions 1669 and 1670, at the start of the A3 domain, were mutated to alanine using the QuikChange XL kit (Stratagene). This approach improved yields of VWF115-A3 and ensured that the conserved A domain disulfide bond between Cys^{1686}-Cys^{1872} was correctly paired. Certain type 2A VWD mutations (R1597W, R1597Q, D1614G, I1628T, G1629R, E1638K) and specific charged residue substitutions (R1583A, D1587A, D1614A, E1615A, K1617A, E1638A, E1640A) were introduced into VWF115 and VWFA2 sequences using the QuikChange XL kit (Stratagene). All vectors were verified by sequencing.

VWF76, VWF115, and VWFA2 constructs were expressed in Rosetta *Escherichia coli* cells (Novagen, Nottingham, UK). VWF115-A3 was expressed in Rosetta-Gami *E. coli* (Novagen), which allows cytoplasmic disulfide bond formation. Transformed bacteria were grown in 2× yeast tryptone cultures at 37 °C with shaking. Once in log-phase growth,

Downloaded from www.jbc.org at Imperial College London on November 2, 2006

recombinant protein expression was induced with 1 mM isopropyl-β-D-thiogalactoside for 16 h. Bacteria were harvested, and soluble (cytoplasmic) or insoluble (inclusion body) fractions were prepared using BugBuster reagent (Novagen). Recombinant His-tagged proteins were purified on an ÄKTA FPLC (Amersham Biosciences) using Ni^{2+}-HiTrap-chelating columns (Amersham Biosciences). VWF76 was purified from the soluble fraction according to the manufacturer's instructions and eluted with 500 mM imidazole. VWF115-A3, VWF115, and VWFA2 inclusion bodies were solubilized in 8 M urea/20 mM Tris-HCl (pH 7.8)/50 mM imidazole and bound to the Ni^{2+}-chelating column. Protein refolding was achieved using an 8–0 M urea linear gradient (1 ml/min for 40 min). Refolded, soluble material was eluted with 500 mM imidazole. Misfolded, precipitated protein was stripped from the column with 6 M guanidine/0.5 M EDTA. All recombinant proteins (eluted and stripped) were dialyzed into 20 mM Tris (pH 7.8) overnight at 4 °C. For VWFA2 and VWF115-A3, the stripped material was refolded by this process. Thereafter, soluble and insoluble protein fractions were separated by centrifugation. The purity of each recombinant protein was assessed by SDS-PAGE and Coomassie staining and quantified using a BCA total protein assay kit (Perbio, Cramlington, UK).

Cleavage of VWF Fragments by ADAMTS13—For time course reactions, recombinant ADAMTS13 (final reaction concentration 5–16.5 nM) was preincubated without substrate at 37 °C for 30 min in reaction buffer (final reaction concentrations 20 mM Tris, pH 7.8/150 mM NaCl/5 mM $CaCl_2$). In preliminary experiments, VWF76, VWF115, VWFA2, or VWF115-A3 were added as final concentrations of 4–8 μM to start each reaction. For analyses of the intact A2 domain, reactions were performed in the presence and absence of 1 M urea. At different time points, 65-μl sub-samples were removed and stopped with EDTA. 15 μl were analyzed by SDS-PAGE (16.5% Tris-Tricine gel; Invitrogen) and Coomassie staining. The remaining 50 μl were analyzed by HPLC. Samples were loaded on a BioBasic C4 column (Thermo Electron, Runcorn, UK), and the full-length and cleaved peptides were eluted/resolved using a specific acetonitrile gradient (20–55% for VWF76, 25–45% for VWF115, 25–60% for VWFA2, 20–65% for VWF115-A3). Mass spectrometry or N-terminal sequencing (Alta Bioscience, Edgbaston, UK) was performed to identify the polypeptide in each eluted peak and establish the precise site of proteolysis. For the determination of the specificity constant, low substrate concentrations $<K_m$ were used (250–500 nM substrate/5.5 nM ADAMTS13). Unicorn analysis software was used to calculate the areas under the peaks of the full-length and cleaved fragments. The measure of the catalytic efficiency, k_{cat}/K_m, was determined using Enzfitter software by fitting the data to Equation 1

$$k_{cat}/K_m = \frac{-\ln(1 - [AP]/[APf])}{et}$$

where $[AP]$ is the area under the cleavage product peak 1 curve at time t, $[APf]$ is the area under cleavage product peak 1 curve after complete cleavage, e is ADAMTS13 concentration, t is time. For individual determination of the K_m, V_{max}, and k_{cat}, the initial rate of proteolysis of VWF115 (after 5–10 min) was measured at varying substrate concentrations (100 nM-50 μM) as outlined above. Data were transformed into Michaelis-Menten and Lineweaver-Burk plots, and the catalytic constants were derived using Prism 4 software (GraphPad, San Diego, CA).

Surface Plasmon Resonance—SPR, using a dual flowcell BIAcore X biosensor system (BIAcore, Eyeworth, UK), was employed for analysis of the interaction between ADAMTS13 and different VWF115 variants. Two different SPR approaches were used. In each case, the surface of a carboxymethylated dextran (CM5) sensor chip (BIAcore) was activated with 0.4 M 1-ethyl-3-(3-dimethylaminopropyl)carbodiimide and 0.1 M *N*-hydroxysuccinimide, according to the manufacturer's instructions. First, ~600 response units of wild-type or variant VWF115 was covalently immobilized by amine coupling to one flow cell. To control for nonspecific binding, 600 response units of human endothelial protein C receptor was immobilized onto the other flow cell. All free reactive surface groups on both flow cells were blocked using 1 M ethanolamine. Different concentrations (10–137 nM) of ADAMTS13 in HBS-P buffer (BIAcore) were injected over both flow cells at 30 μl/min, contact time 1–2 min. After each injection, any bound ADAMTS13 was stripped with 10 mM NaOH prior to subsequent injections. Data analysis was performed using the BIAevalutaion software 3.0 (BIAcore), which allowed determination of k_a, k_d, and K_D values by fitting the derived sensograms to 1:1 Langmuir model. For the second approach, ~8000 response units of ADAMTS13 or anti-endothelial protein C receptor antibody (control) were immobilized to respective flow cells of CM5 chips, as above. Various concentrations (80 nM-1 μM) of VWF115, or VWF115 variants, in HBS-P buffer (BIAcore) were injected over both flow cells at 30 μl/min. The chip surface was regenerated with 10 mM NaOH as before. Using this approach, data were analyzed using a heterogeneous ligand (parallel reaction) model.

Modeling of VWF A2 Domain—The VWF A2 domain was computer modeled using its sequence homology to the VWF A3 domain and the coordinates for the crystal structure of this domain (Protein Data Bank code 1atz_A), according to the method outlined by Sutherland *et al.* (17). Models were manipulated using Protein Explorer (www.molvis.sdsc.edu/protexpl/frntdoor.html).

RESULTS

Purification of Recombinant VWF Fragments—Different human VWF A2 domain substrate fragments (Fig. 1*A*) were expressed in, and purified from, bacteria. VWF76 was purified from the soluble, cytoplasmic fraction by Ni^{2+}-chelating column affinity chromatography (Fig. 1*B*). SDS-PAGE and Coomassie staining demonstrated a purified product of 12.5 kDa. VWF115, VWFA2, and VWF115-A3 were purified from inclusion body preparations. Refolding of these proteins was achieved using an 8–0 M urea linear gradient during purification. This technique produced high yields of soluble VWF115 and VWFA2 of the correct predicted size (16.9 and 26.9 kDa, respectively) that were essentially pure (Fig. 1, *C* and *D*). VWF115-A3 was initially purified and refolded similarly. However, after elution a relatively low yield of soluble material was purified (Fig. 1*E*, *lane 1*). The precipitated protein was stripped from the column and refolded by dialysis, yielding higher amounts of soluble material (*lane 2*) than the on-column refolded preparation. The eluted material and the refolded/solubilized stripped fraction obtained after dialysis contained a product of 38.6 kDa (*lanes 1NR* and *2NR*). The presence of the disulfide bond between Cys^{1686} and Cys^{1872} was confirmed by the band shift upon reduction of this material (*lanes 1R* and *2R*). The insoluble material after dialysis contained VWF115-A3 polymers arising through intermolecular disulfide bond formation (*lane 3*) and was discarded.

Proteolysis of VWF76, VWF115, and VWF115-A3—To first visualize the capability of ADAMTS13 to proteolyze each of the recombinant A2 domain fragment substrates, recombinant ADAMTS13 was incubated at 37 °C with either VWF76, VWF115, or VWF115-A3 in the presence of physiological concentrations of Ca^{2+} and NaCl. Sub-samples were stopped between 0 and 6 h and analyzed by SDS-PAGE and Coomassie staining to give a qualitative assessment of each reaction (Fig. 2, *A–C*). In each case, only the full-length substrate band was visible at 0 h. Thereafter, the intensity of this band diminished and two smaller cleavage

Downloaded from www.jbc.org at Imperial College London on November 2, 2006

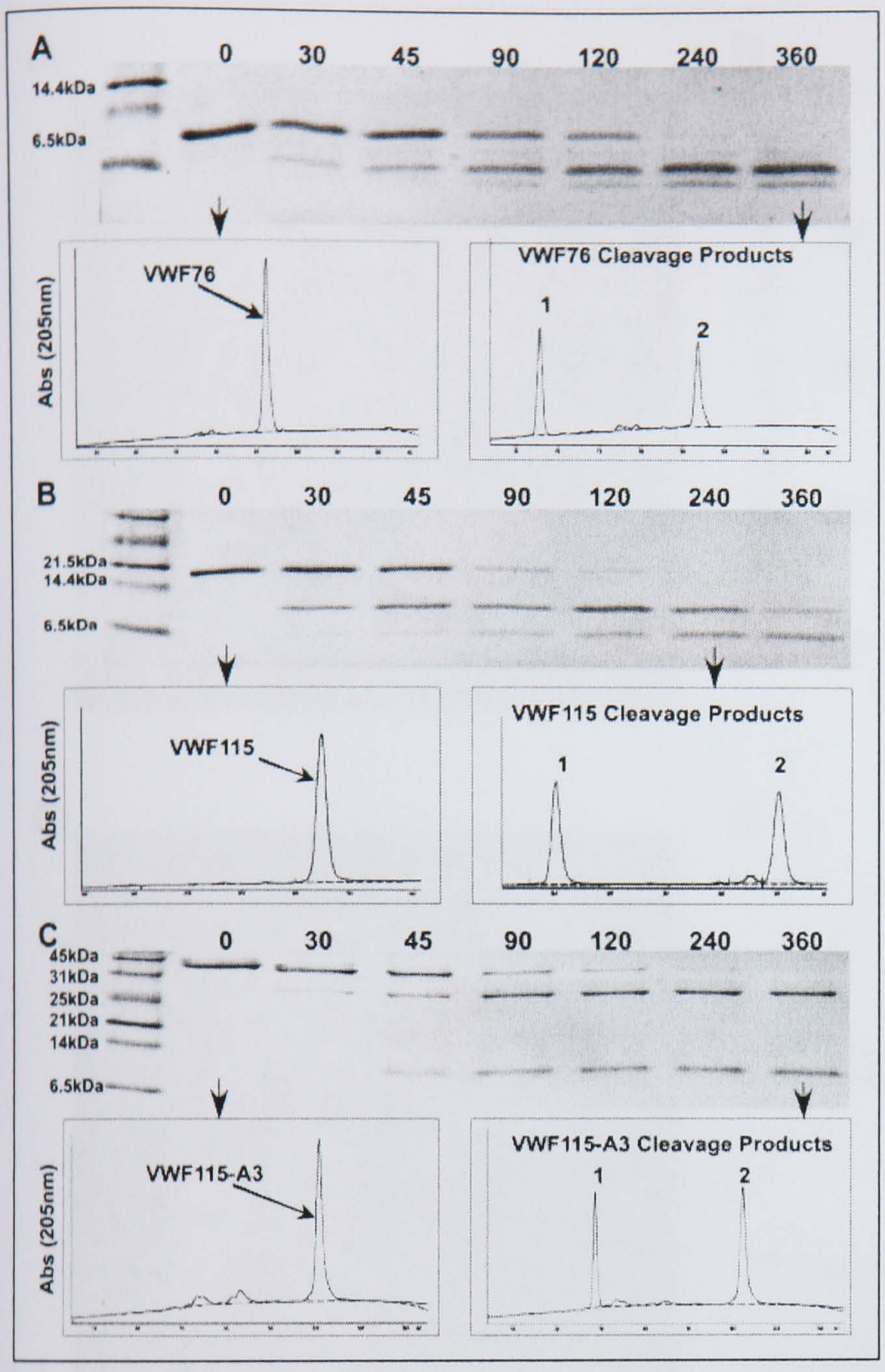


FIGURE 2. **Analysis of VWF76, VWF115, and VWF115-A3 proteolysis by ADAMTS13.** VWF76 (*A*), VWF115 (*B*), and VWF115-A3 (*C*) were incubated with ADAMTS13 as outlined under "Experimental Procedures." At various time points (0–6 h), sub-samples were stopped with EDTA and analyzed by SDS-PAGE/Coomassie staining and by HPLC, using a BioBasic C4 column. In each case (*A–C*), both techniques resolved the full-length substrate from the two cleavage products generated by ADAMTS13 proteolysis. Using the area under peak 1 as a measure of the extent of substrate proteolysis, this technique enabled quantification of the extent of proteolysis at each time point.

product bands appeared. In each case, these bands corresponded to the predicted molecular masses of fragments generated following cleavage at the Tyr^{1605}–Met^{1606} bond. N-terminal sequencing was performed upon the smallest cleavage product and confirmed that proteolysis had occurred between the Tyr^{1605}–Met^{1606} bond. Visually, VWF76, VWF115, and VWF115-A3 appeared to be proteolyzed by ADAMTS13 at similar rates. Parallel samples were also analyzed by HPLC. The resolution of the full-length substrate from the two cleavage fragments (*peaks 1* and *2*) arising from proteolysis (Fig. 2) of each different substrate allowed precise quantification of the extent of cleavage at each time point, confirming that the rates of proteolysis of VWF76, VWF115, and VWF115-A3 were, as indicated by the Coomassie staining, very similar (not shown).

To confirm specific proteolysis by ADAMTS13 and to identify each peak, cleavage product fractions were collected and analyzed by mass spectrometry. For all substrates, peak 1 corresponded to the tagged N-terminal cleavage product up to Tyr^{1605}. Peak 2 corresponded to the C-terminal fragment, in each case starting at Met^{1606}.

Type 2A VWD Mutations and ADAMTS13 Proteolysis—The scissile bond in VWF is predicted from a homology model (17) to be located in the center of the folded A2 domain (Fig. 3*A*). Given that VWF is the only known substrate for ADAMTS13 and that it is proteolyzed at just a single site, we hypothesized that other A2 domain amino acids that flank this site dictate the specificity of ADAMTS13 for the 1605–1606 bond. As an initial step toward identifying A2 domain residues that influence VWF proteolysis, we individually introduced six type 2A VWD mutations (see www.sheffield.ac.uk/vwf/) into the VWF115 construct (Fig. 3*A*). By mutating VWF115, which unlike the intact A2 domain naturally adopts a conformation that is permissive to ADAMTS13 proteolysis, the influence of specific mutations upon substrate specificity (as opposed to effects upon overall A2 domain structure) could be assessed under physiological ionic conditions. HPLC analysis of the proteolysis of VWF115 and VWF115 type 2A mutants (R1597W, R1597Q, D1614G, I1628T, G1629R, and E1638K) demonstrated that most of these mutations (R1597W, R1597Q, I1628T, and G1629R) had little or no effect upon VWF115 proteolysis (Fig. 3*B*). However, the E1638K mutant was proteolyzed slightly slower than VWF115, and the D1614G mutant was cleaved ~8 times slower (Fig. 3*B*). As Glu^{1638} and Asp^{1614} are charged residues that are predicted to be located in close proximity to each other on the surface of the VWF A2 domain homology model, we hypothesized that such residues might comprise part of an ADAMTS13 interaction site. Using this model, we subsequently identified additional acidic or basic amino acids predicted to lie on the surface of the A2 domain in the vicinity of Asp^{1614} and Glu^{1638} (Fig. 3*C*) and individually mutated each residue (Arg^{1583}, Asp^{1587}, Asp^{1614}, Glu^{1615}, Lys^{1617}, Glu^{1638}, Glu^{1640}) in VWF115 to alanine (Fig. 3*D*).

Kinetic Analysis of VWF76, VWF115, VWF115-A3, and VWF115 Charged Mutant Proteolysis—As a qualitative assessment of the relative ability of ADAMTS13 to proteolyze each of the charged residue mutants compared with the wild-type VWF76, VWF115, and VWF115-A3 substrates, we analyzed cleavage reactions by SDS-PAGE and Coomassie staining (Fig. 4*A*). From these gels, it seemed as if all of the mutants exhibited reduced rates of proteolysis. However, the concentrations of substrates needed to facilitate visualization by gel staining were high. To perform kinetic analysis of proteolysis for different substrates, it was necessary to monitor cleavage using substrate concentrations below the K_m for the reaction. Consequently, we determined the individual kinetic constants (K_m, k_{cat}) of VWF115 by measuring the initial rates of proteolysis at different concentrations (100 nM-50 μM). For the ADAMTS13-dependent proteolysis of VWF115 ($n = 4$), we derived a k_{cat} of $0.14 \pm 0.06\ s^{-1}$. The K_m for this reaction was determined to be $1.61 \pm 0.47\ \mu M$, from which a value for the specificity constant (catalytic efficiency, k_{cat}/K_m) of $8.70 \times 10^4\ M^{-1}\ s^{-1}$ could be derived.

For separate determination of the catalytic efficiency of VWF115, repeated time course experiments were performed using low substrate concentrations (250–500 nM). Repeated time course experiments ($n = 8$) gave a mean value of $7.83 \times 10^4\ M^{-1}\ s^{-1}$ for k_{cat}/K_m (Table 1). Confirmation of the pseudo-first order conditions was obtained by deriving the same k_{cat}/K_m value for VWF115 proteolysis at both 250 and 500 nM. Determination of k_{cat}/K_m for VWF76 and VWF115-A3 gave values of $6.39 \times 10^4\ M^{-1}\ s^{-1}$ and $6.70 \times 10^4\ M^{-1}\ s^{-1}$, respectively (Table 1). These kinetic data confirmed that the VWFA3 domain does not significantly contribute to the rate of A2 domain proteolysis, despite containing an ADAMTS13 binding site (18).

The contribution of each selected charged amino acid to VWF proteolysis was assessed by determination of the catalytic efficiency of all the mutant VWF115 substrates at 500 nM (Fig. 4*C* and Table 1). The rate

Downloaded from www.jbc.org at Imperial College London on November 2, 2006

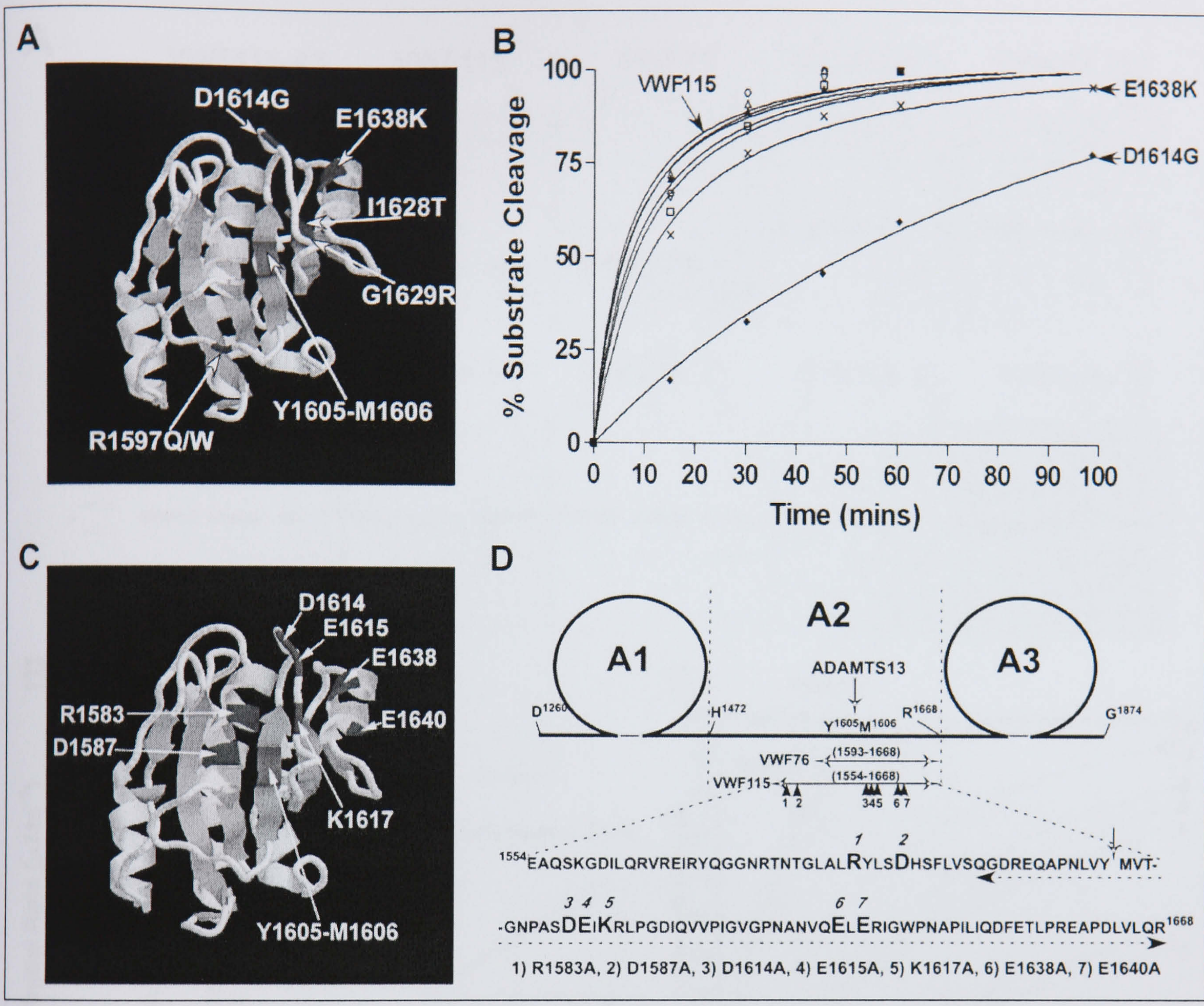


FIGURE 3. **Mutagenesis of VWF115.** *A*, predicted model of the VWF A2 domain. The Tyr[1605]–Met[1606] scissile bond in the center of the A2 domain is highlighted in *green*. The positions of certain type 2A (group II) VWD mutations that were introduced into VWF115 are labeled and highlighted in *red*. *B*, VWF115 and VWF115 type 2A mutants (R1597W, R1597Q, D1614G, I1628T, G1629R, E1638K) were proteolyzed with 10 nM ADAMTS13 and time course reactions analyzed by HPLC and represented graphically as in *panel B*). Although VWF115 and the R1597W, R1597Q, I1628T, and G1629R mutants were proteolyzed at very similar rates, the VWF115(E1638K) mutant was cleaved slightly slower. The VWF115(D1614G) mutant was proteolyzed at a markedly slower rate. *C*, predicted model of the VWF A2 domain. The Tyr[1605]–Met[1606] scissile bond in the center of the A2 domain is highlighted in *green*. The positions of the acidic/basic amino acids predicted to form a charged patch on the surface of the A2 domain in the vicinity of the most affected type 2A VWD mutants at Asp[1614] and Glu[1638] are highlighted in *red*. *D*, diagram of the VWF A1A2A3 domains. VWF76 and VWF115 regions are marked by *arrows*. The single letter amino acid sequence of VWF115 is given (VWF76 sequence is underlined with a *dashed arrow*). The ADAMTS13 cleavage site is marked (⇓). Locations of acidic and basic amino acids mutated to alanine and predicted to form a charged patch on the surface of the VWF A2 domain are highlighted (1–7).

of proteolysis of the R1583A mutant was not significantly different from that of VWF115, suggesting that this residue is not important for cleavage. Mutation of Glu[1638] and Glu[1640] induced a mild (2–3-fold) reduction in catalytic efficiency. The most affected (>12-fold reduction) single mutant was D1587A, the k_{cat}/K_m of which was $0.64 \pm 0.10 \times 10^4$ M^{-1} s^{-1}. The k_{cat}/K_m for K1617A, D1614A, and E1615A, which are predicted to lie on the same surface-exposed loop, were 1.90, 1.36, and 1.13×10^4 M^{-1} s^{-1}, respectively. These results implied that this loop might play an important role in the cleavage reaction. Consequently, we generated a triple mutant DEK1614/5/7AAA) containing all 3 residues substituted for alanine. Whereas individually these mutations caused a 4–7-fold reduction in k_{cat}/K_m, in combination the catalytic efficiency was >13-fold less than wild-type VWF115, implying that the amino acids in this charged loop may act in synergy.

Influence of D1587A, D1614A, and E1615A upon VWFA2 Proteolysis—To test whether the effects of the above mutations were maintained in a fully folded A2 domain, we introduced the most affected single charged mutants into the whole A2 domain. A variety of VWF A2 domain mutations appear to alter the conformation of the domain, such that the scissile bond is more readily exposed and thus more accessible for ADAMTS13 cleavage under normal physiological ionic conditions. Therefore, this approach also served to ascertain whether the most affected charged residue mutants (D1587A, D1614A, E1615A) induced gross structural changes. Despite using increased concentrations of ADAMTS13 (16.5 nM) in the absence of a denaturant, the intact wild-type A2 domain was proteolyzed very slowly, as visualized by gel staining (Fig. 5*A*), when compared with the A2 domain fragments VWF115, VWF76, and VWF115-A3. When samples containing 500 nM VWFA2

Downloaded from www.jbc.org at Imperial College London on November 2, 2006

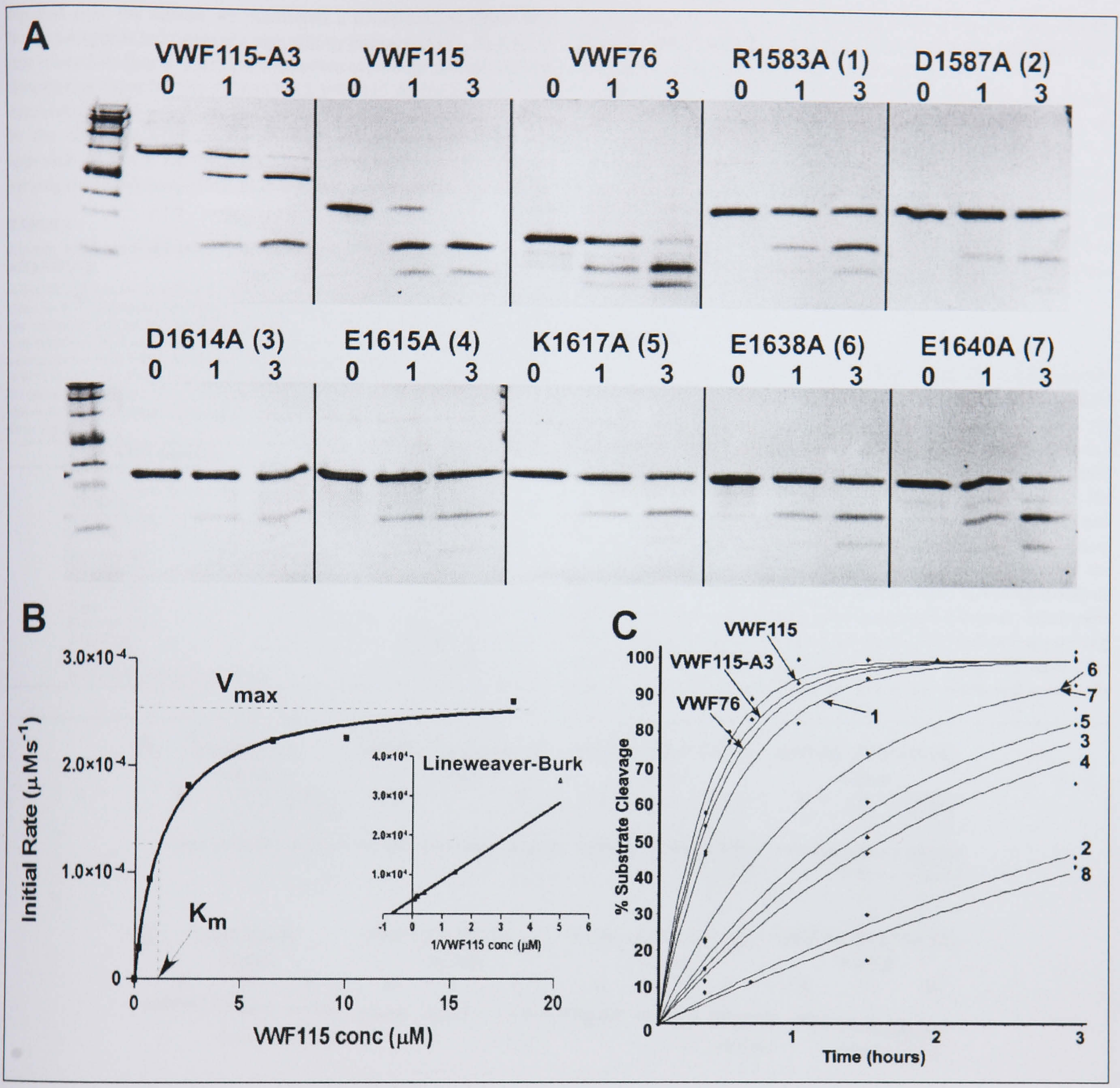


FIGURE 4. **Proteolysis of VWF76, VWF115, VWF115-A3, and VWF115 mutants by ADAMTS13.** *A*, SDS-PAGE and Coomassie staining of different substrate proteolysis. ADAMTS13 was incubated with different wild-type VWF A2 domain fragments or mutant VWF115 as indicated, using high substrate concentrations (4–8 μM). Samples analyzed were 0-, 1-, and 3-h time points. *B*, determination of the individual rate constants (K_m and k_{cat}) for VWF115 proteolysis by HPLC analysis of the initial rate of VWF115 proteolysis at different substrate concentrations (100 nM-50 μM). Michaelis-Menten and Lineweaver-Burk (*inset*) plots are shown. Values for K_m and k_{cat} for VWF115 proteolysis were 1.61 ± 0.47 μM and 0.14 ± 0.06 s^{-1}, respectively. *C*, HPLC analysis of time course reactions of different substrates shown in *panel A* are represented graphically. Reactions employed 500 nM substrate (marked as in *panel A*) and 8 nM ADAMTS13. The catalytic efficiency (k_{cat}/K_m) of proteolysis of each substrate was derived using Enzfitter software as shown in Table 1.

were analyzed by HPLC (Fig. 5*C*), it was clear that the cleavage reaction did not proceed toward completion (~28% after 5 h), as previously reported (13). The D1587A, D1614A, and E1615A VWFA2 mutants were proteolyzed either at a similar or slower rate (Fig. 5, *A* and *C*), suggesting that these mutations do not alter the A2 domain structure markedly. Under denaturing conditions (1 M urea), the wild-type VWFA2 was proteolyzed faster, although it still did not reach completion (~50% after 5 h) (Fig. 5, *B* and *D*). Although all the mutants were cleaved at a higher rate under denaturing conditions, they were cleaved appreciably slower than VWFA2, corroborating the direct influence of these mutations upon VWF115 proteolysis.

Confirmation of ADAMTS13 Binding Site Residues in VWFA2 Domain—We hypothesized that the most likely cause of the reduced catalytic efficiency of the affected VWF115 charged mutants was impaired binding to ADAMTS13. To measure the influence of each mutation upon the interaction of VWF115 with ADAMTS13, we performed SPR analysis. Monoclonal antibody-mediated orientation-specific coupling of either VWF115 or ADAMTS13 to the sensor chip was not possible due to the relatively fast off-rates of these molecules with the available antibodies to each ligand (not shown). Consequently, we covalently bound either VWF115 or ADAMTS13 to the sensor chip by amine coupling. With VWF115 bound to the chip and ADAMTS13

Downloaded from www.jbc.org at Imperial College London on November 2, 2006

injected over the sensor, we monitored a concentration-dependent binding response indicative of a high affinity interaction (K_D, 20 nM) for this interaction (Fig. 6, *inset*). Determination of both the association and dissociation rates for the ADAMTS13-VWF115 interaction ($n = 3$) demonstrated a slow off-rate ($1.72 \times 10^{-3}\ s^{-1}$), which would appear to be the major determinant for the high affinity binding. A second approach, in which ADAMTS13 was coupled to the sensor chip and varying concentrations of VWF115 injected, gave a similar high affinity binding component ($K_D \sim 15$ nM, not shown). These data demonstrate that the affinity of ADAMTS13 for VWF115 is significantly higher than is suggested by the K_m for VWF115 proteolysis.

SPR analysis of VWF115 mutants (D1587A, D1614A, E1615A, and DEK1614/5/7AAA) using both binding approaches revealed a markedly reduced affinity of ADAMTS13 for each of the mutants when compared with wild-type VWF115 (Fig. 6). Because of the low binding response measured, an accurate K_D could not be derived from the VWF115 mutant data. Despite the poor fitting the estimate for the K_D for the DEK1614/5/7AAA mutant was ~1.3 μM. It was clear that for each variant the binding with ADAMTS13 was appreciably compromised and thus the likely cause of their reduced specificity constants.

TABLE 1

Kinetic analysis of different VWF substrate proteolysis by ADAMTS13.

ADAMTS13 was incubated with 500 nM substrate under physiological ionic conditions at 37 °C. Sub-samples from each time course reaction were taken (0–6 h) and the extent of proteolysis measured by HPLC. The catalytic efficiency (k_{cat}/K_m) of proteolysis of each substrate was derived using Enzfitter software. The specificity constants for each VWF substrate/VWF115 variant is given (±S.E.). For VWF115, VWF115-A3, and VWF76, $n = 8$. For the least affected VWF115 variants (R1583A, D1640A, E1638A, and K1617) and the triple mutant DEK1614/5/7AAA, $n = 1$. For the most affected single mutants (D1614A, E1615E, and D1587), $n = 3$. Numbering as in Fig. 4.

VWF substrate	k_{cat}/K_m
	$\times 10^4\ M^{-1}\ s^{-1}$
VWF115	7.83 ± 1.18
VWF115-A3	6.70 ± 2.78
VWF76	6.39 ± 1.18
R1583A (1)	6.19
D1640A (7)	2.74
E1638A (6)	2.74
K1617A (5)	1.90
D1614A (3)	1.36 ± 0.26
E1615 (4)	1.13 ± 0.30
D1587A (2)	0.64 ± 0.10
D1614A/E1615A/K1617A (8)	0.59

DISCUSSION

ADAMTS13 cleaves a single bond within the VWF A2 domain (9). Under static or low shear conditions, proteolysis is slow because of the globular conformation adopted by multimeric VWF. Moreover, the complex folding of the A2 and surrounding domains further conceals the scissile bond (10). The isolated intact A2 domain is also not readily proteolyzed by ADAMTS13 (19). In the absence of a denaturant, the intact domain (VWF residues Met^{1473}-Arg^{1668}) adopts a "non-permissive" structure that restricts access of ADAMTS13 (13). This is potentially explained by a VWF A2 domain model that suggests that the Tyr^{1605}–Met^{1606} bond lies buried within the center of the folded domain (17) and is thus not normally solvent exposed. However, incomplete VWF A2 domain fragments that span the ADAMTS13 cleavage site (*e.g.* VWF73 Asp^{1595}-Arg^{1668} and VWF115 Glu^{1554}-Arg^{1668}) have been shown, here and elsewhere (12, 20, 21), to be readily and specifically

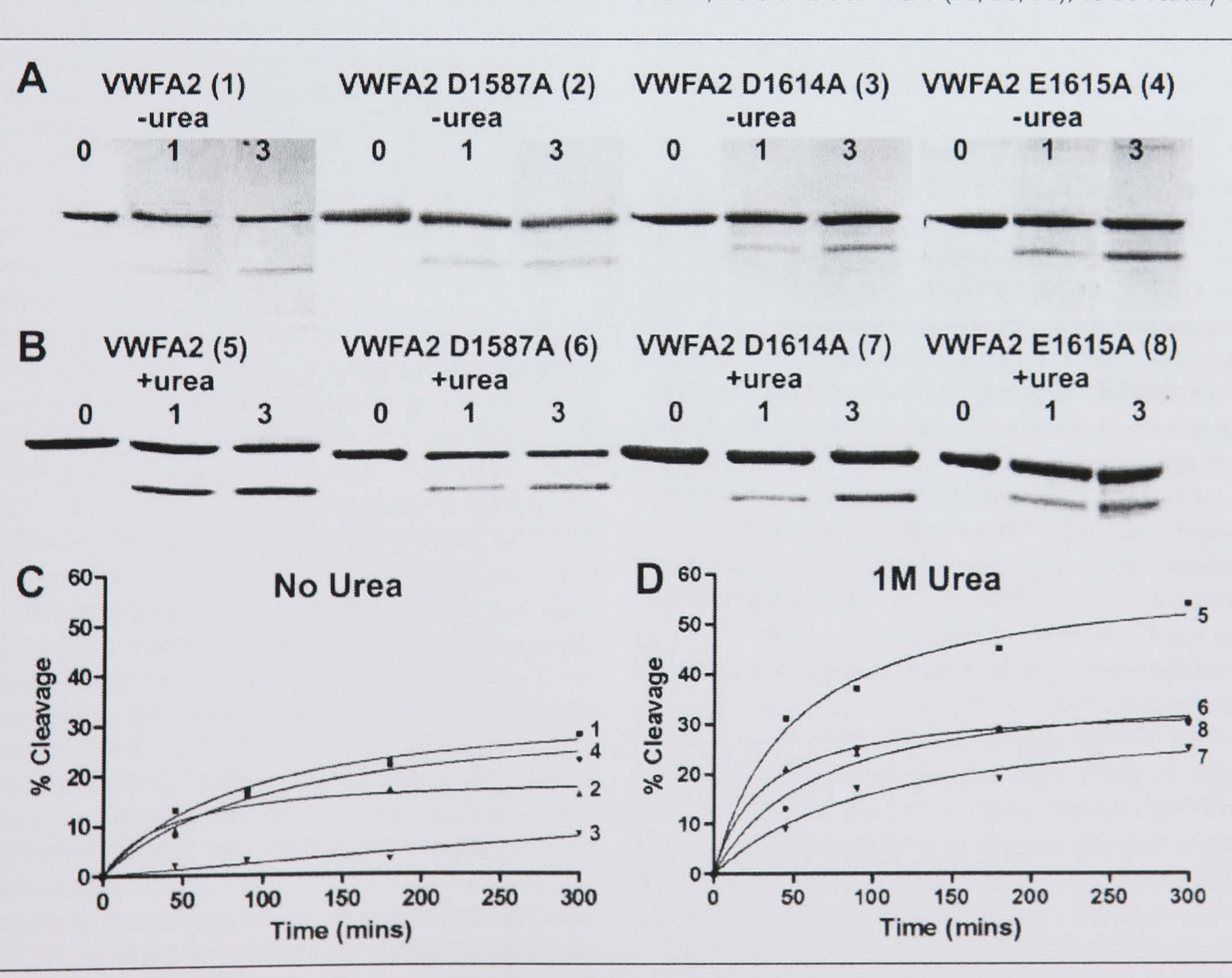


FIGURE 5. **VWFA2 and VWFA2 charged mutant proteolysis.** *A*, 6 μM VWFA2 (*1*) or VWFA2 carrying D1587A (*2*), D1614A (*3*), or E1615A (*4*) was incubated with 16.5 nM ADAMTS13 in the absence of denaturant and analyzed by SDS-PAGE and Coomassie staining. Samples were incubated for 0, 1, and 3 h as indicated. *B*, 6 μM VWFA2 (*5*) or VWFA2 carrying D1587A (*6*), D1614A (*7*), or E1615A (*8*) mutations was incubated with ADAMTS13 as in *panel A* in the presence of 1 M urea. Samples were analyzed as in *panel A*. *C*, graph of HPLC analysis of time course reaction samples 1–4 (*panel A*) set up in parallel reactions containing 500 nM of each substrate. *D*, graph of HPLC analysis of time course reaction samples 5–8 (*panel B*) set up in parallel reactions containing 500 nM of each substrate.

Downloaded from www.jbc.org at Imperial College London on November 2, 2006

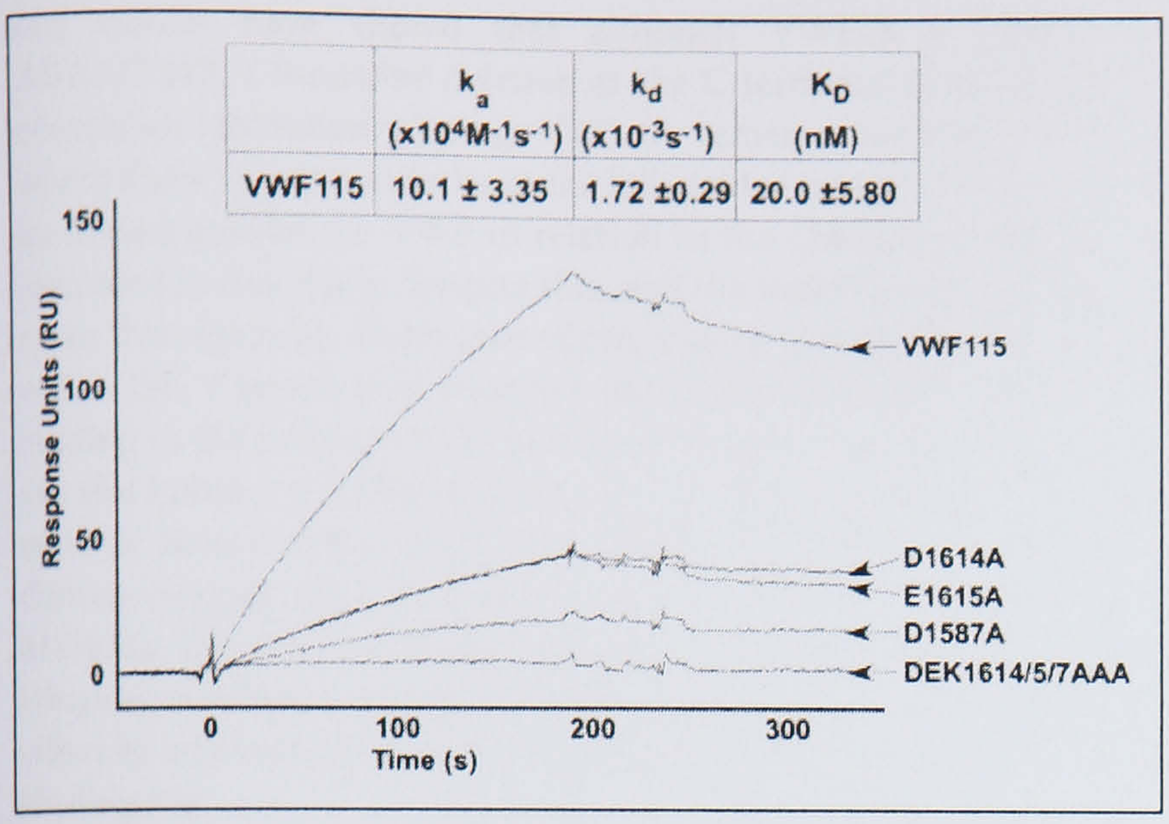


FIGURE 6. **Binding of ADAMTS13 to VWF115 and VWF115 mutants.** VWF115 was immobilized by covalently coupling 600 response units of VWF115 to one flow cell of a CM5 sensor chip and human endothelial protein C receptor to the control flow cell. Sequential injections of ADAMTS13 (10–137 nM) in HBS-P buffer were injected over the surface of each chip. Data were fitted using a 1:1 Langmuir model. Individual association (k_a) and dissociation (k_d) rates for the ADAMTS13-VWF115 interaction are given, from which the K_D (20.0 nM) was derived (k_d/k_a). Comparative SPR analysis was performed by covalently coupling VWF115, VWF115(D1587A), VWF115(D1614A), VWF115(E1615A) or VWF115(DEK1614/5/7AAA) as above. Results shown are overlaid data for VWF115 and VWF115(D1587A), VWF115(D1614A), VWF115(E1615A), or VWF115(DEK1614/5/7AAA) as marked, using 27.5 nM ADAMTS13.

cleaved at the Tyr^{1605}–Met^{1606} site under normal physiological ionic conditions, suggesting that these fragments not only contain important recognition sequences for specific ADAMTS13-dependent proteolysis but also that their structure presents the cleavage site in a permissive conformation, more akin to unraveled/denatured VWF (12). In the present study, we have expressed and purified a number of related VWF A2 and A2/A3 domain fragments to delineate those regions important for A2 domain proteolysis. Previous studies have employed SDS-PAGE and/or Western blotting to monitor proteolysis, the latter to achieve high sensitivity in the early stages of the cleavage reaction (13). Cleavage of VWF fragments by ADAMTS13 was quantified here by HPLC, allowing for the first time accurate and fully quantitative analysis of the kinetics of these reactions.

In our hands, most likely as a result of the smaller recombinant protein tag used in this study, VWF115 was marginally more susceptible to cleavage than the shorter substrate VWF76 (very similar to VWF73 that has been reported elsewhere (12, 20)) when the cleavage reaction was fully quantified. Its K_m was ~1.6 μM, $k_{cat} \sim 0.14\ s^{-1}$, and its specificity constant (k_{cat}/K_m) $\sim 8 \times 10^4\ M^{-1}\ s^{-1}$. This estimate of specificity is quite similar to that recently reported for ADAMTS13 cleavage of full-length VWF multimers under conditions of low ionic strength (22). This is surprising, considering those experiments were performed under denaturing conditions and without the advantage of a released peptide with which to accurately quantitate the rate of proteolysis. VWF115-A3 gave similar values for the specificity constant, suggesting that the A3 domain makes no appreciable contribution to the cleavage reaction despite its reported high affinity binding site (18). This finding corroborates previous semi-quantitative data obtained from the comparative analysis of recombinant VWFA2 and VWFA2/A3 proteolysis under denaturing conditions (13).

Residues surrounding the cleavage site are known to influence proteolysis of intact VWF, as they are reported to be dysfunctional in certain cases of type 2A (group II) VWD (15). We therefore introduced some of these mutations into the A2 domain fragment (VWF115) and evaluated proteolysis. Of course, the type 2A (group II) phenotype is generally associated with enhanced, rather than reduced, proteolysis by ADAMTS13. Nevertheless, we selected reported mutations surrounding the cleavage site, as not all had been tested extensively in terms of ADAMTS13 interaction. Interestingly, of those mutations selected, one (D1614G) was proteolyzed significantly slower when introduced into VWF115. To fully characterize how this mutation might exert a type 2A VWD phenotype, further studies examining its influence upon full-length, multimeric VWF will be required. Type 2A group II VWD mutations are generally believed to manifest their phenotype by unfolding of the A1-A2-A3 domain region, increasing ADAMTS13 access to, and therefore cleavage of, the scissile bond. The possibility of reduced, rather than enhanced, rates of cleavage of mutants, such as D1614G, in the vicinity of the cleavage site should be taken into consideration when evaluating the complex phenotype of cases of potential type 2A group II VWD. Because of this finding, we mutated further charged residues thought to be in proximity with Asp^{1614} on the basis of primary sequence and the homology model of the A2 domain. Of eight such mutants introduced into VWF115, six (D1587A, D1614A, E1615A, K1617A, E1638A, and E1640A) had clearly reduced cleavage rates. The triple mutant, DEK1614/5/7AAA, had ~13-fold reduction in the specificity constant for proteolysis. To confirm that the delayed cleavage of the VWF115 substrate was not merely a feature of this particular substrate, three of the mutations (D1587A, D1614A, and E1615A) were introduced into the fully folded intact A2 domain. Under denaturing conditions (1 M urea), proteolysis of all three substrates was reduced in rate and extent when compared with the wild-type VWFA2. Even under non-denaturing conditions, where under the conditions used proteolysis of the A2 domain did not exceed 30% at 300 min, proteolysis of D1587A and D1614A was appreciably impaired. These results with both VWF115 and A2 substrates suggested that specificity is appreciably influenced by a charged patch on the surface of the A2 domain.

Binding of ADAMTS13 to multimeric VWF and A2 domain fragment substrates has been reported to be of high affinity (23). Physiologically, ADAMTS13 seems to circulate in complex with VWF. However, the binding of ADAMTS13 to VWF need not necessarily be accompanied by proteolysis. Although Ca^{2+} ions are required for efficient proteolysis (10), they are not necessary for high affinity binding (21, 23). A recent report of binding of ADAMTS13 to VWF73 in the absence of Ca^{2+} ions using a microtiter plate-based immunoassay for ADAMTS13 suggested a K_D of 4.6 nM (21). Because of uncertainties surrounding the use of antibody detection and equilibrium perturbation in the detection step of binding in such assays, we used the alternative approach of SPR. Coupling VWF115 directly to the sensor chip and injecting different concentrations of ADAMTS13 yielded a K_D of ~20 nM. This high affinity interaction appeared to be conferred by a slow dissociation rate (k_d). Confirmation of tight binding was obtained by covalently immobilizing ADAMTS13 and then injecting VWF115 over the sensor chip. In this case, a K_D of 15 nM was obtained. However, there was also some evidence for heterogeneity of binding, and a lower affinity component was also apparent using this second approach. Importantly though, both SPR approaches demonstrated substantial loss (>10-fold) in binding affinity of ADAMTS13 to the mutant VWF115 fragments D1587A, D1614A, and E1615A and the triple mutant DEK1614/5/7AAA irrespective of whether SPR was performed with these fragments as analyte or ligand. This provides direct evidence that these residues form part of a docking site for ADAMTS13 on the VWFA2 domain.

The present investigation has for the first time identified critical residues within the VWF A2 domain that are important for both binding to ADAMTS13 and for proteolysis at the Tyr^{1605}–Met^{1606} bond. Given its specificity, proteolysis is unlikely to be determined solely by interaction with a limited number of residues surrounding the cleavage site. Previ-

Downloaded from www.jbc.org at Imperial College London on November 2, 2006

ous studies have shown that although VWF73 is cleaved by ADAMTS13, a 9-residue deletion at the C terminus of this fragment completely abolished cleavage (12). It remains uncertain precisely where these 9 amino acids lie in the fully folded intact A2 domain or in unraveled multimeric VWF in relation to the charged patch/residues identified in this study. Despite this, and the inability of a peptide that spans this region to inhibit proteolysis, it remains possible that residues within this 9-amino acid sequence contribute directly to high affinity binding to the protease (12). Structures remote from the cleavage site are also known to influence proteolysis. The A1 domain of VWF was recently demonstrated to inhibit access of ADAMTS13 to the A2 domain cleavage site (13). This inhibition was removed in the presence of GpIbα, the principal A1 domain ligand, suggesting that under physiological conditions platelet binding may enhance VWF proteolysis either by increasing scissile bond access or by revealing an ADAMTS13 binding site.

Acknowledgment—We thank Dr. James Rance for help in the early phase of this work.

REFERENCES

1. Sadler, J. E. (1998) *Annu. Rev. Biochem.* **67,** 395–424
2. Roth, G. J., Titani, K., Hoyer, L. W., and Hickey, M. J. (1986) *Biochemistry* **25,** 8357–8361
3. Siedlecki, C. A., Lestini, B. J., Kottke-Marchant, K. K., Eppell, S. J., Wilson, D. L., and Marchant, R. E. (1996) *Blood* **88,** 2939–2950
4. Ruggeri, Z. M., De Marco, L., Gatti, L., Bader, R., and Montgomery, R. R. (1983) *J. Clin. Investig.* **72,** 1–12
5. Zwaal, R. F., Comfurius, P., and Bevers, E. M. (1998) *Biochim. Biophys. Acta* **1376,** 433–453
6. Bajaj, M. S., Kuppuswamy, M. N., Manepalli, A. N., and Bajaj, S. P. (1999) *Thromb. Haemostasis* **82,** 1047–1052
7. Haberichter, S. L., Fahs, S. A., and Montgomery, R. R. (2000) *Blood* **96,** 1808–1815
8. de Wit, T. R., and van Mourik, J. A. (2001) *Best Pract. Res. Clin. Haematol.* **14,** 241–255
9. Furlan, M., Robles, R., and Lammle, B. (1996) *Blood* **87,** 4223–4234
10. Tsai, H. M. (1996) *Blood* **87,** 4235–4244
11. Dong, J. F., Moake, J. L., Nolasco, L., Bernardo, A., Arceneaux, W., Shrimpton, C. N., Schade, A. J., McIntire, L. V., Fujikawa, K., and Lopez, J. A. (2002) *Blood* **100,** 4033–4039
12. Kokame, K., Matsumoto, M., Fujimura, Y., and Miyata, T. (2004) *Blood* **103,** 607–612
13. Nishio, K., Anderson, P. J., Zheng, X. L., and Sadler, J. E. (2004) *Proc. Natl. Acad. Sci. U. S. A.* **101,** 10578–10583
14. Tsai, H. M. (2004) *J. Thromb. Haemostasis* **2,** 2057
15. Tsai, H. M., Sussman, I. I., Ginsburg, D., Lankhof, H., Sixma, J. J., and Nagel, R. L. (1997) *Blood* **89,** 1954–1962
16. Crawley, J. T., Lam, J. K., Rance, J. B., Mollica, L. R., O'Donnell, J. S., and Lane, D. A. (2005) *Blood* **105,** 1085–1093
17. Sutherland, J. J., O'Brien, L. A., Lillicrap, D., and Weaver, D. F. (2004) *J. Mol. Model (Online)* **10,** 259–270
18. Dong, J. F., Moake, J. L., Bernardo, A., Fujikawa, K., Ball, C., Nolasco, L., Lopez, J. A., and Cruz, M. A. (2003) *J. Biol. Chem.* **278,** 29633–29639
19. Cruz, M. A., Whitelock, J., and Dong, J. F. (2003) *Thromb. Haemostasis* **90,** 1204–1209
20. Kokame, K., Nobe, Y., Kokubo, Y., Okayama, A., and Miyata, T. (2005) *Br. J. Haematol.* **129,** 93–100
21. Ai, J., Smith, P., Wang, S., Zhang, P., and Zheng, X. L. (2005) *J. Biol. Chem.* **280,** 29428–29434
22. De Cristofaro, R., Peyvandi, F., Palla, R., Lavoretano, S., Lombardi, R., Merati, G., Romitelli, F., Di Stasio, E., and Mannucci, P. M. (2005) *J. Biol. Chem.* **280,** 23295–23302
23. Majerus, E. M., Anderson, P. J., and Sadler, J. E. (2005) *J. Biol. Chem.* **280,** 21773–21778

Downloaded from www.jbc.org at Imperial College London on November 2, 2006

ADDENDA AND CORRIGENDA

1. p. 20, line 11: platelet dense granules do not contain thromboxane A2.
2. p. 57, Section 1.3.6.1, line 12: 'Tsai *et al*' should be replaced by 'Tsai'.
3. p.61, Section 1.3.6.6.4, lines 7 and 8: the sentence '…the quencher is no more able to absorb the fluorescence then thus is emitted…' should be replaced with ' …the quencher is no longer able to absorb the fluorescence which is emitted…'.
4. p. 62, line 1: 'peripheal' should be replaced with 'peripheral'.
5. p. 62, lines 28 and 33: 'activated microvenules' refers to microvenules activated with calcium ionophore A23187 (a secretagogue of Weibel-Palade bodies).
6. p. 62, line 34: 'base' should be replaced with 'basis'.
7. p. 90, Fig. 2.6 : 'dymamic' should be replaced by 'dynamic'.
8. p. 92, line 4: ' …during the all course of the experiment…' should be altered to '… during the entire course of the experiment..'
9. p.169, line 8: 'Of the all above residues…' should be replaced with 'Of all the above residues…'.
10. p. 181, line 4: 'extents' should be replaced by 'extends'.